

**EXPERIMENTAL INVESTIGATION OF
THE INFLUENCE OF LUBRICANT ADDITIVES ON
RHEOLOGY OF ELASTOHYDRODYNAMIC FILMS**

by

HE-JIN YU

A thesis

presented to the University of Waterloo

in fulfillment of the

thesis requirement for the degree of

Doctor of Philosophy

in

Mechanical Engineering

Waterloo, Ontario, Canada, 1997

© He-Jin Yu 1997



**National Library
of Canada**

**Acquisitions and
Bibliographic Services**

395 Wellington Street
Ottawa ON K1A 0N4
Canada

**Bibliothèque nationale
du Canada**

**Acquisitions et
services bibliographiques**

395, rue Wellington
Ottawa ON K1A 0N4
Canada

Your file Votre référence

Our file Notre référence

The author has granted a non-exclusive licence allowing the National Library of Canada to reproduce, loan, distribute or sell copies of his/her thesis by any means and in any form or format, making this thesis available to interested persons.

The author retains ownership of the copyright in his/her thesis. Neither the thesis nor substantial extracts from it may be printed or otherwise reproduced with the author's permission.

L'auteur a accordé une licence non exclusive permettant à la Bibliothèque nationale du Canada de reproduire, prêter, distribuer ou vendre des copies de sa thèse de quelque manière et sous quelque forme que ce soit pour mettre des exemplaires de cette thèse à la disposition des personnes intéressées.

L'auteur conserve la propriété du droit d'auteur qui protège sa thèse. Ni la thèse ni des extraits substantiels de celle-ci ne doivent être imprimés ou autrement reproduits sans son autorisation.

0-612-21401-X

The University of Waterloo requires the signatures of all persons using or photocopying this thesis. Please sign below, and give address and date.

Abstract

An experimental investigation was conducted to study the influence of additives on lubricant rheology in elastohydrodynamic lubrication (ehl) and micro-ehl as found in applications such as gears and rolling element bearings. The lubricants were subjected to very high pressures which acted globally over the apparent area of contact in ehl and to even higher pressures which acted locally at asperity contacts in micro-ehl. For ehl, calculations were described for evaluating the effective film thickness parameter λ (theoretical central film thickness divided by measured composite RMS surface roughness). This parameter determined an approximate point of transition to micro-ehl. As well, an analytical procedure was developed for determining the limiting shear stress, which was considered an important parameter in high pressure rheology. For micro-ehl, a calculation procedure, based on measured surface roughness parameters and a modified Greenwood and Williamson type model, was developed to evaluate the real area of contact.

A side-slip disc machine was used to measure friction forces which sheared elastohydrodynamic lubricant films as slip-roll ratio increased from zero. Major disc machine modifications included adding devices to measure surface temperature, using an electrical resistance circuit to measure cross film voltage drop, and providing an automatic data acquisition system. Lubricant additives, in the general categories of friction modifier, anti-wear, and extreme pressure, were studied in disc machine experiments involving rough and smooth disc surfaces.

Friction force rose rapidly to achieve a maximum value at a slip-roll ratio of about 5%. In ehl, with the smooth discs, small but distinct and repeatable differences in the friction forces were caused by the additives. These differences permitted evaluation of limiting shear stress expressions which were functions of pressure for each lubricant. In micro-ehl, with a rough disc surface, the friction force was 2 - 3 times higher than occurred with smooth disc surfaces

and the additives had significant influence on friction forces. The measured friction force divided by the estimated real area of contact gave an alternative evaluation of the limiting shear stress, which agreed quite closely with the limiting shear stress predictions based the expressions derived from testing in ehl. This agreement suggested that friction measurements under ehl could be used to evaluate and explore the influences of additives on the limiting shear stress. Thus, the lubricant chemistry could be designed to give an optimal limiting shear stress using disc machine measurements, under conditions of ehl, for guidance.

Acknowledgements

I would like to express my sincere gratitude to my supervisor, Professor John. B. Medley, for his invaluable guidance and encouragement throughout my studies at the University of Waterloo. I am thankful not only for his expertise in tribology and the countless extra hours working on my research but also for his infinite enthusiasm and truthful friendship.

I would also like to express my thanks to Mr. Ernst Huber and Mr. Paul Renkema, Tribology Laboratory technicians, and to Mr. Dieter Raude, Engineering Machine Shop mechanist, for their effective support during my experimental work.

I am indebted to my fellow graduate students for many lively discussions, enthusiastic help and constructive criticism. With them I shared a very friendly study environment.

I also thank Imperial Oil Ltd., Sarnia, Canada and the Natural Sciences and Engineering Research Council of Canada for providing a financial support through the Department of Mechanical Engineering, University of Waterloo, for this study.

Finally, I give my sincerest thanks to Chao-Wu Sheng and all of my family members for their understanding and encouragement.

To my dear parents and my beloved husband.

Table of Contents

Abstract	iv
Acknowledgements	vi
Table of Contents	viii
List of Tables	xiv
List of Figures	xvi
Nomenclature	xxiv
Chapter 1 Introduction	1
1.1 Tribology Mechanism and Lubricant Rheology	1
1.2 Objective and Chosen Approach.....	5
1.3 Thesis Layout.....	6
Chapter 2 Background	8
2.1 Mineral Oils and Additives	8
2.1.1 Low pressure rheological properties.....	8
• Viscosity	
• Density	
• Viscosity-temperature relationship	
• Viscosity-pressure relationship	
• Viscosity variation with both temperature and pressure	
2.1.2 Functions of additives	15
• Friction modifier	

• Antiwear additive	
• Extreme pressure additive	
2.2 Elastohydrodynamic Lubrication.....	21
2.2.1 Regimes of lubrication	22
• Hydrodynamic lubrication	
• Elastohydrodynamic lubrication	
• Boundary lubrication	
• Mixed film lubrication	
• Some comments on lubrication failure	
2.2.2 Fundamentals of ehl theory	24
• Hertzian theory for nominal point contact	
• Reynolds equation	
• Pressure distribution and film shape	
2.2.3 Film thickness equation.....	35
2.3 Mixed Film Lubrication	40
2.3.1 Surface roughness.....	40
2.3.2 Effective film thickness parameter (λ)	44
2.3.3 Area of asperity contact.....	45
• Contact spot density between flat rough and smooth surfaces	
• Determining surface and asperity height distributions	
• Determining the real area of contact for a specified load	
• Extension to a sphere-on-flat configuration	
2.3.4 Micro-ehl approach.....	59
• Average flow factor approach	
• Deterministic solution model	
• Physical influence in micro-ehl	
2.4 Friction and Rheological Models	66
2.4.1 Friction behaviour.....	66

2.4.2 High pressure rheological models.....	70
• The Eyring thermal activation model	
• Limiting shear stress model	
• Comparison of the models	
2.4.3 Limiting shear stress from ehl friction measurement.....	82
2.4.4 Friction in rough surface lubricated contact.....	85
Chapter 3 Development of Test Facility.....	90
3.1 Disc Machine	90
3.1.1 Main components.....	91
• Lubricant supply system	
• Driving system	
• Loading system	
• Traction measuring system	
3.1.2 Operating principles	101
3.2 Temperature Measurement.....	106
3.2.1 Temperature of supplied lubricant.....	106
3.2.2 Contact zone temperature measurement.....	107
3.3 Electrical Resistance Method for Detecting Film Breakdown.....	111
3.3.1 Electrical resistance circuit.....	112
3.3.2 Output voltage.....	112
3.4 Data Acquisition and Data Processing	117
3.4.1 Data acquisition system.....	117
• Hardware	
• Software	
• Specific application of Virtual Instrument program	
3.4.2 Power spectrum analysis and sampling frequency	123
3.4.3 Analog filter.....	127

Chapter 4 Materials and Methods	130
4.1 Lubricants	130
4.1.1 Base stock oil	131
4.1.2 Formulated oils	134
• Friction modifier formulation	
• Anti-wear additive formulation	
• Extreme pressure additive formulation	
4.2 Design of Experiments	135
4.2.1 Disc surface roughness control.....	136
• Smooth surface	
• Rough surface	
• Roughness measurements	
• BA and HSC for rough surface discs	
4.2.2 Operating conditions.....	148
• Applied load	
• Entrainment velocity	
• Inlet zone lubricant temperature and ambient pressure viscosity	
• Disc surface roughness and λ ratio arrangement	
4.3 Sequence of Experiments	154
 Chapter 5 Results	 163
5.1 Friction Force Measurements	163
5.1.1 Results for full ehl.....	166
• Traction curves	
• Maximum friction force	
5.1.2 Results for mixed film lubrication.....	181
• Traction curves	
• Maximum friction force	

5.2	Some Observations from Traction Curves.....	203
5.2.1	Characteristics from ehl.....	203
	• Influences of operating conditions on friction force	
	• Lubricant additives in smooth disc experiments	
5.2.2	Characteristics from mixed film lubrication.....	209
	• Effects of surface roughness on friction force	
	• Lubricant additives in rough disc experiments	
5.3	Accuracy and Precision	211
	• Determining the origin of friction force at zero skew angle	
	• Error in F_f caused by friction of top disc supporting bearing	
	• Top disc alignment	
	• Disc surface cleaning	
	• Repeatability	
Chapter 6	Analysis and Discussion.....	222
6.1	Influence of λ -Ratio on Friction Coefficient	222
6.2	Empirical Approach to Determine Limiting Shear Stress.....	230
6.2.1	Determining the limiting shear stress index number.....	231
6.2.2	Empirical expression of τ_L as a function of film pressure.....	234
6.3	Real Area of Contact for the Rough Surface Discs.....	234
6.3.1	Bearing area and high spot count	235
6.3.2	Surface separation and real area of contact.....	240
6.4	Comparison of τ_L from Experiments with Smooth and Rough Top Discs	244
	• τ_{Lavg} from friction measurements a smooth top disc	
	• τ_{Lavg} from friction measurements a rough top disc	
	• Comparison of τ_{Lavg} values	

Chapter 7 Conclusions and Recommendations	253
7.1 Summary	253
7.2 Conclusions	255
7.3 Recommendations of Further Research	256

References	259
-------------------------	------------

Appendix A Influence of Lubricant Additives on Friction in a Disc Machine (Paper accepted for publication in the “Fundamentals and Applications in Lubrication and Traction”, Tribology Series, 32, Elsevier)	271
--	------------

List of Tables

2.1	Coefficients of expansion of mineral oils (from <i>Handbook of Lubrication</i> , 1984)	11
2.2	Viscosity and Density of SAE 5W Engine Oil (from Cameron, 1981)	13
2.3	Discrete data of $F_j(\zeta)$'s for GW type model	57
3.1	Measurement results of output voltage V_o for various u	115
4.1	Inspection data of mineral oils used in present study (from Imperial Oil Ltd.).....	131
4.2	Measurement results of η_o and ρ	132
4.3	Alloy composition of disc materials	136
4.4	Roughness measurement records for smooth top and bottom discs	141
4.5	Roughness measurements for rough surface contact disc pairs and matched smooth surface contact disc pairs	143
4.6	Talysurf measured data for rough surface disc R1	147
4.7	Talysurf measured data for rough surface disc R2.....	147
4.8	Applied load levels and corresponding contact area and pressure	149
4.9	Conversion of pulse rate ψ and rolling speed u	149
4.10	Experiment sequence for smooth disc tests	155
4.11	Experiment sequence for rough disc tests	158
4.12	Experiment sequence for matched smooth disc tests	160
5.1	The $F_{f_{max}}$ in smooth surface disc measurements	180
5.2	The $F_{f_{max}}$ in rough surface top disc measurements.....	201
5.3	The $F_{f_{max}}$ in matched reference smooth top disc measurements	202
5.4	Error in friction force caused by friction of top disc supporting bearings	215
5.5	The $F_{f_{max}}$ in two repeated sets of smooth disc tests for MCT 5	217

5.6 Multiple $F_{r\max}$ measurements performed in various experiments	219
6.1 The μ_{\max} in rough disc experiments	224
6.2 The μ_{\max} in matched smooth disc experiments.....	225
6.3 Constants for the expression of τ_L versus p	234
6.4 Curve fitting data for rough surface disc R1.....	237
6.5 Calculation of β, A_r and A_r / A_a	244
6.6 Measured and predicted $\tau_{L,avg}$ for ehl conditions.....	246
6.7 Measured and predicted $\tau_{L,avg}$ for micro-ehl conditions.....	247
6.8 Predicted $\tau_{L,avg}$ from empirical expression with p_{avg}	248

List of Figures

1.1 Tribological mechanisms of thin film lubrication in concentrated contacts	2
2.1 Physical illustration of Newtonian fluid.....	10
2.2 Viscosities of SAE lubricating oils at atmospheric pressure (from Hamrock, 1994)	12
2.3 Lubrication mechanism by FM additives	17
(a) adsorption lubrication mechanism (from Stachowiak and Batchelor, 1993)	
(b) chemical structure of fatty acid (from Liston, 1992)	
2.4 Effects of friction modifiers (from O'Brien, 1983)	18
(a) on friction coefficient	
(b) on engine power loss	
2.5 Chemical structure of zinc dialkyldithiophosphate (from Stachowiak and Batchelor, 1993)	20
2.6 Lubrication mechanism by EP additives (from Liston, 1992).....	20
2.7 Nominal point contact	26
(a) geometry of contacting elastic solid (from Hamrock and Dowson, 1981)	
(b) a circular contact area from a contact of a sphere and a plane	
2.8 Typical bearing illustration for deriving Reynolds equation	29
(a) a bearing with converging-diverging surfaces	
(b) control volume for conservation of momentum	
(c) control volume for conservation of mass	
2.9 Typical pressure and film thickness profiles for ehl contact	32
2.10 Typical ehl film between an elastic sphere and a rigid plane.....	34
2.11 A simple computational scheme for isothermal ehl	36
2.12 Lubrication regime chart for nominal point contact (from Hamrock, 1994, based on the results of Esfahanian and Hamrock, 1991).....	38

2.13 Geometric characteristic of solid surface (from Halling, 1976).....	41
2.14 Surface roughness measurement (from Talysurf 5 Operator's Handbook).....	43
(a) RMS of a Gaussian surface	
(b) BA and HSC at a separation z	
2.15 Variation of friction coefficient with film parameter (from Hamrock and Dowson, 1981).....	46
2.16 Representation of contact between a rigid plane and a rough surface	48
2.17 Average trace cross a circular asperity contact spot.....	50
2.18 Determination of d_{avg} and σ from a probability plot of BA versus z	52
2.19 Determination of d^*_{avg} and σ^* from a probability plot of n/n_{max} versus z	53
2.20 Numerical results of pressure and film thickness profiles and contour plots (from Lubrecht et al, 1988)	61
(a) for longitudinal roughness	
(b) for transverse roughness	
2.21 Micro-interferograms of rough surface lubricated contact (from deSilva et al, 1985).....	62
(a) for longitudinal roughness	
(b) for transverse roughness	
2.22 Solution of asperity flattening model (from Kweh et al, 1989).....	64
2.23 Discontinuous pressure distribution in rough surface contact (from Evans and Johnson, 1985)	65
2.24 Typical friction curves from disc machine	68
2.25 Visco-elastic nature for rheological model	71
2.26 Relationship of shear stress and shear strain rate for lubricant under extremely high pressure (from Smith, 1960)	75
2.27 Comparison of friction results from different measurement methods (from Bair and Winer, 1979b)	77
2.28 Observation of Shear bands (from Bair et al., 1993).....	79
2.29 Traction map for Santotric 50 (from Evans and Johnson, 1986).....	81

2.30	Variation of τ_L with p at various temperatures (from Wu and Cheng, 1994).....	86
2.31	Influence of λ ratio on friction coefficient (from Evans and Johnson, 1985)	88
3.1	Side-slip disc machine (photo)	92
3.2	Schematic representation of the lubricant supply system	93
3.3	Schematic representation of the side-slip disc machine	96
3.4	Friction force measurement	
(a)	strain gauge ring load cell	98
(b)	load cell calibration	99
3.5	Skew angle measurement	
(a)	direct current displacement transducer for measuring skew angle	100
(b)	DCDT calibration	102
3.6	Rolling with side-slip kinematic principles on disc machine	103
(a)	Arrangement of discs	
(b)	Vectors of shear strain rate in contact zone	
(c)	Vectors of total shear strain in contact zone	
3.7	Typical traction curve from side-slip disc machine	105
3.8	Schematic representation of disc surface temperature measurement	108
3.9	Influence of thermocouple contact force on disc surface temperature	110
3.10	Electrical resistance circuit for detecting film breakdown	113
3.11	Output voltage from electrical resistance circuit	114
3.12	Typical plot of output voltage versus rolling speed for various loads	116
3.13	Configurations for PC-LPM-16 data acquisition system	118
3.14	A graphical program "AITOWAVE.VI" for traction measurement	
(a)	Front panel	120
(b)	Block diagram	120
(c)	Hierarchy diagram	121
3.15	Typical power spectrum analysis for measured traction curve	125
3.16	High frequency noise from unfiltered traction curve	126

3.17	Circuit of low-pass analog filter	128
3.18	Low-pass analog filter property curve.....	129
4.1	Comparison of viscosity at various temperatures	133
	(a) for MCT 5	
	(b) for MCT 5 and MCT 5 + FM	
	(c) for MCT 5 and MCT 5 + AW	
	(d) for MCT 5 and MCT 5 + EP	
4.2	Main description of experimental design	137
4.3	Typical segment of measured surface profile of smooth top disc S0 ₁	139
	(a) in circumferential direction	
	(b) in axial direction	
4.4	Photo of smooth and rough top discs.....	140
4.5	Surface profiles of rough top disc R2.....	142
	(a) at beginning	
	(b) after run-in	
	(c) after friction measurement	
4.6	Typical Talysurf measurement records for rough top disc R1	145
	(a) surface profile (after run-in)	
	(b) data for BA and HSC at various depths	
4.7	Typical plot of output voltage vs. film parameter	153
5.1	Typical repeated traction plots from same operating conditions	164
5.2	Traction curves from smooth disc tests for MCT 5	168
	(a) T = 30°C, 4 load levels, 4 lower u's	
	(b) T = 30°C, same 4 loads, 4 higher u's	
	(c) T = 40°C, 4 load levels, 4 lower u's	
	(d) T = 40°C, lower 2 loads, 2 higher u's	

(e) T = 55°C, 4 load levels, 4 higher u's	
5.3 Traction curves from smooth disc tests for MCT 5 + FM	171
(a) T = 30°C, 4 load levels, 4 lower u's	
(b) T = 30°C, same 4 loads, 4 higher u's	
(c) T = 40°C, 4 load levels, 4 lower u's	
(d) T = 40°C, lower 2 loads, 2 higher u's	
(e) T = 55°C, 4 load levels, 4 higher u's	
5.4 Traction curves from smooth disc tests for MCT 5 + AW	174
(a) T = 30°C, 4 load levels, 4 lower u's	
(b) T = 30°C, same 4 loads, 4 higher u's	
(c) T = 40°C, 4 load levels, 4 lower u's	
(d) T = 40°C, lower 2 loads, 2 higher u's	
(e) T = 55°C, 4 load levels, 4 higher u's	
5.5 Traction curves from smooth disc tests for MCT + EP	177
(a) T = 30°C, 4 load levels, 4 lower u's	
(b) T = 30°C, same 4 loads, 4 higher u's	
(c) T = 40°C, 4 load levels, 4 lower u's	
(d) T = 40°C, lower 2 loads, 2 higher u's	
(e) T = 55°C, 4 load levels, 4 higher u's	
5.6 Traction curves from rough top disc tests and matched smooth top disc tests for MCT 5 at T = 30°C.....	183
(a) 2 load levels, highest u's	
(b) 2 load levels, high u's	
(c) 2 load levels, low u's	
(d) 2 load levels, lower u's	
(e) 2 load levels, lowest u's	
5.7 Traction curves from rough top disc tests and matched smooth top disc tests for MCT 5 at T = 40°C.....	186

(a) 2 load levels, highest u's	
(b) 2 load levels, high u's	
(c) 2 load levels, low u's	
(d) 2 load levels, lower u's	
(e) 2 load levels, lowest u's	
5.8 Traction curves from rough top disc tests and matched smooth top disc tests	
for MCT 5 + FM T = 30°C	189
(a) 2 load levels, highest u's	
(b) 2 load levels, high u's	
(c) 2 load levels, low u's	
(d) 2 load levels, lower u's	
(e) 2 load levels, lowest u's	
5.9 Traction curves from rough top disc tests and matched smooth top disc tests	
for MCT 5 + FM at T = 40°C.....	192
(a) 2 load levels, highest u's	
(b) 2 load levels, high u's	
(c) 2 load levels, low u's	
(d) 2 load levels, lower u's	
(e) 2 load levels, lowest u's	
5.10 Traction curves from rough top disc tests and matched smooth top disc tests	
for MCT 5 + EP at T = 30°C	195
(a) 2 load levels, highest u's	
(b) 2 load levels, high u's	
(c) 2 load levels, low u's	
(d) 2 load levels, lower u's	
(e) 2 load levels, lowest u's	
5.11 Traction curves from rough top disc tests and matched smooth top disc tests	
for MCT 5 + EP at T = 40°C	198

(a) 2 load levels, highest u's	
(b) 2 load levels, high u's	
(c) 2 load levels, low u's	
(d) 2 load levels, lower u's	
(e) 2 load levels, lowest u's	
5.12 Influence of applied loads on friction force in smooth disc tests	204
5.13 Influence of rolling speed on friction force in smooth disc tests	205
5.14 Effect of inlet lubricant temperature on friction force in smooth disc test	
(a) results for $F = 829.5 \text{ N}$	206
(b) results for $F = 244.5 \text{ N}$	207
5.15 Effects of surface roughness on friction force ($F_{f \max}$ versus u plot from rough	
top disc tests and matched smooth top disc tests at $T = 30^\circ\text{C}$)	210
(a) results for MCT 5	
(b) results for MCT 5 + FM	
(c) results for MCT 5 + EP	
5.16 Error caused by friction of top disc supporting bearings.....	213
(a) free body diagram of top disc and shaft assembly	
(b) true friction force	
5.17 Comparison of $F_{f \max}$ for smooth top disc tests before and after	
rough disc experiments	218
5.1 Comparison of multiple $F_{f \max}$ measurements	220
6.1 Plots of the maximum friction coefficient versus λ ratio at $T = 30^\circ\text{C}$	
(a) top discs S1 and R1, $F = 147.0 \text{ N}$	226
(b) top discs S2 and R2, $F = 244.5 \text{ N}$	227
6.2 Plots of the maximum friction coefficient versus λ ratio at $T = 40^\circ\text{C}$	
(a) top discs S1 and R1, $F = 147.0 \text{ N}$	228
(b) top discs S2 and R2, $F = 244.5 \text{ N}$	229

6.3 Polynomial curve fitting of BA versus z	236
6.4 Plot of BA on probability paper for determining d_{avg} and σ	238
6.5 Polynomial curve fitting of HSC versus z	239
6.6 Plot of HSC on probability paper for determining d^*_{avg} and σ^*	241
6.7 Comparison of predicted and measured $\tau_{L,avg}$ in ehl and micro-ehl	
(a) at T = 30°C.....	249
(b) at T = 40°C.....	250
6.8 Comparison of present $\tau_{L,avg}$ vs. p_{avg} with other researcher's values	252

Nomenclature

A_a	apparent contact area
A_r	real contact area
a	radius of Hertzian contact circle
BA	bearing area in unit length at measured surface height
C	average constant in empirical expression of τ_L vs. p
C_T	thermal effect correction factor
d	surface height
d^*	asperity height
d_{avg}	average surface height
d^*_{avg}	average asperity height
E_1, E_2	elastic modulus of contact body 1 or 2
E'	reduced elastic modulus
F	load
F_f	friction (or traction) force
$F_{f_{max}}$	maximum friction force
$F_j(\zeta)$	common form of probability density function ($j = 0,1,1.5$)
F_T	applied force in tangent direction
f_N	Nyquist frequency
f_s	sampling frequency (scan rate) of data acquisition system
G	elastic shear modulus of lubricant in rheological models
g_E	dimensionless elasticity parameter
g_V	dimensionless viscosity parameter
HSC	high spot count in unit length at measured surface height
HSC*	measured HSC over traverse length
\hat{H}_{min}	reduced dimensionless minimum film thickness parameter in Eq. 2.23
h	fluid film thickness

h_c	central film thickness
h_{min}	minimum film thickness
h_0	constant separation
L	apparent traverse length of surface profile
l_i	contact lined which passes through the material side of the profile
m	index number for limiting shear stress distribution
N	total sampling number (scan number) of data acquisition system
n	asperity density
n_{max}	maximum asperity density
p	lubricant film pressure
p_{avg}	average film pressure
p_{max}	maximum film pressure
q_x, q_y	mass flow rate per unit width in x or y direction
R	reduced radius
R_a	central line average of surface roughness profile
R_q	RMS of surface roughness profile
R_{max}	the maximum peak to valley height of surface roughness profile
R_x, R_y	reduced radius in x or y direction
R_{x1}, R_{x2}	radius of contact body 1 or 2 in x direction
R_{y1}, R_{y2}	radius of contact body 1 or 2 in y direction
S_0	dimensionless constant used in Eq. 2.7
s	number of discrete contact lines at measured surface height
T	temperature
T_P (%)	bearing area in percentage at measured surface height
T_r	reference temperature
t	time
Δt	sampling interval for data acquisition system
u	fluid velocity in the entrainment direction
u_1, u_2	surface velocity of contact body 1 or 2

V_i, V_o	input or output voltage of electrical resistance circuit
V_h, V_v	horizontal or vertical magnification of Talysurf profilometer
v	sliding velocity in the direction perpendicular to entrainment velocity
x, y, z	Cartesian coordinate system
Z	viscosity-pressure index, a dimensionless constant in Eq. 2.7
z	separation from mean line to contact line
z_m, z_m^*	dimensionless separation parameters
z_L	particular separation at which $n = n_{max}$
α	pressure-viscosity coefficient
α	dimensionless roughness parameter defined in Eq. 2.41
α^*	Roelands pressure-viscosity coefficient
β	asperity tip radius
$\dot{\gamma}$	shear strain rate
$\dot{\gamma}_e$	linear elastic shear strain rate
$\dot{\gamma}_v$	non-linear viscous flow shear strain rate
δ	elastic deformation of contact body
δ_c	elastic deformation at contact center
η	viscosity
η_0	viscosity at atmospheric pressure
λ	effective film thickness parameter (defined as h_c/σ_C in this thesis)
λ^*	effective film thickness parameter (defined as h_{min}/σ_C)
μ	coefficient of friction
μ_{max}	maximum coefficient of friction
ν	kinematic viscosity
ν_1, ν_2	Poisson's ratio of contact body 1 or 2
ρ	density
ρ_T	lubricant density at required temperature
σ	standard deviation of surface heights, i.e. RMS surface heights

σ^*	standard deviation of asperity heights
σ_C	composite RMS surface roughness of contact surfaces
σ_T, σ_B	RMS surface roughness of the top or bottom disc
σ_1, σ_2	RMS surface roughness of contact surface 1 or 2
τ	shear stress within fluid film
τ_L	limiting shear stress
$\tau_{L,avg}$	average limiting shear stress
$\tau_{L,max}$	maximum limiting shear stress
τ_0	Eyring shear stress
$\dot{\tau}$	shear stress rate
ϕ	skew angle
ψ	pulse rate for bottom disc rolling speed represented in holes/s
%err	percent error in Eq. 6.4
ϵ	sum of the squared residuals
ϵ_{min}	minimum sum of the squared residuals

Chapter 1 Introduction

1.1 Tribological Mechanisms and Lubricant Rheology

The investigation of the rheology in very thin lubricant films under high pressures is an important topic in tribology because many concentrated contacts in rolling and sliding motion are lubricated to some extent by these films. These contacts are found in machine elements such as gears, rolling element bearings and bearings in vehicle engines. The lubricant films are formed by a physical process known as elastohydrodynamic lubrication (ehl), in which average pressures typically exceed 1 GPa and film thicknesses are in the range of about 0.1 ~ 1.0 μm (Figure 1.1a). The high film pressure causes a significant increase in lubricant viscosity and a shift from Newtonian to non-linear viscoelastic rheological behaviour, as well as elastic deformations of the machine element surfaces. Shearing of an ehl film results in quite a high friction force because of the higher viscosity, however, as shear strain rates increase, temperature also increases which, in turn, decreases both the viscosity and the friction force. The understanding of the complex physics of ehl (Hamrock and Dowson, 1981) is a major tribological achievement of the twentieth century.

Under various combinations of contact conditions, ehl films are thin enough to allow individual asperities to play a role. In these cases, the film thickness is less than 0.1 μm , which is of the same order as root mean square (RMS) surface roughness of typical bearing surfaces in concentrated contacts. Conventional ehl theory, in which perfectly smooth surfaces are assumed, cannot work well for these films. There has been an increasing realization that the asperity contacts themselves behave as “micro” bearings and some form of fluid film lubrication may persist under quite extreme conditions. Consequently, micro-ehl theory was developed (Christensen, 1969; Fowles, 1971; Tallian, 1972; Cheng, 1978).

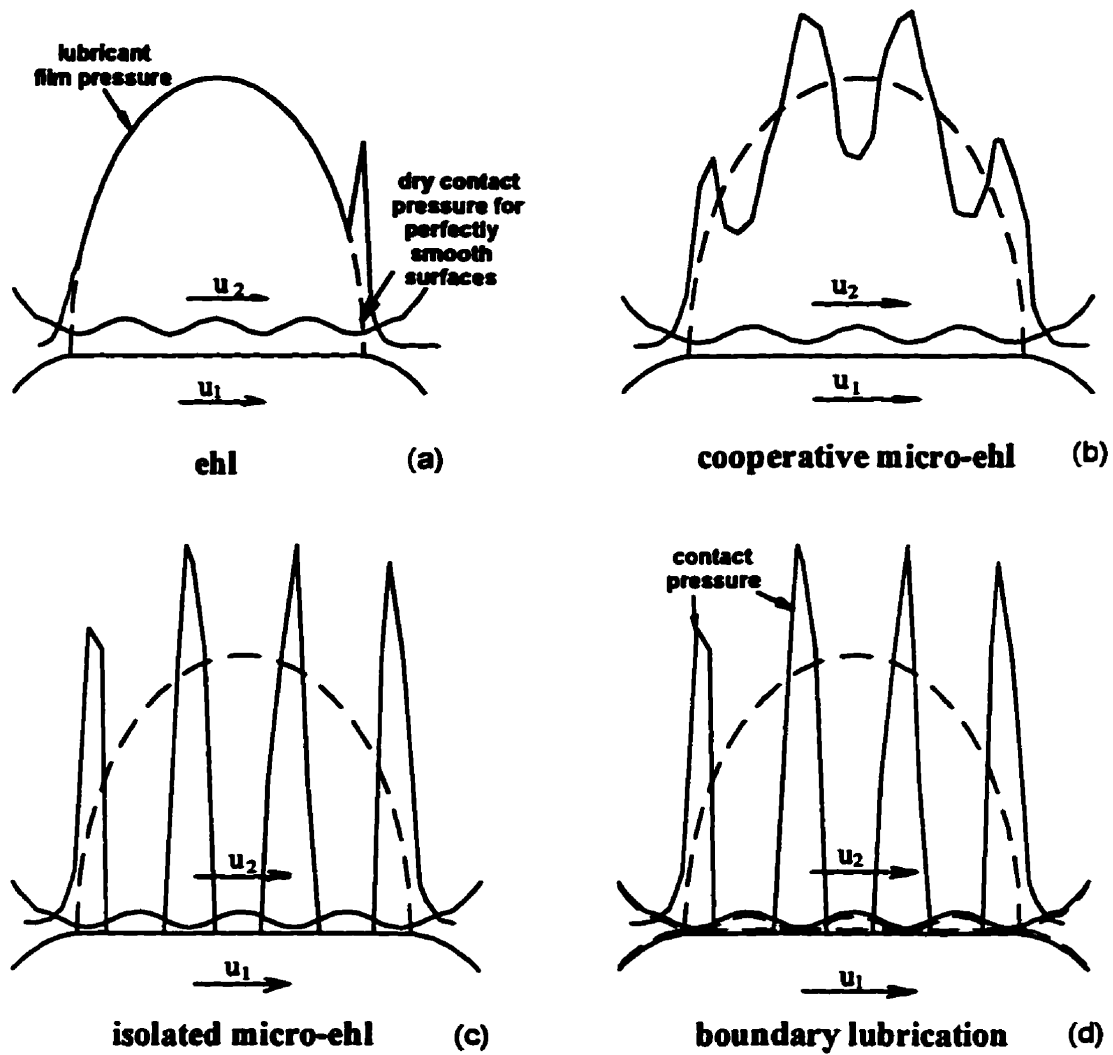


Figure 1.1 Tribological mechanisms of thin film lubrication in concentrated contacts
(u_1, u_2 - contact surface velocities)

When the asperities deform elastically, ripples are generated on the pressure distribution which occurs for perfectly smooth surfaces. The asperity interactions are “cooperative” if these ripples remain relatively small compared to the smooth surface pressure distribution (Figure 1.1b) and, thus, a relatively continuous lubricant film is maintained. However, as the surfaces approach more closely, there may be a transition to “isolated” micro-ehl, in which each asperity contact acts as an individual bearing (Figure 1.1c). As a result, the pressure may become insignificant between the asperity contacts and all the applied load is supported on the asperity contacts (Kingsbury, 1985; Shieh and Hamrock, 1991; Chang and Webster, 1991; Sutcliffe, 1991; Huang and Wen, 1993). Much of the recent understanding of micro-ehl comes from theoretical studies because suitable experiments are very difficult to perform.

In micro-ehl, the friction force depends on the rheology of the lubricant film which, as mentioned previously, tends to follow a non-linear viscoelastic behavior. The shearing may occur between molecules or between large groups of molecules but the slip planes are distributed to some extent through the lubricant film thickness. During relative sliding between the solid bearing surfaces, the micro-ehl shear action may be considered analogous to a continuous “ductile” fracture process.

Most lubricants contain additives that are designed to form very thin surface layers of molecular dimensions (about 5 - 10 nm) that adhere chemically to the machine element surface asperities. As tribological conditions become more extreme and lubricant film thickness decreases (Figure 1.1d), these surface layers begin to interact at the asperity tips. Their life in the contact during sliding action depends on the strength of the chemical attachment to the surface, and while they exist in the contact the friction force is influenced. The friction force may arise from shearing at a layer-surface interface or at some intermediate plane between contacting surface asperities. If shearing occurs at a layer-surface interface, friction force is influenced directly by the strength of the adherent chemical bonds. On the other hand, if the shearing occurs at an intermediate plane, the friction force may correlate with the strength of the adherent chemical bonds, but the relationship is not direct, because

the bonding across the intermediate plane must be considered. In any case, the shearing involves slip at a plane rather than a distributed deformation through the film thickness, and is perhaps analogous to a “brittle” rather than a “ductile” fracture process. When the friction is dominated by the lubricant surface chemistry, the phenomena is described as boundary lubrication.

The tribological mechanisms of thin film lubrications are summarized in Figure 1.1. Actual contacts may exhibit a blending of two or more of these mechanisms. The combination of ehl and boundary lubrication and the combination of isolated micro-ehl and boundary lubrication are of particular interest to the present research.

Mineral oils are extensively used as lubricants to reduce friction and wear. Although mineral oils are graded according to their viscosity variation with temperature, additive packages that make them formulated oils are also part of their overall classification. The additive packages are considered to be developed for boundary lubrication. However, they may be influential and perhaps beneficial in ehl or micro-ehl films and therefore the performance of additives under these conditions is an interesting and important topic.

New additives are proposed frequently by lubricant chemists who concentrate their efforts on characterizing the chemical properties. The rheological behaviour of lubricant additives received much less attention. It is not economically feasible to evaluate all additive formulations in the field or in test programs with comprehensive simulator devices. The low cost, standard lubricant screening tests, such as 4-ball (ASTM D 2266) and Timken (ASTM D 2509), may be helpful indicators of the chemical-rheological behaviour of the additives, but often are not related directly to the performance in situ. Therefore, it would be useful to develop a screening test which quantified the rheological influences of lubricant additives more precisely than the existing standard tests and related more directly to the lubricant performance in final applications or full simulation devices.

One approach to investigating the lubrication of very thin films is to measure the friction in contacts that simulate some of the key conditions found in machine elements, and then to determine the lubricant rheology based on these measurements. In particular, it would be useful to perform tests under controlled conditions of low slip-roll ratio which, for example, occurs in gears and rolling element bearings. Under these conditions thermal effects are much less dominant and lubricant behaviour is not well represented by standard lubricant tests that involve pure sliding. Friction (or traction) force measurement in a disc machine provides this control over the slip-roll ratio and has been used to study ehl and various combinations of the mechanisms shown in Figure 1.1 (Smith, 1959; Johnson and Jeffieris, 1968; Johnson and Roberts, 1974; Wu and Cheng, 1994). Various rheological models were developed to characterize this behavior (Johnson and Tevaarwerk, 1977; Bair and Winer, 1979). Quite recently, interest has been focused on the effects of surface roughness on ehl friction (Evans and Johnson, 1987; Johnson and Higginson, 1988; Sutcliffe, 1991). However, less experimental work was found for conditions involving asperity interactions with randomly rough surfaces and formulated oils, although such contacts are common in practice.

1.2 Objective and Chosen Approach

The objective of present research is to explore the influence of lubricant additives on the rheology of ehl and micro-ehl. A side-slip disc machine with a particular nominal point contact geometry was used to measure the friction forces with four formulated versions of MCT 5 lubricating oil (Imperial Oil Ltd, Sarnia, Ontario). The formulated oils are designated as MCT 5, MCT 5 + FM, MCT 5 + AW and MCT 5 + EP where the additives are indicated by FM for friction modifier, AW for anti-wear and EP for extreme pressure. In the contact between the top and bottom discs, the oil is subjected to a high pressure, while maintaining an almost constant elastohydrodynamic film thickness. When a side-slip velocity is introduced by skewing the top disc, a friction force perpendicular to the rolling direction occurs. The

friction force increases with increasing skew angle until it reaches a relatively constant value before thermal influences cause its decline. Therefore, the friction force measurement is linked directly to the lubricant rheology. The top disc has either a very smooth surface or a randomly rough surface, which produces ehl and micro-ehl conditions. In this manner, a particular set of formulated oils is studied and a procedure is developed for investigating additive influence on the rheology of ehl and micro-ehl.

1.3 Thesis Layout

The remainder of this thesis contains six chapters. Chapter 2 provides a brief literature review of lubricant properties, lubrication in concentrated contacts and experimental and analytical methods which related to the present study. First, low pressure properties of mineral oil and functions of additives are considered. Then, some basic concepts and research achievements of ehl are presented. Following that, the effects of surface roughness on ehl are considered. Finally, the development of rheological models from friction force measurements are introduced.

In Chapter 3 the experimental facility is described. Following a general description of the components and operating principles of the side-slip disc machine, three modifications of this test rig are discussed. These modifications are the installation of a temperature measurement instrumentation, a data acquisition system, and an electrical resistance circuit for detecting a lubricant film breakdown.

Chapter 4 describes the experimental materials and methods. The relevant properties of four formulations of a lubricating mineral oil, which are used in the present study, are discussed. For the experimental design, the tribological characteristics, including two types of disc surface roughness and various combinations of the conditions of load, lubricant temperature, ambient pressure viscosity and rolling speeds are presented. The experiments are arranged in

groups under various operating conditions for each lubricating oil. Finally, the central film thickness and the effective film thickness parameter is estimated for each of the test condition and given a consequent experiment number for all of them.

In Chapter 5, the results of friction force measurements are reported for the various lubricants and test conditions. The maximum friction forces are determined for traction curves, and the features from both smooth and rough disc experiments are discussed in a preliminary fashion.

In Chapter 6, a further discussion and analysis of the results is presented. From the friction force measurements with smooth disc, a limiting shear stress for each formulation is determined by using an empirical approach developed by Wu and Cheng (1994), and an expression of the relationship between the limiting shear stress and film pressure is found. Using this expression a limiting shear stress under any pressure can be predicted. For rough disc experiments, assuming that loads are carried only by the asperity contacts and using an estimate of the real area of contact which is obtained by a modified Greenwood and Williamson type model, the average pressure is calculated by dividing applied load by the real area of contact. Also, the average maximum shear stress for various lubricating oils are found from measured maximum friction forces. A comparison of these values to the predicted values, using the expression of limiting shear stress versus pressure, is made to show the influences of lubricant additives in ehl and micro-ehl.

Chapter 7 summarizes the present study and presents conclusions and recommendations for future work.

Chapter 2 Background

This chapter presents background related to the present research. Conventional “low pressure” rheological properties of mineral oils are discussed along with various functions of additive packages. Brief descriptions of lubrication regimes and ehl theory are presented, followed by discussions on the influence of contact surface roughness on ehl and the concepts of micro-ehl. Finally, friction force measurements on a disc machine are described along with the relationship between these measurements and “high pressure” lubricant rheology.

2.1 Mineral Oils and Additives

A lubricant is any substance that is used to reduce friction and wear between moving surfaces. However, only mineral oils, which are low cost liquid lubricants derived from petroleum fractions, are considered in the present research. Various additives are usually added in very small quantities to give the base stock mineral oils a wider range of applications. To a large extent, the rheological properties of mineral oils are determined by the base stock, while the chemical interactions of mineral oils with the contact surface are determined by the additives.

2.1.1 Low pressure rheological properties

The fundamental rheological behavior of mineral oils depends on the pressure and the shear strain rate. Under low pressures and shear strain rates, mineral oils have a classical Newtonian fluid rheology. Consequently, viscosity alone is sufficient to describe the rheology with further adjusting relationships to account for the influences of temperature and pressure. This rheological description is a conventional approach used to grade engine and gear oils.

- **Viscosity**

Viscosity is a measure of a resistance of a mineral oil to a shear strain rate. This resistance is caused by continually shifting weak bonds between adjacent layers of mineral oil as it is subjected to shear. In 1687, Newton suggested that shear stress within a fluid might be directly proportional to shear strain rate and this proportionality constant became known as viscosity. In a simple shear flow (Figure 2.1), the viscosity may be calculated as follows:

$$\eta = \frac{\tau_x}{\dot{\gamma}} = \frac{\frac{F_T}{A}}{\frac{u_2}{h}} = \frac{F_T h}{u_2 A} \quad (2.1)$$

where η - viscosity (Pa·s)

τ_x - shear stress within the fluid in the x-direction

$\dot{\gamma}$ - shear strain rate

F_T - force driving upper solid

A - contact surface area

u_2 - velocity of solid 2 in the x-direction

h - thickness of sheared lubricant film

Viscosity is an important property for most contacts in which fluid film lubrication occurs. Unfortunately, a lubricant may not have a uniform viscosity throughout the film because of variations in the pressure and/or temperature that cause subsequent changes in the value of viscosity.

- **Density**

Density is important to “low pressure” rheology because it is required in some standard measurement procedures to determine viscosity. Almost all the liquid mineral oils are incompressible unless under extremely high pressure (Dowson and Higginson, 1966), but

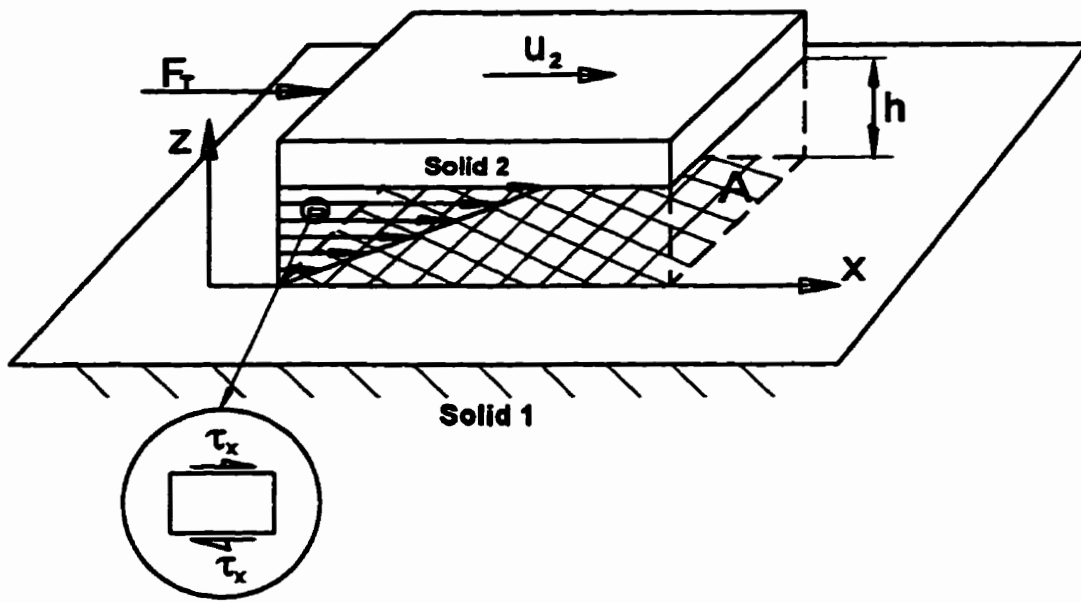


Figure 2.1 Physical illustration of Newtonian fluid

their densities change with temperature even at low pressure. In the present study, an expression from Cameron (1976) for a density at a specified temperature was adopted to give

$$\rho_T = \rho_{15} \cdot [1 - \gamma \cdot (T - 15)] \quad (2.2)$$

where ρ_T - density at temperature T

ρ_{15} - measured density at 15°C

γ - coefficient of thermal expansion (1/°C)

T - temperature in Celsius scale¹

The coefficients of thermal expansion (γ) for various ranges of ρ_{15} were provided by a commercial handbook² (Table 2.1) with some confirmation provided by Booser (1984).

Table 2.1 Coefficients of thermal expansion of mineral oils

ρ_{15} (kg/m ³)	γ (1/°C)
1075 - 965	0.00063
965 - 850	0.00072
850 - 775	0.00090
775 - 742	0.00108

Thus, given a measured value for ρ_{15} , the density can be calculated using Eq. 2.2 with support from Table 2.1.

• Viscosity-temperature relationship

Viscosity of a mineral oil decreases with increasing temperature (Figure 2.2). The Society of Automotive Engineers (SAE) has defined different viscosity grades for engine oils which depend on their viscosity-temperature behavior. An example of the viscosities of a typical

¹ All temperatures are in °C through this thesis.

² The relevant ranges of density were quoted from *Production Information Lubricants and Specialties*, 7th Edition (1990), Imperial Oil Ltd. Canada.

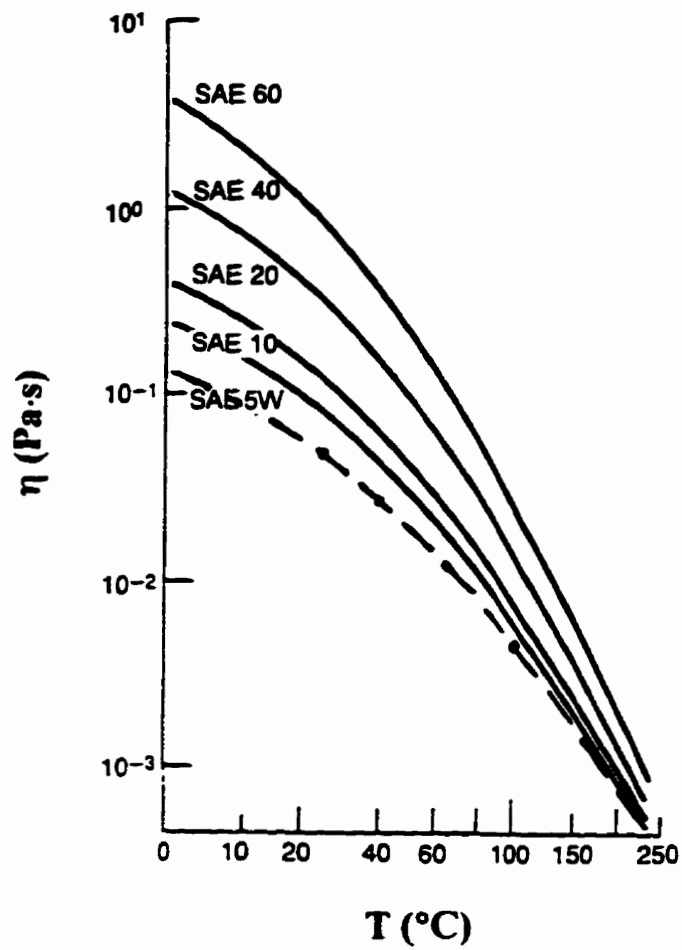


Figure 2.2 Viscosities of SAE lubricating oils at atmospheric pressure
(from Hamrock, 1994)

SAE 5W engine oil at various temperatures is given in Table 2.2. The viscosity (η) is the product of kinematic viscosity (ν) and density (ρ).

$$\eta = \nu \cdot \rho \quad (2.3)$$

where ν - kinematic viscosity

ρ - density

Table 2.2 Viscosity and Density of SAE 5W Engine Oil (from Cameron, 1981)

T (°C)	ν (m ² /s)	ρ (kg/m ³)	η (Pa·s)
25	4.82×10^{-5}	860	0.0415
40	2.545×10^{-5}	851	0.0217
100	4.994×10^{-6}	812	0.00406

The American Society of Testing and Materials (ASTM) advocates the use of a viscosity-temperature relationship, which was derived from a large number of mineral oil viscosities, called the Walther equation (Briant, et al. 1989)

$$\log(\log(\nu + 0.7)) = A - B \cdot \log(T + 273.15) \quad (2.4)$$

where ν - kinematic viscosity varied from 2.0 to 2.0×10^7 cSt

(1 cSt = 1×10^{-6} m²/s)

A, B - constants determined from ν measurements at two different temperatures for a specific oil

Using the above relationship with two values of ν measured in cSt at 40°C and 100°C, the constants A and B can be found. Then, the ν -T behaviour is represented quite accurately, providing ν is always within the range $2.0 \sim 20 \times 10^6$ cSt and T is within the range -70°C ~ 370°C. To determine viscosity (η) at a given temperature, the density must be calculated as described previously, and then both ν and ρ substituted into Eq. 2.3.

- **Viscosity-pressure relationship**

A simple relationship between pressure and viscosity is given by the Barus equation (Cameron, 1981).

$$\eta = \eta_0 \cdot e^{\alpha p} \quad (2.5)$$

where η_0 - viscosity at atmospheric pressure and a particular reference temperature

p - pressure

α - pressure-viscosity coefficient at the reference temperature

The Barus equation is used extensively, but it is valid as a reasonable approximation only at low to moderate pressures and becomes inaccurate (overestimating viscosity) as pressure increases beyond 0.5 GPa (Hamrock, 1991) or 0.85 GPa (Wu and Cheng, 1994). If the reference temperature is high, this inaccuracy occurs at even lower pressures.

- **Viscosity variation with both temperature and pressure**

Some more comprehensive expressions which include the simultaneous effects of both temperature and pressure on viscosity have been given by Crook (1961),

$$\eta = \eta_0 \cdot e^{\alpha p - \beta(T - T_r)} \quad (2.6)$$

where β - constant

T_r - reference temperature

η_0 - viscosity at atmosphere pressure and T_r

and by Roelands et. al. (1963)

$$\eta = \eta_0 \cdot e^{\alpha^* p} \quad (2.7)$$

$$\text{where } \alpha^* = \frac{1}{p} \cdot [\ln(\eta_0) + 9.67] \cdot \left\{ \left(\frac{T - 138}{T_r - 138} \right)^{-s_0} \cdot (1 + 1.5 \times 10^{-9} \cdot p)^z - 1 \right\}$$

- Roelands pressure-viscosity coefficient

$$Z = \frac{\alpha}{5.1 \times 10^{-9} \cdot [\ln(\eta_0) + 9.67]}$$

- viscosity-pressure index, which is usually constant

over a wide temperature range

$$S_0 = \frac{\beta \cdot (T_r - 138)}{\ln(\eta_0) + 9.67}$$

- dimensionless constant which establishes slope of

viscosity-temperature relationship

α, β - constants

The expression of Roelands et. al. is considered the most accurate but the required constants are not readily available.

2.1.2 Functions of additives

Hydrocarbons are the main chemical constituents of mineral oils. Hydrocarbon chains along with various incorporated compounds can interact with the contact surfaces to produce chemically attached layers which improve tribological performance. In general, the chemical layers are designed to protect the surfaces from wear and reduce friction. Most of the compounds required to form the attached layers are not found in refined petroleum fractions that form the "base stock" oil and must be added. The surface chemistry of mineral oil depends to a large extent on these "additives".

Additives may be classified according to their functions. There are many types of additives, some of them, such as antioxidants, anti-foaming agents, etc. are not involved directly in the friction and wear. In the present study, typical examples of a friction modifier, an antiwear additive and an extreme pressure additive are considered.

- **Friction modifier**

Friction modifier (FM) additives reduce the friction by forming layers of low shear strength on the contact surfaces. In current usage, the FM additives are mostly fatty acids and esters. The molecules generally contain unbranched long chains of carbon atoms, which are at least ten atoms in length and are classified as the oil-solubilizing portion, plus a polar group at one end, which reacts with the contact surfaces by a mechanism known as adsorption (Fein, 1983; Liston, 1992; Stachowiak and Batchelor, 1993). The molecular layers generated by this mechanism cover the contact surfaces as shown in Figure 2.3 and effectively prevent the high friction associated with direct surface contact.

O'Brien (1983) reported experiments which investigated the effect of a friction modifier in automatic transmission oil (Figure 2.4). According to O'Brien, FM additives reduced the friction coefficient in the transmission, especially at low sliding velocity where the oil film was relatively thin and surface asperities might have made contact with each other. This reduction decreased with increasing sliding speeds since the asperities were separated by a thicker oil film and the FM additives did not have as much opportunity to act as that at the lower sliding velocities.

- **Antiwear additive**

Antiwear (AW) additives reduce wear usually at low sliding velocities by helping to initiate chemical reactions at the surface which form layers of sulphide and phosphate compounds. These chemical reactions, which are classified as chemisorption (Stachowiak and Batchelor,

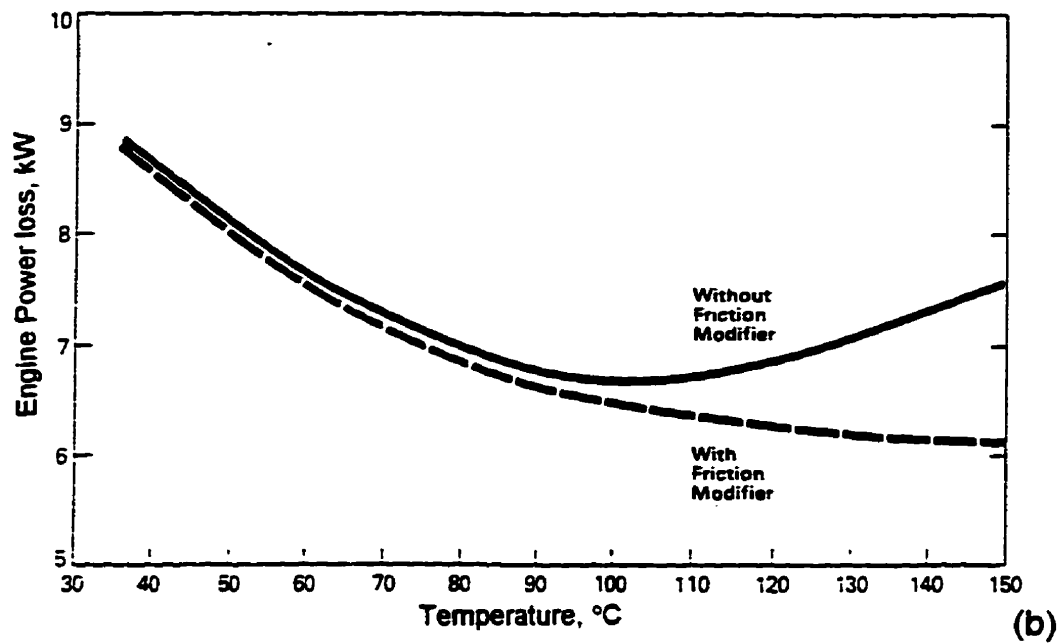
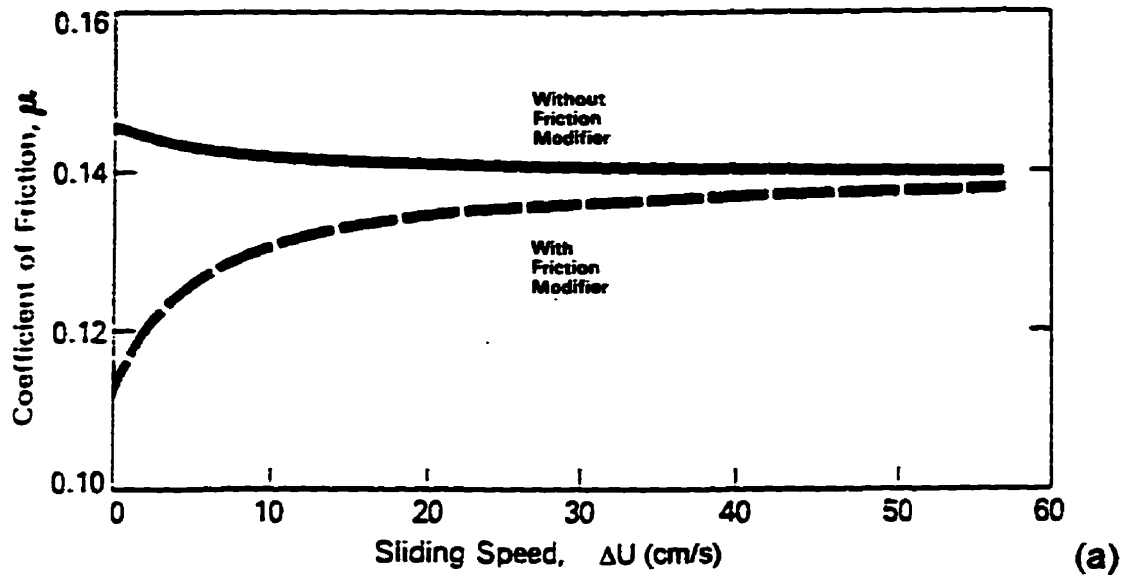


Figure 2.4 Effects of friction modifiers (from O'Brien, 1983)

(a) on friction coefficient

(b) on engine power loss

1993), require initial input energy which is provided by frictional heating during the sliding of one surface over the other. However, this chemisorption is only used at moderate loads and temperatures. If frictional heating continues to occur, it can damage the surface layers that have just been formed or impair their formation. When these surface layers do form, they wear out during sliding but at a lower rate than would occur with direct contact of the original surfaces. The surface layer produced by chemisorption of AW additive is much more durable than the layer produced by a FM additive through the mechanism of attachment called adsorption.

The most commonly used AW additive in engine oils is zinc dalkyldithiophosphate (ZDDP), in concentrations of 1% ~ 3% by weight. Its chemical structure is given in Figure 2.5. The layer formed from ZDDP additives effectively reduces wear rate. The presence of zinc in ZDDP plays an important role. Zinc gives the lowest wear rate compared with other metals, such as nickel, silver, lead and tin (Stachowiak and Batchelor, 1993). The lubrication mechanism of ZDDP is complex and the current understanding is that the surface layer is subject to a “sacrificial” wear, which is lower than the wear which would occur without it.

- **Extreme pressure additive**

Extreme pressure (EP) additives are essentially designed as AW additives but work under high contact pressures and sliding velocities in which lubricant and surface temperatures are high. EP additives usually contain phosphorus, sulphur or chlorine, plus water and oxygen (Fein, 1983; Liston, 1983; Stachowiak and Batchelor, 1993). When they are exposed to hot surfaces they are activated and react with the surfaces through a mild corrosion mechanism (Stachowiak and Batchelor, 1993). Figure 2.6 shows a typical EP additive protective film (Liston, 1983). They contain complex inorganic and organic reaction products, which are often phosphorus, sulphur and chlorine containing compounds, as mentioned previously, as well as almost all of the chemical elements which present in the lubricant and contact surfaces (Fein et al. 1986). Care should be taken while selecting types of EP additives and determining

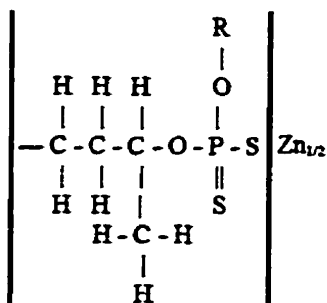


Figure 2.5 Chemical structure of zinc dialkyldithiophosphate
(from Stachowiak and Batchelor, 1993)

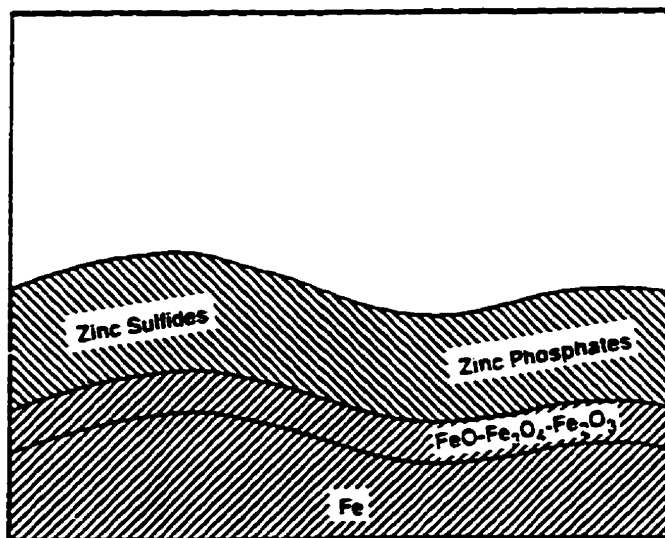


Figure 2.6 Lubrication mechanism by EP additives (from Liston, 1992)

their concentrations for individual applications, in order to minimize corrosion and control the formation of low shear strength surface layers. For example, if the concentration of EP additive is too high, then excessive corrosion may occur, while if it is too low, then the surfaces may not be fully protected.

Surface layers produced from EP additives remain stable at quite high temperatures and provide a “sacrificial” low wear rate in the same manner as AW additives. They extend the load-carrying capacity preventing any unacceptably high rate wear or surface damages, such as scuffing and seizing.

Sometimes the same additive can perform more than one functions. For example, zinc dithiophosphate has been used as both an AW and an EP additive. At low temperatures associated with low sliding velocity and contact pressure, surface layers form since the thermal activation energy is low. At higher temperatures, the surface layers form even more readily and remain stable. However, many additives do not work at both high and low temperatures.

2.2 Elastohydrodynamic Lubrication

In general, the purpose of lubrication is to protect two contact surfaces during relative motion and to reduce friction. Based on the physics of the surface interaction, lubrication can be classified into various regimes. Elastohydrodynamic lubrication (ehl) is one of them, which is found extensively in engineering practice. In order to understand the context in which ehl occurs, a brief description of lubrication regimes and their mechanisms is given and the fundamentals of ehl theory are discussed in detail.

2.2.1 Regimes of lubrication

Conventionally, there are four lubrication regimes: hydrodynamic lubrication, elasto-hydrodynamic lubrication, boundary lubrication, and mixed film lubrication. The characteristics of each regime are determined by the contact geometry, material of the contact surfaces, kinematic conditions, applied loads, and lubricant properties.

- **Hydrodynamic lubrication**

Hydrodynamic lubrication can give low friction and virtually zero wear. It usually occurs in conformal surface geometries. The applied load is carried by a pressure generated within the fluid film. This pressure develops during relative motion in the region where the surfaces converge. The motion of the surfaces pulls lubricant into the gap between them and the decreasing of available space causes the pressure generation. In hydrodynamic lubrication, the gap between the surfaces must diverge eventually to permit the lubricant to flow through the region of close proximity (known as the contact zone). Contact pressure in hydrodynamic lubrication is low enough that the effects of elastic deformations of contact surfaces and of pressure on viscosity do not influence film thickness significantly.

- **Elastohydrodynamic lubrication**

In ehl, however, both elastic deformation of the contact surfaces and the lubricant pressure-viscosity effect act to increase the lubricant film thickness. Usually, ehl occurs in non-conformal surface geometries. For materials of low elastic modulus, such as rubber, surface deformation is more important than the pressure-viscosity effect, while the converse is found for materials of high elastic modulus, such as metals or ceramics. According to Hamrock (1994), lubricant viscosity can vary up to 10 orders of magnitude under a pressure up to 3 GPa, which can occur with metallic surface materials. Thus, despite high film pressures, continuous lubricant films can be generated which prevent asperity contact and associated surface damage.

- **Boundary lubrication**

Eventually, a combination of factors such as high load, low surface velocity, very nonconformal surface geometry, and low lubricant viscosity with a weak pressure viscosity effect, prevents fluid film formation. However, boundary lubrication may exist to protect the contact surfaces. Boundary lubrication locates at the other end of the lubrication spectrum from hydrodynamic lubrication. The opposing contact surfaces are only separated by very thin surface layers of molecular proportions. As mentioned in Chapter 1, the chemical bonding of the lubricant layers to the surface determines the friction and wear of the contact, and the layers themselves usually involve additive compounds. In boundary lubrication, the friction force is usually higher than that in ehl, but still lower than in dry contact. Sometimes the layer forms by a chemical reaction between surface and lubricant. Therefore, the formation is often temperature, pressure and time dependent. The layer thickness depends on the size of the composing molecules, and is typically within 1 to 10 nm.

- **Mixed film lubrication**

The behaviour during the transition from ehl to boundary lubrication is known as mixed film lubrication. As the film thickness in ehl decreases, the asperities begin to interact and a phenomena known as micro-ehl may occur, in which the asperity geometry and deformation influence the lubricant film thickness. At first the asperities may interact in a cooperative fashion where lubricant flow at an individual asperity is influenced by nearby asperities. As the film thickness decreases, the asperities begin to act in isolated individual contacts. When the tribological conditions become more severe, the lubricant film becomes even thinner and a chemical attachment of additives to the surfaces leads to boundary lubrication. There is a progression from a lubricant film rheology to an interaction of solid surface layers, and the mode of deformation changes as discussed in Chapter 1.

Although the above behaviour is plausible, it is not accepted universally. A constitutive equation of similar form governs the deformation of both a micro-ehl film and a solid boundary lubrication layer (Dowson, 1995; Dowson, 1992). Therefore, experimental studies of typical contacts involving specific formulated lubricants have difficulty determining whether the transition from ehl to boundary lubrication occurs directly or with an intermediate micro-ehl behavior. If asperities begin to interact through boundary lubricant layers, then there can still be a transitional behaviour as pressure is shared between ehl film and asperity contacts, which would constitute a mixed film lubrication regime. In other words, the mixed film lubrication regime is composed of some combination of ehl, micro-ehl and boundary lubrication but the physics governing the proportions of each is not well established.

- **Some comments on lubrication failure**

From the above discussion of lubrication regimes, a conclusion can be drawn that lubricants protect the machine elements from dry contact in a number of different ways. In most cases, tribologists strive to avoid dry contact, which often causes a drastic increase in friction coefficient and wear rate, by introducing liquid lubricants. However, dry contact can occur when ehl films break down and the boundary lubricant layers are sheared from the surface. When the lubricants are effective, whether with fluid films or surface layers, the lives of machine elements are extended, but eventually long term damage caused by phenomena, such as surface fatigue, corrosion or solid particle abrasion (perhaps from lubricant contaminants), results in component failure.

2.2.2 Fundamentals of ehl theory

The theory of ehl explains the physical action in the lubrication of many non-conformal machine element contacts, such as rolling element bearings, gears, piston rings and cam-follower pairs. A considerable development has occurred since the pioneering work of Ertel and Grubin, (Grubin, 1949), on the solutions of ehl problems. A brief review of elastic

deformation in contact mechanics and viscous flow in fluid mechanics is provided in this section, and then the main features of ehl are discussed. In the last part of this section the dimensionless parameters and film thickness equations, as well as the ehl regime charts are discussed.

- **Hertzian theory in nominal point contact**

Hertzian theory gives formulae for contact stress and elastic deformation in dry static contact (there is no liquid lubricant or surface velocities). Smooth surfaces are assumed with no surface tractions. The surfaces are also elastic, isotropic and homogeneous half spaces. Finally, Hertzian theory assumes that the contact dimensions are small compared to the radii of curvature of the surfaces. A nominal point contact occurs when two smooth surface ellipsoids are loaded together and the very small contact area is elliptical in shape. Hamrock and Dowson (1981) provide formulae which allow load (F), the curvature sum (R*), along with the elastic modulus (E) and Poisson's ratio (ν) of each surface to give the dimensions of the contact ellipse, the contact stress distribution and the total deflection of the centers of the two ellipsoids.

The R* is calculated from the radii of curvature of the ellipsoidal contact surfaces (Figure 2.7a) as follows:

$$\frac{1}{R^*} = \frac{1}{R_x} + \frac{1}{R_y} = \left(\frac{1}{R_{x1}} + \frac{1}{R_{x2}} \right) + \left(\frac{1}{R_{y1}} + \frac{1}{R_{y2}} \right) \quad (2.8)$$

where R_x, R_y - effective radii in the x and y directions

The formulae can be simplified for the circular contact area of the experimental apparatus in the present study. In this case, $R_x = R_y$ and the circular contact area can be considered equivalent to that which occurs when a sphere of radius R makes contact with a flat plane (Figure 2.7b), where R is defined as the effective radius for contacting spherical surfaces.

$$R = R_x = R_y \quad (2.9)$$

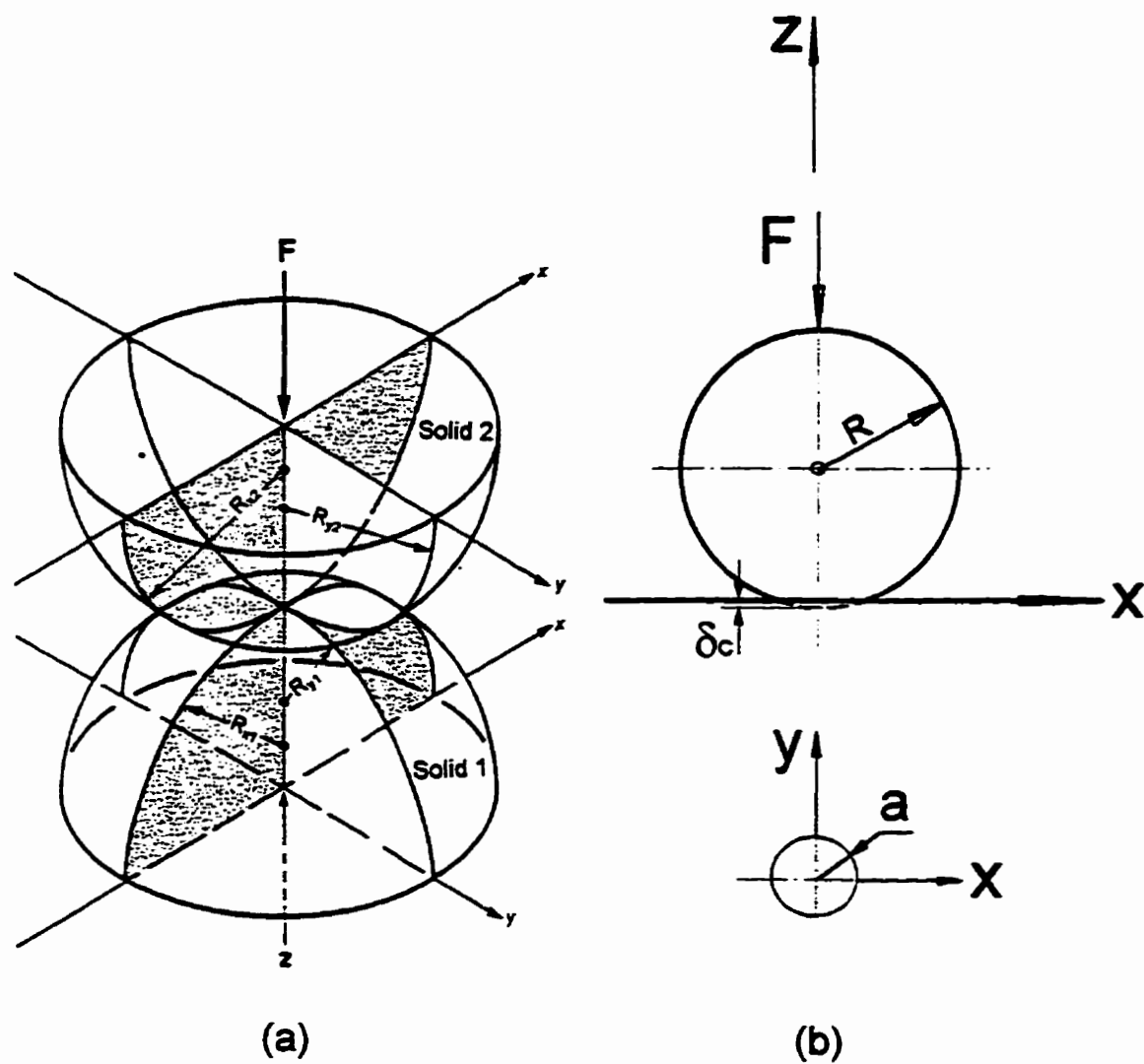


Figure 2.7 Nominal point contact

(a) geometry of contacting elastic solid (from Hamrock and Dowson, 1981)

(b) circular contact area from a contact of a sphere and a plane

The formulae of Hamrock and Dowson can be reduced to the following well established Hertzian equations for contacting spherical surfaces (Cameron, 1966; Halling, 1975).

$$a = \left(\frac{3FR}{2E'} \right)^{\frac{1}{3}} \quad (2.10)$$

$$A_a = \pi a^2 \quad (2.11)$$

$$p = \frac{3F}{2\pi a^2} \cdot \sqrt{1 - \frac{r^2}{a^2}} \quad (0 \leq r \leq a) \quad (2.12)$$

$$\delta_c = \frac{a^2}{R} \quad (2.13)$$

where a - radius of the apparent circular contact area

A_a - apparent contact area (real contact area is calculated by considering the additional effect of surface roughness)

E' - reduced elastic modulus

$$\frac{1}{E'} = \frac{1}{2} \cdot \left(\frac{1 - \nu_1^2}{E_1} + \frac{1 - \nu_2^2}{E_2} \right) \quad (2.14)$$

F - applied load

p - contact pressure (or normal stress) acting on the contact surfaces

δ_c - elastic deformation at contact center

- **Reynolds equation**

The Reynolds equation is a partial differential equation describing the pressure distribution in fluid film lubrication. It combines the physical principles of conservation of mass and conservation of momentum for thin film flow. Various versions of the Reynolds equation can be found in the literatures, depending on the assumptions made in the derivation. The following assumptions are made in the present research to obtain a version of the Reynolds equation.

- (1) The film thickness is small, compared to the radii of curvature of the surfaces and the contact dimensions.
- (2) Inertial and body forces are negligible compared to shear and pressure forces.
- (3) Load and surface velocity are constant so that flow is steady and film thickness is constant with respect to time.
- (4) The lubricant is a Newtonian liquid, flow is laminar and viscosity is constant through the thickness of the film.
- (5) There is no slip at the surface-fluid interface.
- (6) The lubricant is incompressible.

Considering a typical bearing with converging-diverging surfaces (Figure 2.8a), the first assumption allows the elimination of shear stresses acting on the side faces of control volume (Figure 2.8b). A conservation of momentum is applied, which is a static force balance because inertial forces are negligible. Take limits as the control volume and follow the Newtonian laminar flow assumption with constant viscosity through the film thickness, a reduced version of the Navier-Stokes equations is obtained as follows:

$$\begin{aligned}\frac{\partial p}{\partial x} &= \eta \cdot \frac{\partial^2 u}{\partial z^2} \\ \frac{\partial p}{\partial y} &= \eta \cdot \frac{\partial^2 v}{\partial z^2} \\ \frac{\partial p}{\partial z} &= 0\end{aligned}\tag{2.15}$$

where p - pressure of lubricant film

η - lubricant viscosity

u, v - lubricant velocities in the x and y directions

Since the third equation above indicates that the pressure in the z direction is a constant, it is possible to integrate the first two equations twice with respect to z , where the boundary conditions are described by the assumption of no slip at the interface as follows:

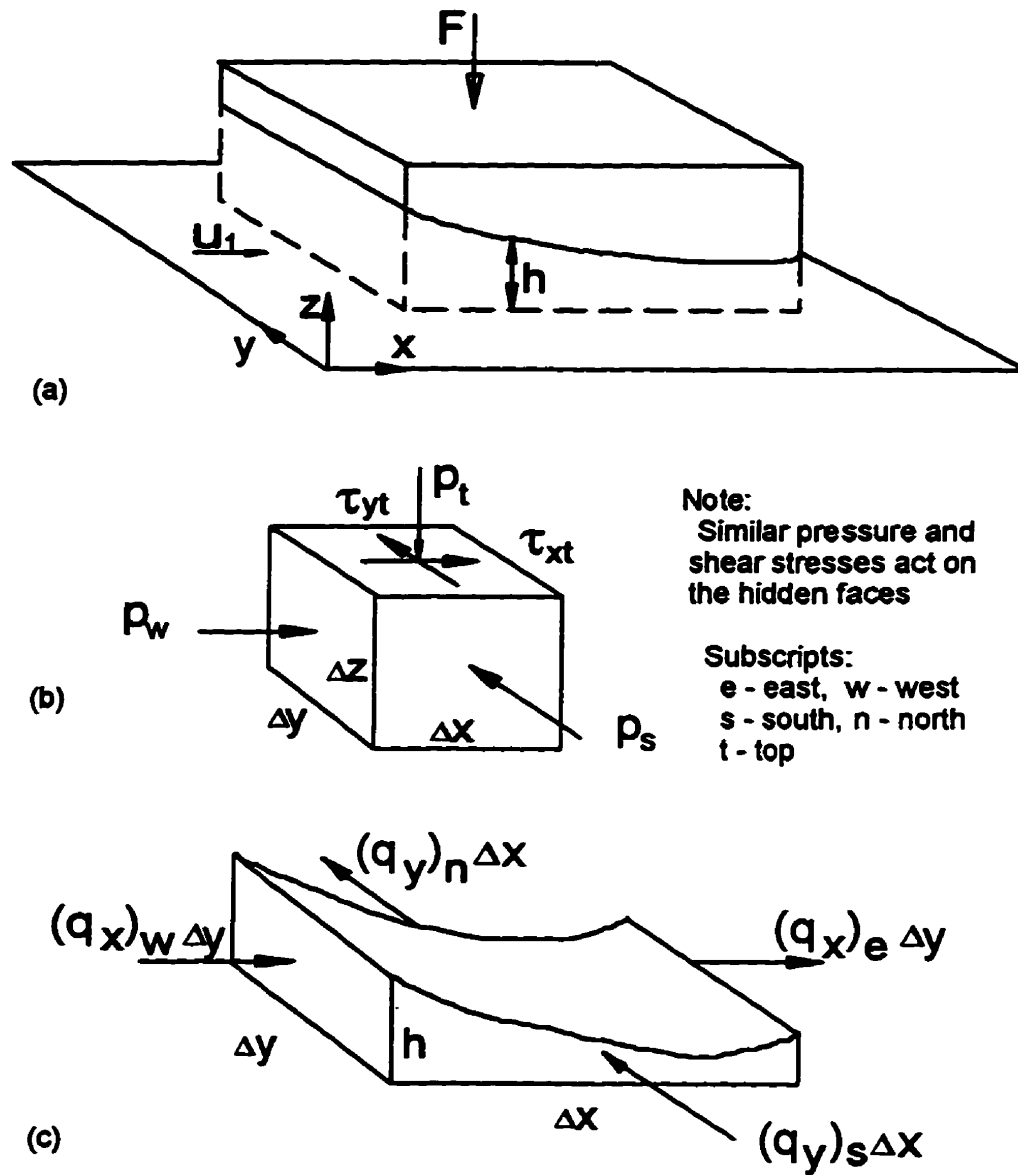


Figure 2.8 Typical bearing illustration for deriving Reynolds equation
 (a) a bearing with converging-diverging surfaces
 (b) control volume for conservation of momentum
 (c) control volume for conservation of mass

$$u = u_1, v = 0 \quad \text{at } z = 0$$

$$u = 0, v = 0 \quad \text{at } z = h$$

Then the lubricant velocities, u and v , are

$$\begin{aligned} u &= -z \cdot \left(\frac{h-z}{2\eta} \right) \cdot \frac{\partial p}{\partial x} + u_1 \cdot \left(\frac{h-z}{h} \right) \\ v &= -z \cdot \left(\frac{h-z}{2\eta} \right) \cdot \frac{\partial p}{\partial y} \end{aligned} \quad (2.16)$$

The lubricant velocities may be integrated across the film thickness to obtain the volume flow rates per unit width in the x and y directions as follows:

$$\begin{aligned} q_x &= \int_0^h u \cdot dz = -\frac{h^3}{12\eta} \cdot \frac{\partial p}{\partial x} + \frac{u_1 h}{2} \\ q_y &= \int_0^h v \cdot dz = -\frac{h^3}{12\eta} \cdot \frac{\partial p}{\partial y} \end{aligned} \quad (2.17)$$

Take a control volume that stretches across the film thickness (Figure 2.8c), the conservation of mass for the incompressible fluid in this control volume implies

$$(q_x \cdot \Delta y)_w + (q_y \cdot \Delta x)_s - (q_x \cdot \Delta y)_e - (q_y \cdot \Delta x)_n = 0 \quad (2.18)$$

Dividing both sides of Eq. 2.18 by $\Delta x \cdot \Delta y$, taking limits as Δx and Δy approach zero, and substituting in Eq. 2.17 yields the following version of the Reynolds equation.

$$\frac{\partial}{\partial x} \cdot \left(\frac{h^3}{12\eta} \cdot \frac{\partial p}{\partial x} \right) + \frac{\partial}{\partial y} \cdot \left(\frac{h^3}{12\eta} \cdot \frac{\partial p}{\partial y} \right) = u \cdot \frac{\partial h}{\partial x} \quad (2.19)$$

where $u = u_1 / 2$ - entrainment velocity, i.e. average lubricant velocity in the contact zone.

If both contacting elements are in a pure rotation with surface velocities u_1 and u_2 , then a similar derivation reveals that $u = \frac{u_1 + u_2}{2}$.

- **Pressure distribution and film shape**

Determining the pressure distribution in an isothermal ehl film is a complex problem. The pressure generated in the contact zone changes both viscosity and film thickness; thus, Eq. 2.19 is a highly non-linear partial differential equation when applied to ehl.

In typical ehl, the elastic flattening becomes large compared with the film thickness and the pressure distribution approaches the Hertzian contact pressure for most of the contact area. However, an inlet pressure “sweep” occurs, in which pressure gradually increases as the lubricant is drawn into the contact by the moving surfaces rather than the rapidly increasing Hertzian pressure in the same inlet zone (Figure 2.9). At the exit of the contact zone, the pressure drops rapidly to ambient pressure. The influence of this ambient pressure on the exit zone surface is to reduce deformation, thus producing a constriction down to the minimum film thickness. This constriction occurs because deformation is influenced by the total pressure field not just the local film value. Pressure rises rapidly when the lubricant flow is confronted with the constriction. This abrupt rise in pressure is defined as a pressure spike and is an important feature of ehl. The details of the pressure distribution and the film shape are shown simultaneously in Figure 2.9 for a simplified case, where only the top surface is elastic. Given the same reduced elastic modulus, the total surface deformation is identical in the contact zone for an elastic-rigid combination as for an elastic-elastic combination as suggested by Eqs. 2.8 to 2.14.

An essential feature for effective lubrication is to maintain an adequate lubricant film thickness. Therefore, it is a very important practical aspect of ehl theory to determine the film thickness within the contact. The fluid film profile through the center of the contact can be

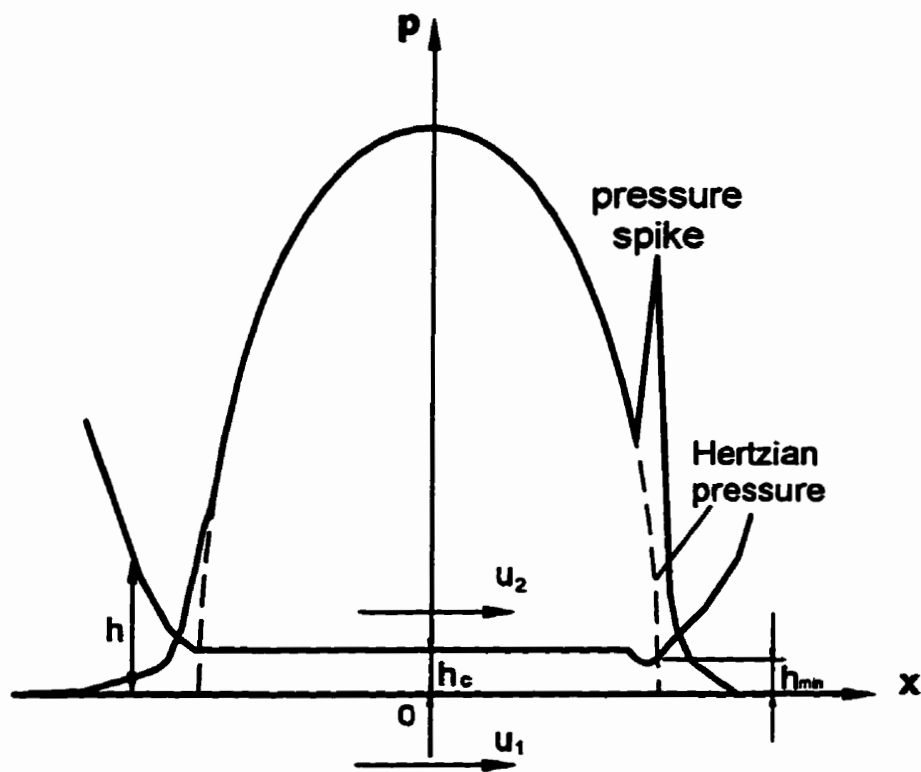


Figure 2.9 Typical pressure and film thickness profiles for ehl contact

represented by the following expression and shown in the simplified case where only the upper surface is elastic (Figure 2.10).

$$h = h_0 + \frac{x^2}{2R} + \delta \quad (2.20)$$

where h_0 - separation of the undeformed surface at the contact center

δ - elastic deformation

The elastic deformation can be calculated by a “surface element” procedure as described by Hamrock and Dowson (1981).

In ehl calculation procedures, the effect of pressure on viscosity can be estimated by the Barus equation (Eq. 2.5), even though it overestimates the viscosity at higher pressures. It is found that using the more realistic Roelands equation (Eq. 2.7) for pressure viscosity effects gives approximately the same film thickness (This result is discussed in a subsequent section). Therefore, computational procedures may use Roelands equation which gives a more precise result (and faster convergence), but the film thickness formulae, which are correlated from the numerical solutions, use the pressure-viscosity coefficient (α) from the Barus equation for the lubricant. The α value may be measured for a given lubricant at relatively low pressures, and thus, it is fairly easy to obtain.

Furthermore, in ehl, the pressures are high enough to change density, and thus, the lubricant is not incompressible. Inclusion of this effect in ehl calculation procedures is not difficult and often makes convergence easier, but it does not change film thickness significantly compared to calculations considering the lubricant as incompressible (Cameron, 1976). Thus, ehl formulae do not need to include a pressure-density term.

The Reynolds equation, as derived in the previous section, can be used to investigate the ehl film thickness with the provision that the pressure generated in the contact zone increases the

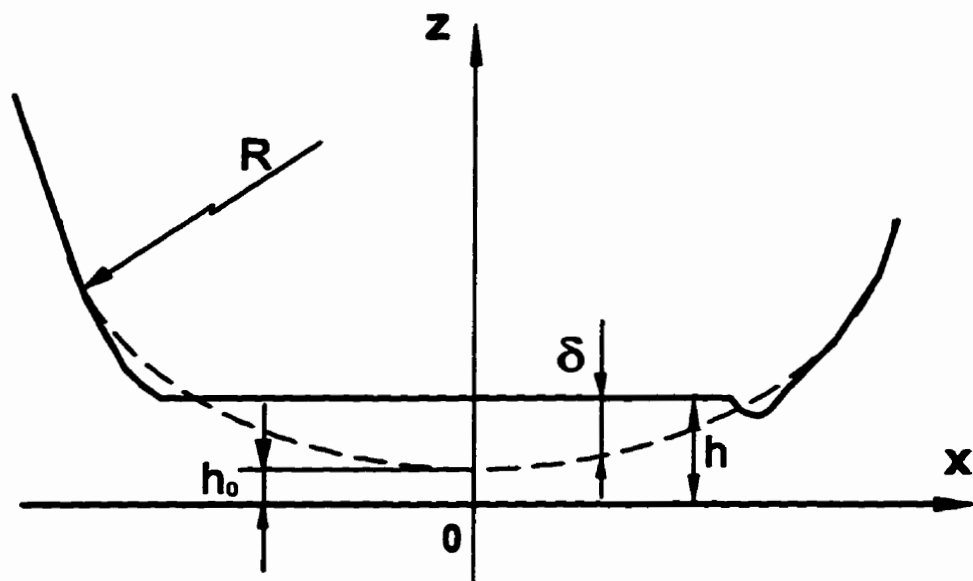


Figure 2.10 Typical ehl film between an elastic sphere and a rigid plane

lubricant viscosity and causes the elastic deformation. As mentioned previously, both the variations in viscosity and elastic deformation make the Reynolds equation highly non-linear. The most common inlet pressure boundary condition is $p = 0$ at a large enough negative x -value, so that moving this inlet boundary further from the contact has a negligible effect on the converged pressure distribution. The most common outlet pressure boundary condition is $p = dp/dx = 0$ at some positive x -value close to the outermost edge of the Hertzian dry contact area. The location of this outlet “cavitation” boundary is determined within the numerical solution procedure. A numerical analysis and computation technique was developed by Hamrock and Dowson (1981) for solving an isothermal ehl in an elliptical contact. An equivalent, but somewhat simpler, computation scheme to solve the Reynolds equation in isothermal ehl is presented in Figure 2.11 to provide the basic approach.

The typical ehl film thickness profile presented in Figure 2.10 shows that, over most of the contact zone, the film thickness is almost constant, and thus, the central film thickness (h_c) provides a good estimate of the average value. Under the pressure spike at the exit of the ehl contact, there is a film constriction as mentioned previously. The minimum film thickness (h_{min}) occurs at the constriction and is approximate 75 ~ 80 % of the h_c .

2.2.3 Film thickness equation

Elastohydrodynamic lubrication involves the effect of pressure on lubricant viscosity and on surface elastic deformation. Thus, the film thickness in ehl depends on the relative influences of film pressure on the increase in viscosity and the elastic deformation. To quantify these influences, Johnson (1970) developed a “regime” chart. These regimes of ehl are specified by calculating the magnitude of a dimensionless elasticity parameter (g_E), which is proportional to the maximum rigid isoviscous film pressure divided by the maximum Hertzian pressure as shown below and quantifies the effect of pressure on surface deformation.

lubricant viscosity and causes the elastic deformation. As mentioned previously, both the variations in viscosity and elastic deformation make the Reynolds equation highly non-linear. The most common inlet pressure boundary condition is $p = 0$ at a large enough negative x -value, so that moving this inlet boundary further from the contact has a negligible effect on the converged pressure distribution. The most common outlet pressure boundary condition is $p = dp/dx = 0$ at some positive x -value close to the outermost edge of the Hertzian dry contact area. The location of this outlet “cavitation” boundary is determined within the numerical solution procedure. A numerical analysis and computation technique was developed by Hamrock and Dowson (1981) for solving an isothermal ehl in an elliptical contact. An equivalent, but somewhat simpler, computation scheme to solve the Reynolds equation in isothermal ehl is presented in Figure 2.11 to provide the basic approach.

The typical ehl film thickness profile presented in Figure 2.10 shows that, over most of the contact zone, the film thickness is almost constant, and thus, the central film thickness (h_c) provides a good estimate of the average value. Under the pressure spike at the exit of the ehl contact, there is a film constriction as mentioned previously. The minimum film thickness (h_{min}) occurs at the constriction and is approximate 75 ~ 80 % of the h_c .

2.2.3 Film thickness equation

Elastohydrodynamic lubrication involves the effect of pressure on lubricant viscosity and on surface elastic deformation. Thus, the film thickness in ehl depends on the relative influences of film pressure on the increase in viscosity and the elastic deformation. To quantify these influences, Johnson (1970) developed a “regime” chart. These regimes of ehl are specified by calculating the magnitude of a dimensionless elasticity parameter (g_E), which is proportional to the maximum rigid isoviscous film pressure divided by the maximum Hertzian pressure as shown below and quantifies the effect of pressure on surface deformation.

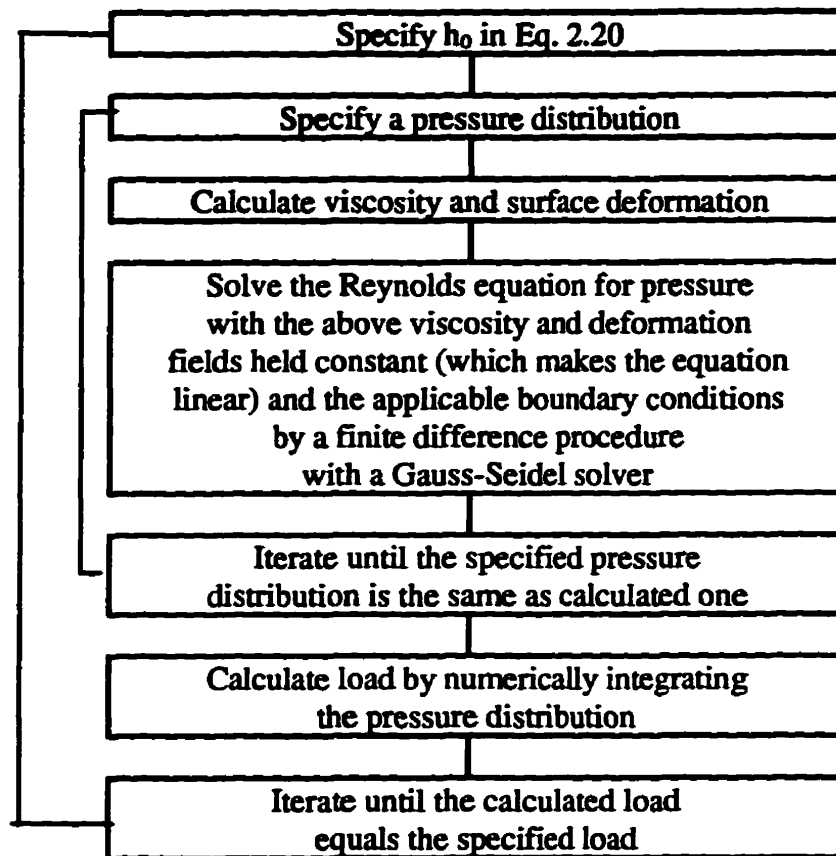


Figure 2.11 A simple computational scheme for isothermal ehl

$$g_E = \frac{F^{\frac{2}{3}}}{(\eta_0 \mu)^2 (E' R^5)^{\frac{2}{3}}} \quad (2.21)$$

Then, a dimensionless viscosity parameter (g_v) is calculated, which is proportional to the maximum rigid isoviscous film pressure divided by the pressure at which viscosity equals $2.72 \times \eta_0$ as shown below and quantifies the effect of pressure on lubricant viscosity.

$$g_v = \frac{\alpha \cdot F^3}{(\eta_0 \mu)^2 R^2} \quad (2.22)$$

After g_E and g_v are calculated, a dimensionless minimum film thickness parameter (\hat{H}_{\min}) can be considered, which is proportional to the minimum ehl film thickness divided by rigid isoviscous film thickness as shown below.

$$\hat{H}_{\min} = \frac{h_{\min} \cdot F^2}{(\eta_0 \mu)^2 \cdot R^3} \quad (2.23a)$$

Following Johnson (1970), numerical solutions were used to generate unique \hat{H}_{\min} contour lines on a g_v versus g_E plot. The orientation of these contour lines showed a physical interpretation of contact mechanics in four distinct regions. Johnson identified the behaviour in each of these regions as a “regime of ehl” and noted that least squares curve fitting gave unique formulae in each regime of the following general form

$$\hat{H}_{\min} = c \cdot (g_v)^a (g_E)^b \quad (2.23b)$$

where a, b, c — constants for a particular regime

The four regimes of ehl are isoviscous rigid, viscous rigid, isoviscous elastic and viscous elastic. Esfahanian and Hamrock (1991) generated a regime chart (Figure 2.12) for minimum

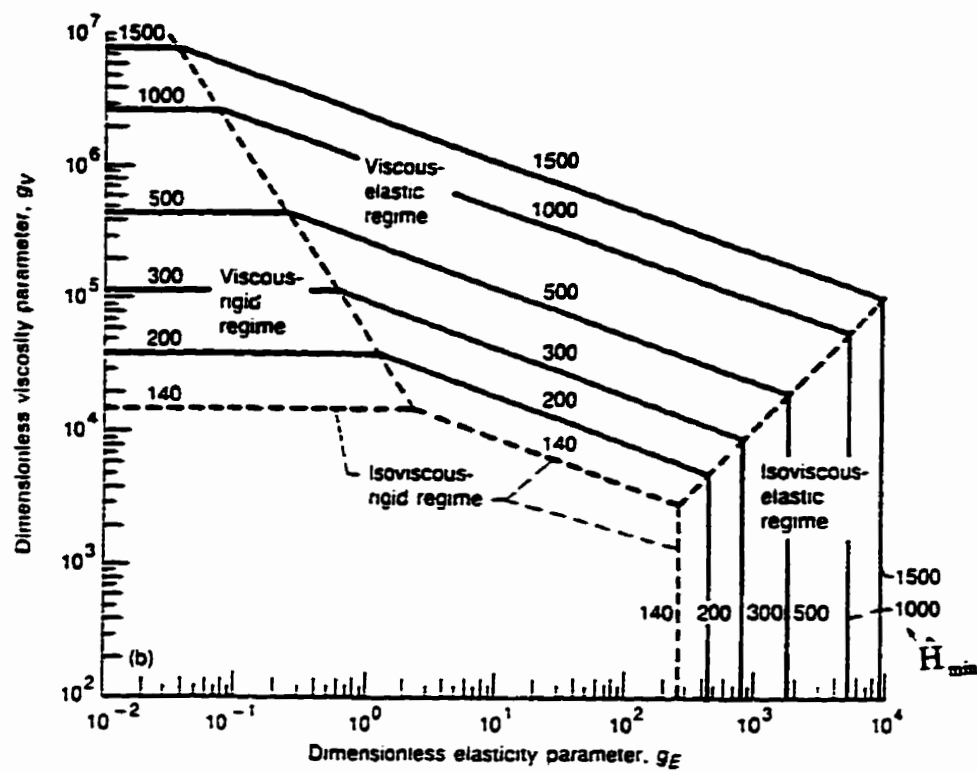


Figure 2.12 Lubrication regime chart for nominal point contact
(from Hamrock, 1994, based on the results of
Esfahanian and Hamrock, 1991)

film thickness in nominal point contacts with circular contact areas which defined the regime boundaries accurately. If the calculated values of g_E and g_V indicated that a given contact was in the viscous elastic regime, then using the constants $a = 0.49$, $b = 0.17$ and $c = 1.687$ in Eq. 2.23 allowed an estimate of minimum film thickness (h_{min}).

Hamrock and Dowson (1977) generated the above formula for h_{min} and a formula for central film thickness (h_c) through their numerical solutions in the viscous elastic regime. In the present study, g_E and g_V were calculated and Figure 2.12 was used to confirm that the contact was in the viscous elastic regime. Then, the following formula, which was developed by Hamrock and Dowson with its somewhat simpler dimensionless groupings, was used to calculate h_c .

$$\frac{h_c}{R} = 1.90 \left(\frac{\eta_0 u}{E'R} \right)^{0.67} (\alpha E')^{0.53} \left(\frac{F}{E'R^2} \right)^{-0.067} \quad (2.24)$$

All of the procedures and formulae discussed so far considered a Newtonian lubricant. However, friction measurements indicate that the lubricant behaves in a non-Newtonian manner in many ehl contacts. In spite of this, the film thickness formulae have strong support from actual film thickness measurements. For example, optical interferometry was used by Kunz and Winer (1977) to measure film thickness, as described by Hamrock and Dowson (1981), and the results agreed well with predicted values. Recently, Hamrock and his coworkers (Lee and Hamrock, 1991a, 1991b; Hsiao and Hamrock, 1994) performed numerical analyses of nominal line contact with non-Newtonian fluid models and pointed out that a formula equivalent to Eq. 2.24 based on a Newtonian model gave quite an accurate prediction of film thickness at low entraining velocities and pure rolling conditions. They attributed this convenient result to the Newtonian behavior of the lubricant during the inlet pressure sweep, which apparently set the film thickness throughout the contact.

2.3 Mixed Film Lubrication

When the ehl films are thin enough to allow individual asperities to interact with the opposing surface, the surface roughness is another important factor which affects lubrication. Conventional ehl theory has been remarkably successful in analyzing lubrication when the surfaces are well separated but a comprehensive understanding of asperity interactions and lubricant films under asperity tips has not yet been achieved. The study of thin film lubrication between rough surfaces is called mixed film lubrication (Hamrock and Dowson, 1981) and requires knowledge of surface roughness, effective film thickness, and area of asperity contact.

2.3.1 Surface roughness

The surface roughness causes local changes in the lubricant film thickness and the pressure distribution. Thus, an analysis of a mixed film lubrication in a particular contact begins with the measurement of the roughness of the contact surfaces. All manufactured surfaces are rough to some extent. The actual surface profile is the combination of three types of deviations: form error, waviness and micro-roughness (Figure 2.13). Even after removing all the form error and waviness by careful machining, there is still micro-roughness which cannot be eliminated from metal surfaces by any known polishing techniques.

To determine the surface roughness, many measurement devices have been developed. Among them, devices that use a contacting stylus needle are common. They transform the vertical motion of a stylus tip into an electrical analog signal (voltage) when the stylus traverses on a surface. This voltage is converted to digital information to represent the surface profile. There are several important parameters that can be used to characterize a rough surface.

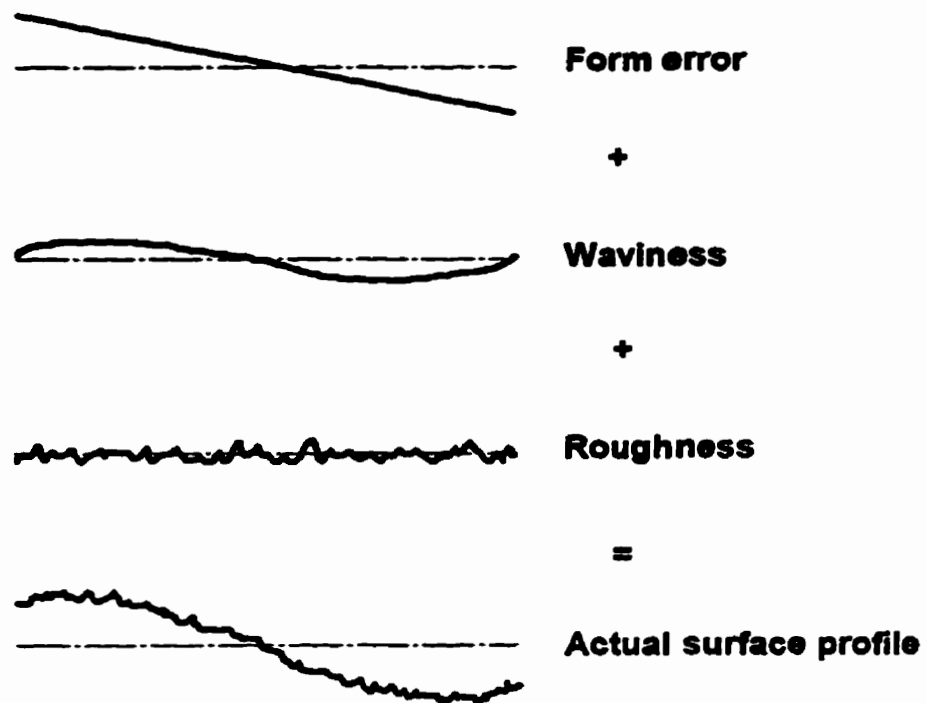


Figure 2.13 Geometric characteristic of solid surface
(from Halling, 1976)

(1) Root mean square of surface height (RMS)

The RMS is the effective vertical deviation of a surface roughness profile and is given by the geometric average value of the differences of the profile from its mean line. Many manufacturing surfaces have a random or Gaussian distribution of surface heights, where the RMS corresponds to the standard deviation of the distribution (Figure 2.14a). The RMS formula from discretized measurement data is

$$RMS = \sqrt{\frac{1}{m} \sum_{i=1}^m (d_i - d_{avg})^2} \quad (2.25)$$

where d_i - surface height from a reference plane

$$d_{avg} = \frac{1}{m} \sum_{i=1}^m d_i - \text{average surface height}$$

m - number of discretized surface heights

(2) Bearing area curve (BA) and high spot count (HSC)

BA and HSC are not constants for a given profile (like the RMS) but vary with the surface height coordinate (z). They are usually measured at the same time. In a measurement of BA and HSC, a hypothetical smooth flat surface is considered, which is parallel to the mean plane of the flat rough surface. When the smooth surface moves towards to the rough surface and intersects the rough surface profile at a number of levels as a line in the profile view (Figure 2.14b), the BA and HSC are defined by the following expressions.

$$BA = \frac{1}{L} \cdot \sum_{i=1}^s l_i \quad (2.26)$$

$$HSC = \frac{s}{L} \quad (2.27)$$

where L - traverse length

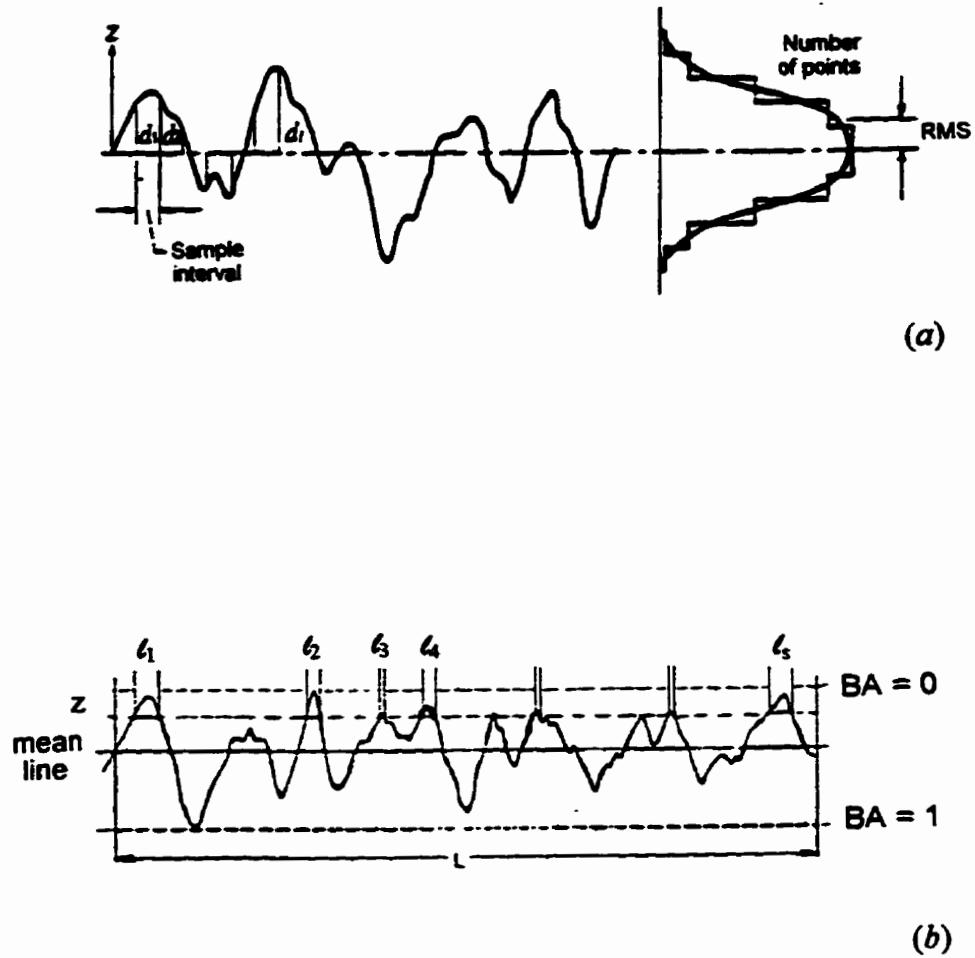


Figure 2.14 Surface roughness measurement
 (from Talysurf 5 Operator's Handbook)
 (a) RMS of a Gaussian surface
 (b) BA and HSC at a separation z

l_i - contact line which pass through the material side of the profile at height z

s - number of l_i 's at height z

2.3.2 Effective film thickness parameter (λ)

In order to evaluate the extent of asperity interaction in ehl, a dimensionless film parameter, known as the λ ratio, is defined as:

$$\lambda = \frac{h_c}{(\sigma_1^2 + \sigma_2^2)^{1/2}} \quad (2.28)$$

where h_c - central film thickness (close to the average film thickness of the contact),

calculated for perfectly smooth surfaces using a formula such as Eq. 2.24

σ_1, σ_2 - RMS surface roughness of contact surfaces 1 and 2

This λ ratio is the same as that used by Johnson et al. (1972). Hamrock and Dowson (1981) and Hamrock (1994) defined a very similar λ^* ratio, in which h_{\min} rather than h_c was used in Eq. 2.28 ($\lambda^* \approx 0.67 \lambda$) and gave the possible values of λ^* in the four lubrication regimes described in Section 2.2.1 as follows:

- (1) hydrodynamic lubrication, $5 \leq \lambda^* \leq 100$
- (2) elastohydrodynamic lubrication, $3 \leq \lambda^* \leq 10$
- (3) mixed (partial) lubrication, $1 \leq \lambda^* \leq 5$
- (4) boundary lubrication, $\lambda^* < 1$

It must be mentioned that the above ranges of the λ^* ratio lack precision because they do not describe the lubrication mechanics uniquely. Rather than modeling the actual surface micro-geometry in a full numerical solution of ehl, a formula for an “average” film thickness of a smooth surface is used with a single “average” roughness parameter.

The variation of the friction coefficient (μ) with the λ^* ratio is shown in Figure 2.15. Many experimental results suggested that the mixed lubrication regime (which is labeled as partial lubrication regime in the figure) has no sharp transitions from the fluid film lubrication or to the boundary lubrication. Therefore, the approximate locations of the various lubrication regimes are drawn as some moveable lines in this figure.

2.3.3 Area of asperity contact

Once roughness has been measured and the calculation of the effective film thickness parameter indicates that asperities affect the lubrication, a detailed examination of the asperity interaction is required. From the surface roughness measurements, the area of asperity contact can be estimated for an unlubricated and static contact. This distributed area of asperity contact indicates the regions in which micro-ehl is possible.

Many efforts have been made to determine the area of asperity contact between rough surfaces. From the microscopic point of view, when two surfaces are pushed into contact, they will touch at a number of discrete asperities which deform either elastically or plastically. The sum of the small areas of all the contact spots will be the real area of contact (A_r) within a specified apparent area of contact (A_a). Some existing models start from the surface roughness measurement, represent the contact through a stochastic process, and determine the real area of contact for a specified load.

Greenwood and Williamson (1966) developed such a model for an elastic contact between a flat rough surface and a flat smooth surface. This model assumed that asperities had spherical tips, deformed independently and the Gaussian distribution could be applied to their height distribution. When the smooth surface was pushed into contact and located at some separation (z), a number of asperities whose height over z would be in contact. To determine A_r within a specified apparent area of contact (A_a), a contact spot density (n) was required, which gave the number of contacted asperities in a unit of A_a . However, n was not measured

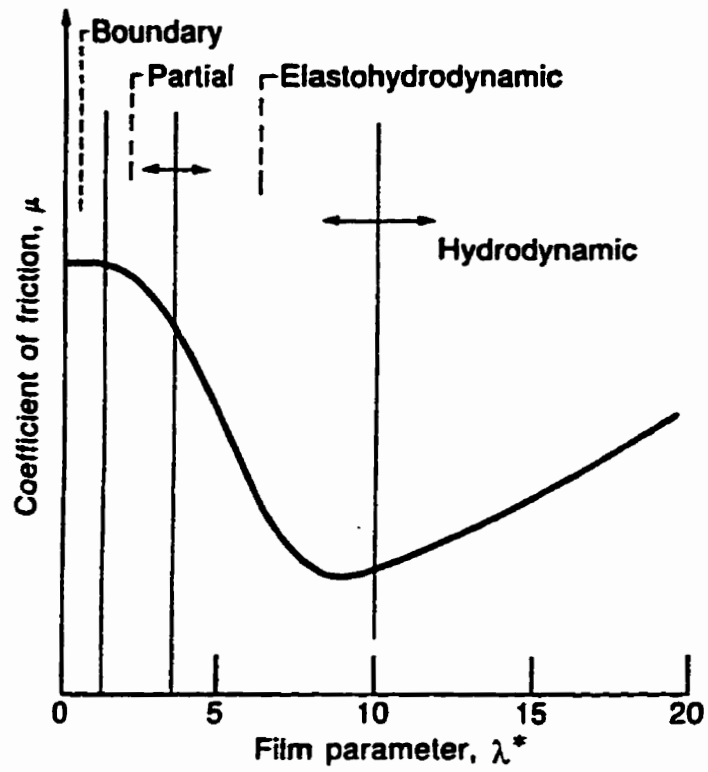


Figure 2.15 Variation of friction coefficient with film parameter
(from Hamrock and Dowson, 1981)

directly when the surface roughness was given as a two dimensional profilometer trace. An expression, which was given originally by Cooper et. al. (1969) in their study of thermal contact conductance, gave the relationship between the n and measured values of HSC and BA. A method of determining an average value of the radius of curvature (β) of the contacting spherical asperity tips at a specified load was given by De Vaal (1983). The work of both Cooper, et al. and De Vaal was adopted to find parameters for a Greenwood and Williamson type model in the present study. Although this model could be extended to the contact of two rough surfaces, such an extension was not required in the subsequent analysis of the present study and thus it is not described here.

- **Contact spot density between flat rough and smooth surfaces**

A derivation of the expression relating n to HSC and BA was given by Cooper et al. (1969) but it was difficult to follow. A somewhat simpler derivation¹ was possible which yielded the same expression.

Following Greenwood and Tripp (1967), asperities were assumed to have spherical tips of about the same radius of curvature but various heights. Here, the n is the same whether both surfaces are elastic or plastic because only size not number or location of contact spots changes. It is convenient for the present derivation, however, to assume a smooth rigid plane in contact with a rough plastic plane. When the rigid smooth plane is pressed into an individual asperity tip, the contact circle increases rapidly after initial contact, then more slowly as the separation z decreases. As a result, all the contact spots have about the same radius (\bar{a}) despite the variation in asperity heights when the smooth plane is at some height z (Figure 2.16).

¹ This derivation was presented first in lecture notes by Dr. J. B. Medley.

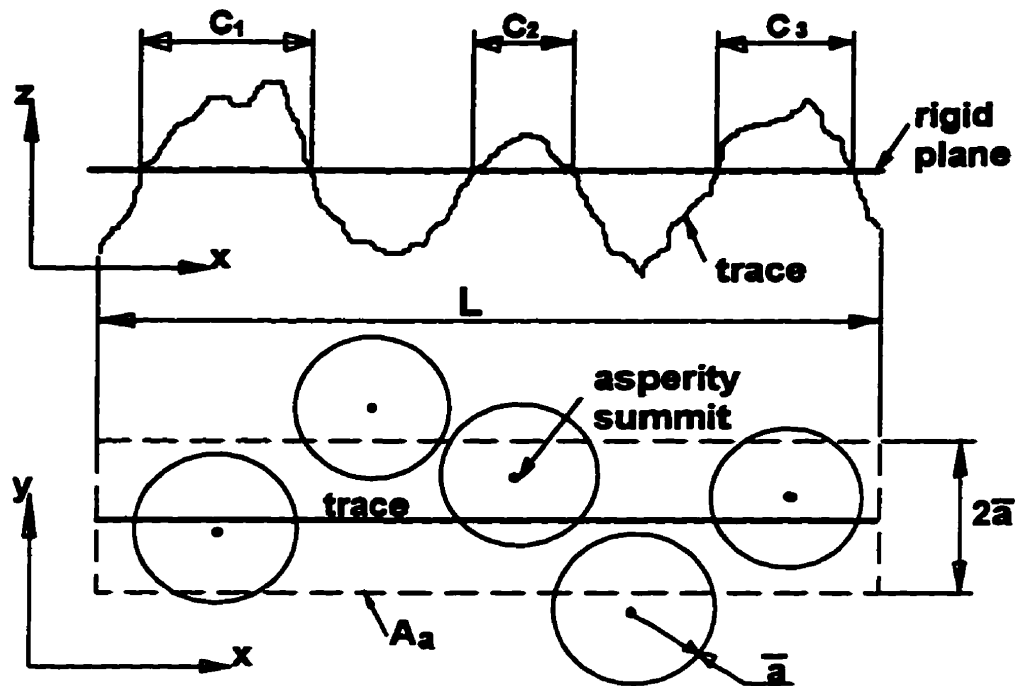


Figure 2.16 Representation of contact between a rigid plane and a rough surface

The A_n shown in Figure 2.16 is chosen to equal $2\bar{a}L$, and it is noted that if asperity contact areas are larger and smaller than those shown, some extra contact spots would be included and some would be missed, but on a long trace n should stay about the same. It follows that

$$n = \frac{HSC}{2\bar{a}} \quad (2.29a)$$

To determine an expression for \bar{a} , consider a long trace that intersects many contact spots. The average length of trace within the contact spots (Figure 2.17) is

$$\frac{BA}{HSC} = 2\bar{x} \quad (2.29b)$$

$$\text{where } \bar{x} = \frac{(1/2)\pi\bar{a}^2}{2\bar{a}} = \frac{\pi\bar{a}}{4}$$

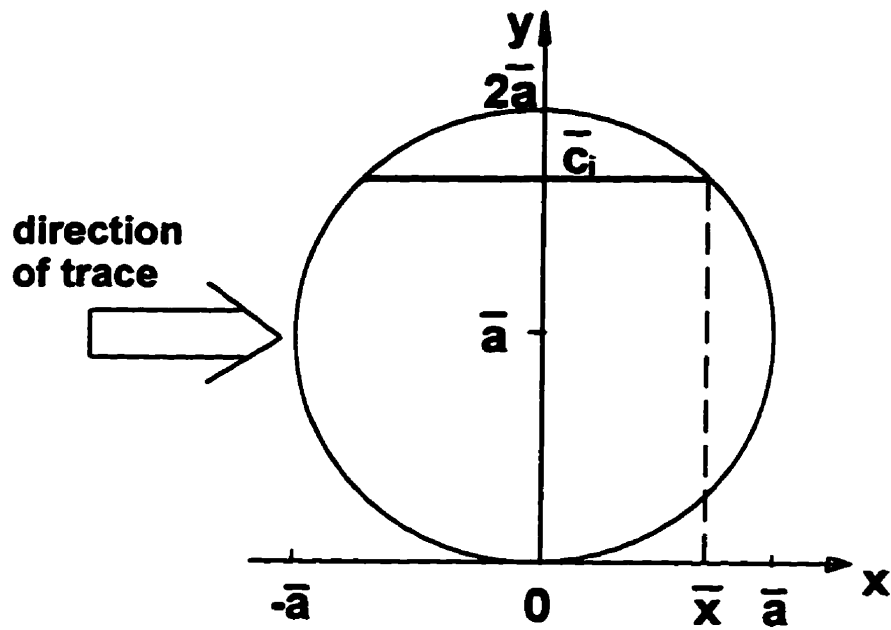
Eqs. 2.29a and 2.29b imply that

$$n = \frac{\pi}{4} \cdot \frac{HSC^2}{BA} \quad (2.30)$$

The above expression is valid for elastic surfaces because only size and not the number or the location of the contact spots changes. The same expression was derived by Cooper et al. (1969).

- **Determining surface and asperity height distributions**

Both the surface height distribution and the asperity height distribution are very important features involved in the analysis of the rough surface contact. The features of these



where $\bar{c}_i = 2\bar{x}$
 - average c_i

Figure 2.17 Average trace across a circular asperity contact spot

distributions can be determined from the BA measurements and the values of n calculated from the BA and HSC measurements.

The values of n increased with decreasing z until asperities began to merge. When this asperity merging occurred, the rate of increase of n declined such that a maximum value (n_{\max}) was reached at a particular separation z_L . It was convenient to have a new definition for asperity, which was any summit on a rough surface with its height greater than z_L .

Since a plot of $BA \times 100$ versus z represented the cumulative frequency distribution of the surface heights, the type and features of the surface height distribution were obtained by plotting BA on a probability paper (Figure 2.18). If the $BA \times 100$ data were oriented along an approximately straight line, the surface heights had a Gaussian distribution (Greenwood and Williamson, 1966). For this distribution, the average surface height (d_{avg}) was the value of z on the fitted line where $BA = 50\%$. The standard deviation (σ) of the surface height was the distance between d_{avg} and the value of z on the fitted line where $BA = 16\%$. The mathematical expressions were

$$d_{\text{avg}} = z_{(BA=50\%)} \quad (2.31)$$

$$\sigma = z_{(BA=16\%)} - z_{(BA=50\%)} \quad (2.32)$$

For convenience in later calculation, the location of the z -axis was adjusted so that $z = 0$ corresponded to the d_{avg} (Figure 2.18).

As mentioned above, an asperity was considered to be any summit on the surface which had a height greater than z_L . The cumulative frequency distribution of the asperity heights was given by $n/n_{\max} \times 100$ versus z plotted on a probability paper (Figure 2.19). Again, if the $n/n_{\max} \times 100$ data were oriented along an approximately straight line, the asperity height had a

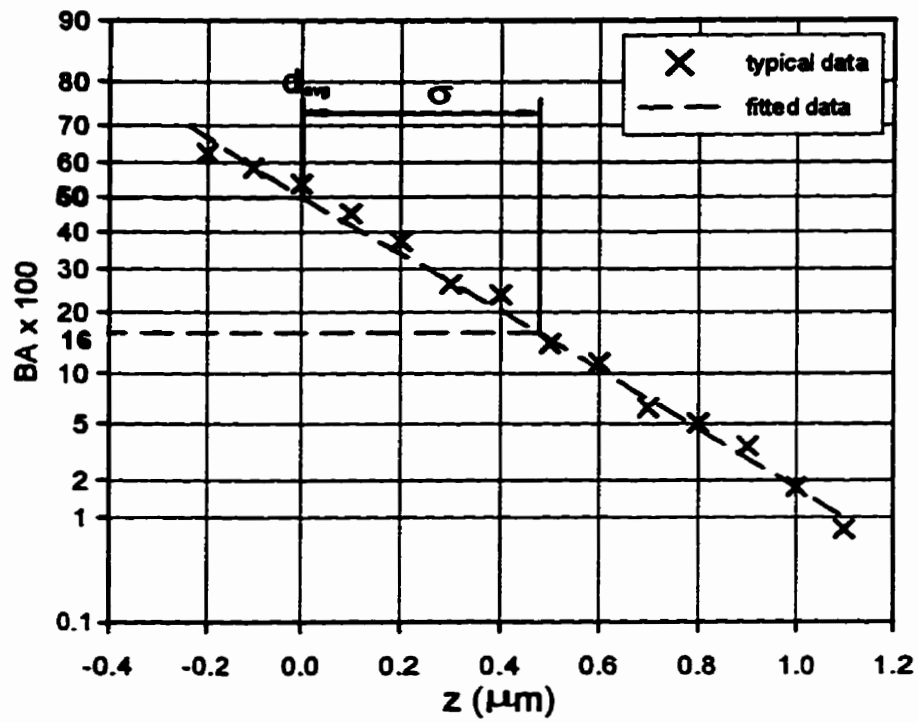


Figure 2.18 Determination of d_{avg} and σ from a probability plot of BA versus z

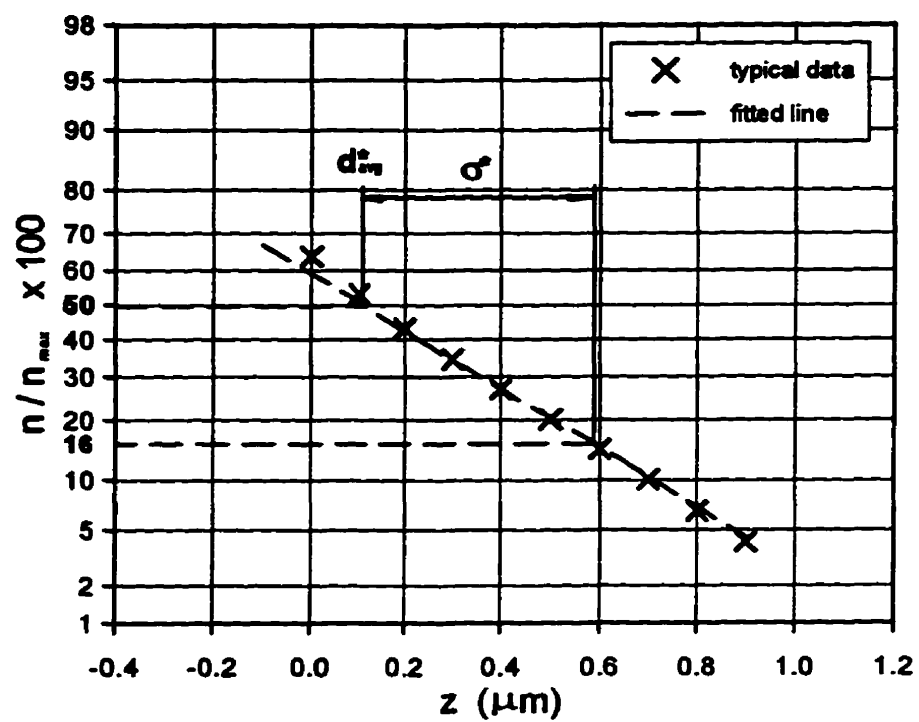


Figure 2.19 Determination of d_{vz}^* and σ from a probability plot of n/n_{\max} versus z

Gaussian distribution. The average asperity height (d^*_{avg}) and its deviation (σ^*) can be obtained from the plot as indicated by the following expressions.

$$d^*_{avg} = z_{\left(\frac{n}{n_{max}}=50\%\right)} \quad (2.33)$$

$$\sigma^* = z_{\left(\frac{n}{n_{max}}=16\%\right)} - z_{\left(\frac{n}{n_{max}}=50\%\right)} \quad (2.34)$$

- **Determining the real area of contact for a specified load**

Assuming that all contacting asperities at a particular z have spherical tips with an average radii of curvature β and that they deform independently, following the approach developed by De Vaal (1983), z , β and A_r can be determined for elastic deformation under a specified load F .

Following Greenwood and Williamson (1966), Hertzian equations are applied to individual asperity contacts and Gaussian distributions of surface and asperity heights are employed to yield the following equations:

(i) for the surface heights

$$A_r = \frac{1}{2} A_a F_0(z_m) \quad (2.35)$$

(From contact mechanics, the elastic Hertzian contact area is half that of purely plastic deformation.)

(ii) for the asperity heights

$$A_r = \pi \cdot \beta \cdot A_a \cdot n_{\max} \cdot \sigma^* \cdot F_1(z_m^*) \quad (2.36)$$

$$F = \frac{2}{3} \cdot E' \cdot \beta^{0.5} \cdot A_a \cdot \sigma^{*1.5} \cdot n_{\max} \cdot F_{1.5}(z_m^*) \quad (2.37)$$

$$\text{where } F_j(\zeta) = \frac{1}{\sqrt{2\pi}} \int_{\zeta}^{\infty} (s - \zeta)^j e^{-\frac{s^2}{2}} ds \quad (j = 0, 1, 1.5)$$

$$z_m = \frac{z - d_{\text{avg}}}{\sigma} \quad (2.38a)$$

$$z_m^* = \frac{z - d_{\text{avg}}^*}{\sigma^*} \quad (2.38b)$$

- dimensionless surface, asperity separation

z - specified separation

$d_{\text{avg}}, d_{\text{avg}}^*$ - average surface or asperity height, respectively

σ, σ^* - standard deviation of surface or asperity heights, respectively

E' - effective elastic modulus

β - average asperity tip radius at z

n_{\max} - the maximum contact spot density (before eventual asperities' merger)

Eqs. 2.35 and 2.36 gave an expression for β at z

$$\beta = \frac{F_0(z_m)}{2 \cdot \pi \cdot \sigma^* \cdot F_1(z_m^*) \cdot n_{\max}} \quad (2.39)$$

and substituting into Eq. 2.37 yielded

$$F_0(z_m) - \frac{4.5 \cdot \pi}{n_{\max}} \cdot \left(\frac{F}{\sigma^* \cdot E' \cdot A_a} \right)^2 \cdot \frac{F_1(z_m^*)}{[F_{1.5}(z_m^*)]^2} = 0 \quad (2.40)$$

Since z_m and z_m^* are functions of z , the above equation can be solved for the only unknown z , which corresponds to a specified load F . However, since z_m and z_m^* are implicit in $F_0(z_m)$, $F_1(z_m^*)$ and $F_{1.5}(z_m^*)$, the solution requires an iterative root finding procedure (implemented in a computer program) with numerous evaluations of the left side of Eq. 2.40. Discrete values of $F_0(z_m)$, $F_1(z_m^*)$ and $F_{1.5}(z_m^*)$ were obtained from McCool (1986) (Table 2.3) and employed with a natural cubic spline interpolation routine to obtain values for any z . This allowed the secant method to be applied to find the root of Eq. 2.40. Once the z is known, the value of z_m can be calculated and the real area of contact A_r can be determined from Eq. 2.35. Also, it is possible to calculate the β from Eq. 2.39.

**Table 2.3 Discrete data of $F_j(\zeta)$'s for GW type model
(from McCool, 1986)**

ζ	$F_0(\zeta)$	$F_1(\zeta)$	$F_{1.5}(\zeta)$
0.0	0.5000	0.3989	0.4299
0.1	0.4602	0.3509	0.3715
0.2	0.4207	0.3069	0.3191
0.3	0.3821	0.2668	0.2725
0.4	0.3446	0.2304	0.2313
0.5	0.3085	0.1978	0.1951
0.6	0.2743	0.1687	0.1636
0.7	0.2420	0.1429	0.1363
0.8	0.2119	0.1202	0.1127
0.9	0.1841	0.1004	0.09267
1.0	0.1587	0.08332	0.07567
1.1	0.1357	0.06862	0.06132
1.2	0.1151	0.05610	0.04935
1.3	0.09680	0.04553	0.03944
1.4	0.08076	0.03667	0.03129
1.5	0.06681	0.02930	0.02463
1.6	0.05480	0.02324	0.01925
1.7	0.04457	0.01829	0.01493
1.8	0.03583	0.01428	0.01149
1.9	0.02872	0.01105	0.8773e-2
2.0	0.02275	0.8490e-2	0.6646e-2
2.1	0.01786	0.6468e-2	0.4995e-2
2.2	0.01390	0.4887e-2	0.3724e-2
2.3	0.01072	0.3662e-2	0.2754e-2
2.4	0.8198e-2	0.2720e-2	0.2020e-2
2.5	0.6210e-2	0.2004e-2	0.1469e-2
2.6	0.4661e-2	0.1464e-2	0.1060e-2
2.7	0.3467e-2	0.1060e-2	0.7587e-3
2.8	0.2555e-2	0.7611e-3	0.5380e-3e
2.9	0.1866e-2	0.5417e-3	0.3784e-3
3.0	0.1350e-2	0.3822e-3	0.2639e-3
3.2	0.6871e-3	0.1852e-3	0.1251e-3
3.4	0.3369e-3	0.8666e-4	0.5724e-4
3.6	0.1591e-3	0.3911e-4	0.2529e-4
3.8	0.7235e-4	0.1702e-4	0.1079e-4
4.0	0.3167e-4	0.7145e-5	0.4438e-5

- **Extension to a sphere-on-flat configuration**

Originally, Greenwood and Williamson (1966) applied their model to a contact between two flat surfaces with apparent area of contact given by the known dimensions. For an elastic sphere-on-flat configuration (with one rough surface), the apparent area of contact could be assumed equal the Hertzian value (Eq. 2.11) according to Johnson et. al. (1972). However, if the variation in surface heights was large compared to the gap just outside the Hertzian contact zone, the apparent area might exceed the Hertzian value.

A non-dimensional roughness parameter (α) was defined by Greenwood et. al. (1984) to estimate if the contact size was close to Hertzian.

$$\alpha = \frac{\sigma \cdot R}{a^2} \quad (2.41)$$

where σ - RMS surface roughness

R - radius of the sphere

a - Hertzian contact radius

If α is less than about 0.1, the apparent area was very close to the Hertzian value.

Some more direct methods have been developed for determining real area of contact with numerical models, which included actual surface microgeometry as input. The numerical models of rough contacts were developed by Bush, Gibson and Thomas (1975), McCool and Gassel (1981), Lai and Cheng (1985), Webster et al. (1985), Lee and Cheng (1992) and Aramaki et al (1993). However, this type of analysis needed long computation time and input maps of surface topography. Therefore, Greenwood and Williamson type models remain popular in contact mechanics.

2.3.4 Micro-ehl approach

As described previously in Chapter 1, lubrication involving rough surface contacts is very complex. Some modeling of micro-ehl has been performed at various research centers. First, average flow factor models were used to offer a simple way to analyze the effects of the asperities. Later on with the improvements in computer techniques, more accurate numerical simulations were performed for the lubrication of rough surfaces specified by a surface topography map. These methods enabled the prediction of the details of pressure variation and film fluctuation, as well as asperity contact temperature and friction in micro-ehl films.

- **Average flow factor approach**

An average flow factor approach to study the mixed film lubrication started in late 60's. Christensen (1969) developed a stochastic theory to predict the average effects of roughness on the integrated load carrying capacity. This approach was used to predict average ehl film thickness and pressure in the contact of rolling elastic cylinders (Johnson et. al., 1972).

Another average flow model for determining the effects of roughness was developed by Patir and Cheng (1978a,b). They considered the effects of the pattern of the roughness and the effective film thickness parameter, and introduced a method of deriving the average Reynolds equation through flow simulation. Their numerical simulation extended the application of the Reynolds equation to the effective film thickness parameter $\lambda < 3$, where the load starts to be shared between the fluid film and the asperity contact films. For a surface with an isotropic Gaussian roughness, the ehl film thickness from formulae based on numerical analysis of perfectly smooth surfaces remains accurate in their prediction of the average film thickness, down to $\lambda = 1$.

The average film thickness is important since it gives the extent of asperity contact in mixed film lubrication. However, Cheng (1993) recently pointed out that his early model seems to

give an over estimation of the roughness effect compared with more accurate numerical simulation results, particularly for the estimation when λ ratio is low.

- **Deterministic solution approach**

The average flow approach considers only the average pressure and film thickness, but it ignores the variation in pressure and film thickness under individual asperities. With the development of modern computers and numerical methods, some deterministic solution models were performed by Cheng (1983), Houpert and Hamrock (1985) and Baglin (1986). In these models, the pressure ripples and film thickness fluctuations around asperities and other irregularities were simulated numerically. They revealed the characteristics of the micro-ehl film in detail.

A full numerical solution is demonstrated in Figure 2.20 for the behaviour of rough surfaces in point contacts (Lubrecht, et.al. 1988). They used the multigrid method to investigate the effects of sinusoidal roughness on the pressure and film thickness in an elliptical Hertzian contact. Their simulation results agree well with the early experimental measurements which were carried out by De Silva, et. al. (1985) using an optical apparatus (Figure 2.21).

- **Physical influences in micro-ehl**

There are many other features of rough surfaces that may have significant effects on lubricant behaviour in micro-ehl. Two of them are the influences of the asperity flattening and the discontinuous pressure distribution.

In practice, the initial surface roughness may decrease, even disappear under the heavy load. The asperity tips are effectively flattened, but in the surrounding low pressure region the surface micro-geometry remains undistorted. This flattening occurs because the load begins to be carried through the micro-contacts at the asperity tips rather than the overall ehl film.

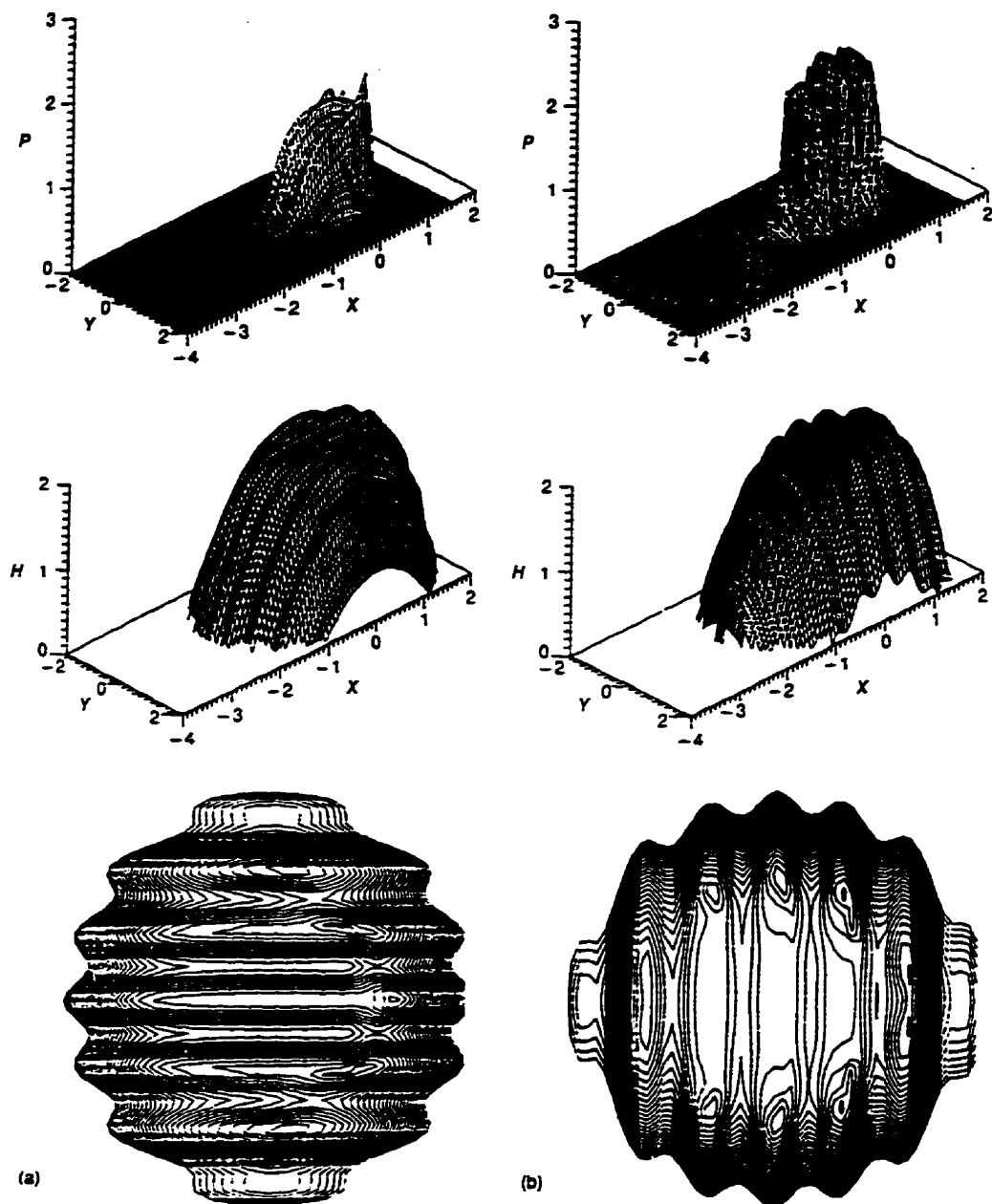


Figure 2.20 Numerical results of pressure and film thickness profiles and contour plots (from Lubrecht et. al., 1988)
(a) for longitudinal roughness (b) for transverse roughness

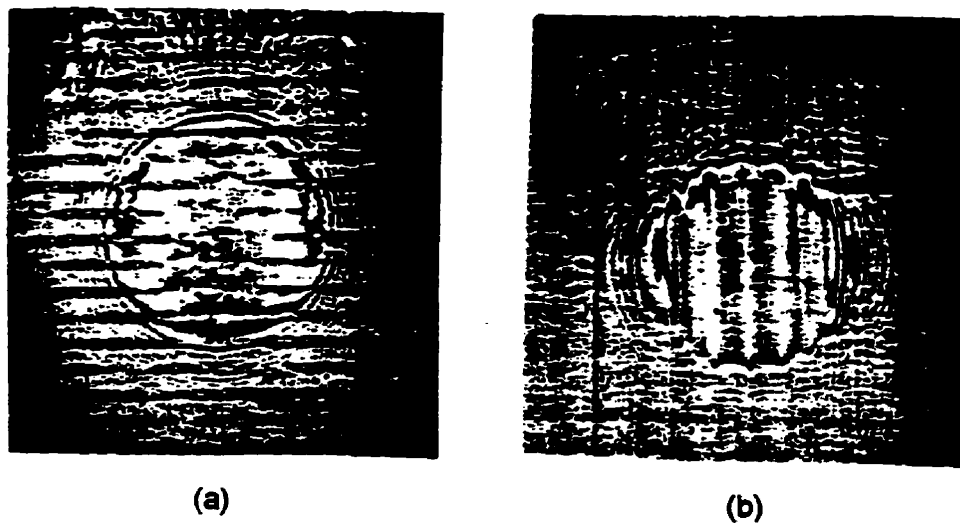


Figure 2.21 Micro-interferograms of rough surface lubricated contact
(from DeSilva et. al., 1985)
(a) for longitudinal roughness (b) for transverse roughness

The local pressures are significantly higher than the corresponding Hertzian pressure, and hence the local viscosities are high. They produce an additional local elastic or plastic deformation at the tips of asperities. As a result of the local deformation, both the effective surface roughness and the pressure ripples are reduced in height within the overall contact zone. An asperity flattening model was suggested by Kweh, Evans and Snidle (1989), in which an isothermal ehl contact between a rough stationary surface and a smooth moving surface was considered (Figure 2.22). If this asperity flattening occurs in practice, it would give continuous ehl films under conditions where such film had been thought impossible.

The amplitude of initial surface roughness influences the pressure distribution and film thickness. As higher amplitude roughnesses are considered, the amplitude of the pressure ripples may make the pressure in the valleys between asperities become insignificant. Thus the viscosity drops and the contribution of the valley regions to the load capacity and the friction force becomes negligible. The pressure distribution becomes discontinuous (Figure 2.23). In such cases, a solution based on the assumption of continuous pressure distribution is not valid.

Several research efforts provided analysis of discontinuous pressure distributions (Karami, et al., 1987; Huang and Wen, 1993). In their models, each asperity contact was considered to behave as an isolated ehl point contact and the Reynolds equation was applied for each individual asperity. The main points of their modeling work involved the treatment of continuity of both flow and surface deformation with the discontinuous pressure and the determination of the beginning of the micro-ehl section (Huang and Wen, 1993). They predicted a critical roughness amplitude value for a sinusoidal roughness in a line contact at which the discontinuous pressure distribution occurs. Although their prediction does not directly relate to the present study, their numerical method can conceivably be used to solve for isolated micro-ehl. In experimental work examining micro-ehl, the discontinuous pressure distribution was also considered as an important end point for the transition from cooperative micro-ehl to isolated micro-ehl (Sutcliffe, 1991).

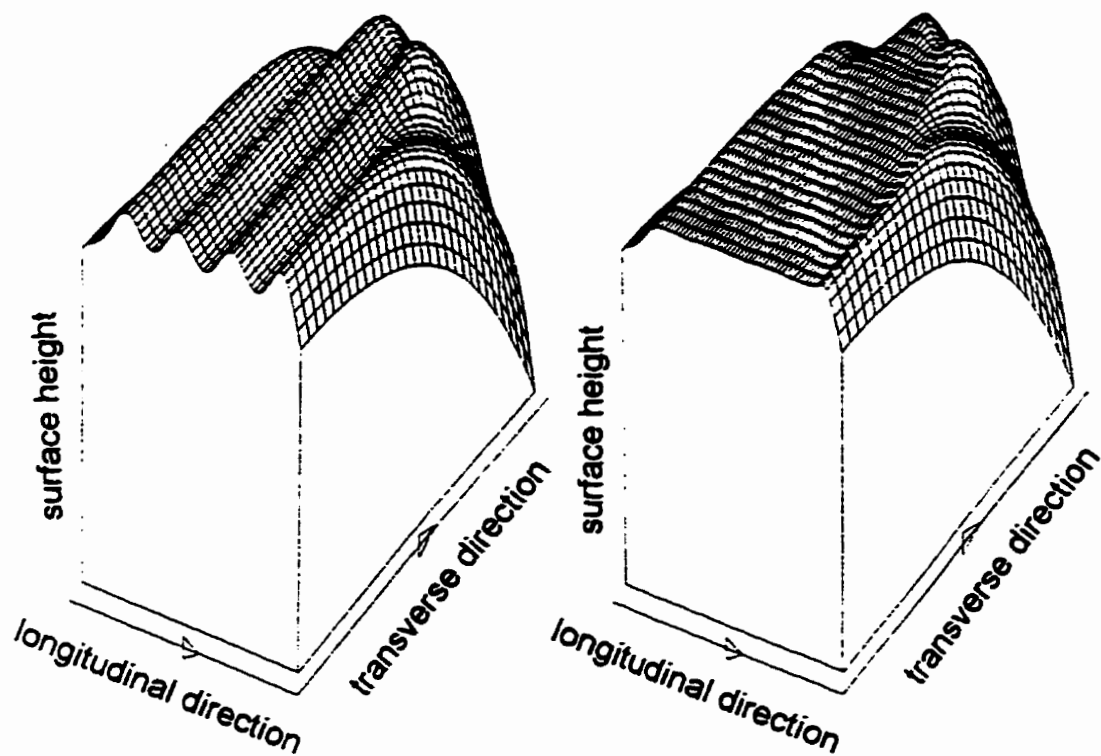


Figure 2.22 Solution of asperity flattening model (from Kweh et. al., 1989)

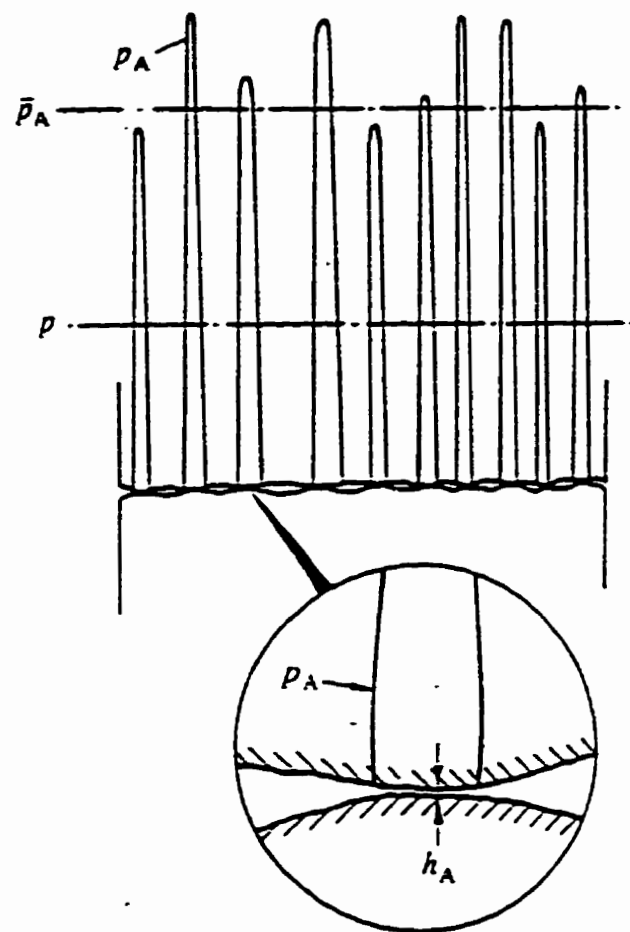


Figure 2.23 Discontinuous pressure distribution in rough surface contact
(from Evans and Johnson, 1985)

Solutions of mixed film lubrication have not been established well enough to provide formulae to predict film thicknesses or friction force. Not even the kinematically simple case of a rough surface in contact with a relatively smooth one has been solved.

2.4 Friction and Rheological Models

Friction is defined as the force generated in the contact that resists relative motion of the bearing surfaces (Hamrock and Dowson, 1981). When the contact surfaces are moving with different speeds then sliding between them exists. The slower moving surface exerts a resistant force on the faster one. Two commonly encountered types of applications in which friction is important are traction components, such as power belts and tires on roads, which require high friction forces, and load transmitting components, such as cranks, gears and all kinds of bearings, which are expected to operate with minimal friction. To reduce friction forces, lubricants may be used. Thus, the friction forces are often very important consequence of the rheological behaviour of the lubricant, particularly in ehl. Friction forces are often studied with a disc machine apparatus, because it permits high rolling speeds with controlled amounts of sliding speed. Therefore, the friction behavior in a disc machine is presented first and some rheological models which explain the features of friction are discussed subsequently.

2.4.1 Friction behaviour

During the past twenty years, friction behaviour has been under intensive study. In typical ehl, the lubricant goes throughout the contact in a very short time (about 1 ms), under very high pressure (about 1 GPa), and shear strain rate (about 2×10^8 1/s). In this contact, the temperature may also vary because of the associated thermal energy dissipation within the film.

Disc machines have been developed to simulate the tribology of counter-formal contacts under conditions of mainly rolling with some sliding, and can be used to study fundamental friction behavior of lubricants in these contacts. Disc machines can apply shear to a lubricant film while avoiding excessive sliding which can lead to high temperatures and complex chains of chemical reactions between the lubricant additives and the surface. In a typical test, the applied load (F) is set to a constant value and surface speeds (u_1) and (u_2) respectively for two discs are controlled. The rolling speed ($u = (u_1 + u_2) / 2$) can be kept constant, but u_1 and u_2 can both be changed so that the sliding speed ($u_s = u_1 - u_2$) varies. When lubricant is drawn into the nip between the discs, it generates a film of approximately uniform film thickness (h) under the pressure (p) which is close to the Hertzian pressure distribution. The variation of friction force (F_f) is measured at increasing values of sliding speed and plotted as a friction or traction curve, which is usually represented as friction force (F_f) or the friction coefficient ($\mu = F_f/F$) versus slide-roll ratio (u_s/u).

The traction behaviour of concentrated contacts is complex and the shape of traction curve depends on the lubricant, contact surfaces and operating conditions. Figure 2.24 is a group of typical traction curves, where a point contact side-slip disc machine is considered. In this case, the sliding speed is in the direction which is perpendicular to the rolling direction, so that $u_s = v$ and the traction curves are plotted by the F_f versus v/u . These traction curves present various rheological behaviours of the sheared lubricant film.

Traction curve A is measured under a low pressure and shows a linear relationship between the F_f and v/u . The lubricant behaves as a Newtonian fluid and the slope of the traction curve is proportional to the viscosity (η) of the lubricant. When the lubricant is subjected to the contact discs, heat may be generated in the inlet zone due to shearing, especially as the sliding speed is high. The shear heating can lower the lubricant viscosity significantly, which is known as shear thinning (Johnson and Tevaarwerk, 1977), and make the traction curve A depart from the solid line to the dash line.

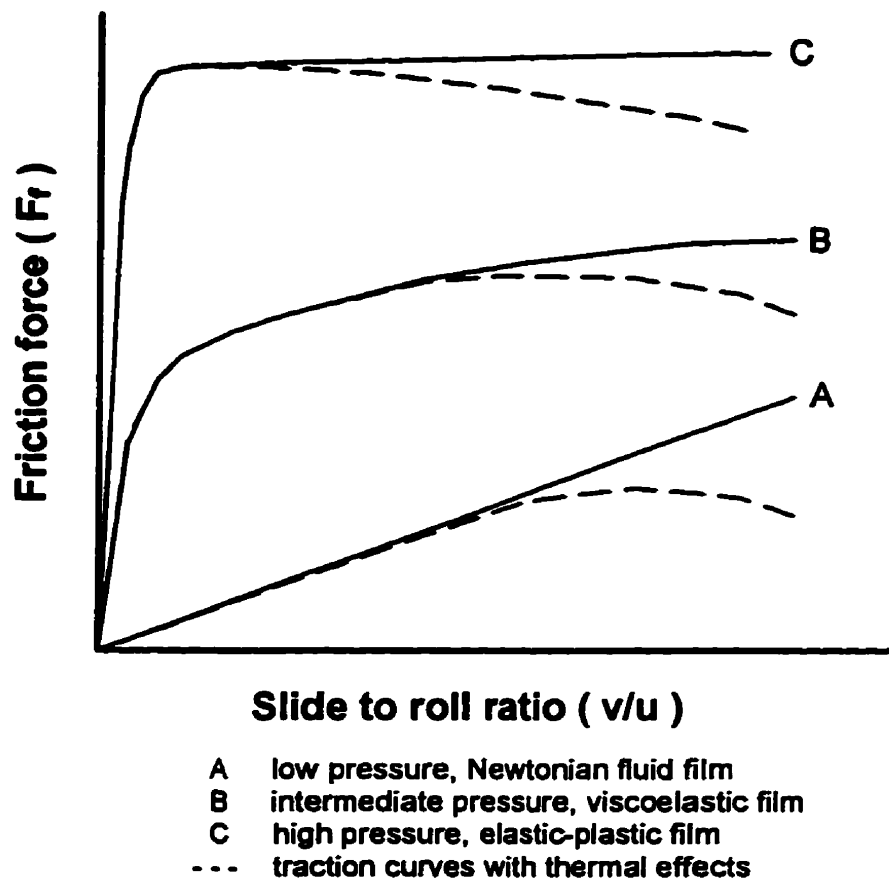


Figure 2.24 Typical traction curves from a disc machine

Traction curve B is measured under an intermediate pressure, where a viscoelastic film exists. Increasing v/u gives a rise of progressive non-linearity in the F_f . This non-linear variation was explained by Hirst and Moore (1974) and Johnson and Tevaarwerk (1977) as a shear rate dependent viscoelastic behaviour. The viscous fluid changes from the Newtonian to a non-Newtonian behaviour because of the cumulated thermal activation energy which was created during shearing according to the Eyring theory of fluid viscosity. Other researchers (Bair and Winer, 1979) attributed this non-linear variation of F_f to the limiting shear stress (τ_L). As soon as localized high pressure made part of the lubricant film reach the τ_L and behave as elastic-plastic solid, then the linear Newtonian response of F_f is modified. Under the intermediate pressure, the entire lubricant film has not reached τ_L , and therefore, the lubricant film appears to exhibit viscoelastic behaviour. When the sliding speed increases, the inlet zone heating due to shear and compression may lead to an increase in film temperature and a consequent decrease in viscosity and τ_L . This thermal effect causes an obvious decline in the traction curve as shown by the dash line.

Traction curve C is measured under a high pressure, where the lubricant film is sheared as an elastic solid rather than a viscous fluid. The slope is then proportional to the elastic shear modulus (G) of the lubricant. As the sliding speed increases, F_f reaches a limit and does not increase continuously with increase in v/u , which shown as a flat part in the traction curve. This type of traction curve indicates that the lubricant film within the whole contact zone reaches the τ_L . Under this τ_L the lubricant behaves as a perfect plastic solid and shears independent of the sliding speed (Smith, 1962; Plint, 1967; Johnson and Cameron, 1967). It has been suggested that τ_L is a fundamental material property of the lubricant (Bair and Winer, 1979a). In the high pressure case, thermal effects may also occur as shown by the dash line. It is possible that the thermal effect occurs before the whole lubricant film reaches the τ_L . Then, the maximum friction force measured on the traction curve may not correspond to the τ_L if the thermal effect exists.

The traction curves in Figure 2.24 suggest that pressure is a dominant parameter. When the pressure is high, such as a mean contact pressure (p_{avg}) above 1.0 GPa for a mineral oil, the linear region is restricted to extremely low sliding speed and friction is dominated by the plastic shearing of the lubricant film. In contrast, when the p_{avg} is below 0.1 GPa, the friction is dominated by the viscosity of the lubricant.

2.4.2 High pressure rheological models

Several rheological models have been developed to explain the highly non-linear relationship between the traction or friction force and the slide-to-roll ratio, which involve the shear stress (τ) and shear strain rate ($\dot{\gamma}$) relation in the lubricant film. The two models that have emerged from research in rheology are the Eyring thermal activation model and the limiting shear stress model.

- **Eyring thermal activation model**

Johnson and Tevaarwerk (1977) described the lubricant behavior that they observed in their disc machine experiments as a non-linear viscous flow superimposed on a linear elastic strain (Figure 2.25). They suggested the following constitutive equation relating τ to $\dot{\gamma}$, which is a nonlinear Maxwell type equation.

$$\dot{\gamma} = \dot{\gamma}_e + \dot{\gamma}_v = \frac{1}{G} \cdot \frac{d\tau}{dt} + F(\tau) \quad (2.42a)$$

where $\dot{\gamma}$ - shear strain rate (subscripts e and v for elastic and viscous components)

τ - shear stress

G - elastic shear modulus of the lubricant

$\frac{d\tau}{dt}$ - shear stress rate

$F(\tau)$ - a shear stress function for nonlinear viscous flow

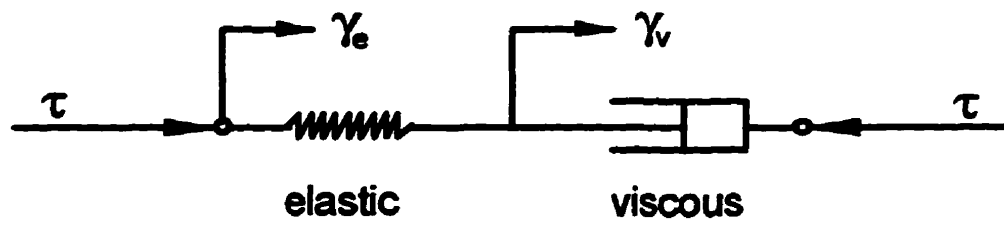


Figure 2.25 Visco-elastic nature for rheological model

Johnson and Tevaarwerk used the following form of the function $F(\tau)$, which was suggested first by Hirst and Moore (1974) and was based originally on a thermal activation theory of fluid viscosity proposed by Eyring (1936).

$$F(\tau) = \frac{\tau_0}{\eta} \cdot \sinh \frac{\tau}{\tau_0}$$

where τ_0 - Eyring shear stress

η - Eyring viscosity

Then the constitutive equation became

$$\dot{\gamma} = \frac{\dot{\tau}}{G} + \frac{\tau_0}{\eta} \cdot \sinh\left(\frac{\tau}{\tau_0}\right) \quad (2.42b)$$

where G , τ_0 and η were specified for particular temperature and pressure.

It is interesting to note that when the viscosity is low, usually under relatively low pressure,

$\frac{\tau_0}{\eta} \cdot \sinh\left(\frac{\tau}{\tau_0}\right) \gg \frac{\dot{\tau}}{G}$ and $\dot{\gamma} \approx \frac{\tau_0}{\eta} \cdot \sinh\left(\frac{\tau}{\tau_0}\right)$. Then, if $\tau \ll \tau_0$, it follows that $\sinh(\tau/\tau_0) \approx \tau/\tau_0$

and the lubricant behaves as a Newtonian fluid with $\dot{\gamma} = \tau/\eta$ (Eq. 2.1). As $\tau \geq \tau_0$, either through higher film pressures, increasing shear strain rates or decreasing temperature, the fluid becomes appreciably nonlinear and the full constitutive equation (Eq. 2.42b) applies.

According to Eq. 2.42b, there are three rheological parameters (G , η and τ_0) for a lubricant under high pressure and each of these parameters vary with both pressure and temperature. Evaluation of these rheological parameters is very difficult. One approach is to use a disc machine which can subject a lubricant to suitably high pressures for relatively short periods of time (typically about 1 ms). Since the disc machine provides a good simulation for ehl contacts, the rheological parameters can be determined under conditions relevant to

engineering application. However, difficulties arise because shear strain rate, pressure, and sometimes temperature vary over the contact.

To address these problems, Johnson and Tevaarwerk (1977) assumed that G , η and τ_0 could be averaged over the varying contact pressure and kept temperature variation small by avoiding high slip velocities. Then, using an ehl formula (Eq.2.24), they estimated the film thickness and determined an average shear strain rate ($\dot{\gamma} = u/h_c$). If time was expressed by $t = x/u$, where x is the position in the contact, and $u = (u_1 + u_2)/2$ (which was the average rate of flow of lubricant through the contact), then, Eq. 2.42b was integrated with the initial condition that the lubricant shear stress was zero as the lubricant entered the Hertzian contact zone. Lubricant shear stress was solved analytically as

$$\tau = f(G, \eta, \tau_0, x, y)$$

Assuming that the contact zone extended over the Hertzian contact area allowed the friction force to be determined by numerically integrating the shear stress over the contact as follows

$$F_f = \int_{-a}^a \int_{-\sqrt{a^2-y^2}}^{\sqrt{a^2-y^2}} \tau \cdot dx \cdot dy$$

It was possible to determine unique values of the rheological parameters (G , η and τ_0), by measuring F_f from a disc machine. Assuming that the lubricant film pressures were close to Hertzian, the values of the rheological parameters were assumed to correspond to the average Hertzian pressure. However, Johnson (1992) noted that the disc machine was not an ideal way to study lubricant properties of mineral oils because pressure varied over the contact.

- **Limiting shear stress model**

When the pressure is very high for a given contact, increasing shear strain rate ($\dot{\gamma}$) from zero causes a rapid increase in shear stress (τ), which levels off at a constant value before thermal effect cause its decline. Smith (1959), based on his disc machine friction measurements, first proposed that the lubricant film was shearing as a plastic solid at the “limiting shear stress” rather than a viscous liquid. From his plot of the τ versus $\dot{\gamma}$ (Figure 2.26), the lubricant was assumed to deform plastically at the τ_L , so that an increase in shear strain rate produces no increase in shear stress if the film temperature was kept constant. In this figure, Smith also pointed out that the τ_L was a function of pressure. Later on, his discoveries were discussed and developed by other researchers.

Johnson and Tevaarwerk (1977) suggested that at high contact pressure the lubricant behaved like a solid more than a liquid. It was fully elastic and linear at lower shear strain rate, but behaved as plastic flow at high shear strain rate when the shear stress reached the τ_L . If this did occur, the elastic-plastic equation could be used to describe relationship of the shear stress and shear strain rate, which was as that indicated by Smith (Figure 2.26)

$$\begin{aligned} \tau &= G \cdot \gamma && (\text{low } \dot{\gamma}) \\ \tau &= \tau_L && (\text{high } \dot{\gamma}) \end{aligned} \tag{2.43a}$$

For low $\dot{\gamma}$ the equation was given by Johnson and Roberts (1974) from their point contact disc machine experiments as

$$\tau = \frac{8}{3\pi} \frac{Ga}{u} \dot{\gamma} \tag{2.43b}$$

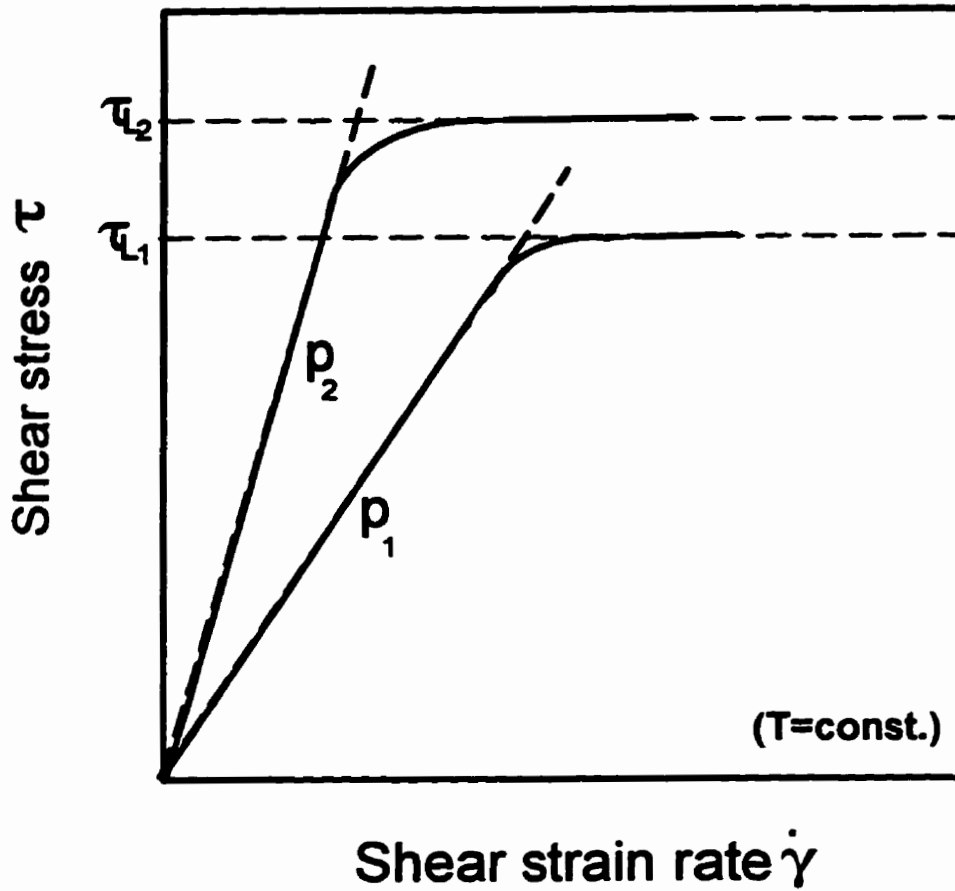


Figure 2.26 Relationship of shear stress and shear strain rate for lubricant under extremely high pressure (from Smith, 1960)

Bair and Winer (1979b) found that the τ_L is a function of film pressure by using a high pressure rheometer to measure the τ_L . They used a linear equation to describe the relation between the τ_L and pressure at a given temperature.

$$\tau_L = A + B \cdot p \quad (2.44)$$

where A, B - constants

p - pressure

To deal with the transition from elastic to plastic behaviour over a wide range of contact pressure, Bair and Winer (1979a,b) proposed a Maxwell type constitutive equation based on measurements with a pressure rheometer (not a disc machine), which had three independent rheological parameters, G , η and τ_L .

$$\dot{\gamma} = \frac{\dot{\tau}}{G} - \frac{\tau_L}{\eta} \ln \left(1 - \frac{\tau}{\tau_L} \right) \quad (2.45)$$

where G - elastic shear modulus

η - viscosity

τ_L - limiting shear stress

This equation was used to predict the friction behavior in eHL. The prediction for lubricant polyphenyl ether 5P4E by using the G , η and τ_L from their high pressure rheometer was compared with the friction for the same lubricant, which was measured by Johnson and Tevaarwerk in their disc machine. The predicted friction agreed quite well with the measured results where the actual average film temperature was considered higher than the bulk temperature and was approximately 50 °C (Figure 2.27).

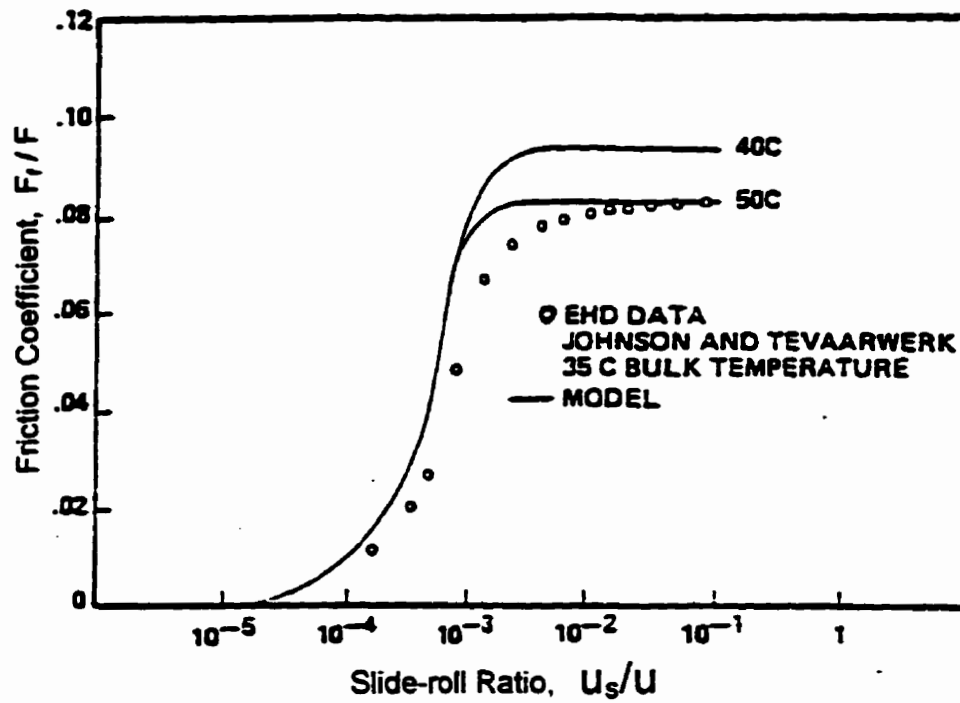


Figure 2.27 Comparison of friction results from different measurement methods (from Bair and Winer, 1979b)

Another version of limiting shear stress model was introduced by Gecim and Winer (1980) as shown below.

$$\dot{\gamma} = \frac{\dot{\tau}}{G} + \frac{\tau_L}{\eta} \cdot \tanh^{-1} \left(\frac{\tau}{\tau_L} \right) \quad (2.46)$$

It predicted the traction curve for the same lubricant with similar accuracy as the other version (Eq.2.45) and was more suitable in computational models due to its symmetry about zero shear stress.

Further examinations of the relationship between τ_L and pressure were performed by many researchers using various experimental devices, such as Höglund and Jacobson (1986a) with a high pressure rheometer, Ramesh and Clifton (1987) with a pressure-shear plate impact device and, Evans and Johnson (1986a) with a disc machine containing heating elements imposing temperature on the lubricant film. Evans and Johnson (1986), referring to the work of Imai and Brown (1976), stated that once τ_L was reached, “the mechanism of fluid flow changes from thermally activated motion of independent molecular segments to the formation of a shear band through the collaborative motion of adjacent segments”. Bair and Winer (1992,1993) observed these shear bands optically using a flow visualization cell (Figure 2.28). They showed the evidence of localized slip mechanism at shear bands in ehl under a pressure range of 0.22 GPa to 0.76 GPa.

● Comparison of the models

The rheological properties of lubricants in ehl have been established by the above models for about twenty years. To specify the lubricant properties which govern the friction behaviour, both models give the relations of the shear stress which is developed in the lubricant film to the shear strain rate which is imposed on the fluid (Eqs. 2.42, 2.43, 2.45 and 2.46). The differences between these models are the explanations of the rheological mechanisms.

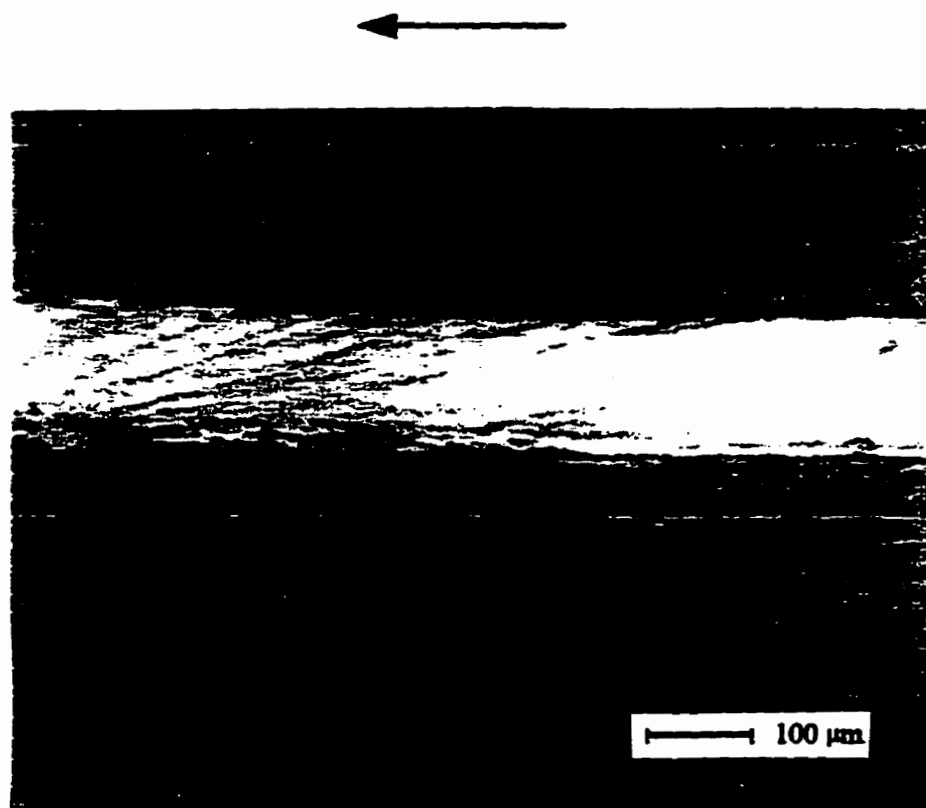


Figure 2.28 Observation of shear bands (from Bair et al., 1993)

(Synthetic oil 5P4E at $P = 220$ MPa, $T = 22^\circ\text{C}$, $\dot{\gamma} = 0.25$ s $^{-1}$)

The thermal activation model is based on an activation energy concept to explain the variation of viscosity with temperature and pressure. Recently, experimental measurements by Evans and Johnson (1986a, 1986b) showed that the friction behaviour with smooth surface discs could take various forms in response to increasing pressure. Figure 2.29 (Evans and Johnson, 1986b) is a typical friction regime map of a synthetic traction fluid, Santotrac 50, where the vertical axis is the dimensionless film thickness parameter of $(\alpha\eta_0 u/R)$ and the horizontal axis is the dimensionless pressure parameter of (αp_{av}) . The map displays four distinct regimes of Newtonian, Eyring, viscoelastic and elastic-plastic rheological behaviour. In order to construct this type of map, i.e. to distinguish boundaries between the regimes, the values of η , τ_0 and τ_L varied with pressure and temperature were measured from their disc machine experiments and some analytical derivations based on the rheological models.

The limiting shear stress model describes the lubricant behaviour in a somewhat simple way. It assumes that the lubricant flows as a plastic solid at some shear stress (τ_L) which varies with temperature and pressure (Smith, 1959; Johnson and Tevaarwerk, 1977; Bair and Winer, 1979, 1980, 1992). As the shear stress is below τ_L , Newtonian behaviour dominates. There is a transition from the linear Newtonian behaviour to the shear strain rate independent plastic behaviour, which was explained by Evans and Johnson with the Eyring thermal activation model. This transition covers a broad range of shear strain rates as pressure is increased. However, Bair and Winer (1991, 1993) disagree with the existence of the Eyring regime. They explained this non-linear transition with the localized shear bands, which were observed from their high pressure flow visualization cell (Figure 2.28). The band occurred at a quite low shear strain rate when a departure from the Newtonian flow began, and it showed the shear stress at that location reached some critical value. The number of shear bands increased with increasing shear strain rate from as few as one at the onset of non-Newtonian flow until the shear region is essentially filled with bands. Therefore, the critical shear stress is statistically distributed by the limiting shear stress τ_L . The functional form of the limiting shear stress model (Eq. 2.45 or Eq. 2.46) is expected to give this distribution.

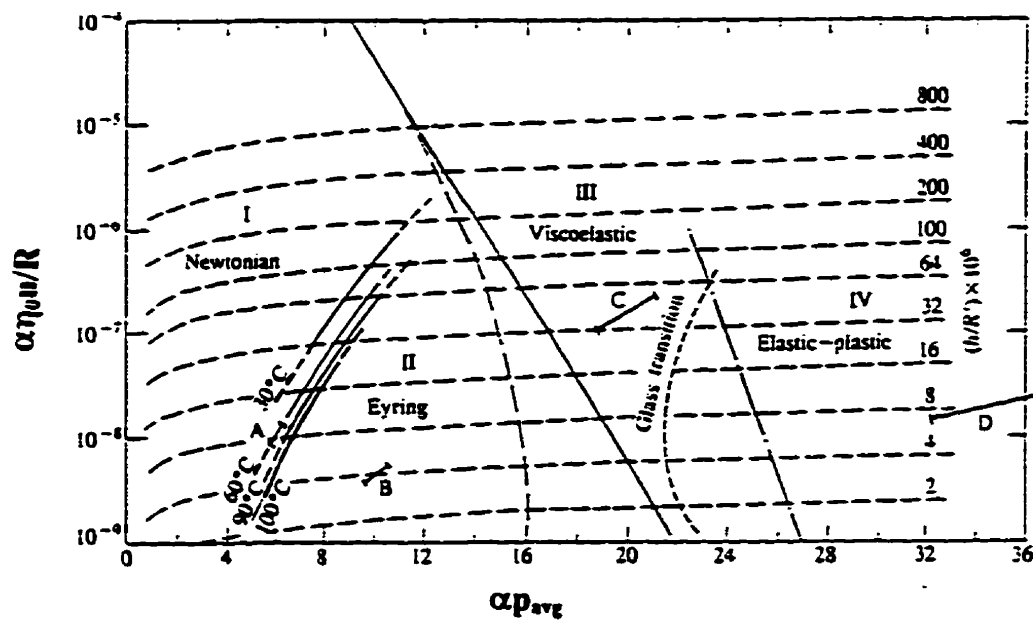


Figure 2.29 Traction map for Santotric 50 (from Evans and Johnson, 1986)

For the high pressure plastic shear behaviour, the two models give a same explanation. Whether the thermal activation exists or not, it is eliminated in this regime. In the present study, the rheological properties of formulated lubricants will be established by the limiting shear stress model.

2.4.3 Limiting shear stress from ehl friction measurement

The rheological models developed to analyze friction behaviour of lubricants in ehl are represented in constitutive equations (Eqs. 2.42b, 2.43, 2.45 and 2.46). They are expressed in terms of certain independent rheological parameters of lubricants. Thus, determining the rheological parameters is the first step to use a rheological model to predict the lubricant behaviour in ehl. Unfortunately, only a limited amount of data of the rheological parameters is available for most of the lubricants in practical situations, although many efforts have been made to determine them since the rheological models were presented.

In general, there are a direct and an indirect approaches to determine the rheological parameters. The direct method requires rather sophisticated devices to impose appropriate constant values of pressure, temperature and shear strain rate and to measure the rheological parameters. The indirect approach uses relatively simple devices but cannot impose constant pressure, temperature and shear strain rate. In fact, even the distribution of these input parameters is not known with certainty for the indirect method. Recently, some data generated by using the direct method were reported (Höglund and Jacobson, 1986; Ramesh and Clifton, 1987), but the indirect method is used widely because of its lower cost and simplicity (Kato, et. al., 1993; Wu and Cheng, 1994).

The limiting shear stress (τ_L), a fundamental rheological parameter, is a function of pressure and temperature. If the traction regime is “elastic-plastic”, the friction may depends only on τ_L . Values for τ_L have been measured with a disc machine (Johnson and Tevaarwerk, 1977) and a high pressure rheometer (Bair and Winer, 1979a, 1979b). A recent approach to

measuring τ_L with a disc machine was developed by Wu and Cheng (1994); it takes into account the distribution of film pressure and was based on the improved version (Eq. 2.46) of limiting shear stress model (Gecim and Winer, 1980). This approach was adopted to determine the τ_L for the present study. The major step in this approach is determining the limiting shear stress index number (m). If the m is determined from the measured friction force, it can be used to generate an empirical expression of the τ_L in terms of the film pressure (p).

For a nominal point contact with an elliptic contact area (πab) in Wu and Cheng's test rig, the lubricant film had a Hertzian pressure distribution

$$p = p_{\max} \cdot \left(1 - \frac{x^2}{a^2} - \frac{y^2}{b^2}\right)^{\frac{1}{2}} \quad (2.47)$$

where $p_{\max} = \frac{1.5F}{\pi ab}$ - the maximum contact pressure

x, y - coordinates

a, b - radius of contact ellipse along x or y direction

The lubricant was assumed to have reached the τ_L throughout the contact zone and had not been subject to significant shear heating which meant that the inlet temperature of the lubricant prevailed throughout the contact. Thus, the τ_L values depended on the lubricant film pressure, which followed the constitutive equation (Eq. 2.43a) originally suggested by Smith (1960), and the τ_L was assumed to have a distribution as follows

$$\tau_L = \tau_{L\max} \cdot \left(1 - \frac{x^2}{a^2} - \frac{y^2}{b^2}\right)^m \quad (2.48)$$

where $\tau_{L\max}$ - the maximum τ_L in contact

m - an index number for limiting shear stress distribution

Under a high shear strain and high load, the maximum traction force ($F_{f \max}$) can be obtained by integrating the τ_L on the ellipse contact area.

$$F_{f \max} = \int_{-b}^b \int_{-a}^a \tau_L dx dy$$

Substituting the τ_L (Eq. 2.48) in and integrating it resulted in

$$F_{f \max} = \tau_{L \max} \cdot \frac{\pi ab}{(m+1)}$$

This can be rewriting as

$$\tau_{L \max} = (m+1) \frac{F_{f \max}}{\pi ab} \quad (2.49)$$

Then, a general expression for τ_L could be obtained by combining Eqs. 2.47, 2.48 and 2.49

$$\tau_L = (m+1) \frac{F_{f \max}}{\pi ab} \left(\frac{p}{p_{\max}} \right)^{2m} \quad (2.50)$$

Since the τ_L was only a function of pressure and temperature, and the temperature was held constant, the τ_L was related to pressure with Eq. 2.50. For a specified load, the contact area (πab) and the maximum Hertzian pressure (p_{\max}) were known. Under a high shear strain rate and high load condition, the $F_{f \max}$ could be measured as the highest constant value in traction curve. Therefore, to determine the index number of m for a particular lubricant, $F_{f \max}$'s were measured at a constant temperature and at a number of various ehl loads. For each load there was a τ_L expression (Eq. 2.50) including the unknown m and the corresponded πab and p_{\max} . The m value was found by "curve-finding" (it was not clear in their paper what was meant by

this expression), and set as a constant for the test lubricant by Wu and Cheng. The plots of τ_L versus p for different lubricant temperatures (Figure 2.30) showed that pressure had a stronger influence on τ_L than temperature.

2.4.4 Friction in rough surface lubricated contact

The friction force increases as the film thickness decreases, especially when the magnitude of the film thickness is comparable with the surface roughness. This increase in friction is a result of asperity interaction. Friction behavior in rough surface lubricated contact has been studied under high pressure and low sliding speed. In the early work of Jefferis and Johnson (1967), the influence of surface roughness on friction was investigated using a disc machine. The measured maximum friction coefficients (0.06 - 0.07) showed little change from those of smooth surface results (0.055). Jefferis and Johnson (1967) suggested that under the conditions of mixed film lubrication the friction is still governed by the bulk lubricant rheological properties. However, the local pressure at the asperity interaction is higher than surrounding pressure; thus, if the shear stress is close to the limiting value, friction force does not increase dramatically.

Later on, Bair and Winer (1982) identified three regimes of friction based on the feature of the effective film thickness parameter (λ). At sufficiently high λ ratio, the friction force was a function of the bulk lubricant rheological properties at operating conditions. There was no surface roughness influence. At medium λ ratio, the film thickness and surface roughness had comparable magnitudes. The friction force was determined by the bulk lubricant properties under conditions of pressure, temperature and load between the local asperity contacts. Bair and Winer (1982) interpreted the friction behaviour in medium λ ratio regime, i.e. the mixed film lubrication, in the same way as Jefferis and Johnson (1967). At $\lambda < 1.0$, the friction force increased in accordance with the properties of films which were adsorbed onto the contact surfaces.

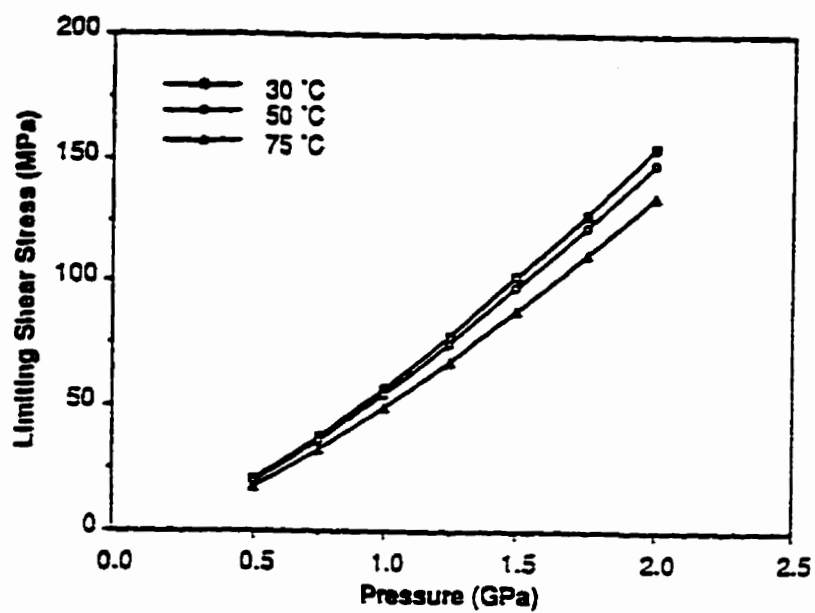


Figure 2.30 Variation of limiting shear stress with pressure at various temperatures (from Wu and Cheng, 1994)

From Evans and Johnson's (1987) friction regime map (Figure 2.29), the value of αp_{avg} would be governed by the pressure at individual asperity tips where the friction force developed between rough surfaces. Since the asperity pressure was greater than the smooth surface pressure, the operating point in the regime map would move to larger αp_{avg} . As the λ ratio decreased, the friction behaviour changed corresponding to the changes from hydrodynamic film pressure to the local asperity pressure.

At the high spots of the asperities, there would be a local thinning of the film, resulting in local increases in pressure, when the shear strain rate is high. Thus, the friction force will be dominated by the shear stress developed in these high pressure and shear strain rate regions. Figure 2.31 (Evans and Johnson, 1987) gives an example of a contact under certain load and kinematic conditions: the mean Hertzian pressure (p_{avg}) of 0.63 GPa and film temperature (T) of 60°C. With an increase in surface roughness, i.e. a reduction of λ , the friction behaviour changed and the traction curves had different shapes. Associated with the regimes map in Figure 2.29, traction behaviour might gradually move to the elastic-perfectly plastic regime.

More recently, Johnson and Higginson (1988), and Sutcliffe (1991) introduced controlled roughness in friction force measurements. Johnson and Higginson's (1988) experiments were carried out on a regular, circumferentially rippled disc in contact with a smooth disc. To establish the mechanism in micro-ehl, they assumed that a thin film separating the asperity contacts, and this lubricant film sheared at a constant limiting shear stress when it was under a sufficiently high pressure. They checked the non-Newtonian effect of sliding in micro-ehl and concluded that asperity contact is significantly increased with increased sliding speed. Sutcliffe (1991) also used the disc machine, but changed his experimental conditions to control the lubricant film pressure from a Hertzian pressure distribution to a discontinuous pressure distribution. In his experiments, the film pressure between the asperity contacts was much higher than the Hertzian pressure, but the pressure surrounded these asperity contacts was reduced to insignificant, which was similar to the pressure distribution (Figure 2.23) described by Evans and Johnson (1985). He defined the friction behaviour governed by the

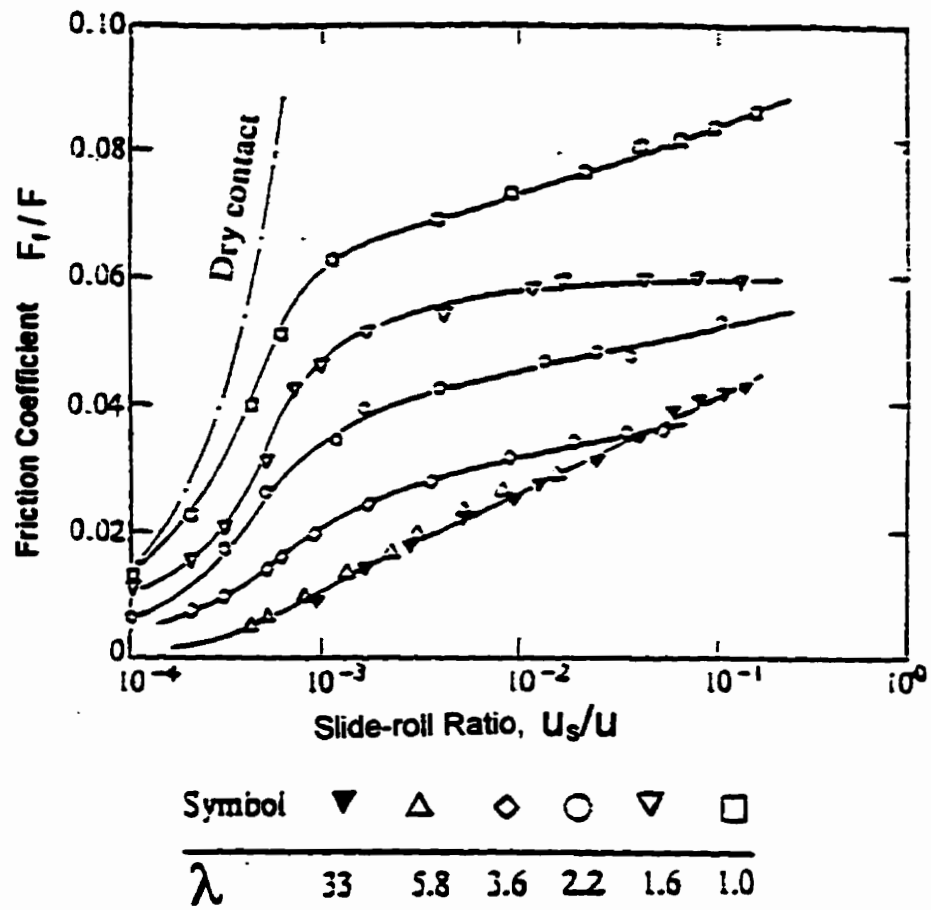


Figure 2.31 Influence of λ ratio on friction coefficient (from Evans and Johnson, 1987)

rheology of the lubricant both within and surrounded asperity contacts as a co-operative micro-ehl, and the friction behaviour governed only by the rheology of the lubricant within the asperity contacts as isolated micro-ehl. He predicted the transition from the co-operative to the isolated micro-ehl for the test conditions with λ ratio between 0.88 and 2. In other words, when $\lambda < 0.88$, the pressure surrounding the asperity contacts was negligible and the friction force was only attributed by the film within the asperity contacts. Sutcliffe (1991) also pointed out that the fluid film did not appear to break down until $\lambda = 0.09$ with the film thickness as small as 8 nm.

Chapter 3 Development of Test Facility

This chapter describes the development of testing facilities used in the present research. A side-slip disc machine was available in the Tribology Laboratory of the Department of Mechanical Engineering, University of Waterloo, but it required some modification. These modifications included the installation of a temperature measurement system, an electrical resistance method for detecting film breakdown, and a data acquisition system consisting of a signal conditioner, digital data acquisition board, and a software package.

3.1 Disc Machine

The ehl of non-conformal contact is very complex. In this contact, typical film thickness is in the order of $0.5 \mu\text{m}$, film pressure exceeds 1 GPa, shear strain rates are up to $4 \times 10^8 \text{ s}^{-1}$, and temperature can rise over 100°C . It is almost impossible to measure these parameters directly in practical machine elements such as gears, cams and rolling element bearings. Therefore, many of the experimental measurements of ehl parameters were made in disc machines.

As mentioned previously, the disc machine provides rolling motion with a small controlled amount of sliding. Fundamental lubricant behaviour can be studied without the excessive temperature rises and associated complex chains of chemical reactions of the lubricant additives on the surface which may occur during pure sliding. Hence, the disc machine is well suited to studying fundamental behaviour and simulating contacts which have mostly rolling motion such as gear teeth and rolling element bearings. On the other hand, the disc machine does not provide a good simulation of pure sliding which occurs in machine elements such as piston rings or flat faced cam followers. However, it may still contribute some useful fundamental insight, including some representation of the initial chemical reactions of the oil additive.

In the present study, a side-slip disc machine similar to that described by Johnson and Roberts (1974) and Johnson and Tevaarwerk (1977) was used to measure the friction (or traction) force in ehl and micro-ehl films and both under approximately isothermal conditions. The lubricating oil was entrained into a nominal point contact of circular contact area and subjected to high pressures and a range of low shear rates while maintaining an almost constant film thickness. The friction force acting through the lubricant film was measured by a transducer consisting of a strain gauged ring. With a suitable analysis, the rheological properties of the lubricant could be estimated for the specific operating pressure, temperature, and shear strain rate.

3.1.1 Main components

The side-slip disc machine apparatus was mounted on a high stand beside an oil supplying tank and a control tower (Figure 3.1). It consisted of systems for lubricant supply, driving, loading, and traction measurement.

- **Lubricant supply system**

The lubricant supply system of the disc machine is shown in Figure 3.2. Lubricant was stored in a tank, which had an electrical heater and a refrigeration unit. A simple feedback control system with an on-off controller allowed the required temperature to be set above or below room temperature.

Lubricant was pumped out from the tank by a gear pump through pipes to an oil filter (17-1704-2 PH8A, Motomaster, Canadian Tire Co., Toronto, Canada). A valve connected to the outlet of the filter determined which side of the contact was supplied with lubricant so that the discs could be run in both directions of rotation. The lubricant was continuously entrained by the rolling motion of discs to form a lubricant film for the friction force measurement. There was a reservoir located under the bottom disc to collect the lubricant which was thrown from

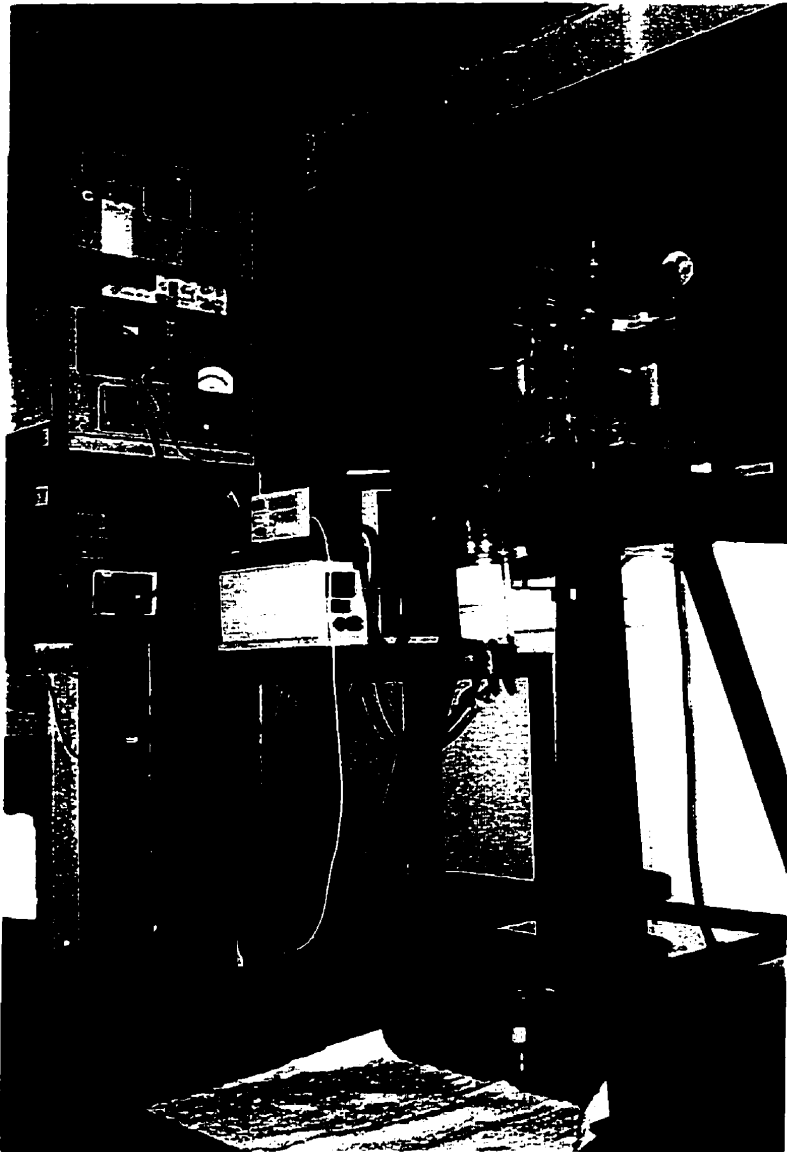


Figure 3.1 Side-slip disc machine

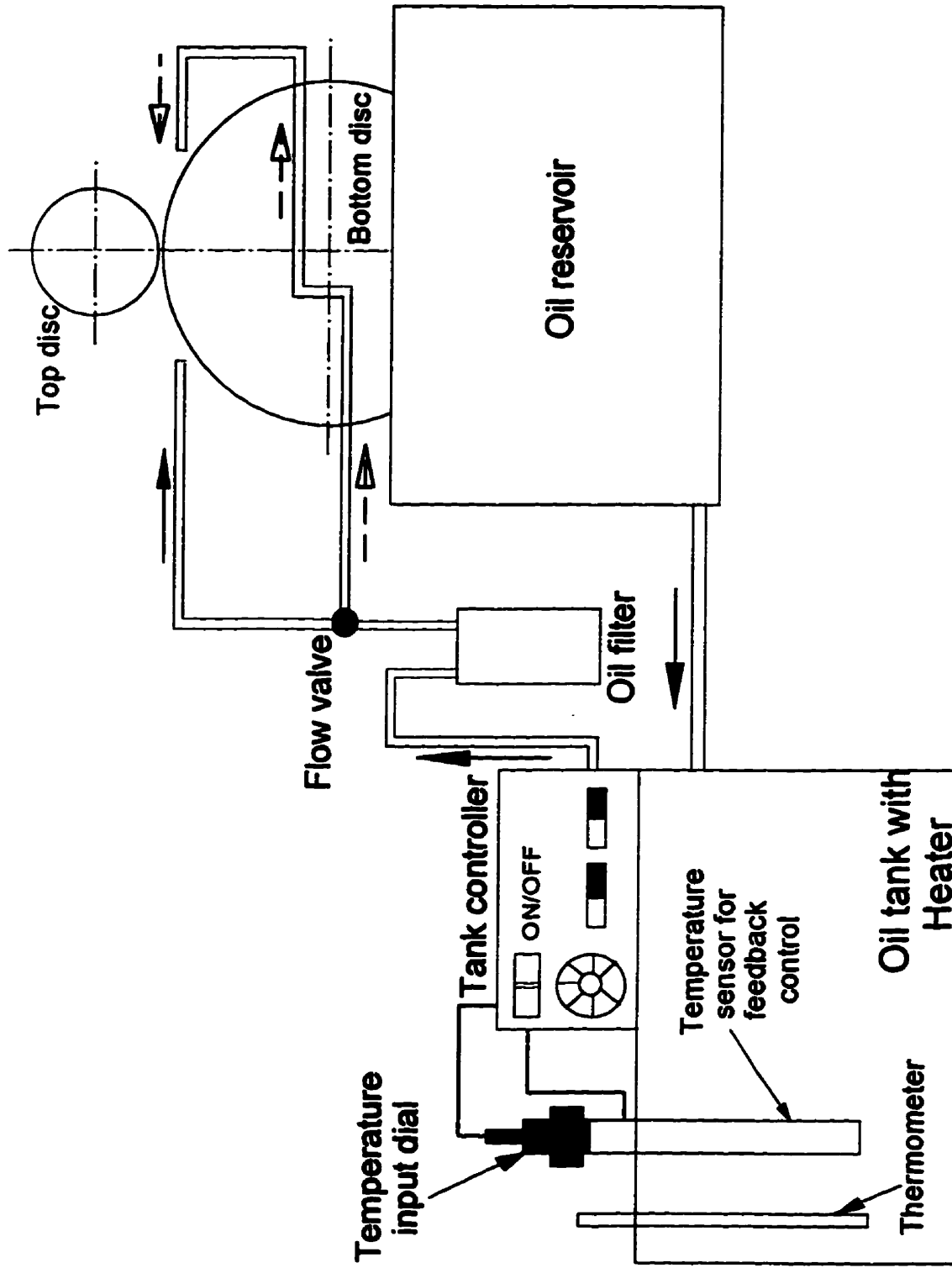


Figure 3.2 Schematic representation of the lubricant supply system

the disc surfaces. Plexiglass shields were placed around the discs to direct oil to the reservoir. After one measurement, the valve of the reservoir was opened and the lubricant flowed back to the oil tank for next measurement.

- **Driving system**

A 746 W (1 HP) DC shunt motor (Reliance Electric Company, Columbus, Ind. 47201, USA) drove the bottom disc which in turn drove the top disc by virtue of friction acting through the lubricant film of the contact. In this way the two discs had about the same surface velocity. The motor had a feedback control system for speed in which the bottom disc rolling speed (u_1) was measured by a photo-electric sensor beam which was cut intermittently by a perforated “target” disc. The aluminium target disc (66 mm in diameter and 2 mm thick) had 20 holes equally spaced around its circumference and was fitted to the shaft of the bottom disc. The pulse rate (ψ) of the photo-transistor was recorded by a frequency counter (John Fluke MFG. Co., Inc., U.S.A.) expressed in hole/s on the counter panel and sent to the motor speed controller where proportional control was exerted. The motor was connected to the bottom disc shaft with a series of timing belts and pulleys giving a speed reduction ratio of 0.67.

The pulse rate (ψ) was converted into the bottom disc surface velocity (u_1) by the following equation

$$u_1 = 2\pi \cdot R_1 \cdot \frac{1}{n} \cdot \psi \quad (3.1)$$

where R_1 - bottom disc radius

n - number of holes in target disc

ψ - pulse rate in holes/s

Inserting the values of $R = 0.071374\text{m}$ and $n = 20$ holes gave the following conversion factor:

$$u = 0.02242 \cdot \psi \quad (3.2)$$

A lateral sliding velocity (v) was obtained by skewing the top disc assembly with a manual gear transmission when the discs were rolling, which is discussed in a subsequent section.

- **Loading system**

The load was applied to the top disc by setting dead-weights on a hanger assembly which consisted of a gimbal and a pair of cables (Figure 3.3). In order to reduce the effect of rotational inertia and mechanical vibration during the skewing of the upper disc at higher loads and rolling speeds, a self-aligned single row tapered roller bearing pivot was provided in the hanger rod and a heavy oil damper was placed below the weights. The bearing pivot separated the upper and lower parts of the weight hanger. The damper supplied strong resistance to vibrations in both vertical and circumferential directions through a plastic disc immersed in a high viscosity gear oil (Industrial Gear Oil 680, Monarch Oil Ltd.). In this way, the weights and the lower part of the hanger remained essentially stationary when the top disc was skewed.

The applied load was equal to the total weight of the hanger, dead-weights and top disc assembly minus the buoyancy force associated with the heavy oil damper. The applied load levels were set by the number of dead-weights.

The mass of the top disc assembly was 1.92 kg and the hanger assembly was 3.321kg. The volume of the part of the hanger assembly immersed in the damper oil was $2.12 \times 10^{-4} \text{ m}^3$. The density of the damper oil was 895 kg/m^3 , the mass of the displaced volume of the oil was 0.19 kg. Each dead-weight had equal mass as 9.94 kg. Therefore the applied load could be calculated from following equation.

$$F = n \cdot (97.51) + 49.55 \quad (3.3)$$

where n - number of dead-weights

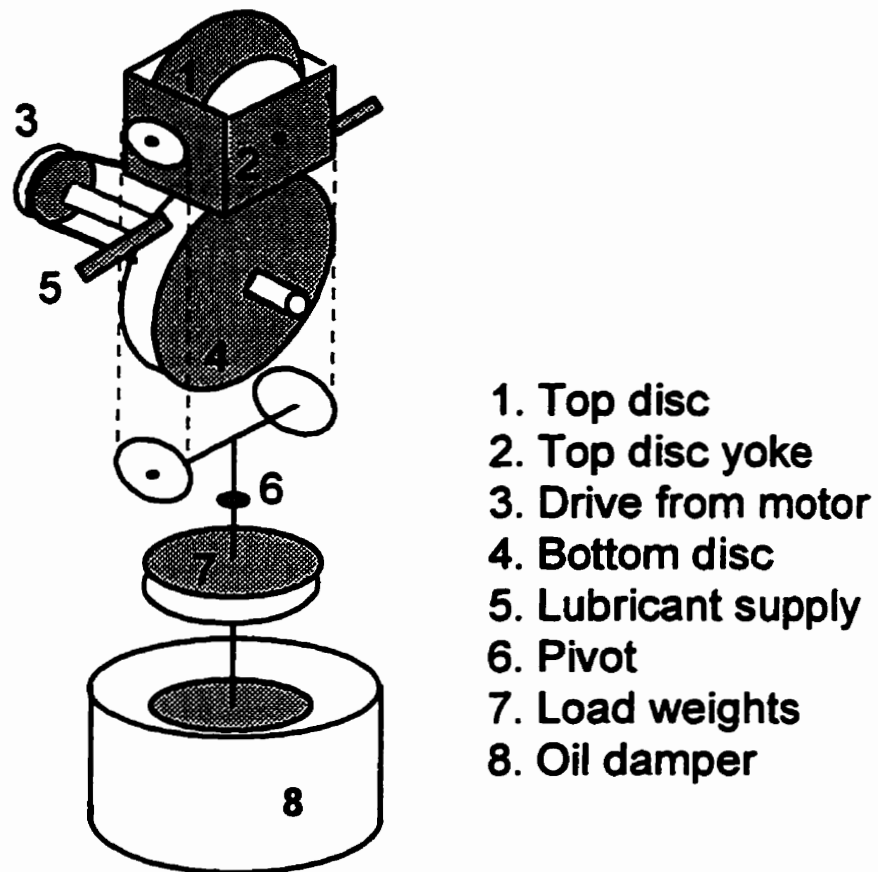


Figure 3.3 Schematic representation of the side-slip disc machine

- **Traction measuring system**

By skewing the top disc slowly about the vertical axis through the contact center over a small angle ϕ , the side-slip velocity v was increased continuously in the direction perpendicular to that of rolling. It sheared the lubricant film between the contact and caused a friction (or traction) force (F_f) which also acted sideways. The variation of F_f with ϕ constituted the basic measurement provided by the disc machine. The F_f was measured by a strain gauge load cell and the ϕ was measured by a direct current displacement transducer (7DCDT-1000, Hewlett Packard, Andover, Mass. JW), referred as DCDT in subsequent of this thesis.

(1) Friction force

The load cell had four strain gauges mounted on a steel ring, two of which were on the outside of the ring and the other two were on the inside. They were connected as a Wheatstone bridge configuration and provided a sensitive measurement. One end of the load cell was fixed rigidly on the top disc support and the other end was fixed on the top disc yoke which was suspended from the top disc support by two sets of leaf springs which held the top disc in place but imposed little resistance to motion in the “side-slip” direction (Figure 3.4a). As the top disc assembly was skewed, the strain gauge output voltage was directly proportional to F_f generated by the shearing of the lubricant film in the side-slip direction. The strain gauge ring was calibrated by placing known weights on a pan which was suspended from a steel cable which went over a pulley and connected to the top disc yoke. The calibration results are shown in Figure 3.4b.

(2) Skew angle

DCDT transducer was held tightly by a split block, which was fixed on the bottom disc support frame (Figure 3.5a). The DCDT plunger was spring loaded against the top disc support frame. As the entire top disc assembly was skewed about the contact center, the

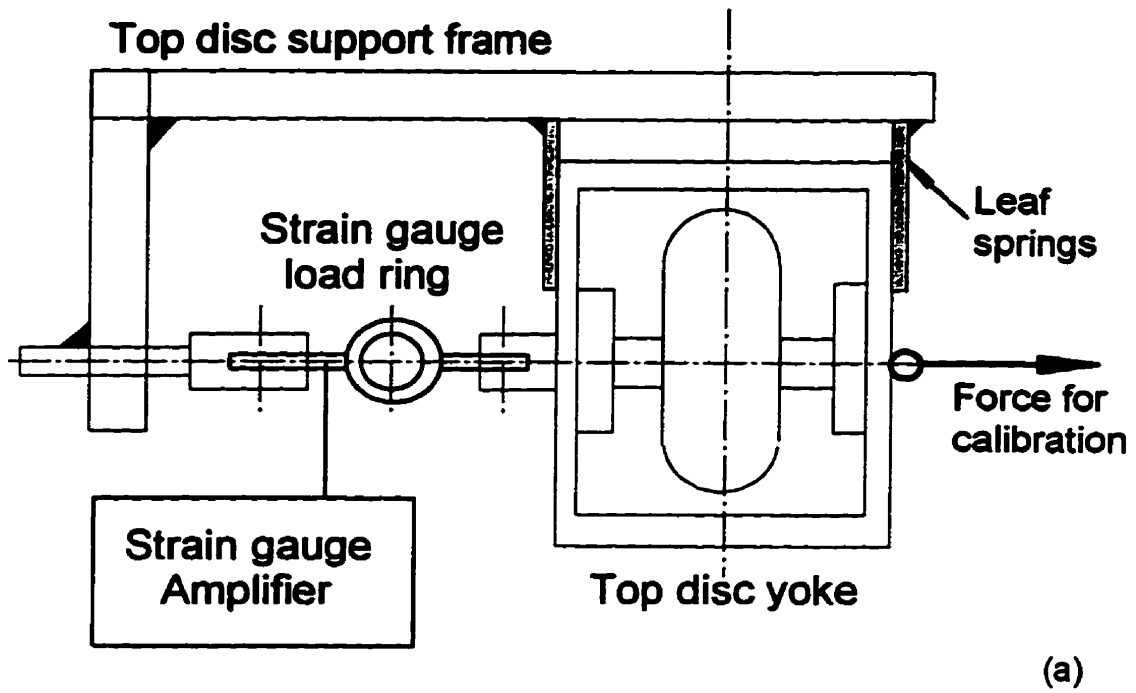


Figure 3.4 Friction force measurement
(a) strain gauge ring load cell

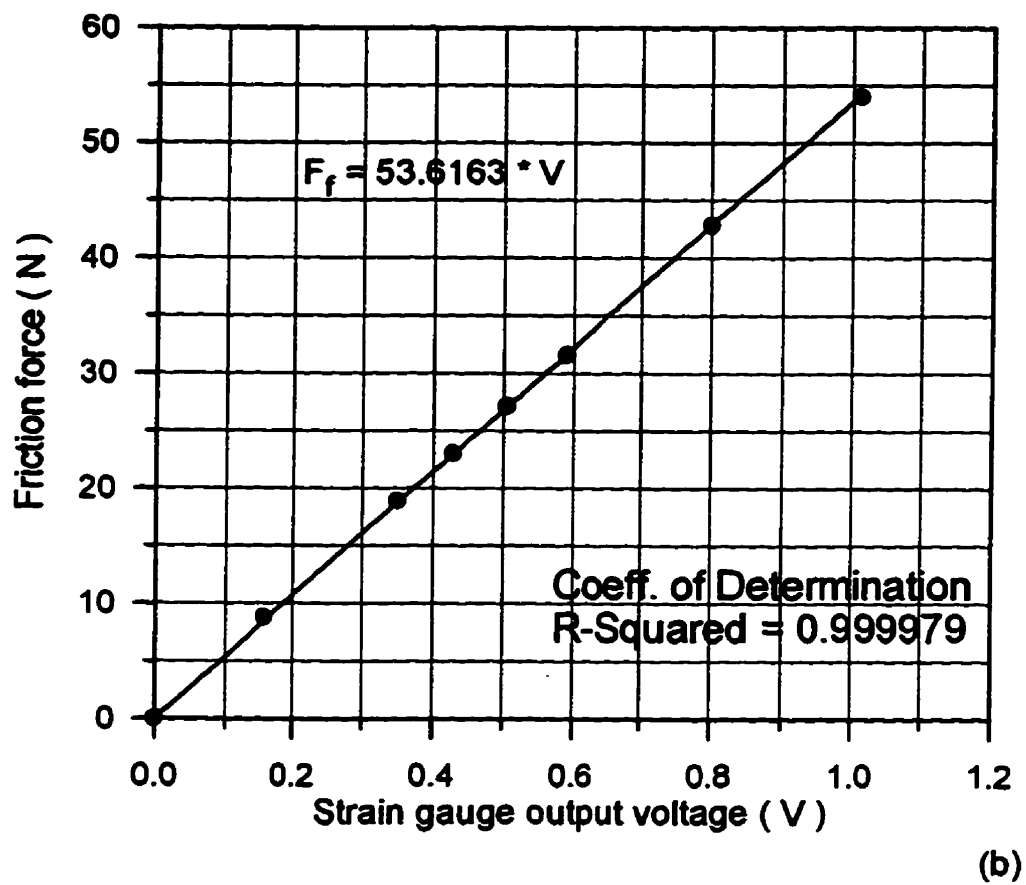


Figure 3.4 Friction force measurement
(b) load cell calibration

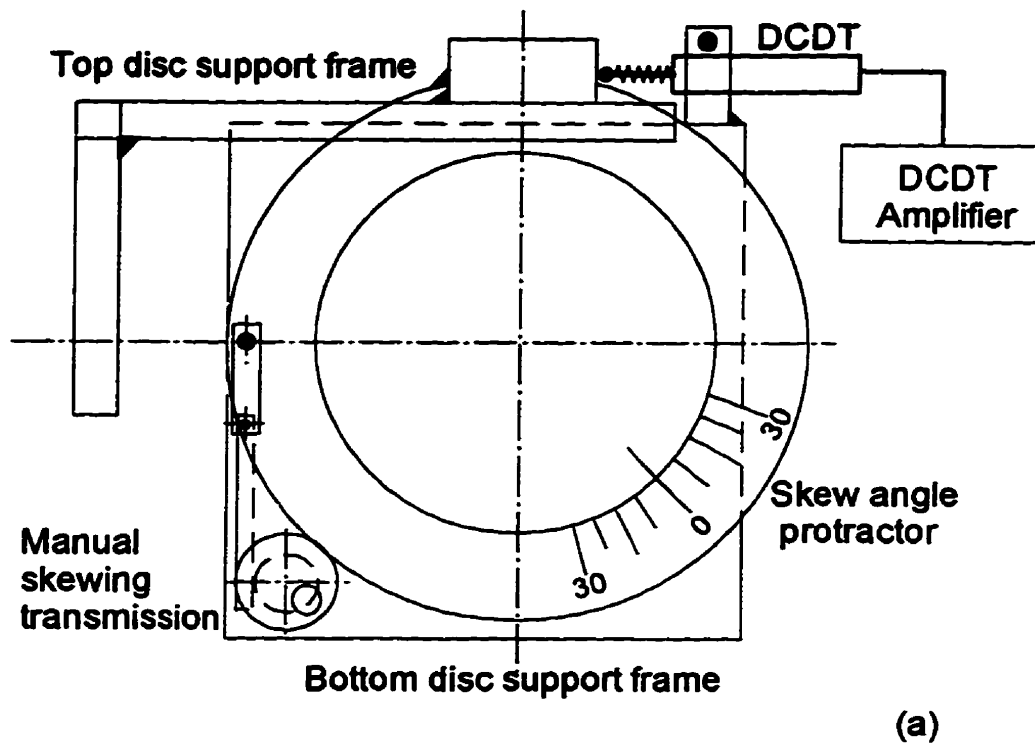


Figure 3.5 Skew angle measurement
(a) direct current displacement transducer

transducer output voltage indicated the variation of the displacement of the measured point on the top disc assembly related to bottom disc supported frame. The measured displacement had linear relationship with the skew angle ϕ when it varied over a very small range. The value of ϕ was measured during the calibration procedure by using a skew angle protractor (Figure 3.5a). The calibration produced a linear relationship as expected (Figure 3.5b). Whenever the DCDT transducer was removed from the holding block or the disc machine was reassembled, a new calibration was performed.

3.1.2 Operating principles

The main objective operation of this disc machine was to measure the F_f when the lubricating film was sheared in the side-slip direction under a high contact pressure at a certain temperature. The kinematics of rolling with side-slip shearing indicated that $v = u_1 \sin \phi = u_2 \tan \phi$ (Figure 3.6a). Since $u = (u_1 + u_2)/2$ and $u_1 = u_2$ throughout small skew angle ϕ , therefore, $v = u \cdot \tan \phi$, which agreed with the expression given by Johnson and Roberts (1974). For the disc machine contact, the rolling speed (u) equaled the entrainment velocity and a lubricant film with an almost constant central film thickness (h_c) was generated over the contact area. The particular nominal point contact geometry of the disc machine had a Hertzian contact radius of a and area of πa^2 .

Similar traction force measurements on side-slip disc machine were described by Johnson and Roberts (1974). Theoretical formulae of side-slip shearing were developed for both pure Newtonian lubricant and pure elastic lubricant films.

(1) For a pure Newtonian fluid film, the shear strain rate $\dot{\gamma}$ (Figure 3.6b) can be approximated as v/h_c , where h_c can be calculated by Eq. 2.24. The shear stress is thus constant and equal to $\tau = \eta \cdot v / h_c$. Integrating shear stress over the contact area gives the F_f , which acts at right angles to the rolling direction.

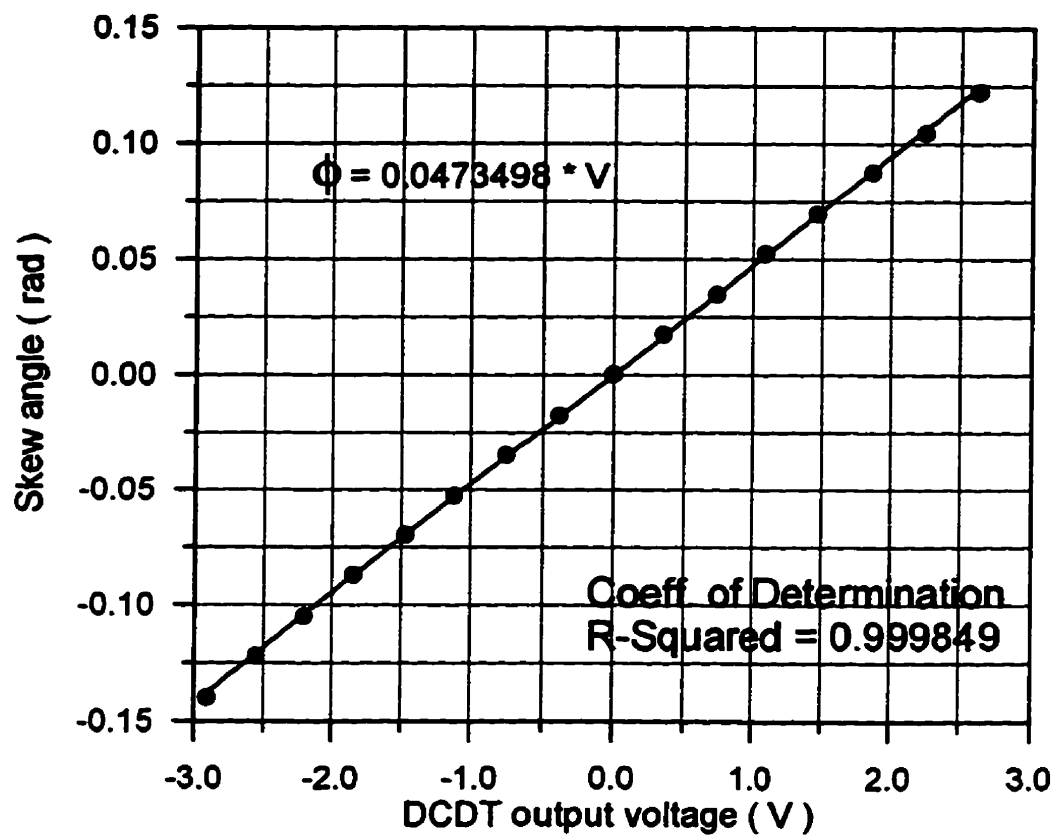


Figure 3.5 Skew angle measurement
(b) DCDDT calibration

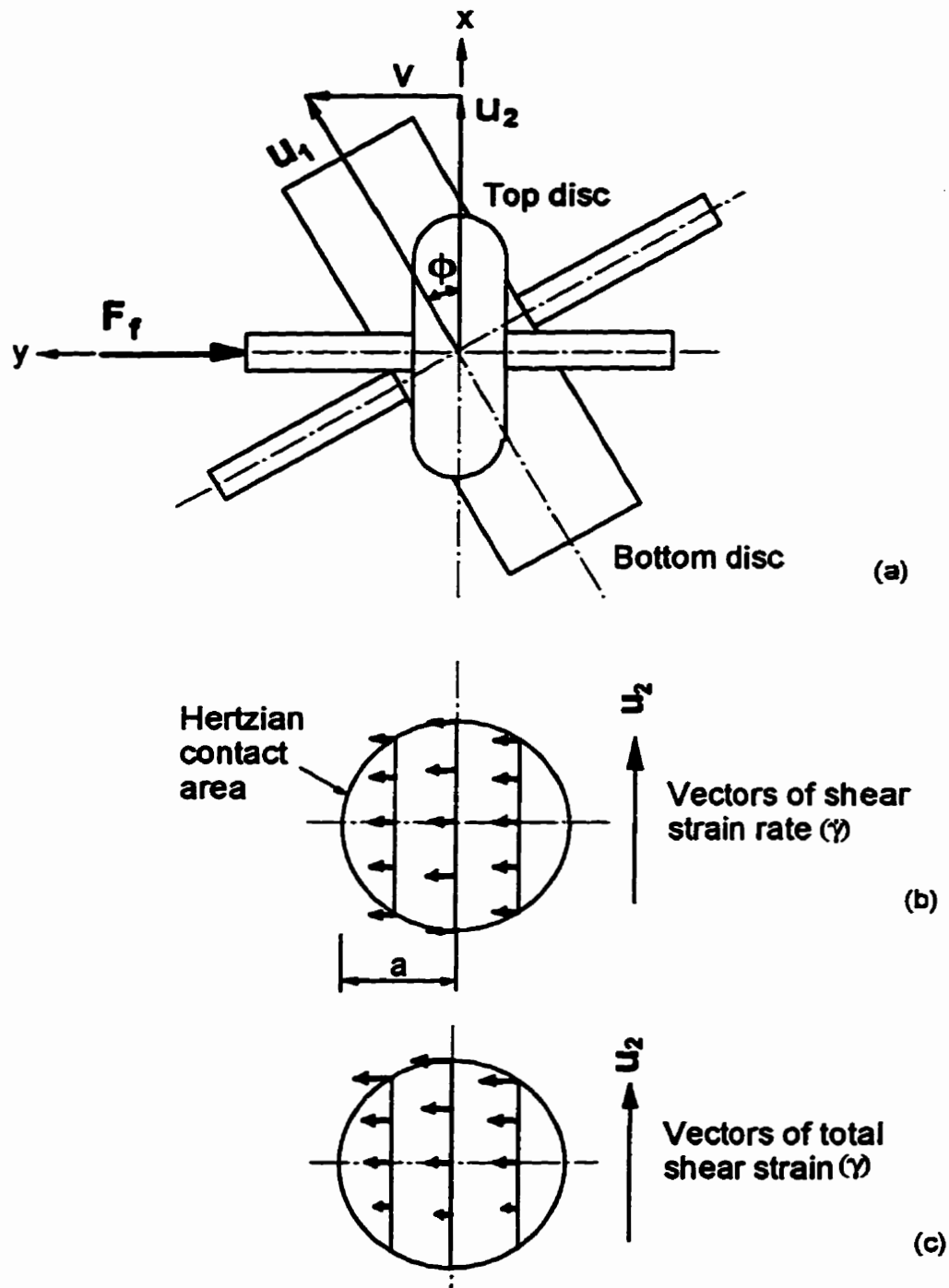


Figure 3.6 Rolling with side-slip kinematic principles on disc machine
 (a) arrangement of discs
 (b) vectors of shear strain rate in contact zone
 (c) vectors of total shear strain in contact zone

$$F_f = \eta \cdot \frac{v}{h_c} \cdot \pi a^2 \quad (3.4)$$

(2) For an elastic solid-like film, the shear stress is proportional to the shear strain, $\tau = G \cdot \gamma$, where, $\gamma = \int_0^t \dot{\gamma} \cdot dt = \int_{-\sqrt{a^2-y^2}}^x (v/h_c) dx/u$ (Figure 3.6c). Integrating the shear stress over the contact area gives

$$F_f = G \cdot \frac{8a^3}{3h_c} \cdot \frac{v}{u} \quad (3.5)$$

However, real ehl films was neither pure Newtonian flow nor pure elastic lubricant deformation. The experimental approach was to measure F_f versus ϕ and subsequently develop a plausible and consistent rheological model of the lubricant flow.

In a typical disc machine friction force measurement (Figure 3.7), ϕ was varied over the range of ± 0.125 rad as specified by the protractor scale on the top disc assembly. When ϕ was small, $v/u \approx \phi$ and thus plotting F_f vs. ϕ showed the friction force behavior as a function of slip-roll ratio. When ϕ is varied through the point of pure rolling at $\phi = 0$ the sliding direction changes causing the direction of F_f to change as well. The measured F_f vs. ϕ , or traction curve, had a sigmoidal shape. Repeating the above act for the opposite direction of rolling gave another measured sigmoidal shape and the cross-over point allowed the origin of the traction curve to be determined exactly. The symmetry of this “traction plot” (Figure 3.7) in the four quadrants provided a method to check the alignment of the disc machine.

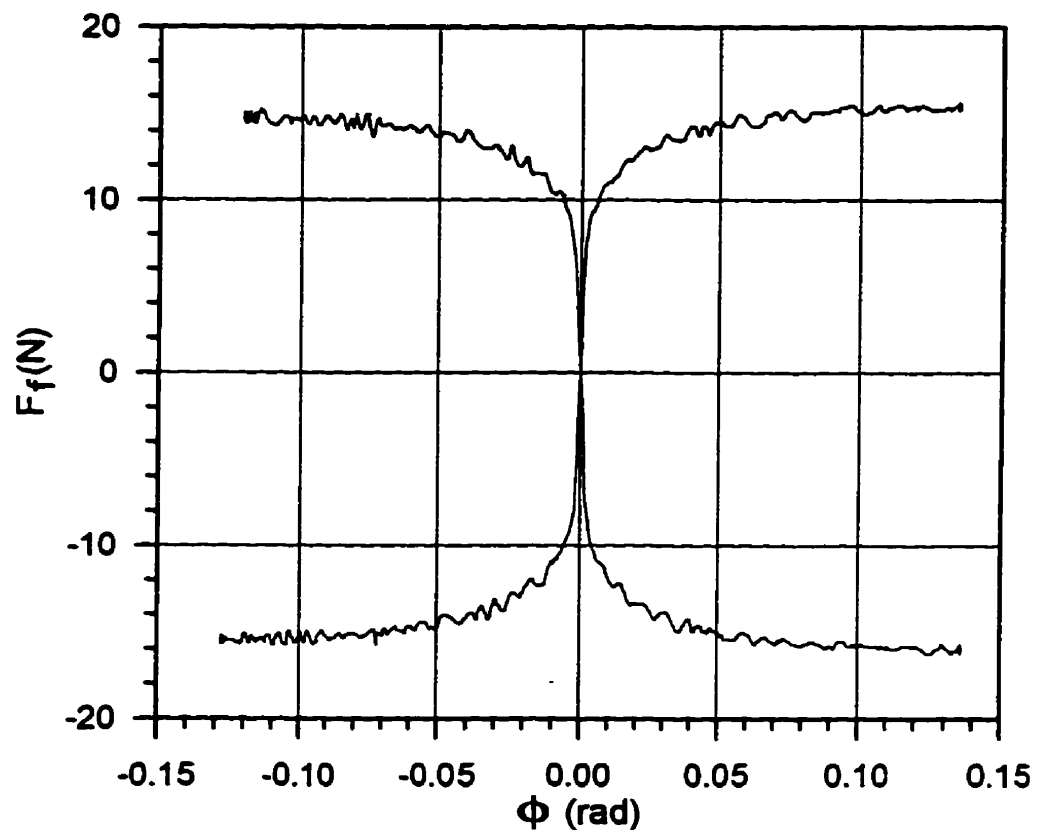


Figure 3.7 Typical traction plot from side-slip disc machine

3.2 Temperature Measurement

Temperature control was very important for an isothermal traction measurement. The lubricant supply system should provide the contact with a lubricant at a known constant temperature and the rise in the lubricant film temperature in the contact zone should be negligible.

3.2.1 Temperature of supplied lubricant

Lubricant supply system of the side-slip disc machine was designed to control and provide the lubricant at a constant temperature during the experiment. The feedback control system with an on-off controller for the heater allowed the tank temperature to be set to a specific value above room temperature. However, the lubricant temperature might have changed when it was pumped out from the tank to the contact. In order to keep the operator informed of the real lubricant temperature, additional temperature checking points were needed in the lubricant supply system.

One thermometer was inserted in the oil tank to get the actual reading of the tank lubricant temperature at any time. Another crucial point to measure the temperature was the entry to the contact. A thermocouple was fixed to the outlet end of the oil supply pipe with its tip immersed in the lubricant outside the jet. If the lubricant temperature dropped during the flow from the tank, then the tank temperature was adjusted to a relatively higher value. Conversely, if the temperature increased for some reason, the tank temperature could be preset at a lower value.

Ensuring that lubricant was supplied to the inlet zone at a known constant temperature was the first step in an isothermal experiment. The next step was keeping the lubricant film temperature constant in contact zone.

3.2.2 Contact zone temperature measurement

As discussed previously, the inlet temperature of the lubricant could be used to give the viscosity in an isothermal ehl formula for film thickness. In a disc machine with ehl conditions close to pure rolling, the appropriate inlet lubricant temperature was likely to equal the average of the disc surface temperature just prior the entering the contact, while, the inlet shear heating associated with the flow field was negligible. Although, the disc surface temperature could also be elevated because of the accumulation of heat from side-slip shear in the contact zone, the steel disc was such a good heat conductor and an elevated surface temperature would require considerable generation of heat within the film. When the side-slip velocity was low, there should not be significant side-slip shear heating in the contact zone. To measure the surface temperature, a thermocouple was placed in light contact with the moving bottom disc surface. But two important things of contacting thermocouple temperature measurements had to be considered in this case: one was the placement and the other was the load between the thermocouple tip and disc surface.

(1) To get an accurate reading, the thermocouple should be placed in the inlet zone as close as possible to the contact zone. But the geometry of the apparatus itself and the size of the thermocouple tip made this difficult. The closest point to measure the inlet zone temperature was along the central line of the contact zone in rolling direction and the distances from the center of contact was 5 mm (Figure 3.8). When the disc machine was kept running, the disc surface temperature changed gradually from the room temperature towards that of inlet oil temperature, until a stable temperature was obtained. Under the same load and kinematic conditions, the outlet zone temperature was checked with the same thermocouple by running the disc machine in the reverse direction. The outlet zone temperature did not show the difference from the inlet zone temperature. This finding suggested that there was no significant accumulation of heat from side-slip shear in the contact zone.

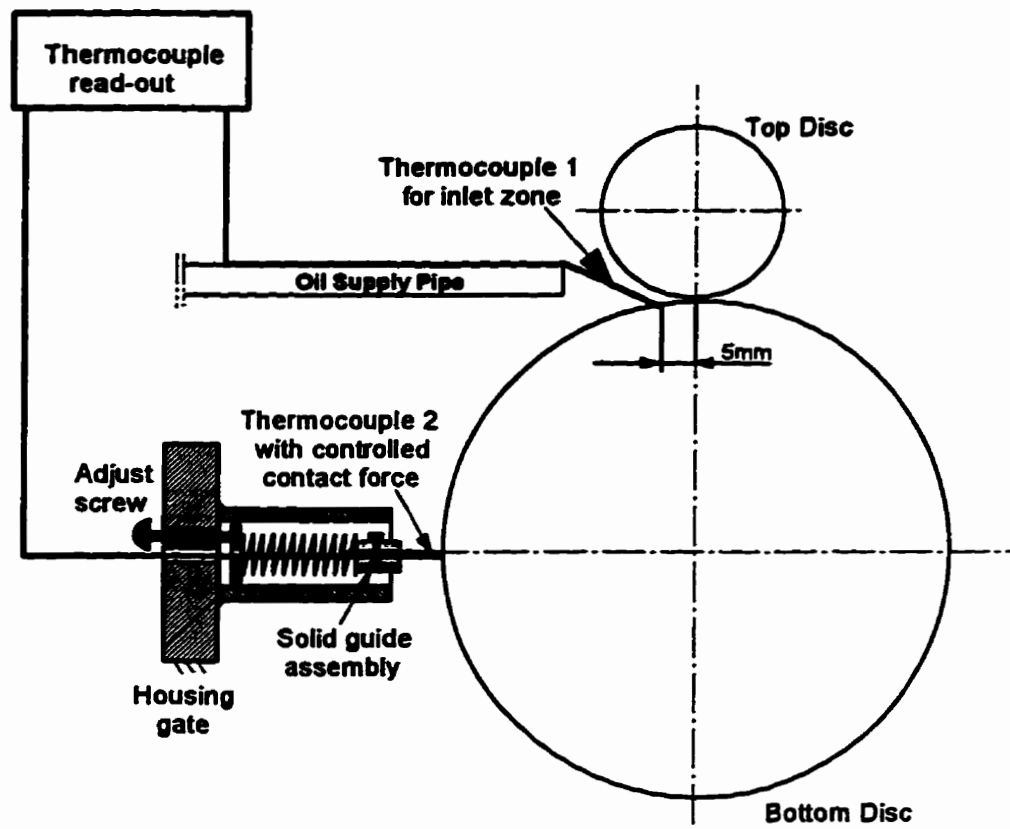


Figure 3.8 Schematic representation of disc surface temperature measurement

(2) Many early papers (Cameron, 1966; Jefferis and Johnson, 1968) discussed how a “surface contacting” and embedded thermocouple could provide the same estimate of the disc surface temperature. For a contacting thermocouple, a suitable force must be determined to push it against the disc surface with sufficient force to measure surface rather than lubricant temperature, yet not such a large force that would cause any false temperature elevation due to friction heating. Since the contact force was not known for the inlet thermocouple (No. 1 in Figure 3.8), a second contacting thermocouple was installed.

A device was designed to push the thermocouple against the disc surface with a controlled contact force (Figure 3.8). The spring constant was determined before it was mounted in the device. The contact force was increased in increments of 3N from the point where the thermocouple seemed first to touch the disc surface very lightly. Unfortunately, due to the space limitation, this thermocouple could not be placed very close to the contact due to the space problem, and to avoid any possible disc surface damage, it was moved 5 mm laterally along the axis of the bottom disc. Thus, this thermocouple provided information on a suitable contact force but would only detect substantial heating of the disc surface.

The test results gave quite a wide range of contact force to obtain a stable and accurate temperature reading before a sudden increase in temperature caused by friction heating between the thermocouple tip and the disc surface at about 15N (Figure 3.9). During the friction force measurements, this device was used along with the inlet zone thermocouple to estimate surface temperature. When the disc machine was kept running, the whole disc surface slowly reached the desired temperature and both thermocouples gave quite stable temperatures. Usually, the thermocouple with controlled contact force recorded a temperature not greater than 1°C below that of the inlet zone thermocouple, although it was located in a distance from contact zone and was offset from the contacting part of the bottom disc by about 5 mm.

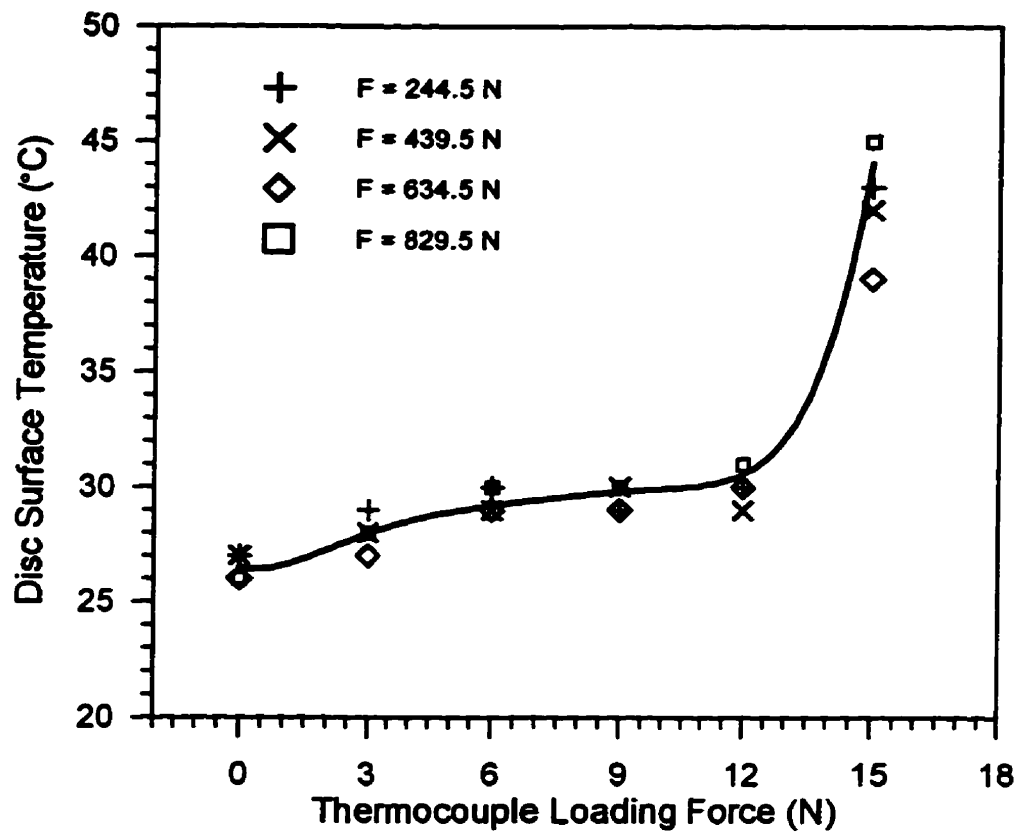


Figure 3.9 Influence of thermocouple contact force on disc surface temperature

Despite these temperature measurements, it was still possible that inlet shear heating could elevate the oil temperature. The evidence of this heating might be removed by heat transfer by conduction and convection. When the film thicknesses were calculated, a further calculation was performed to estimate the influence of inlet shear heating as discussed in a subsequent section.

3.3 Electrical Resistance Method for Detecting Film Breakdown

The objective of adopting an electrical resistance measurement technique was to check whether the ehl formula (Eq.2.24) of Hamrock and Dowson (1977) was appropriate for the present experiments. A drop in film resistance was expected near $\lambda = 3$. Providing this occurred, the tribological conditions for subsequent experiments could be selected to be in the ehl and isolated micro-ehl regimes. No attempt was made to link electrical resistance with the asperity interaction of mixed film lubrication. Such work has been attempted by others (Furey, 1961; Johnson and Higginson, 1988; Yang, et.al., 1996), but it was considered beyond the scope of the present investigations in which friction force was measured to study rheology of lubricant films.

Cameron and his coworkers (1958) used the electrical resistance measurement technique in an attempt to determine the ehl film thickness. Higher resistance occurred between two rolling surfaces when a lubricant film separated them and the resistance level correlated to some extent with its thickness. However, the application of this technique became extremely difficult when the fluid film was very thin, because asperity contact made the electrical resistance drop rapidly instead of decreasing proportionally to the average film thickness. On the other hand, thin surface layers might sometimes form on the contact surfaces and prevent an expected drop in resistance when the lubricant film had broken down. Therefore, the electrical resistance method was considered difficult to apply with precision, yet could be applied to provide useful approximate information regarding the existence of continuous fluid film lubrication (Kato, et al., 1993).

3.3.1 Electrical resistance circuit

The electrical resistance measurement technique was easy to implement. A simple circuit (Figure 3.10) was built up following the design of Furey (1961). The circuit consisted of a power supply battery, two resistors ($R_1 = 1.0 \times 10^6 \Omega$ and $R_2 = 1.0 \times 10^4 \Omega$), and a voltmeter readout. This circuit minimized the occurrence of electrical discharge through the oil film by lowering the applied voltage. When a battery with the input voltage of $V_i = 1.5 \text{ V}$ was used, the maximum measured output voltage was $V_o = 15 \text{ mV}$. The top disc was electrically isolated from the bottom disc by putting isolated epoxy resin rings around the outer race of the top disc supported bearings. The bottom disc was electrical connected to the resistor R_2 through the stand of the disc machine. A carbon brush acted as a pickup, which was spring-loaded against one end of the top disc shaft and electrical connected the top disc to the other end of R_2 .

At a certain load level and temperature, the V_o varied with the electrical resistance of the contact between the two discs. If the disc machine was running at a sufficiently high rolling speed and the two discs were separated by continuous fluid film, the V_o approached 15 mV and no electric current flowed across the contacts. If the rolling speed was low and asperity interactions occurred between the contact surfaces, then the film resistance was reduced and V_o dropped as the electric current began to flow across the contact.

3.3.2 Output voltage

An example set of unfiltered V_o signals was measured and plotted as waveform graphs through a computer program, which simulated an oscilloscope (Figure 3.11). The MCT 5 base stock oil was used with the applied load of $F = 244.5 \text{ N}$ and smooth surface discs. The plots showed visible oscillations superimposed on the average V_o . As u varied from 0 to 4 m/s, the V_o was read from a digital voltmeter as an average value given by a built in processor. The measured V_o for various rolling speeds (u) are listed in Table 3.1. If the h_c

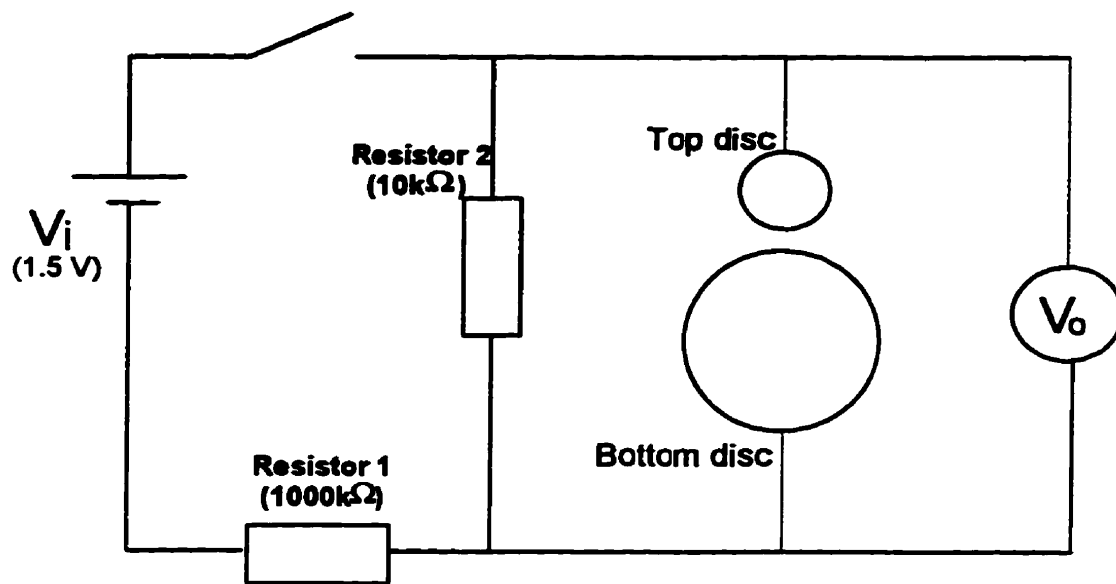


Figure 3.10 Electrical resistance circuit for detecting film breakdown

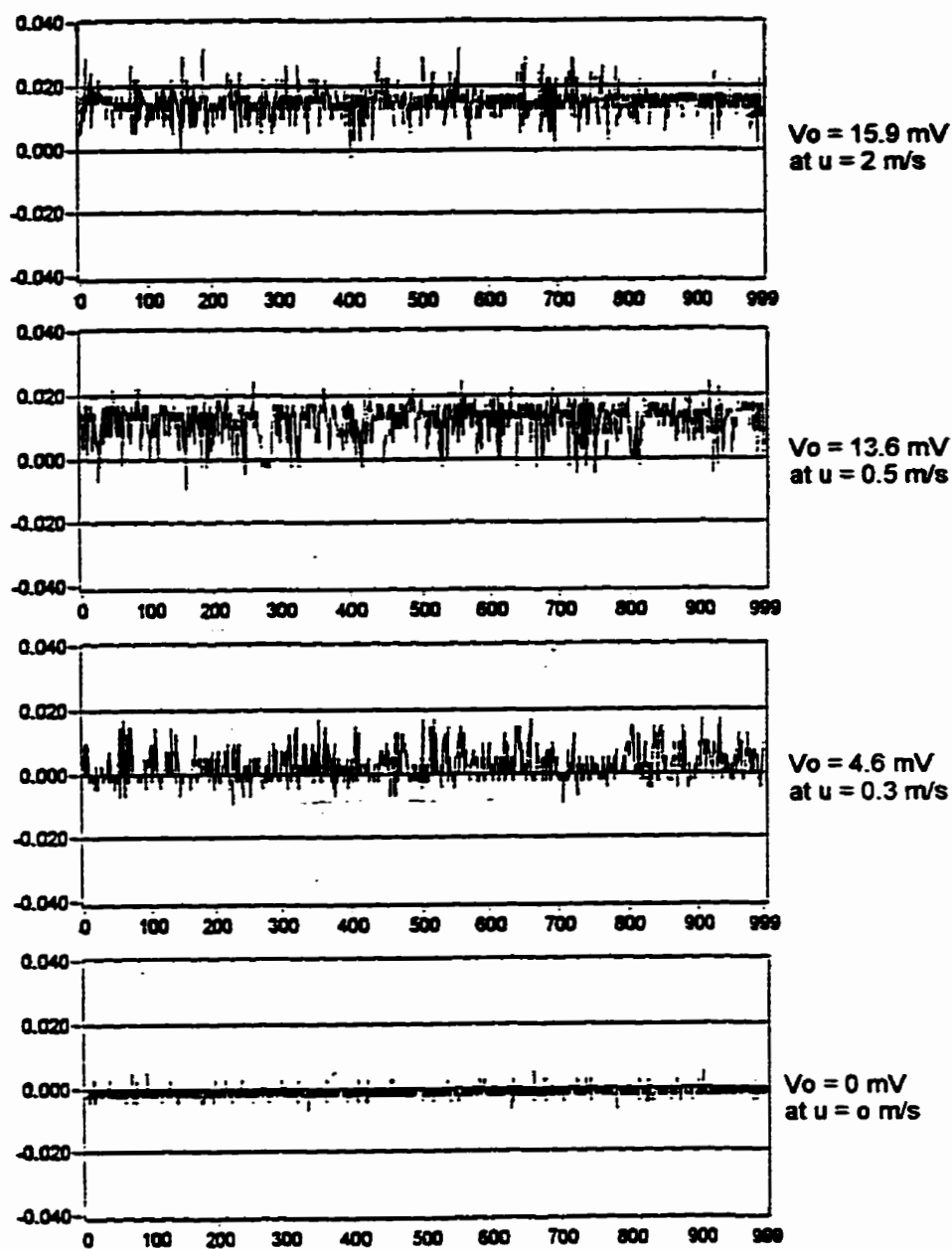


Figure 3.11 Signals of output voltage from electrical resistance circuit
(for MCT 5, $F = 439.5 \text{ N}$ and $V_i = 1.5 \text{ V}$)

was considered together with the u , the full scale V_o output region represented $u > 2.5$ m/s, where $h_c > 0.4$ μm which was three times of composite surface roughness ($\sigma_c \approx 0.1\mu\text{m}$). Below this speed, the film thickness was reduced and the asperity interaction started to occur. The V_o decreased to zero when $u < 0.6$ m/s, corresponding to the $h_c \approx 0.15$ μm , which was comparable with the surface roughness. Thus, more asperity interactions occurred and the full ehl film was replaced by micro-ehl.

**Table 3.1 Measured V_o for various u
(for MCT 5, $F=244.5\text{N}$, smooth disc)**

u (m/s)	V_o (mV)	h_c (μm)
0.0	0.0	0.0
0.2	0.0	0.0835
0.4	0.0	0.1329
0.6	0.0	0.1743
0.8	0.1	0.2114
1.0	0.2	0.2455
1.1	0.375	0.2617
1.2	1.225	0.2774
1.3	2.525	0.2926
1.4	4.235	0.3075
1.5	6.775	0.3221
1.6	9.325	0.3363
1.7	11.85	0.3503
1.8	13.25	0.3639
1.9	14.05	0.3774
2.0	14.65	0.3906
2.5	15.75	0.4535
2.8	15.9	0.4893
3.0	15.9	0.5125
4.0	16.2	0.6214

V_o versus u plots, for the data from this example and for the other three loads of 439.5 N, 634.5 N and 829.5 N, showed as sigmoidal functions (Figures 3.12). From these plots, it was easy to find the asperity interaction starting point, where the lubricant additive might have significant influence on friction between contacts. Eventually, these plots could be used to decide the tribological conditions for the friction force measurements in the present study.

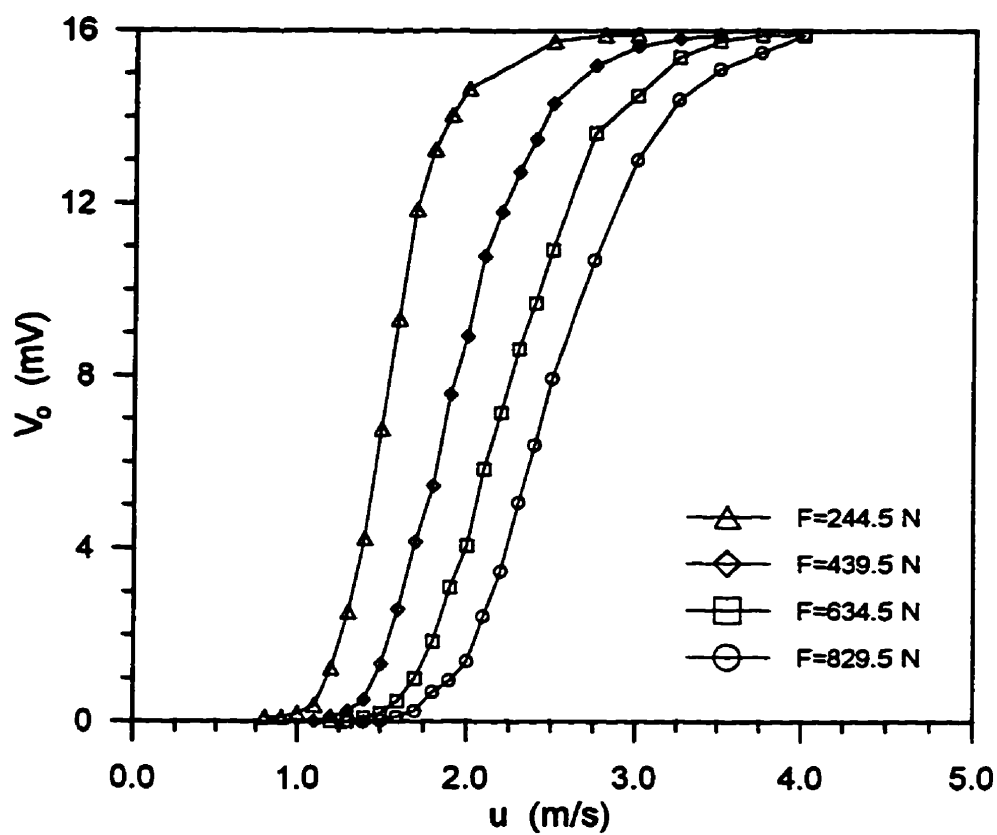


Figure 3.12 Typical plot of output voltage versus rolling speed for various loads
($T=30^{\circ}\text{C}$, $V_i = 1.597\text{ V}$, $V_o \text{ max} = 15.9\text{ mV}$)

3.4 Data Acquisition and Processing

The most important modification of the disc machine for the present research was an installation of a computer data acquisition system. Previously, friction force and skew angle measurements from the disc machine were recorded on an x-y plotter. The computer data acquisition system facilitated recording, storing and processing of the experimental data. A software package was chosen to implement the data acquisition and processing.

3.4.1 Data acquisition system

- **Hardware**

A PC-LPM-16 data acquisition hardware board (National Instrument Corporation, Austin, TX, USA) was selected and plugged into the personal computer. It was a low power multichannel input and output board with 16 digital I/O lines which were useful in high resolution applications. A hardware configuration was used to set certain analog inputs and outputs, such as polarity range, jumper setting, etc. Then, a software configuration was set up as a currently selected device in the main lists (Figure 3.13) and as the default set-up for the friction measurement.

The I/O connector for the PC-LPM-16 was located on the back panel of the board. Two analog signal input channels were connected with disc machine: one for F_f from the strain gauge load cell through an amplifier, and the other for ϕ from the DC displacement transducer. A ground pin on the connector was chosen for analog input ground signals.

- **Software**

The computer software package used in the present study was LabVIEW, standing for Laboratory Virtual Instrument Engineering Workbench (National Instruments Corporation, Austin, TX, USA). It worked within Microsoft Window 3.1 operating system. LabVIEW uses a graphical programming language to create programs in block diagram form for

DEVICE SELECTED

Device #:

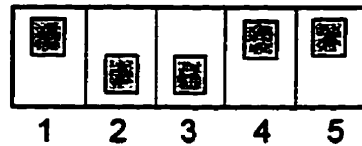
Device Name:

Base Address:

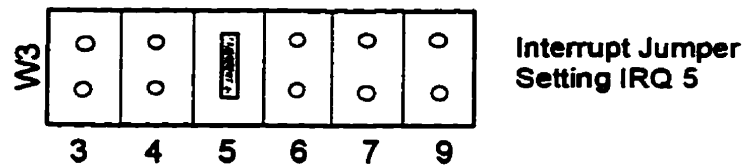
DMA Channels:

IRQ Levels:

Base I/O Address Switch Settings



Interrupt Selection



ANALOG INPUT

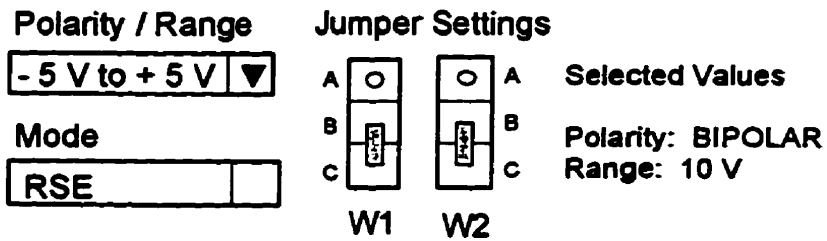


Figure 3.13 Configurations for PC-LPM-16 data acquisition system

scientific computation, process control, and measurement applications. This program allows “virtual instrument” (VI) to be constructed which attempt to imitate actual instruments. Libraries of functions and tools are available to build up the VIs. The most valuable feature of LabVIEW is its ability to acquire data from almost any sources.

A computer data acquisition system was set up for the disc machine and included some VIs for controlling data acquisition and data processing for the friction force measurements.

- **Specific application programs**

Analog input signals from the disc machine were recorded in a waveform graph and stored in a digital data file. A program (AITOWAVE.VI) was written to perform this process. The graphical program had three features: front panel, block diagram and hierarchy diagram (Figures 3.14a, 3.14b and 3.14c) as discussed below.

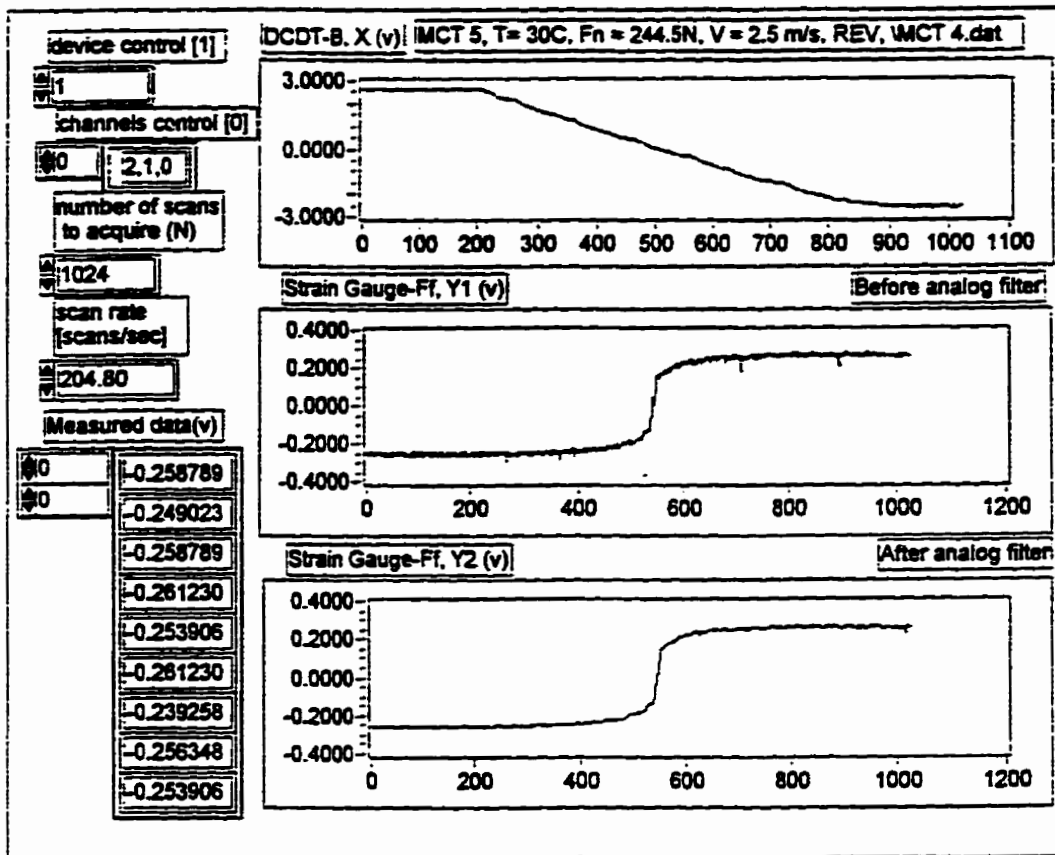
The “front panel” was an operating interface which provided a visual image that resembled an instrument front panel. The commands to acquire signals were input from controllers on the front panel in a manner similar to select settings on a conventional voltmeter or a plotter. The output data were stored in tables and presented in graphs. The graphs were similar to those from a plotter, but the stored discrete data allowed scale changes to be performed long after data collection.

In the front panel of AITOWAVE.VI (Figure 3.14 a), the PC-LPM-16 (*Device control*) and its three working channels (*channels control*) should be selected first. Two channels (one with an analog filter and one without it) collected discrete voltage from the strain gauged load cell which measured the friction force. The last channel collect discrete voltages from DCDT. Then, the total scan number (N) and the scan rate (f_s) were set considering the friction measuring operation time and the resolution of signals. At the chosen interval, the continuous analog signal was converted to a series of digital values. These discrete values were also

Dwave.vi
10/13/95 12:51 PM

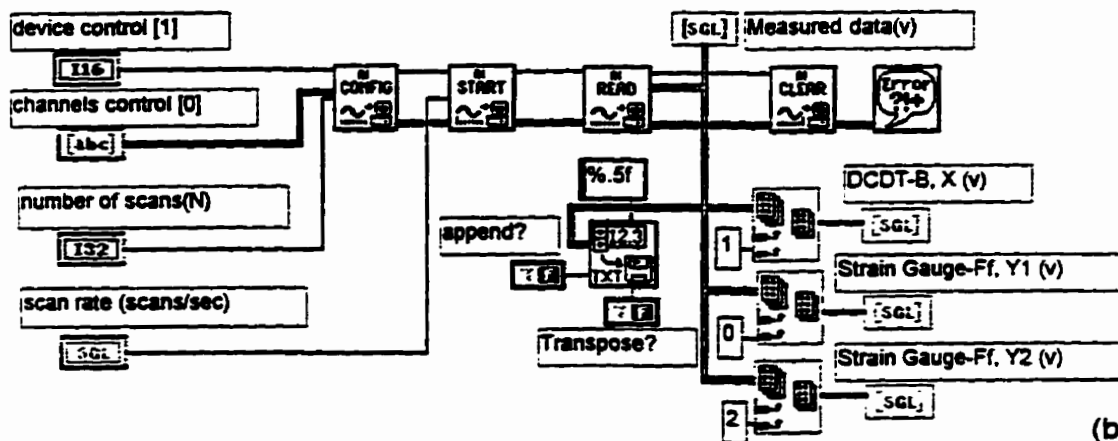


Front Panel



(a)

Block Diagram



(b)

Figure 3.14 Graphical program "AITOWAVE.VI" for traction measurement
(a) Front Panel (b) Block Diagram

Dwave.vi
10/24/96 11:27 AM

Position in Hierarchy

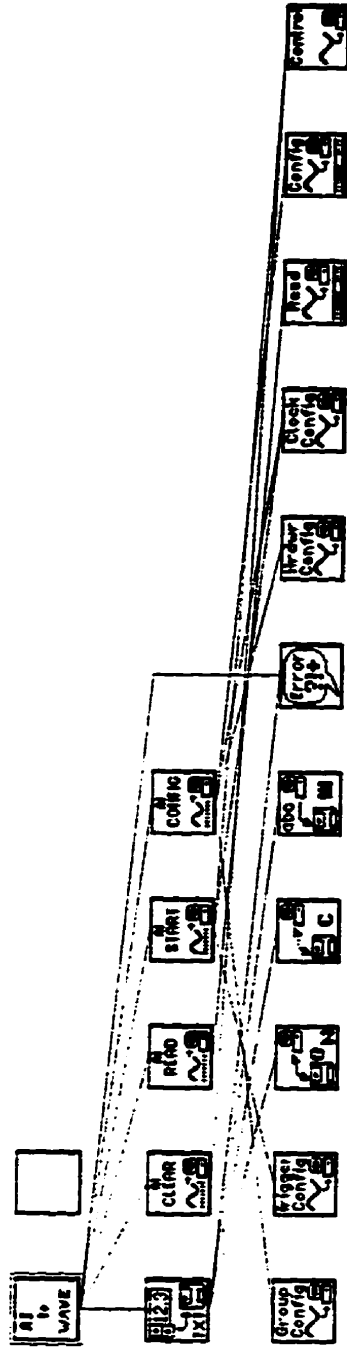


Figure 3.14 Graphical program "AITOWAVE.VI" for traction measurement
(c) Position in Hierarchy

plotted as three “waveform” graphs of voltage versus the sequential data point number (0 – 1023). The operating conditions and the output file name were labeled at the top of the front panel.

The block diagram was a pictorial representation, i.e. a logical flow chart of the program which was created on the front panel. It was constructed by linking descriptive program icons that performed specific data acquisition functions. A LabVIEW program received instructions from its block diagram which transferred data, performed specific functions and controlled the order of execution.

In the block diagram of AITOWAVE.VI (Figure 3.14b), all the “controllers and indicators” from the front panel were automatically shown as terminals. They were linked with some specific operation sub-programs, which were sub-VIs and shown as icons (AI CONFIG, AI START, etc.), to construct the desired logical relationship of the program and to control the collection of the analogue input signals.

The hierarchical diagram was a tree of all VIs and sub-VIs currently being utilized. Each VI had its icon in the hierarchical diagram. When the main VI was open all the corresponding VIs had to be loaded in the memory. VI hierarchy describes a map showing the interaction and sequencing of an application.

In Figure 3.14c the AITOWAVE.VI was the currently used VI which was highlighted. It required five sub-VI to complete the data acquisition. The five data acquisition sub-VIs needed more sub-VIs to support their work. Therefore the hierarchical diagram for this program shows three levels of VIs which were connected by lines.

3.4.2 Power spectrum analysis and sampling frequency

As mentioned above, data acquisition involves digitizing analog signals. A number of general references (Bendat and Piersol, 1980; LabVIEW Analysis VI Reference Manual, 1993; Johnson, 1994) provided some background information of a digital signal processing. When continuous analog signals are digitized at a constant time interval Δt , the corresponding sampling frequency is $f_s = 1/\Delta t = n/t$, where n is the number of samples and t is the total time. The value of f_s can be selected following the Nyquist criterion, which indicates that f_s must be at least twice as large as the highest frequency component in the input signals, in order to avoid its misrepresentation known as aliasing. In other words, for a specified f_s , the highest possible frequency component which can be represented properly is the corresponding “Nyquist frequency”.

$$f_n = \frac{f_s}{2} \quad (3.6)$$

To select a suitable f_s , a power spectrum analysis of the signals provided some guidance. Power spectrum analysis is performed a fast Fourier transformation (FFT) to transform linear time sequence signals into the frequency domain. This transformation can be used to show individual frequency components of analog signals that can be related to measured physical phenomenon. Furthermore, this analysis can be used to help avoid either a too low sampling rate which may cause aliasing or an unnecessary high sampling rate which is often expensive.

In the present study, the power spectrum analysis for the data acquisition and digital processing was performed by a program, PS.VI. This program read recorded data representing F_f or ϕ from a spreadsheet file written by AITOWAVE.VI. It chose a series of data by using an index array function and sent it to the sub-program, POWER SPECTRUM.VI. The time based data were transformed into the frequency domain, and the power spectrum (square of the amplitude of the transformed individual frequency component)

was found and plotted (Figure 3.15). The highest peak on the power spectrum plot occurred at a particular frequency which indicated that the original analog signal (which could be considered a summation of many individual sinusoidal components) had a dominant component with a large amplitude at that frequency.

The PS.VI program was used to analyze the data which were collected at various f_s increasing up to 4096 Hz within the same period of measuring time ($t=5\text{sec}$). For a number of experiments with smooth top disc, the results showed that the highest power spectrum peak was always located at the position close to zero frequency, since the traction curve measurement had an overall sigmoidal shape. Comparing with the highest peak (which represented the maximum friction force and was a quantity of interest in the experiment) there were no other large peaks shown on the power spectrum plot and this did not change with the increasing in sampling number n , as well as f_s . If f_s was increased, then the f_N also increased and the possibility of aliasings decreased for the friction measurements. For aliasing to have had a significant influence on friction measurement, a large amplitude component would have to be present with a very high frequency.

Subsequent work with a rough top disc might have shown somewhat different results. However, the lack of influence of f_s on the power spectrum and the time required for subsequent data manipulation and processing were considered. Thus, a suitable value for f_s was selected as follows:

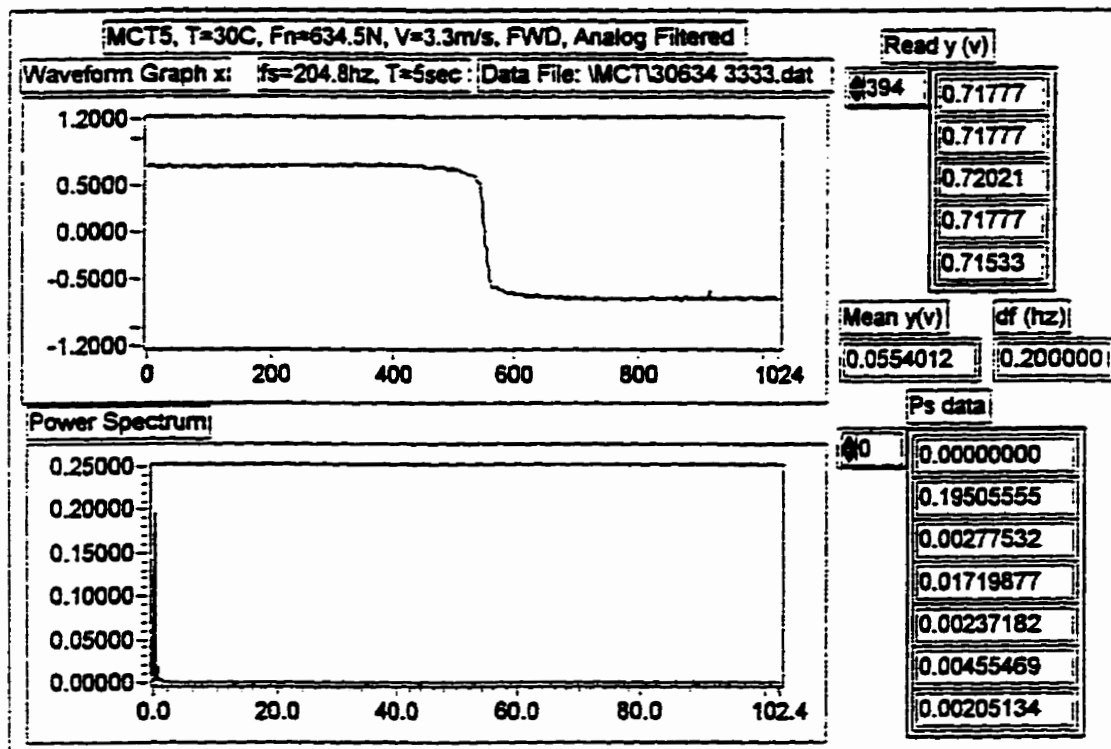
$$f_s = \frac{n}{t} = \frac{1024}{5} = 204.8(\text{Hz})$$

As the f_s was selected, any signals with the frequency higher than $f_N = f_s/2 = 102.4(\text{Hz})$ would cause aliasing. Actually, besides of the highest peak, there were some smaller peaks which did not show on the plot. By changing the scale to let them become visible, it was found that these peaks occurred at multiples of 60 Hz (Figure 3.16). Therefore, they were

PS.vi
10/23/96 09:45 PM

PS.VI

Front Panel



Block Diagram

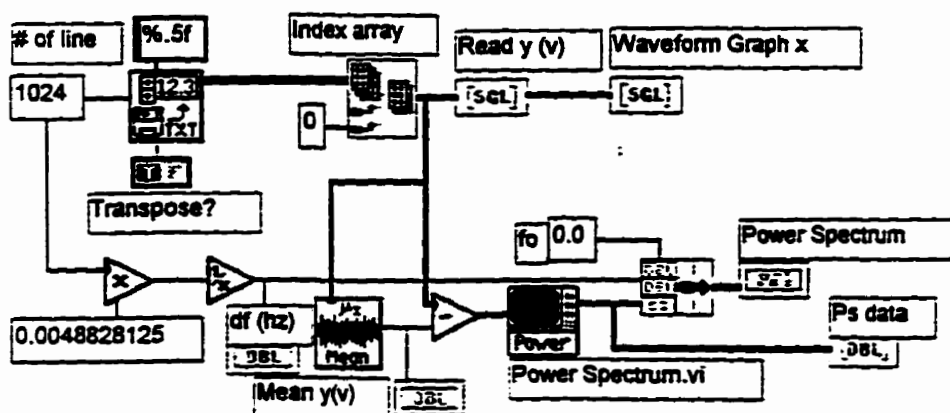


Figure 3.15 Typical power spectrum analysis for measured traction curve

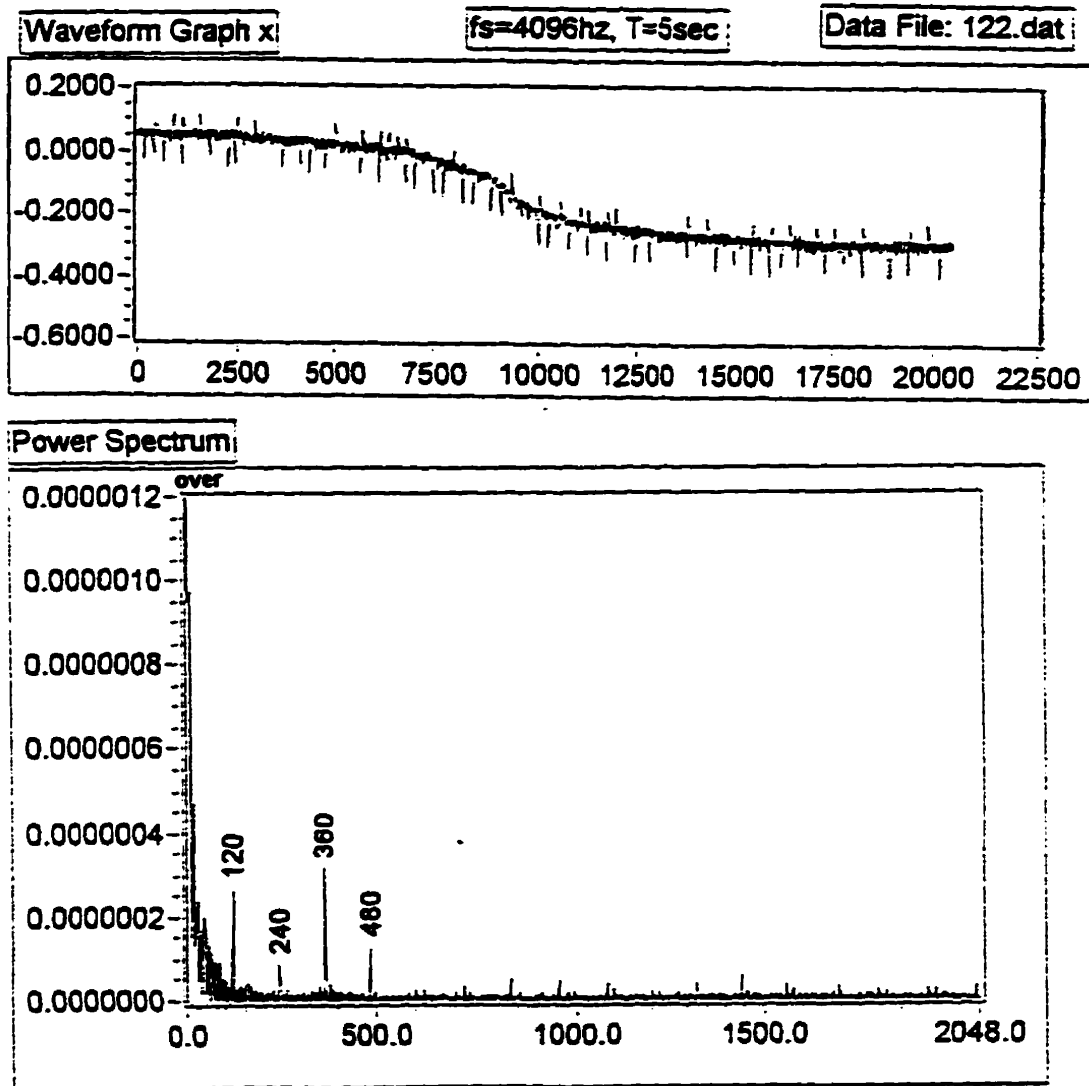


Figure 3.16 High frequency noise from unfiltered traction curve

considered to be noise from the electric circuits of the instrumentation. To avoid possible signal distortions from the electric circuits and other possible physical phenomena in subsequent tests which were not of primary interest, an analog filter was applied before any digital signal processing occurred.

3.4.3 Analog filter

The analog filter allowed signals of low frequencies to pass but rejected or attenuated those of higher frequencies. It was a simple low-pass filter (Hilburn and Johnson, 1983) with standard capacitors, resistors and operational amplifier (Figure 3.17) with a low cutoff frequency of 20 Hz. This cutoff frequency would not give any possible signal distortion of the friction measurement results which had a frequency close to zero. Also, it would have little possible distortion of the 9 Hz component which corresponded to the angular rotational speed of the bottom disc shaft.

The filter was tested by the sinusoidal signals from a signal generator. The responses for three series of input signals with various amplitudes, $RMS = 0.5V$, $1V$ and $2V$, were quite consistent (Figure 3.18). The test results showed that any signals with a frequency greater than 100 Hz would almost totally be filtered out. As mentioned above, the sampling rate was chosen as $f_s = 204.8$ Hz and the Nyquist frequency was $f_N = 102.4$ Hz. If this filter is used in the data acquisition system on disc machine, no significant aliasing is possible. The filter was built into the amplifier between the strain gauge load cell and data acquisition board. The difference between the curves with and without the analog filter (Figure 3.14a) gave a clear view of the benefit in signal clarity of the filtering.

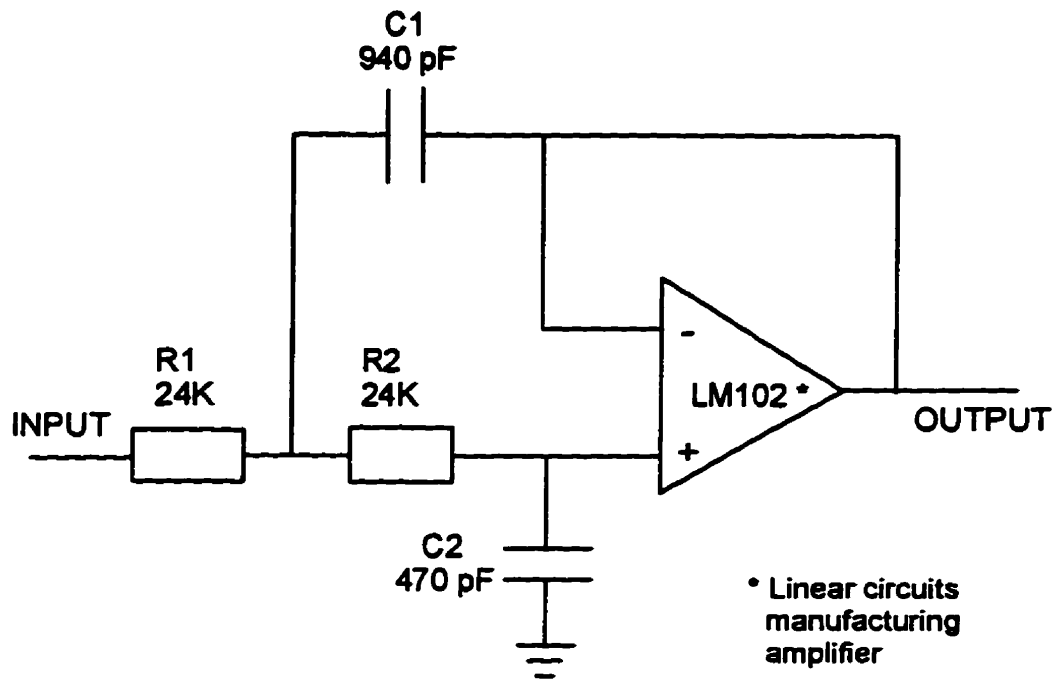


Figure 3.17 Circuit of low pass analog filter

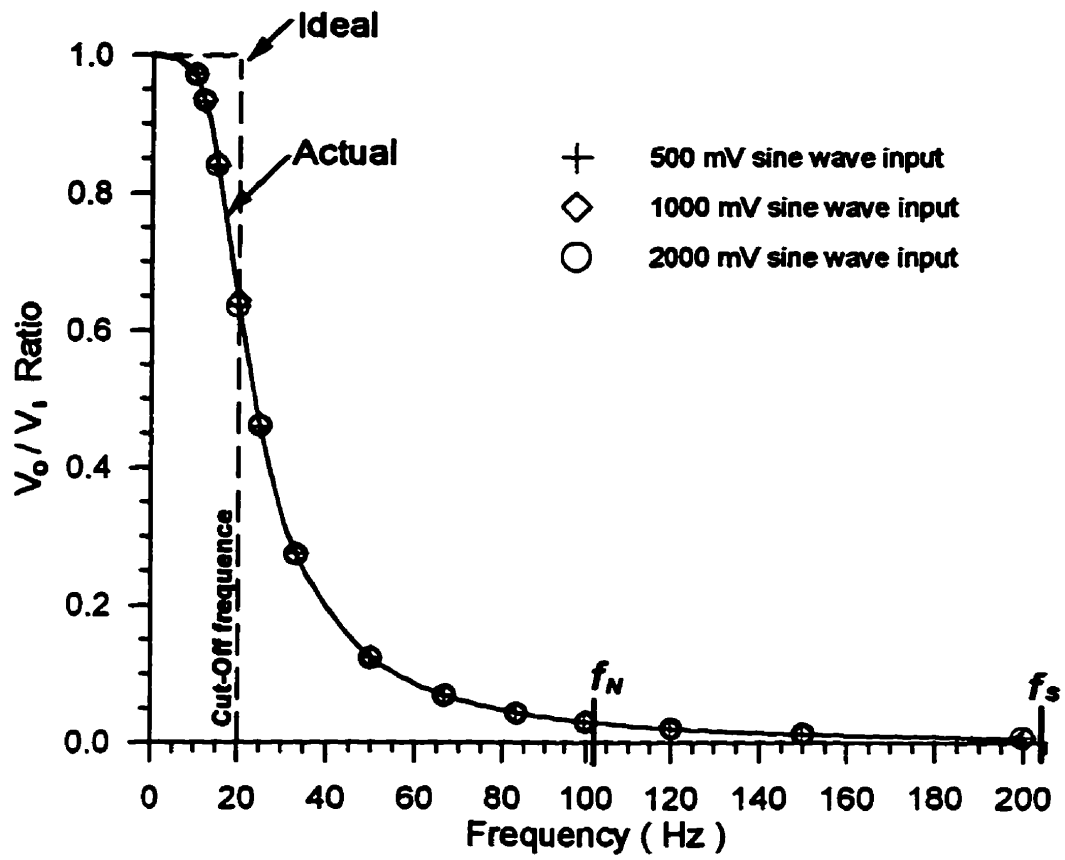


Figure 3.18 Low-pass analog filter property curve

Chapter 4 Materials and Methods

This chapter describes materials and methods used in the present experimental work. First, the properties lubricants, both base stock and formulated oils, are introduced. Secondly, the experimental design is explained, in which the experiments are grouped under various operating conditions. Finally, each of the friction force experiments under specific operating conditions is given a number and estimates of the central film thickness (h_c) and the effective film thickness parameter (λ) are made for each experiment.

4.1 Lubricants

The lubricating oils used in the present research were made by Imperial Oil Limited, Canada. Four formulations of a low viscosity oil were base stock alone (MCT 5), base stock with a friction modifier additive (MCT 5 + FM), base stock with an anti-wear additive (MCT 5 + AW), and base stock with an extreme pressure additive (MCT 5 + EP). The base stock oil was a commercial product directly refined from crude petroleum.

To show the influence of lubricant additives on friction in ehl and mixed film lubrication, each of the formulated oils and the base stock oil were tested under exactly the same operating conditions. With the base stock as a reference, the effects of lubricant additives on the rheological behaviour were evaluated directly from the comparison of the friction force measurements in the side-slip disc machine.

4.1.1 Base stock oil

The inspection data of MCT 5 base stock oil (IMP 4805) provided by Imperial Oil Limited are listed in Table 4.1. By comparing the viscosity to the Society of Automotive Engineers (SAE) grading system, revealed that it might be an SAE 5W ($\nu_{100} = 3.8\text{cSt}^1$, but insufficient information was provided to make a definite identification of the grade).

Table 4.1 Inspection data of mineral oils used in present study (from Imperial Oil Ltd.)

INSPECTIONS	MCT 5	MCT 5 + FM	MCT 5 + AW	MCT 5 + EP
ν_{40} (cSt)	18.47	19.12	18.13	18.46
ν_{100} (cSt)	3.796	3.803	3.800	3.800
ρ_{15} (kg/m ³)	863.0	863.5	865.5	866.8

From the given data of the ν_{40} and ν_{100} , the ν_T of a lubricant at any required temperature T could be calculated from Eq. 2.4 as discussed previously. An example of a calculation of the ν_{30} for MCT 5 is shown below. From Table 4.1, $\nu_{40} = 18.47$ cSt and $\nu_{100} = 3.796$ cSt, the constants in Eq. 2.4 were $A = 9.72319$ and $B = 3.85258$. Inserting $T = 30^\circ\text{C}$ into Eq. 2.4 with these constants gave

$$\log(\log(\nu_{30} + 0.7)) = 9.72319 - 3.85258 \times \log(30 + 273.15)$$

$$\nu_{30} = 27.71 \text{ cSt}$$

The density (ρ) of a lubricant at any required temperature T was calculated using Eq. 2.2 with $T = 30^\circ\text{C}$, $\rho_{15} = 863.0 \text{ kg/m}^3$ and $\gamma = 7.2 \times 10^{-4} \text{ 1}^\circ\text{C}$,

$$\rho_{30} = 863.0 \times [1 - 0.00072 \times (30 - 15)] = 853.7 \text{ kg/m}^3$$

Finally, viscosity (η_0) at atmospheric pressure and 30°C was calculated from Eq. 2.3,

$$(\eta_0)_{30} = \nu_{30} \cdot \rho_{30} = 27.71 \times 853.7 \times 10^{-3} = 23.656 \text{ mPa}\cdot\text{s}$$

¹ cSt - kinematic viscosity unit ($1\text{cSt} = 1 \times 10^{-6} \text{ m}^2/\text{s} = 1 \text{ mm}^2/\text{s}$).

Viscosity was checked using the Brookfield Synchro-Lectric viscometer (Brookfield Engineering Laboratories, Stoughton, Mass., USA) and density was checked by a floating densimeter (ERT Co. USA), both at a number of temperatures (Table 4.2).

Table 4.2 Measurement results of η_0 and ρ

T (°C)	MCT 5		MCT 5 + FM		MCT 5 + AW		MCT 5 + EP	
	η_0 (mPas)	ρ (kg/m ³)	η_0 (mPas)	ρ (kg/m ³)	η_0 (mPas)	ρ (kg/m ³)	η_0 (mPas)	ρ (kg/m ³)
25	31.2	855	31.5	857	30.5	861	32.5	861
30	24.5	851	25.0	854	24.7	858	26.1	858
35	21.5	848	19.7	850	20.9	854	20.7	856
40	18.1	845	17.0	846	17.2	852	17.3	853
45	14.9	840	14.5	843	14.0	849	14.5	850
50	12.4	837	12.5	840	12.0	846	12.5	848
55	11.1	835	10.5	837	10.5	842	11.0	845
60	9.6	833	9.7	834	10.0	838	9.3	842

Comparisons of the viscosities and densities between the data measured at the Tribology Lab, University of Waterloo, with the inspection data provided by Imperial Oil Ltd. at the same temperature showed little difference. These comparisons between measured viscosities and those calculated by the ASTM procedure from inspected data were made by plotting them versus temperature (Figure 4.1). Once again, little difference was shown between the two methods of determining viscosity. As a final example, MCT 5 at 30°C showed a relative difference of 3.6% for viscosity and 0.3% for density when comparing the measured data to the results of ASTM calculation procedure. Since the viscosity of lubricant was measured on the Brookfield viscometer in an opened system and it was difficult to keep a uniform temperature when the spindle was rotating in the lubricant, especially when the temperature was much higher than the room temperature, an unavoidable temperature decrease might have occurred. Therefore, the measured values were usually higher than those from ASTM calculation.

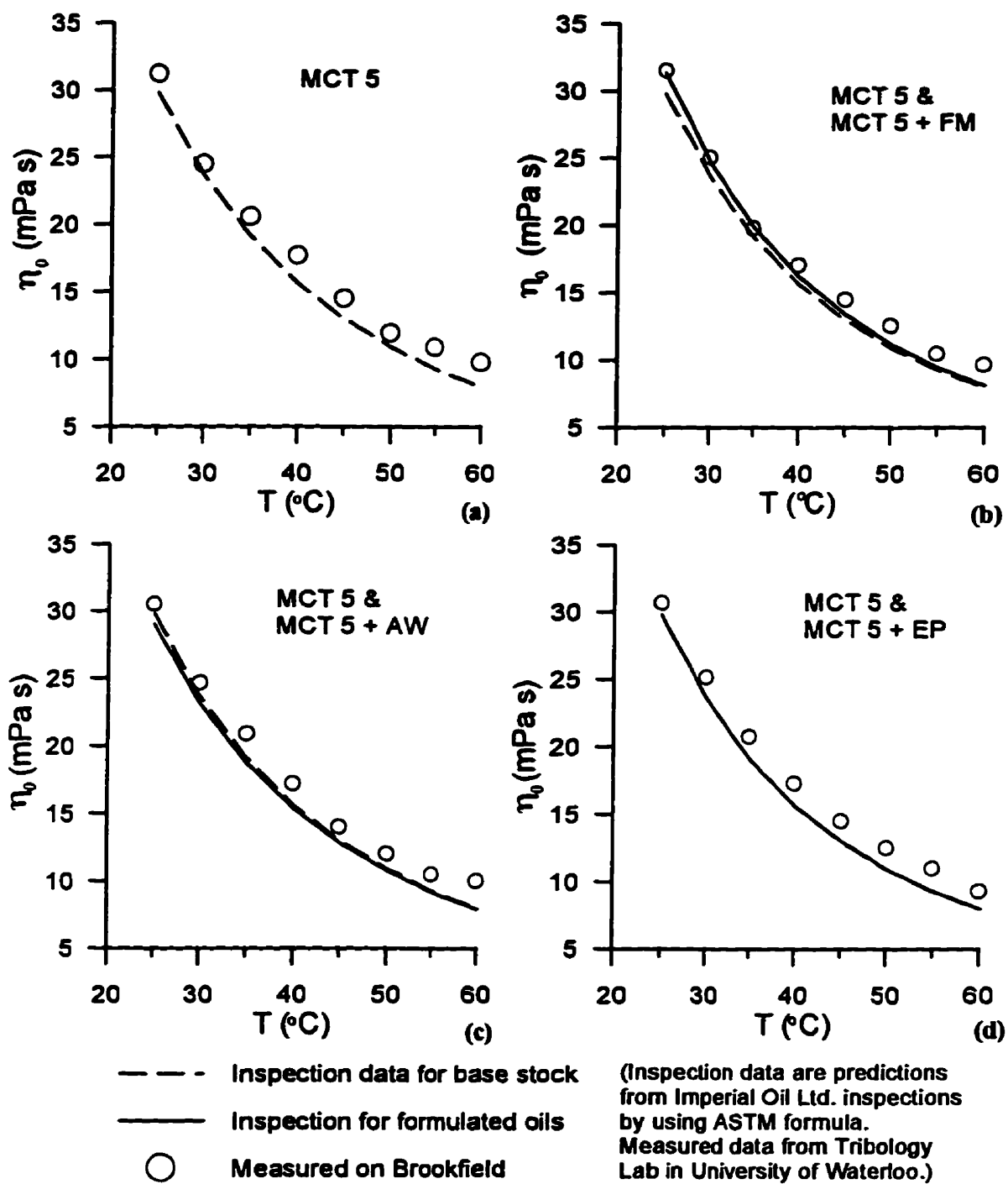


Figure 4.1 Comparison of viscosity at various temperatures for
 (a) MCT 5 (b) MCT 5 + FM (c) MCT 5 + AW (d) MCT 5 + EP

In subsequent calculation of ehl central film thickness, the measured viscosities were used because at that time the inspection data were not available. When the inspection data became available and the ASTM calculation procedure gave almost the same results for $T = 30\text{ }^{\circ}\text{C}$ and $40\text{ }^{\circ}\text{C}$, it was deemed unnecessary to recalculate the central film thickness.

4.1.2 Formulated oils

- **Friction modifier formulation**

MCT 5 + FM formulation (IMP4806) was the MCT 5 base stock oil with 0.5% (wt) friction modifier. This proprietary friction modifier had a long chain polar molecular structure which attached ionically to metal surfaces. These molecules were intended to reduce the amount of metal-metal contact. Some automobile engine tests had been done by Imperial Oil Limited to compare the fully formulated oil with this FM additive and without it. The detailed results of the tests were confidential but they showed a successful performance of the FM additive in that the fuel consumption in automobile engines decreased.

The FM additive did not cause much change in viscosity and density under atmospheric pressure. The viscosity η_0 and density ρ of MCT 5 + FM were checked by measurements in the same manner as MCT 5 (Table 4.2). The η_0 vs. T plot for the MCT 5 + FM formulation in the range of $T = 25^{\circ}\text{C} \sim 60^{\circ}\text{C}$ almost coincided with that of base stock alone MCT 5 (Figure 4.1b).

- **Anti-wear additive formulation**

MCT 5 + AW formulation (IMP 4807) was the base stock MCT 5 with 1.2% (wt) zinc dialkyl dithio phosphate (ZDDP). The ZDDP is a commonly used additive which is added to all crank case oils to control the wear in automobile engines. This additive is made from primary and secondary alcohols. The ZDDP was designed to decompose and form surface compounds.

The η_0 and ρ of MCT 5 + AW were checked by measurements (Table 4.2). The comparison of the viscosity-temperature relations (η_0 vs. T) between AW additive formulation and base stock alone is shown in Figure 4.1c. There was no significant difference in viscosities in the whole range of temperatures, which is similar to the FM additive formulation.

- **Extreme pressure additive formulation**

MCT 5 + EP formulation (IMP 4808) was the base stock MCT 5 with 2% (wt) *anglamol 33* additives. This additive was a sulphur-phosphorus compound, often used in gear oils. The effects of the EP additive could be tested in an FZG gear test apparatus (a German test machine). It could also be evaluated in a special four-ball test, in which the load was as high as 2 to 6 kN and running time was as short as 10 second or until the balls were seized together. The effects of EP additives could also be indicated by the fuel consumption data in automobile engines.

The η_0 and ρ values of MCT 5 + EP formulation were measured using the same method described before (Table 4.2). The EP additive did not change the η_0 vs. T plot significantly from that of the base stock MCT 5 alone under atmospheric pressure and in the whole range of temperatures (Figure 4.1d).

4.2 Design of Experiments

The experiments in the present research involved the use of a side-slip disc machine with a circular point contact geometry to measure the friction force by shearing an isothermal lubricant film under conditions of mainly rolling with a small amount of sliding. The disc machine was run with two levels of disc surface roughness: one was a contact between two smooth surface discs to simulate elastohydrodynamic lubrication (ehl), the other was a contact

between a rough surface disc and a smooth surface disc to simulate mixed film lubrication. Lubricating oils were sheared under various operating conditions. During each measurement, the inlet oil temperature was kept constant. Several rather elaborate series of experiments were performed (Figure 4.2).

4.2.1 Disc surface roughness control

The bottom cylindrical disc was always kept as smooth as possible, and the roughness of the top “crowned” disc surface was either very smooth or quite rough depending on whether ehl or micro-ehl were sought. Both discs were made of wrought tool steel: SAE O1 (The Society of Automotive Engineers, Oil quenched tool steel) for the bottom disc and Keewatin (Atlas Steel, wrought tool steel) for the top discs. The compositions of these two steels were listed in Table 4.3. They had very good hardenability and were hardened to a Rockwell C value of 63. Special cutting and polishing processes were needed to produce smooth and rough disc surfaces at such a high hardness level.

Table 4.3 Alloy composition of disc materials (%wt)

Material	C	Mn	Si	Cr	Ni	V	W
Keewatin	0.89	1.25	0.42	0.47	-	0.14	0.43
SAE O1	0.85-1.0	1.0-1.4	0.5 _{max}	0.4-0.6	0.3 _{max}	0.3 _{max}	0.4-0.6

● Smooth surface disc

The bottom and top smooth discs were cut to the required geometry before hardening. After heat treatment, the disc surfaces were lathe turned with a diamond tip cutting tool first. The feed rate and cut depth were controlled precisely. Then they were lapped carefully with fine diamond paste in the circumferential direction, until the a “mirror” finish was achieved. This procedure gave a root mean square (RMS) surface roughness of 0.08 ~ 0.11 μm .

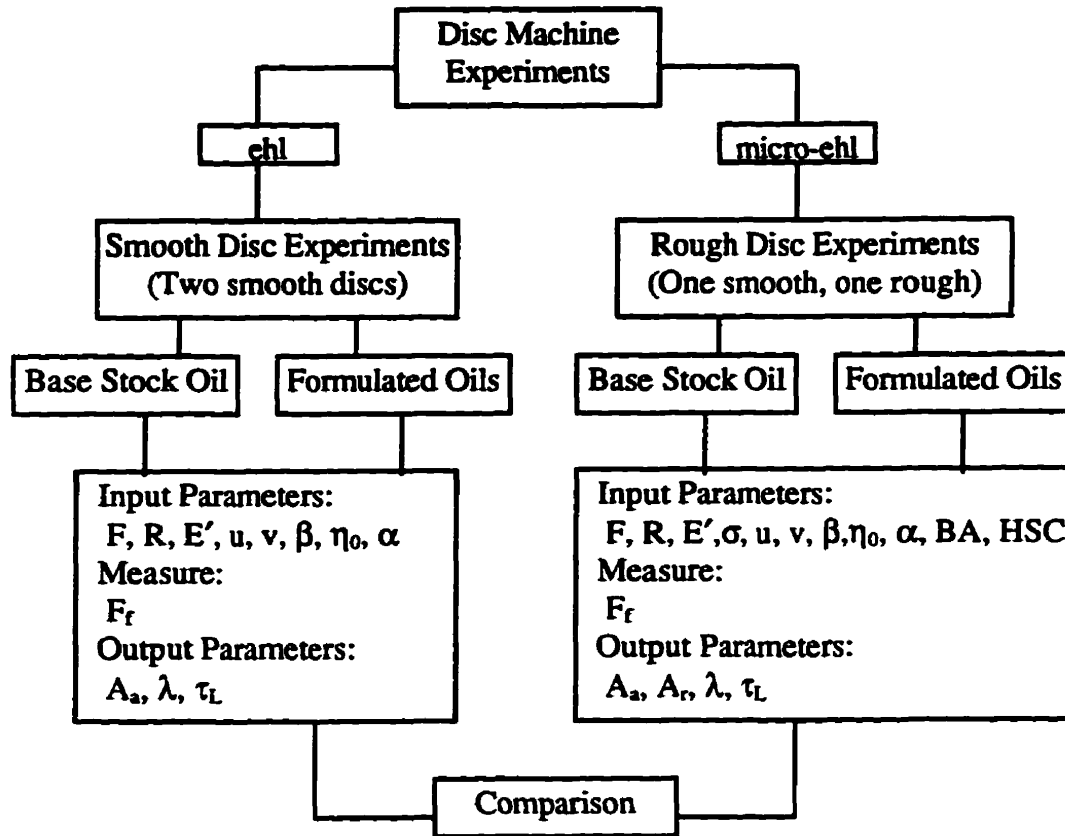


Figure 4.2 Main description of experimental design

The surface roughness was checked on a Talysurf 5 profilometer (Rank Taylor Hobson, Leicester, UK). It had a processor (5M model) to provide a set of values for the selected roughness parameters and a profile graph. All the commands for a measurement were given through the processor, which contained the circuits for providing necessary functions, such as selecting measurement conditions, controlling parameter requirements, collecting signals, processing data, creating and storing the surface profile. The processor printed out the required parameter values and plotted the surface profile. Although, the Talysurf is an independent system, it was connected in parallel to a personal computer (PC) and data acquisition system. Thus, the binary data file obtained from the Talysurf for the surface profile could be saved in an ASCII file by running a Quick Basic program: CONBD.BAS on PC. Then, the surface profile could be plotted on PC with much more flexible control of the size and other characteristics than the original Talysurf plot. It provided more possibilities for further analysis. Typical smooth disc surface roughness measurements before the experiments showed a somewhat rougher surface in the axial direction than in circumferential direction (Figure 4.3).

- **Rough surface**

The rough surface top disc was first prepared following exactly the same processes as for the smooth surface disc. Then, a desired roughness was produced by sandblasting. The sand used in blasting was a graded silica abrasive. The size of the abrasive particles, according to American Foundrymen's Association rating, was No. 60 AFA, and had a mean diameter of about 1.524mm (0.060 inch). The abrasives were shot on the smooth disc surface by compressed air in an industrial surface cleaning machine. The air pressure level provided some control over the resulting surface roughness. It was chosen as 690 kPa (100 psi) in the present study. The abrasive gun kept shooting at a fixed angle while the disc was rotated slowly on a holder. Usually, after one rotation the disc surface changed from that of a mirror finish to a uniformly shaded appearance, without appreciably affecting surface dimensions (Figure 4.4). Measured RMS surface roughness about 1.0 ~ 1.5 μm .

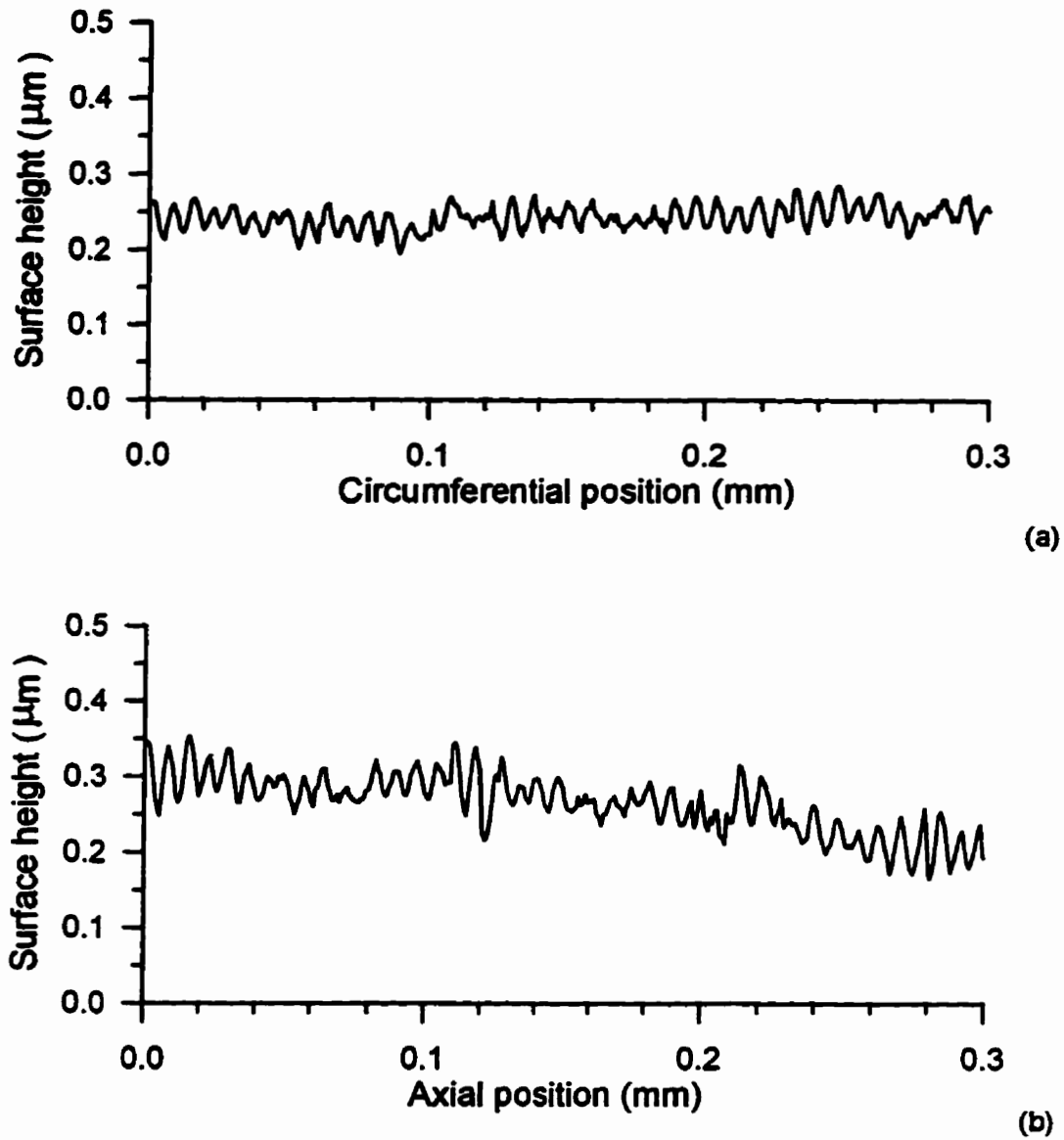


Figure 4.3 A typical segment of the measured surface profile of smooth disc SQ
(a) in circumferential direction (b) in axial direction

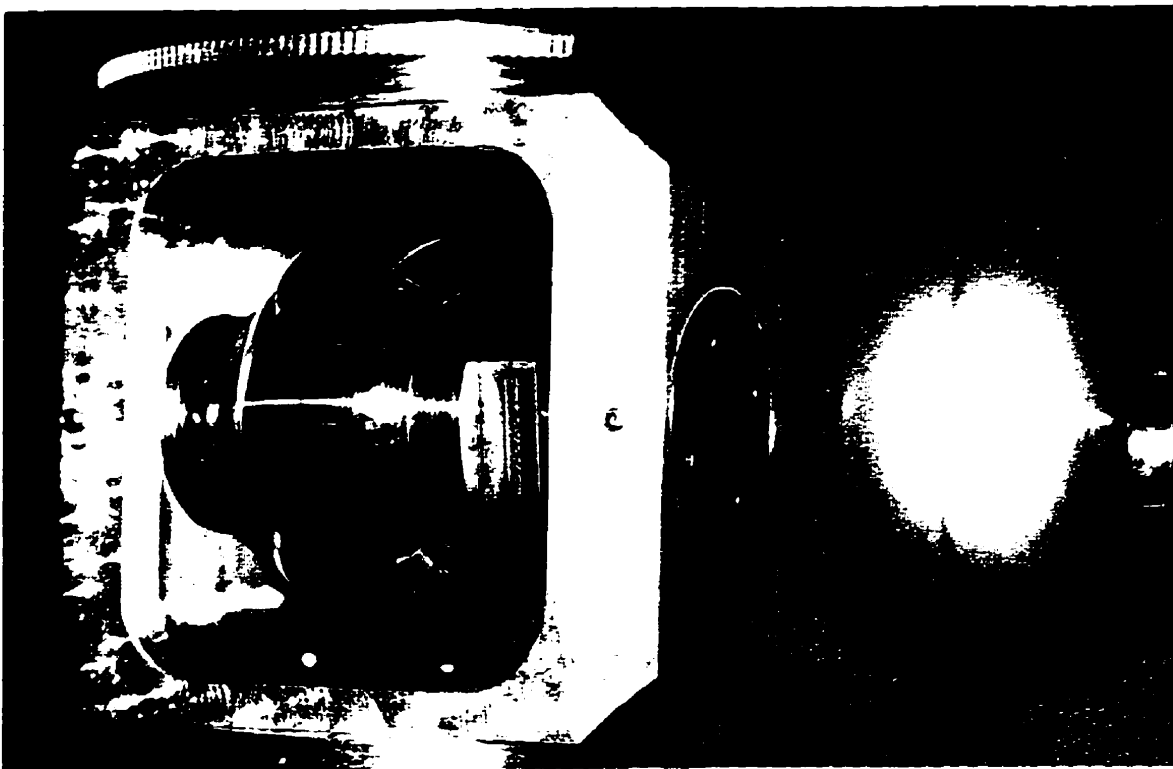


Figure 4.4 Smooth and rough top discs

• **Roughness measurements**

The roughness of disc surfaces was measured after 10 ~ 15 minutes “run-in” when the surface roughness had stabilized. Run-in had a significant influence on the sandblasted rough surfaces in particular (Figure 4.5). Both axial and circumferential directions were measured. The parameters, such as the central line average (R_a), the RMS (R_q) and the maximum peak-to-valley height (R_{max}) were selected on the processor 5M in Talysurf 5 profilometer. The measured conditions, vertical and horizontal magnifications (V_v and V_h), traverse length (T.L.), and cut-off (C.O.), were selected to be as large as possible for each case. However, if T.L. was too large, it became more difficult to remove the underlying curvature of the surfaces and smaller C.O. lengths were required. The data given in Table 4.4 are the measurement results of two pairs of top and bottom discs, which were labeled as ($S0_1$, $B0_1$) and ($S0_2$, $B0_2$) and were used for two repeated sets of smooth disc experiments. Each value was an average from three measurements on the same disc.

Table 4.4 Roughness measurement records for smooth discs

Disc	Direction	V_v	V_h	T.L. (mm)	C.O. (mm)	R_a (μm)	R_q (μm)	R_{max} (μm)
Top($S0_1$)	Axial	10000	5	5.6	0.8	0.051	0.064	0.594
	Circumf.	5000	5	7.2	0.8	0.052	0.065	0.326
	Average	-	-	-	-	0.0515	0.0645	-
Bottom($B0_1$)	Axial	5000	5	7.2	0.8	0.056	0.070	1.083
	Circumf.	10000	5	7.2	0.8	0.049	0.061	0.838
	Average	-	-	-	-	0.0525	0.0655	-
Top($S0_2$)	Axial	10000	5	5.6	0.8	0.050	0.063	0.576
	Circumf.	5000	5	7.2	0.8	0.053	0.066	0.469
	Average	-	-	-	-	0.0515	0.0645	-
Bottom($B0_2$)	Axial	5000	5	7.2	0.8	0.059	0.074	0.895
	Circumf.	10000	5	7.2	0.8	0.053	0.066	0.927
	Average	-	-	-	-	0.056	0.070	-

Note: Each individual parameter in the axial or circumferential direction is the average of 3-4 measurements at different locations on the disc surface.

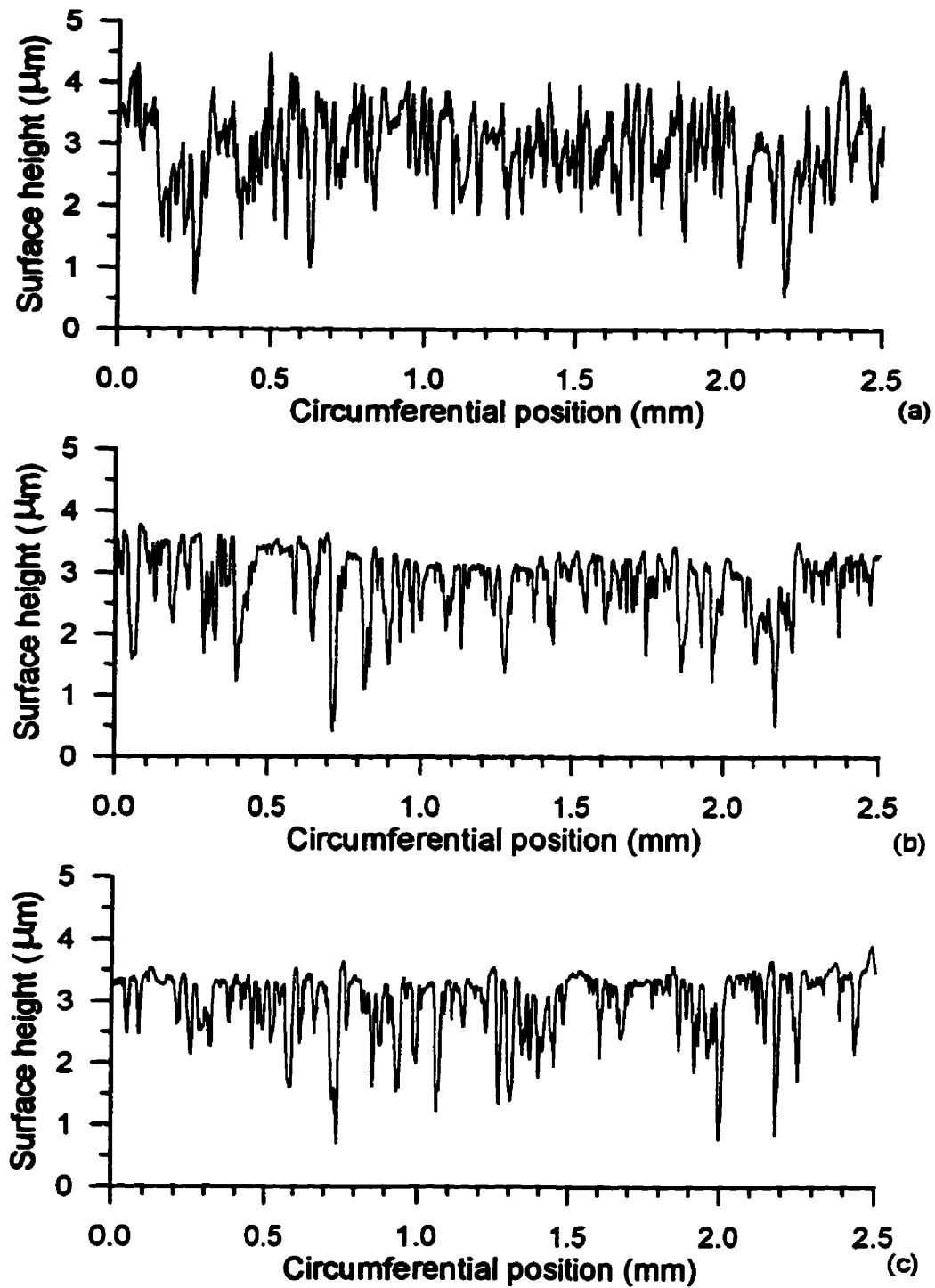


Figure 4.5 Surface profile of the rough top disc R2
(a) at beginning
(b) after run-in
(c) after friction measurements

For the second set of experiments ("Rough Disc Experiments" - Figure 4.2), the bottom disc was repolished and two new top discs were prepared by sandblasting. The roughnesses of the top and bottom discs were measured on the Talysurf (Table 4.5). There were two rough surface top discs (R1 and R2) which were used for two applied load levels, 147.0 N and 244.5 N, respectively. Both were used with the repolished bottom disc (BR). Another two top discs (S1 and S2) were used for matched sets of experiments which paralleled those involving the two rough top discs (R1 and R2) and involved the same bottom disc (BR). The smooth top discs (S1 and S2) had RMS roughnesses an order of magnitude lower than the rough top discs (R1 and R2) (Table 4.5).

Table 4.5 Roughness measurements for discs used in rough disc experiments and matched smooth disc experiments

Disc	Direction	V _v	V _b	T.L. (mm)	C.O. (mm)	R _a (μm)	R _q (μm)	R _{max} (μm)
Top(R1)	Axial	2000	5	2.5	2.5	0.855	1.175	8.884
	Circumf.	2000	5	2.5	2.5	0.843	1.117	8.069
	Average	-	-	-	-	0.847	1.146	-
Top(R2)	Axial	2000	5	2.5	2.5	0.646	0.889	6.761
	Circumf.	2000	5	2.5	2.5	0.853	1.233	10.27
	Average	-	-	-	-	0.750	1.061	-
Bottom(BR)	Axial	5000	5	7.2	0.8	0.055	0.074	1.351
	Circumf.	10000	5	7.2	0.8	0.051	0.069	0.935
	Average	-	-	-	-	0.053	0.072	-
Top(S1)	Axial	2000	5	5.6	0.8	0.059	0.073	1.074
	Circumf.	2000	5	5.6	0.8	0.046	0.063	1.472
	Average	-	-	-	-	0.0525	0.068	-
Top(S2)	Axial	2000	5	5.6	0.8	0.062	0.077	1.230
	Circumf.	2000	5	5.6	0.8	0.046	0.058	1.583
	Average	-	-	-	-	0.054	0.0675	-
Bottom(BS)	Axial	5000	5	7.2	0.8	0.050	0.063	1.055
	Circumf.	5000	5	7.2	0.8	0.057	0.071	1.138
	Average	-	-	-	-	0.0535	0.067	-

Note: Each individual parameter in the axial or circumferential direction is the average of 3-4 measurements at different locations on the disc surface.

- **BA and HSC for rough surface discs**

As mentioned previously, the two sandblasted rough surface discs R1 and R2 were tested under two load levels. The roughness of the surfaces was checked at least three times during the experiments. The first profile before testing showed a Gaussian distribution (Figure 4.5a). It had a symmetrical distribution about the mean line, but after 10 to 15 minutes “run-in” under the applied load, the profile had a serious skewness (Figure 4.5b), because the asperity tips had been worn down or flattened by local plastic deformations. However, as the local contact stress decreased, elastic deformation dominated so that the last check which was made after the friction experiments (Figure 4.5c) showed virtually the same profile as that after run-in. The profile checking mentioned above, included three or four measurements on each disc in the circumferential directions at locations separated circumferentially by 120° or 90°. By measuring in the circumferential direction only, it was possible to keep the trace within the contact zone which was visible as a darkened line on the disc surface.

To determine the real area of contact, two other parameters bearing area (BA or Tp% according to the Talysurf processor) and high spot count (HSC) were measured at various height levels. To illustrate the measurement procedure, data for disc R1 was used which had been collected after a set of friction force measurements under an applied load of 147.0 N. Conditions of measurement were $V_v \times 5000$, $V_h \times 5$, T.L. = 2.5 mm, and C.O. = 2.5 mm. Three unfiltered profiles were taken in the circumferential direction and gave the BA and HSC data which were directly related to the contact zone. The measured results were first shown on the screen of processor 5M. Then, they were printed out as required. The output data (Figure 4.6) included three columns: the increment of Depth (μm), the BA in unit traverse length (Tp%) and the high spot count over the whole traverse length (HSC*). The Tp% and HSC* were measured at equal increments of Depth (μm), which started from the highest asperity tip, across the mean line and to the lowest valley. The interval depended on the selection of the vertical magnification and was one-twentieth (1/20) of the full scale range in

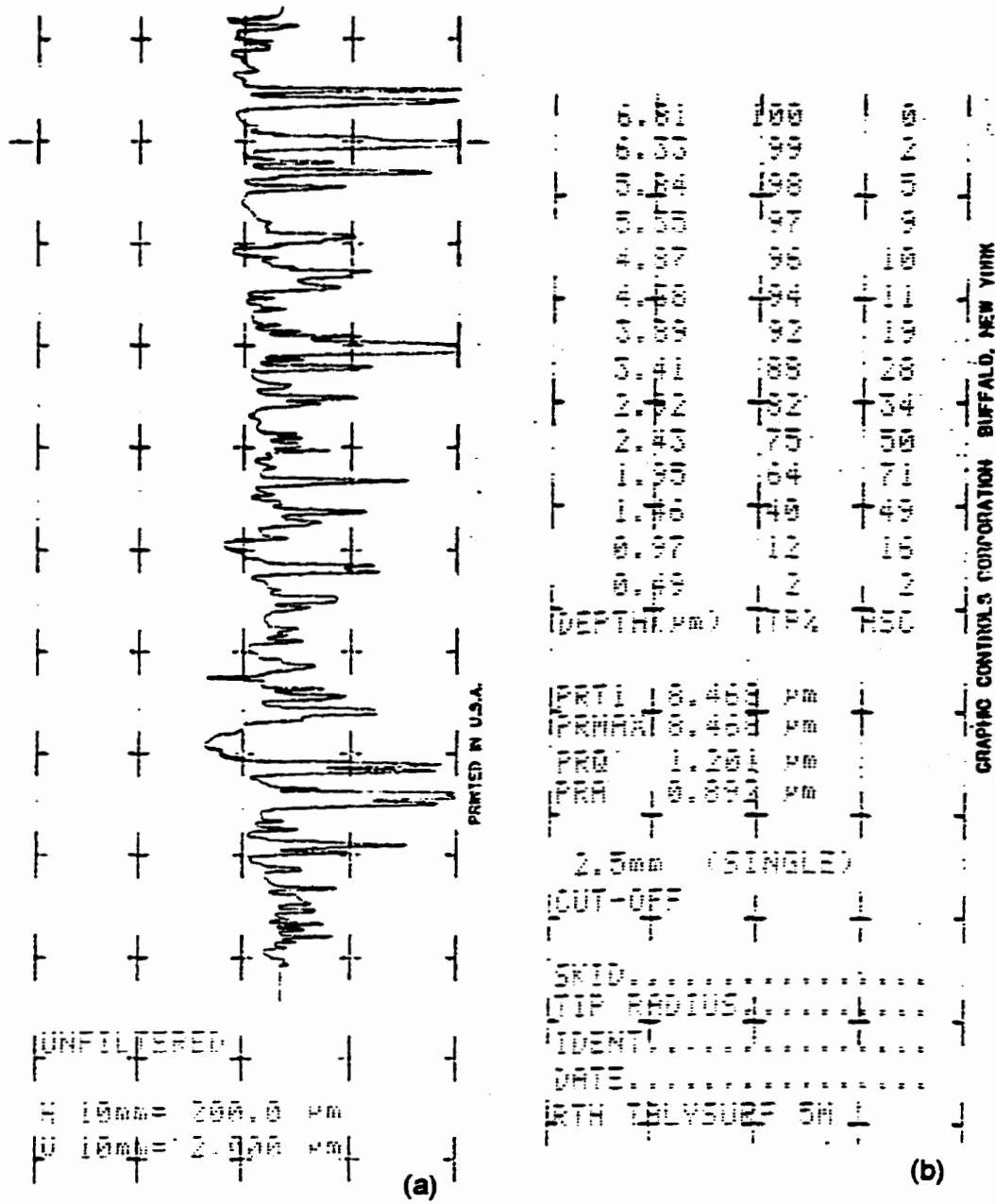


Figure 4.6 Talysurf measurement records
(a) profile of run-in rough top disc R1
(b) data for BA and HSC at various depths
(corresponding to 4.dat in Table 4.6)

each case. In this example, the selected V_v was $\times 5000$. Then the increments of level was $0.50\mu\text{m}$ (Talysurf 5 System, Operator's Handbook).

If the mean line of the profile was set as the origin of vertical axis (z), the relationship between z and measured Depth was given by Eq. 4.1.

$$z = \text{Depth}_{(Tp\%=50)} - \text{Depth}_{(\text{Measured})} \quad (4.1)$$

where $\text{Depth}_{(Tp\%=50)}$ - linear interpolation value of Depth at $Tp(\%) = 50$

The BA and HSC in unit length had the following relations with measured values $Tp\%$ and HSC^*

$$BA = Tp(\%) / 100 \quad (4.2)$$

$$HSC = HSC^* / L \quad (4.3)$$

where L - traverse length

and for the trace in Figure 4.6, $L = 2.5$ mm. The printed values of $Tp\%$ and HSC^* from the trace were converted into HSC and BA for further analysis to determine the real area of contact (Table 4.6). Similarly, Table 4.7 gave the same converted data set for rough disc R2.

**Table 4.6 Talysurf measured data for rough surface disc R1
(3.dat, 4.dat and 5.dat for three traverses)**

Depth (μm)	3.dat			4.dat			5.dat		
	z (μm)	BAC	HSC(1/mm)	z (μm)	BAC	HSC(1/mm)	z (μm)	BAC	HSC(1/mm)
0.49	5.676	0.07	5.2	1.174	0.02	0.8	1.098	0.0	0.8
0.97	0.196	0.40	22.0	0.694	0.12	6.4	0.618	0.10	8.0
1.46	-0.294	0.65	21.6	0.204	0.40	19.6	0.128	0.44	28.4
1.95	-0.784	0.76	16.4	-0.286	0.64	18.4	-0.362	0.67	27.2
2.43	-1.264	0.84	12.0	-0.766	0.75	20.0	-0.842	0.77	18.4
2.92	-1.754	0.90	10.4	-1.256	0.82	13.6	-1.332	0.84	13.2
3.41	-2.244	0.94	6.8	-1.746	0.88	11.2	-1.822	0.89	10.4
3.89	-2.724	0.97	3.2	-2.226	0.92	7.6	-2.302	0.92	7.6
4.38	-3.214	0.97	2.0	-2.716	0.94	4.4	-2.792	0.95	4.0
4.87	-3.704	0.98	2.4	-3.206	0.96	4.0	-3.282	0.97	3.2
5.35	-4.184	0.99	2.0	-3.686	0.97	3.6	-3.762	0.98	2.0
5.84	-4.674	0.99	0.8	-4.176	0.98	2.0	-4.252	0.99	1.2
6.33	-5.164	1.00	0.0	-4.666	0.99	0.8	-4.742	0.99	0.4
6.81				-5.146	1.00	0.0			

**Table 4.7 Talysurf measured data for rough surface disc R2
(6.dat, 7.dat, 8.dat and 9.dat for four traverses)**

Depth (μm)	6.dat			7.dat			7.dat			8.dat		
	z (μm)	BAC	HSC	z (μm)	BAC	HSC	z (μm)	BAC	HSC	z (μm)	BAC	HSC
0.5	0.583	0.14	5.6	0.021	0.49	20.0	0.045	0.16	5.6	0.077	0.46	22.8
1.0	0.083	0.46	20.0	-0.479	0.73	22.4	-0.455	0.60	28.0	-0.423	0.72	25.2
1.5	-0.417	0.70	24.0	-0.979	0.82	20.8	-0.955	0.75	22.0	-0.923	0.82	18.4
2.0	-0.917	0.79	18.8	-1.479	0.90	12.0	-1.455	0.83	14.8	-1.423	0.90	14.0
2.5	-1.417	0.86	12.8	-1.979	0.94	9.2	-1.955	0.88	11.6	-1.923	0.94	7.6
3.0	-1.917	0.90	9.2	-2.479	0.97	4.8	-2.455	0.92	8.0	-2.423	0.96	4.8
3.5	-2.417	0.92	7.6	-2.979	0.98	2.4	-2.955	0.94	5.6	-2.923	0.98	3.6
4.0	-2.917	0.95	5.2	-3.479	0.99	1.2	-3.455	0.96	3.2	-3.423	0.99	2.4
4.5	-3.417	0.96	3.6	-3.979	1.00	0	-3.955	0.97	2.4	-3.923	1.00	0.4
5.0	-3.917	0.97	2.4	-4.479	1.00	0	-4.455	0.98	1.2	-4.423	1.00	0.4
5.5	-4.417	0.98	2.0	-4.979	1.00	0	-4.955	0.99	1.2	-4.923	1.00	0
6.0	-4.917	0.99	2.0				-5.455	0.99	0			

4.2.2 Operating conditions

The operating conditions were directly related to the determination of the lubrication regimes. When the test facility and method were chosen, some of the conditions were fixed for all of the experiments, such as the geometry of the disc machine, the disc material, the range of skew angle, room temperature oil viscosity, etc. But some other conditions had to be selected carefully for each group of tests, even each test, since they affected the rheological behaviour of the lubricant film directly and their choice placed the lubrication in a specific regime. The applied load (F), entrainment velocity (u), composite disc surface roughness (σ_c) and inlet zone lubricant temperature (T) were considered as crucial parameters of testing conditions. As they were selected, the contact pressure (p), inlet lubricant viscosity (η_0), film thickness (h_c), as well as the effective film thickness parameter λ could be calculated and the lubrication regimes could be determined.

- **Applied load**

Applied load system of the disc machine included the top disc assembly, weight holder assembly, dead-weights and heavy oil damper, which was discussed in Chapter 3 (Figure 3.4). Eight load levels could be used on this disc machine (Table 4.8). Once a load was selected, the apparent area of contact (A_a) as well as the average pressure (p_{avg}) and maximum pressure (p_{max}) could be calculated (Table 4.8) following the Hertzian equations for nominal point contact (Eqs. 2.11 and 2.12).

Table 4.8 Applied load levels and corresponding contact area and pressure

Weights	F (N)	A_c (m ²)	p_{avg} (GPa)	p_{max} (GPa)
1	147.0	2.515e-7	0.5845	0.8767
2	244.5	3.531e-7	0.6924	1.0387
3	342.0	4.416e-7	0.7745	1.1617
4	439.5	5.220e-7	0.8420	1.2629
5	537.0	5.966e-7	0.9001	1.3502
6	634.5	6.667e-7	0.9517	1.4276
7	732.0	7.334e-7	0.9981	1.4971
8	829.5	7.972e-7	1.0405	1.5608

Four load levels of 244.5N, 439.5N, 634.5N and 829.5N with 2, 4, 6 and 8 weights were selected for the smooth disc tests. However, only two load levels of 147.5N and 244.5N with 1 and 2 weights, respectively, were selected for the rough disc tests because it was hoped that the progressive plastic deformation of asperity tips would be limited and a stable surface profile would develop after a run-in period.

- **Entrainment velocity**

Entrainment velocity (u) was a crucial parameter to determine the film thickness in ehl. As mentioned in Chapter 3, assuming the surface velocities of the top and bottom discs were the same, the u was adjusted by the pulse rate ψ (Eq. 3.1). However, a high u might introduce high mechanical vibrations on the test rig when the load F was also high. Therefore, the ranges of u and corresponding ψ for this disc machine are listed in Table 4.9.

Table 4.9 Conversion of pulse rate ψ and rolling speed u

u (m/s)	0.1	0.2	0.25	0.3	0.4	0.5	0.6	0.7	0.75	0.8	0.9	1.0
ψ (hole/s)	5	9	11	13	18	22	27	31	33	36	40	45
u (m/s)	1.25	1.5	1.75	2.0	2.25	2.5	2.75	3.0	3.5	4.0		
ψ (hole/s)	56	67	78	89	100	112	123	134	156	178		

- **Inlet zone lubricant temperature and ambient pressure viscosity**

Inlet lubricant viscosity varied with temperature, which affected both film thickness and the friction force. In the present experiments, oil was drawn into the inlet contact zone at a specified temperature. Thus, the central film thickness h_c which depends on the inlet zone viscosity could be determined by using Eq. 2.24, as discussed previously. However, the inlet temperature was measured about 5 mm from the contact centre and some inlet shear heating could have occurred before entrainment into the contact zone. Such heating could rapidly dissipate in the outlet zone because of the high thermal conductivity of the steel discs, and thus running the discs in reverse as discussed in Chapter 3 might not detect a temperature rise in the outlet zone. Fortunately, a calculation of a correction for thermal effects in the contact could be performed (Mobil EHL Guidebook, 4th edition, 1992; Cheng, 1970). The calculated correction factors, at all the applied load levels and the highest rolling speed, were quite close to 1, $C_T = 0.9712 \sim 0.9988$. They were much greater than the criterion of $C_T \leq 0.9$ which was suggested as significant by Cheng (1970). Therefore, according to these calculations, the inlet shear heating effect could be ignored and no thermal correction was necessary for film thickness calculations. As discussed in Chapter 3, preliminary tests for temperature measurement showed that disc surface temperatures in both inlet and outlet zone during a friction experiment were approximately the same. These measurements suggested that the side-slip velocity did not introduce significant heating in the contact zone. Furthermore, thermal effects caused by the side-slip would cause a decline in the friction force with increasing amounts of side-slip (increasing skew angle). Such a decline was not seen in any of the preliminary friction experiments. Therefore, all the friction measurements in the present study were considered to be under isothermal conditions. The inlet temperature T , as measured by the inlet thermocouple 1 (Figure 3.8), was used for the experimental plan and the ambient pressure viscosity η_0 at T and a constant pressure-viscosity coefficient α were used to calculate the h_c .

During the friction force measurements, T was measured and controlled. Most of the experiments were performed at 30°C, but some tests were performed at the higher temperatures of 40°C and 55°C. The ambient pressure viscosities η_0 of the base stock and formulated oils at the three temperatures were measured (Table 4.2). When the temperature increased from 30°C to 55°C, the viscosity dropped from 25 mPa·s to 11 mPa·s for all of the oils. Since it was less than half of the original value, some effect on friction measurement results would be expected.

The inlet lubricant temperature might also effect the value of pressure-viscosity coefficient α , and various formulae were available to calculate it, but they were not particularly accurate (Cameron, 1966; Stachowiak and Batchelor, 1993). In engineering practice, α is often considered as a function of the molecular structure of the lubricant and usually used as a constant within quite a wide range of temperatures. In the present study, the α was considered as a constant, $\alpha = 2.21 \times 10^{-8} \text{ m}^2/\text{N}$, within the inlet lubricant temperature variation referring the Mobil EHL Guide Book (1992).

● Disc surface roughness and λ ratio arrangement

The last important operating condition was the composite roughness of contact disc surfaces, which was defined as $\sigma_c = (\sigma_T + \sigma_B)^{1/2}$. As mentioned in Chapter 2, λ was the ratio of central film thickness to the composite roughness ($\lambda = h_c / \sigma_c$), and it gave some indication of lubrication regimes. When the F , T , η_0 , α and u were selected, the central film thickness h_c for isothermal ehl nominal point contact could be calculated using Eq. 2.24. Therefore, the experiments in the present study were arranged in various regimes based on the values of λ .

The average roughness values of smooth top disc $S0_1$ and bottom disc $B0_1$, $\sigma_T = 0.0645 \text{ }\mu\text{m}$ and $\sigma_B = 0.0655 \text{ }\mu\text{m}$, were taken from the Talysurf measurements (Table 4.4). The composite roughness was $\sigma_c = 0.092 \text{ }\mu\text{m}$. From the results of the preliminary electrical resistance circuit

for an inlet temperature T of 30°C and applied loads F of 244.5N , 439.5N , 634.5N and 829.5N , the output voltage V_0 had a relationship with the entrainment velocity u (Figure 3.12). If the calculation of h_c and the measurement of σ_c were accurate, it was expected that V_0 would start to drop at $\lambda \approx 3$. This behaviour did occur (Figure 4.7) and by setting experimental conditions such that $\lambda < 3$, it was possible to expect varying degrees of asperity interaction with the assurance of both theoretical calculations and experimental measurements. On the other hand, setting $\lambda > 3$ ensured virtually zero direct asperity interaction with the same assurances.

The average RMS roughness values for the rough surface top discs were $\sigma_T = 1.146 \mu\text{m}$ (R1) and $\sigma_T = 1.061 \mu\text{m}$ (R2), and for the same smooth surface bottom disc BR was $\sigma_B = 0.072 \mu\text{m}$ (Table 4.5). The composite roughness for R1 and BR contact was $\sigma_c = 1.148 \mu\text{m}$, and for R2 and BR contact was $\sigma_c = 1.063 \mu\text{m}$. If F , T , η_0 , α and u were selected with similar ranges as that for smooth disc tests, and the h_c was calculated by Eq. 2.24, then the λ ratio would have values $\lambda < 1$. This range was traditionally located in boundary lubrication (Figure 2.15). However, some recent research on mixed film lubrication argued that the division between mixed film lubrication and boundary lubrication might be moved to λ values well below 1.0 (Evans and Johnson, 1987; Sutcliffe, 1991; Johnson, 1992; Cheng, 1992). They pointed out that the effect of asperity interaction on friction was still governed by the rheological properties of the bulk lubricant, but at a pressure corresponding to the asperity contact pressure. It was noted that friction was strongly influenced by non-Newtonian behaviour but the effect of additives was not investigated.

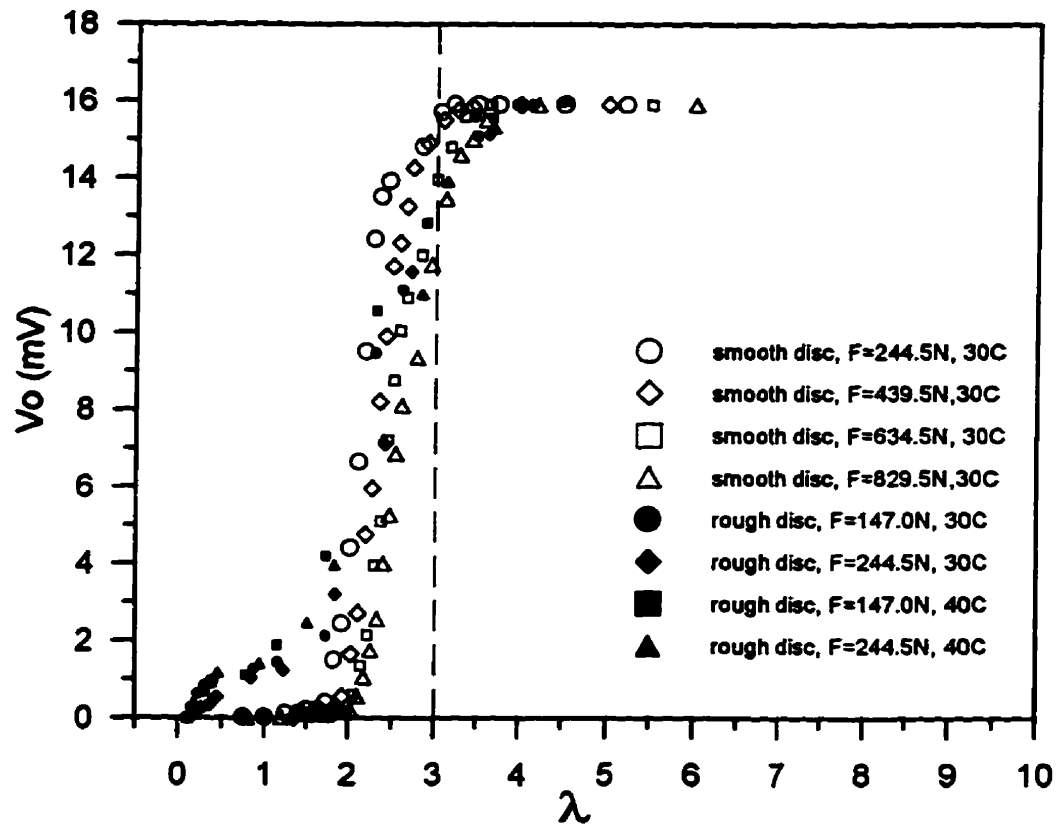


Figure 4.7 Typical plot of output voltage vs. λ
 (for MCT 5, various F , T , u and composite RMS surface roughness)

4.3 Sequence of Experiments

In the present study, λ was used to arrange some experiments in the range $\lambda < 1.0$, others in the range $\lambda > 3.0$ and a few in between. All the experimental conditions of F , T , u and σ_c , as well as the calculated central film thickness h_c and value of λ ratio for each experiment, are grouped and listed in Tables 4.10 ~ 4.12. The group of the smooth disc experiments (Table 4.10) included the base stock alone (MCT 5) and three formulated oils (MCT 5 + FM, MCT 5 + AW and MCT 5 + EP). The groups of the rough disc experiments (Table 4.11) and the matched smooth disc experiments (Table 4.12) included only the MCT 5, MCT 5 + FM and MCT 5 + EP. Each individual experiment had a unique number in a sequence from 1 to 210. However, each individual experiment represented at least two (sometimes three or four) sets of measurements, where each set (Figure 3.7) involved measuring friction force from negative to positive skew angles in both forward and reverse directions. Therefore, over a thousand measurements have been done in the present study.

Table 4.10 Experiment sequence for smooth disc tests

Expt. No.	Lubricant	α_c (μm)	T ($^{\circ}\text{C}$)	F (N)	u (m/s)	h_c (μm)	λ ratio					
1	MCT 5 (S0 ₁ , B0 ₁)	0.092	30	244.5	1.6	0.336	3.7					
2				439.5	1.9	0.363	3.9					
3				634.5	2.2	0.391	4.2					
4				829.5	2.3	0.395	4.3					
5				244.5	2.5	0.454	4.9					
6				439.5	3.0	0.493	5.4					
7				634.5	3.3	0.512	5.6					
8				829.5	3.75	0.548	5.9					
9			40	0.092	30	244.5	2.0	0.358	3.9			
10						439.5	2.25	0.372	4.0			
11						634.5	2.75	0.416	4.5			
12						829.5	3.0	0.433	4.7			
13						244.5	3.25	0.495	5.4			
14						439.5	3.75	0.524	5.7			
15						55	0.092	30	244.5	3.5	0.464	5.0
16									439.5	3.75	0.467	5.1
17			634.5	3.8	0.460				5.0			
18			829.5	4.0	0.467				5.1			
19	MCT 5+FM (S0 ₁ , B0 ₁)	0.092	30	244.5	1.6				0.341	3.7		
20				439.5	1.9				0.368	4.0		
21				634.5	2.2	0.396	4.3					
22				829.5	2.3	0.401	4.4					
23				244.5	2.5	0.460	5.0					
24				439.5	3.0	0.499	5.4					
25				634.5	3.3	0.519	5.6					
26				829.5	3.75	0.556	6.0					
27			40	0.092	30	244.5	2.0	0.338	3.7			
28						439.5	2.25	0.351	3.8			
29						634.5	2.75	0.392	4.3			
30						829.5	3.0	0.408	4.4			
31						244.5	3.25	0.467	5.1			
32						439.5	3.75	0.494	5.4			
33						55	0.092	30	244.5	3.5	0.445	4.8
34									439.5	3.75	0.448	4.9
35			634.5	3.8	0.441				4.8			
36			829.5	4.0	0.448				4.8			

(Table 4.10 continued)

Expt. No.	Lubricant	α_c (μm)	T ($^{\circ}\text{C}$)	F (N)	u (m/s)	h_c (μm)	λ ratio			
37	MCT 5+AW (S0 ₁ , B0 ₁)	0.092	30	244.5	1.6	0.338	3.7			
38				439.5	1.9	0.365	4.0			
39				634.5	2.2	0.393	4.3			
40				829.5	2.3	0.397	4.3			
41				244.5	2.5	0.456	5.0			
42				439.5	3.0	0.495	5.4			
43				634.5	3.3	0.515	5.6			
44				829.5	3.75	0.551	6.0			
45				40	244.5	2.0	0.351	3.8		
46				439.5	2.25	0.365	4.0			
47				634.5	2.75	0.408	4.4			
48				829.5	3.0	0.425	4.6			
49				244.5	3.25	0.486	5.3			
50				439.5	3.75	0.514	5.6			
51	55	0.092	30	244.5	3.5	0.448	4.9			
52				439.5	3.75	0.451	4.9			
53				634.5	3.8	0.444	4.8			
54				829.5	4.0	0.452	4.9			
55				MCT 5+EP	0.092 (S0 ₁ , B0 ₁)	30	244.5	1.6	0.351	3.8
56				439.5			1.9	0.379	4.1	
57				634.5			2.2	0.408	4.4	
58	829.5	2.3	0.412	4.5						
59	244.5	2.5	0.473	5.1						
60	439.5	3.0	0.514	5.6						
61	634.5	3.3	0.535	5.8						
62	829.5	3.75	0.572	6.2						
63	40	244.5	2.0	0.349			3.8			
64	439.5	2.25	0.363	3.9						
65	634.5	2.75	0.405	4.4						
66	829.5	3.0	0.422	4.6						
67	244.5	3.25	0.483	5.2						
68	439.5	3.75	0.511	5.6						
69	55	0.092	30	244.5	3.5	0.450	4.9			
70				439.5	3.75	0.453	4.9			
71				634.5	3.8	0.446	4.8			
72				829.5	4.0	0.454	4.9			

(Table 4.10 continued)

Expt. No.	Lubricant	α_c (μm)	T ($^{\circ}\text{C}$)	F (N)	u (m/s)	h_c (μm)	λ ratio
73	MCT 5	0.095	30	244.5	1.6	0.336	3.5
74		(SO ₂ , BO ₂)		439.5	1.9	0.363	3.8
75				634.5	2.2	0.391	4.1
76				829.5	2.3	0.395	4.2
77				244.5	2.5	0.454	4.8
78				439.5	3.0	0.493	5.2
79				634.5	3.3	0.512	5.4
80				829.5	3.75	0.548	5.8
81			40	244.5	2.0	0.358	3.8
82				439.5	2.25	0.372	3.9
83				634.5	2.75	0.416	4.4
84				829.5	3.0	0.433	4.6
85				244.5	3.25	0.495	5.2
86				439.5	3.75	0.524	5.5
87			55	244.5	3.5	0.464	4.9
88				439.5	3.75	0.467	4.9
89				634.5	3.8	0.460	4.8
90				829.5	4.0	0.467	4.9

Table 4.11 Experiment sequence for rough disc tests

Expt. No.	Lubricant	α_c (μm)	T ($^{\circ}\text{C}$)	F (N)	u (m/s)	h_c (μm)	λ ratio
91	MCT 5	1.15	30	147.0	3.1	0.542	0.47
92		(R1, BR)			2.4	0.457	0.40
93					1.7	0.362	0.32
94					1.1	0.271	0.24
95					0.6	0.180	0.16
96		1.06	30	244.5	3.3	0.546	0.52
97		(R2, BR)			2.5	0.454	0.43
98					1.8	0.364	0.34
99					1.2	0.277	0.26
100					0.65	0.184	0.17
101		1.15	40	147.0	3.7	0.559	0.49
102		(R1, BR)			2.8	0.464	0.40
103					2.0	0.370	0.32
104					1.3	0.277	0.24
105					0.7	0.183	0.16
106		1.06	40	244.5	3.9	0.560	0.53
107		(R2, BR)			3.0	0.470	0.44
108					2.1	0.370	0.35
109					1.4	0.282	0.27
110					0.75	0.186	0.18
111	MCT 5+FM	1.15	30	147.0	3.1	0.549	0.48
112		(R1, BR)			2.4	0.463	0.40
113					1.7	0.367	0.32
114					1.1	0.274	0.24
115					0.6	0.181	0.16
116		1.06	30	244.5	3.3	0.554	0.52
117		(R2, BR)			2.5	0.460	0.43
118					1.8	0.370	0.35
119					1.2	0.281	0.26
120					0.65	0.186	0.18
121		1.15	40	147.0	3.7	0.527	0.46
122		(R1, BR)			2.8	0.438	0.38
123					2.0	0.349	0.30
124					1.3	0.262	0.23
125					0.7	0.173	0.15

(Table 4.11 continued)

Expt. No.	Lubricant	α_c (μm)	T ($^{\circ}\text{C}$)	F (N)	u (m/s)	h_c (μm)	λ ratio
126		1.06		244.5	3.9	0.528	0.50
127		(R2, BR)			3.0	0.443	0.42
128					2.1	0.349	0.33
129					1.4	0.266	0.25
130					0.75	0.175	0.17
131	MCT 5+EP	1.15	30	147.0	3.1	0.566	0.49
132		(R1, BR)			2.4	0.476	0.41
133					1.7	0.378	0.33
134					1.1	0.282	0.25
135					0.6	0.188	0.16
136		1.06	30	244.5	3.3	0.570	0.54
137		(R2, BR)			2.5	0.473	0.45
138					1.8	0.380	0.36
139					1.2	0.289	0.27
140					0.65	0.192	0.18
141		1.15	40	147.0	3.7	0.545	0.47
142		(R1, BR)			2.8	0.452	0.39
143					2.0	0.361	0.31
144					1.3	0.271	0.24
145					0.7	0.179	0.16
146		1.06	40	244.5	3.9	0.546	0.51
147		(R2, BR)			3.0	0.458	0.43
148					2.1	0.360	0.34
149					1.4	0.275	0.26
150					0.75	0.181	0.17

Table 4.12 Experiment sequence for matched smooth disc tests

Expt. No.	Lubricant	α_c (μm)	T ($^{\circ}\text{C}$)	F (N)	u (m/s)	h_c (μm)	λ ratio
151	MCT 5	0.095	30	147.0	3.1	0.542	5.7
152		(S1, BS)			2.4	0.457	4.8
153					1.7	0.362	3.8
154					1.1	0.271	2.8
155					0.6	0.180	1.9
156		0.095	30	244.5	3.3	0.546	5.8
157		(S2, BS)			2.5	0.454	4.8
158					1.8	0.364	3.8
159					1.2	0.277	2.9
160					0.65	0.184	1.9
161		0.095	40	147.0	3.7	0.559	5.9
162		(S1, BS)			2.8	0.464	4.9
163					2.0	0.370	3.9
164					1.3	0.277	2.9
165					0.7	0.183	1.9
166		0.095	40	244.5	3.9	0.560	5.9
167		(S2, BS)			3.0	0.470	4.9
168					2.1	0.370	3.9
169					1.4	0.282	3.0
170					0.75	0.186	2.0
171	MCT 5+FM	0.095	30	147.0	3.1	0.549	5.8
172		(S1, BS)			2.4	0.463	4.9
173					1.7	0.367	3.9
174					1.1	0.274	2.9
175					0.6	0.181	2.0
176		0.095	30	244.5	3.3	0.554	5.8
177		(S2, BS)			2.5	0.460	4.8
178					1.8	0.370	3.9
179					1.2	0.281	3.0
180					0.65	0.186	2.0
181		0.095	40	147.0	3.7	0.527	5.5
182		(S1, BS)			2.8	0.438	4.6
183					2.0	0.349	3.7
184					1.3	0.262	2.8
185					0.7	0.173	1.8

(Table 4.12 continued)

Expt. No.	Lubricant	α_c (μm)	T ($^{\circ}\text{C}$)	F (N)	u (m/s)	h_c (μm)	λ ratio	
186	MCT 5+FM	0.095	40	244.5	3.9	0.528	5.6	
187					(S2, BS)	3.0	0.443	4.7
188						2.1	0.349	3.7
189						1.4	0.266	2.8
190						0.75	0.175	1.8
191	MCT 5+EP	0.095	30	147.0	3.1	0.566	6.0	
192					(S1, BS)	2.4	0.476	5.0
193						1.7	0.378	4.0
194						1.1	0.282	3.0
195						0.6	0.188	2.0
196		0.095	30	244.5	3.3	0.570	6.0	
197					(S2, BS)	2.5	0.473	5.0
198						1.8	0.380	4.0
199						1.2	0.289	3.0
200						0.65	0.192	2.0
201		0.095	40	147.0	3.7	0.545	5.7	
202					(S1, BS)	2.8	0.452	4.8
203						2.0	0.361	3.8
204						1.3	0.271	2.8
205						0.7	0.179	1.9
206		0.095	40	244.5	3.9	0.546	5.7	
207					(S2, BS)	3.0	0.458	4.8
208						2.1	0.360	3.8
209						1.4	0.275	2.9
210						0.75	0.181	1.9

In the above experimental plan, the entrainment velocities were limited by the disc machine used in the present study, i.e. $u \leq 4$ m/s, or $\psi \leq 178$ Hz. For example, the tests at temperature of 40°C and loads of 634.5 N and 829.5 N could not run properly. Therefore, they were not in the smooth surface experimental plan. Neither were the tests at temperature of 55°C for all four loads.

The experiments 73 to 90 (Table 4.10) were performed under the same operating conditions as experiments 1 to 18. Therefore, the base stock oil (MCT 5) had a repeated set of smooth disc tests, but there was a small difference in the top and bottom disc surface roughnesses.

As mentioned previously, for rough surface tests, it was noted that too high applied loads might cause progressive and continuous plastic deformation of the asperity tips during an experiment. Therefore, only two applied load levels were selected, 147.0 N and 244.5 N. Experiments 91 to 150 and 151 to 210 were matched in that they were performed with the same oil and under the same operating conditions. The top discs, however, had different surface roughnesses, the first set with RMS roughness about ten times that of the second set. Therefore, they represented different lubrication regimes, although their film thicknesses should be the same for equal loads and entrainment velocities.

A short FORTRAN program, THICK.FOR, was written to calculate h_c and λ . The inputs of the program included F , η_0 , α , R , E' , σ_T and σ_B . In general, at the selected temperatures, the lubricant viscosity had only little variation among the formulations (Table 4.2 and Figure 4.1). Also, the same disc pair, i.e. the same σ_T and σ_B , was used to test each of the lubricants. Therefore, the calculated values of λ ratio for all of the smooth disc experiments were found in a range of $3.7 \leq \lambda \leq 6.2$ (Table 4.10), which was satisfied the required range for ehl regime, $\lambda \geq 3$. Thus, the smooth disc experiments were assumed to simulate ehl.

On the other hand, the rough disc experiments (91 to 150) had values of λ ratio under both load levels between 0.15 ~ 0.55, whereas the matched smooth disc experiments (151 to 210) had λ ratio in the range of $1.8 \leq \lambda \leq 6.0$. Thus, it is possible to show the effects of asperity interactions and the influences of lubricant additives in the rough disc experiments. The results of experiments are discussed in the consequent chapters.

Chapter 5 Results

This chapter presents the results obtained from the main experiments performed on the side-slip disc machine. In all cases, the friction force (F_f) in the side-slip direction is presented as a function of the skew angle (ϕ) in a single traction curve. The results are organized in groups. First, the results for full ehl with smooth disc surfaces are presented, followed by the results for the mixed film lubrication with the rough top discs. Major findings of the present thesis can be observed directly from the comparisons of the traction curves, either under the same set of conditions but for different lubricant additives, or under different test conditions but for the same lubricant formulation. The accuracy and precision of test results are discussed briefly in the last part of this chapter.

5.1 Friction Force Measurement

Following the experimental plan, hundreds of friction force measurements were performed for ehl and mixed film lubrication. The friction force data was obtained from the data acquisition system which featured the software package, LabVIEW for Windows, as described in Chapter 3. The analog F_f signal was digitized with a specified sampling frequency and stored in a data file. The analog ϕ signal was treated in the same manner. Then, all the F_f vs. ϕ curves were plotted from these data files using a software package, GRAPHER for Windows (Golden Software, Inc. Golden, Colorado, USA, 1994). For a particular set of conditions, a traction plot was obtained, which included measured F_f versus ϕ from - 0.125 to + 0.125 rad, in both forward (FWD) and reverse (REV) rolling directions to give two sigmoidal curves (Figure 5.1) which intersect at $F_f = 0$ as described previously in Chapter 3.

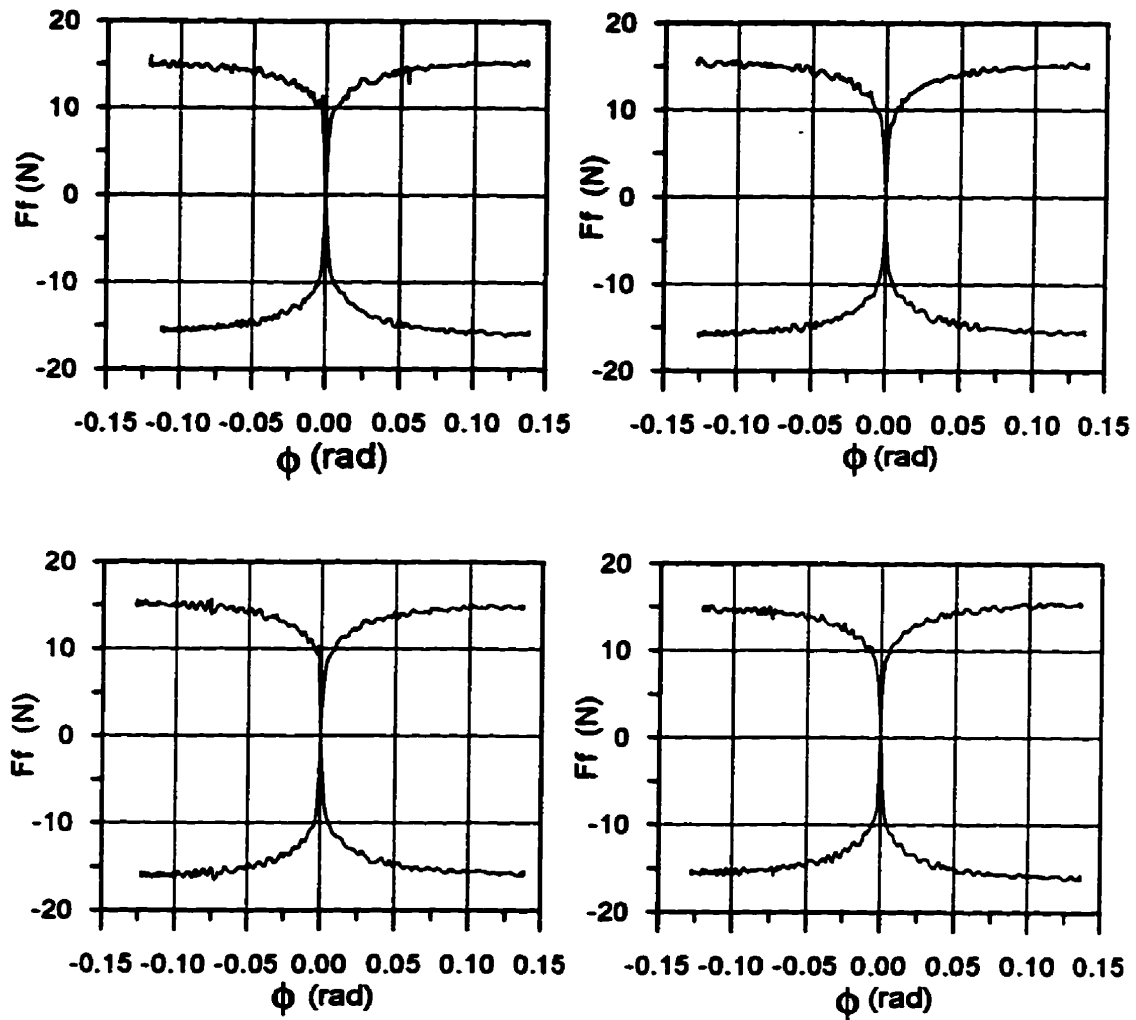


Figure 5.1 Typical repeated traction plots for the same operating conditions (for MCT 5 + FM at $T=30$ C, $u=2.5$ m/s and $F=244.5$ N)

In most cases, rolling speed (u) was the first parameter after ϕ to be varied sequentially and a corresponding sequence of traction plots was obtained. It was standard practice to repeat the sequence of u and thus the corresponding sequence of traction plots. Sometimes, the disc machine was stopped, restarted later, run until the thermal conditions stabilized and the same sequence of u repeated again and then again. As a consequence, many sets of conditions had four corresponding traction plots (Figure 5.1) although, more often, only the first two traction plots were obtained. If a single F_f vs. ϕ curves was required from $\phi = 0$ rad to $\phi = 0.125$ rad, each traction plot provided four choices, one in each quadrant. If four traction plots had been obtained, then, sixteen choices were available. In order to avoid excessive data management problems and because the curves were all very similar, the present author selected a single typical F_f vs. ϕ curve from one quadrant to represent one set of conditions for the specific purpose of presenting typical curves in this chapter.

A summary of the results of each of the experiments was given by quoting the maximum friction force ($F_{f \max}$). To determine $F_{f \max}$, a number of the traction curves with low levels of signal oscillation were identified from a total of two or four "traction plots" (usually from the first and fourth quadrants). Then, the friction force at $\phi = 0.05$ rad (corresponding to a slide-roll ratio of 5%) was identified for each curve and all of these friction forces were averaged. In this manner, it was hoped that the most consistent value of $F_{f \max}$ was obtained. This selection of $\phi = 0.05$ rad for $F_{f \max}$ was made because in all cases F_f was very close to its maximum value, whereas for higher values of ϕ some traction curves had decreases in F_f caused by thermal effects (Figure 5.2b, Expt. No. 8). Also, using ϕ to represent the slide-roll ratio, i.e. $v/u = \tan \phi \approx \phi$ (rad), was correct only when ϕ was small, and thus, accuracy would be reduced when ϕ was large.

5.1.1 Results for full ehl

- **Traction curves**

The smooth disc tests with S0₁ top disc and B0₁ bottom disc were arranged in one group for all four formulations: MCT 5, MCT 5 + FM, MCT 5 + AW and MCT 5 + EP. The traction plots were obtained at various rolling velocities, under four loads (244.5 N, 439.5 N, 634.5 N and 829.5 N) and at three temperatures (30°C, 40°C and 55°C). Traction curves which were measured under the same temperature and similar λ ratios, but various loads and rolling velocities, were grouped together and plotted in individual figures. In this manner, all the data could be presented as a series of 25 plots (Figures 5.2a to 5.5e) with corresponding experiment numbers which were related to the exact conditions in Table 4.10. Thus, a rigorous representation of the variation of F_f with ϕ was given for each experimental condition. The shape of each individual traction curve was influenced by the load, rolling velocity and inlet lubricant temperature, as well as the thermal effects and mechanical vibrations, as discussed in subsequent sections.

LIST OF TRACTION CURVES FROM SMOOTH DISC EXPERIMENTS

(Figures 5.2a to 5.5e on page 168 to 179)

Figure	Lubricant	Temp. (°C)	Expt. No.
5.2 (a)	MCT 5	30	1, 2, 3, 4
5.2 (b)		30	5, 6, 7, 8
5.2 (c)		40	9, 10, 11, 12
5.2 (d)		40	13, 14
5.2 (e)		55	15, 16, 17, 18
5.3 (a)	MCT 5 + FM	30	19, 20, 21, 22
5.3 (b)		30	23, 24, 25, 26
5.3 (c)		40	27, 28, 29, 30
5.3 (d)		40	31, 32
5.3 (e)		55	33, 34, 35, 36
5.4 (a)	MCT 5 + AW	30	37, 38, 39, 40
5.4 (b)		30	41, 42, 43, 44
5.4 (c)		40	45, 46, 47, 48
5.4 (d)		40	49, 50
5.4 (e)		55	51, 52, 53, 54
5.5 (a)	MCT 5 + EP	30	55, 56, 57, 58
5.5 (b)		30	59, 60, 61, 62
5.5 (c)		40	63, 64, 65, 66
5.5 (d)		40	67, 68
5.5 (e)		55	69, 70, 71, 72

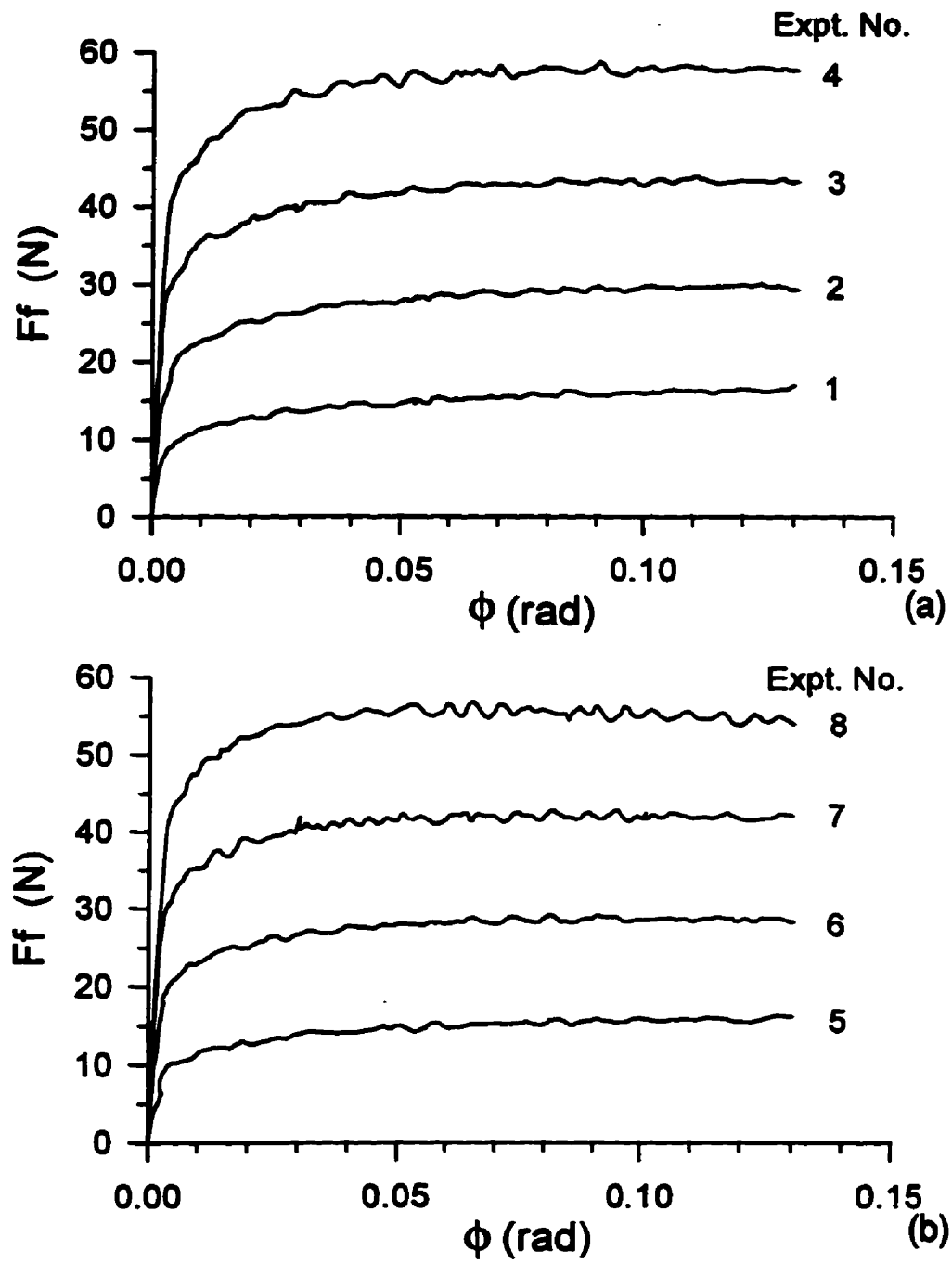


Figure 5.2 Traction curves from smooth disc tests for MCT 5
(a) $T = 30^\circ\text{C}$, 4 load levels, 4 lower u 's
(b) $T = 30^\circ\text{C}$, same 4 loads, 4 higher u 's

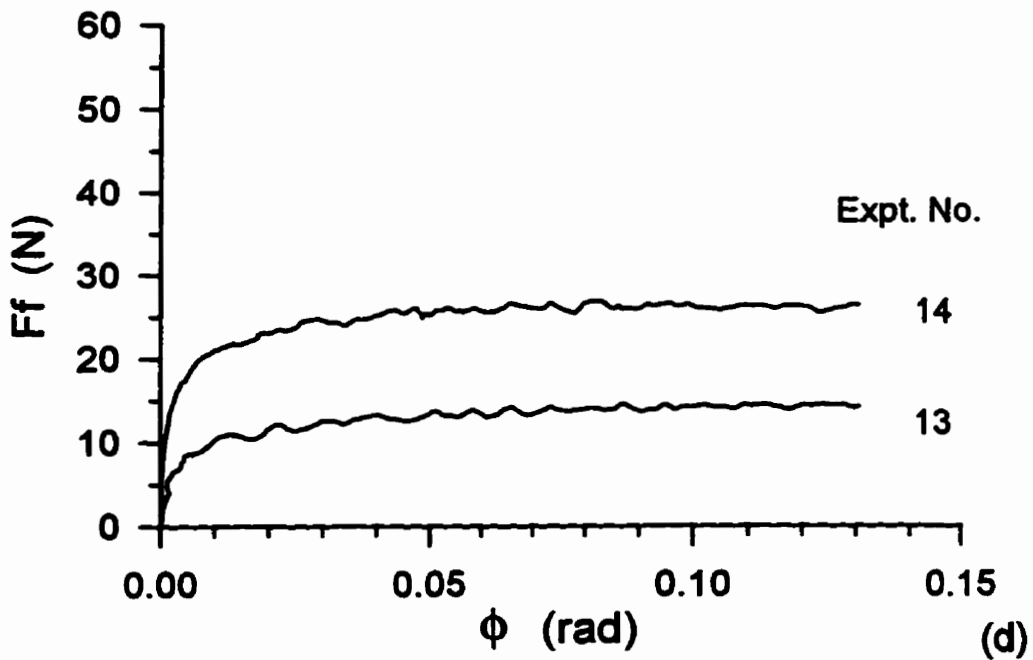
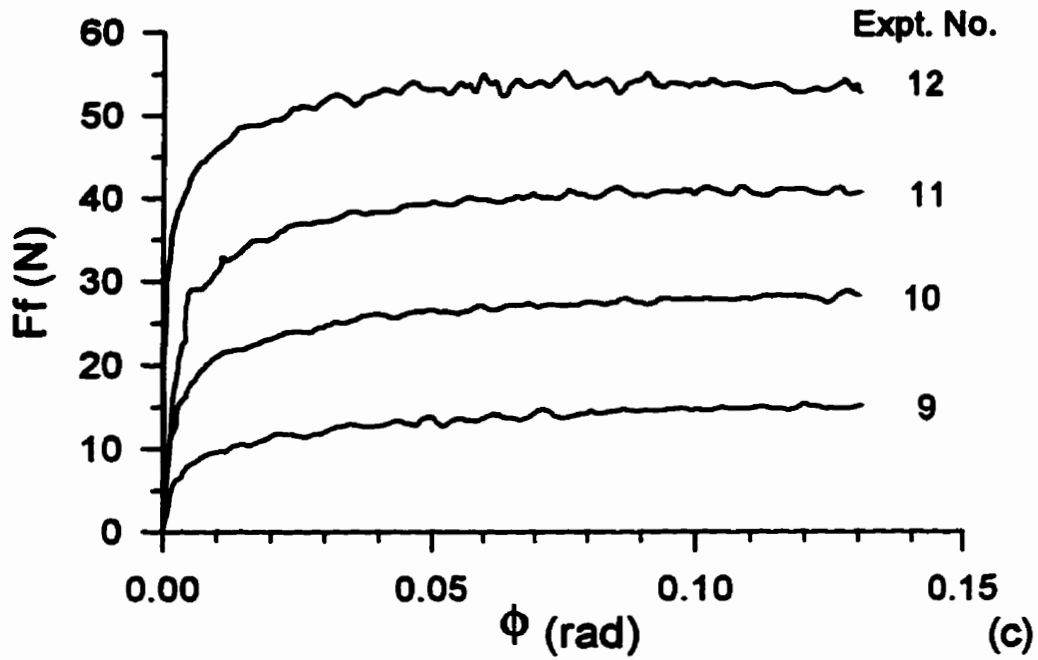


Figure 5.2 Traction curves from smooth disc tests for MCT 5
 (c) $T = 40^\circ\text{C}$, 4 load levels, 4 lower u 's
 (d) $T = 40^\circ\text{C}$, lower 2 loads, 2 higher u 's

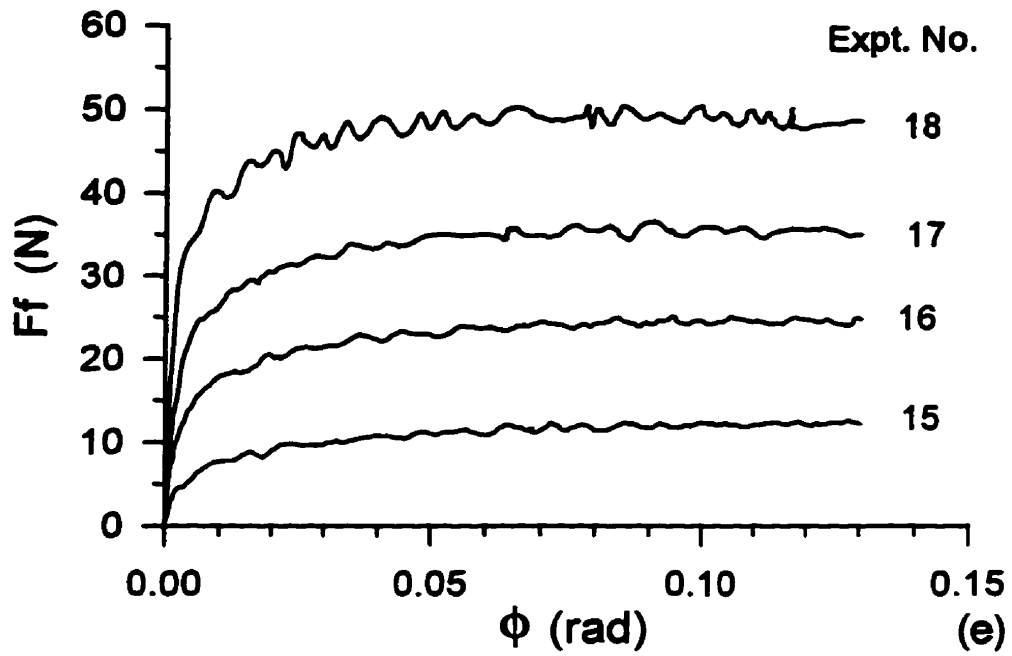


Figure 5.2 Traction curves from smooth disc tests for MCT 5
(e) $T = 55^\circ\text{C}$, 4 load levels, 4 higher u 's

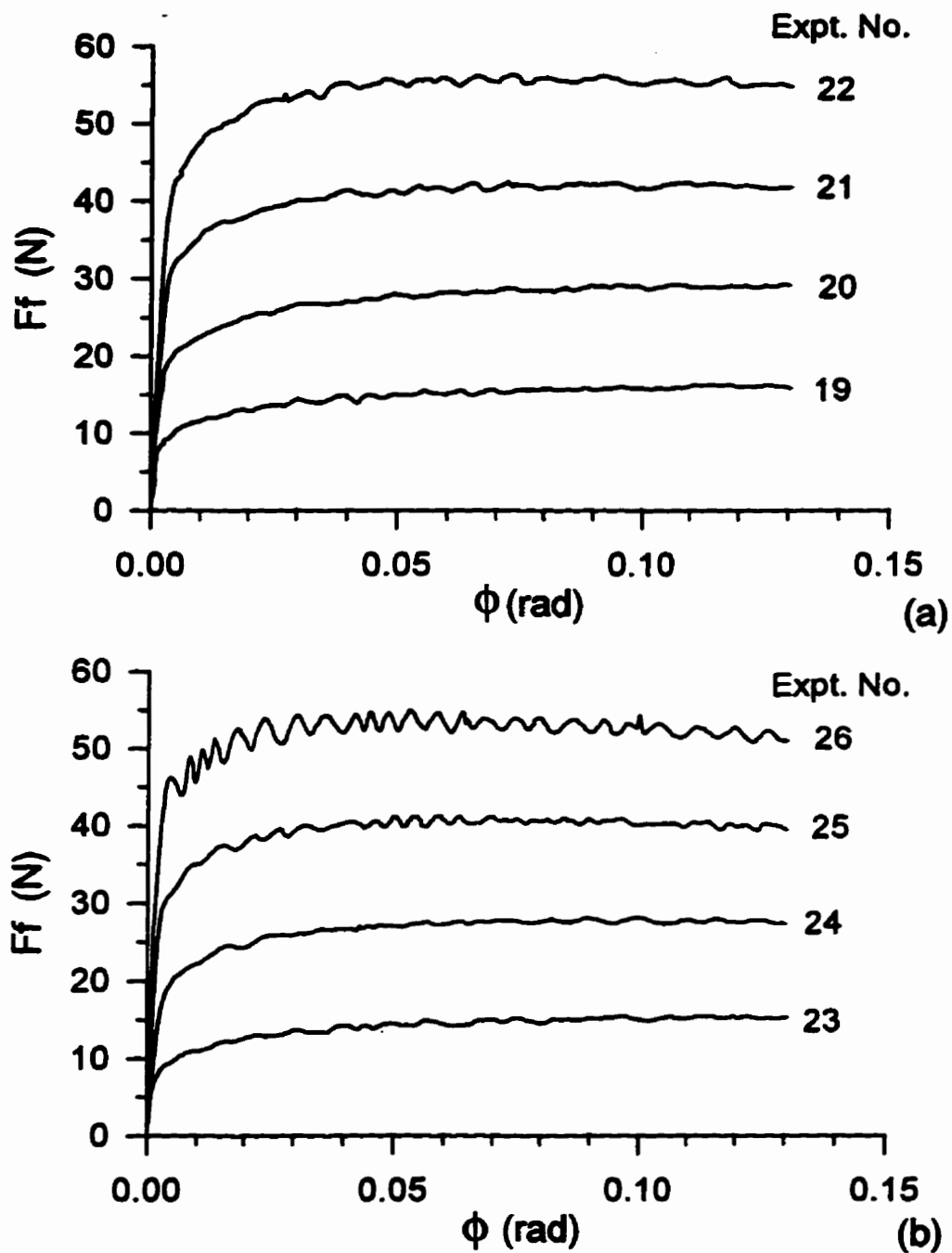


Figure 5.3 Traction curves from smooth disc tests for MCT 5+FM
 (a) $T = 30^\circ\text{C}$, 4 load levels, 4 lower u 's
 (b) $T = 30^\circ\text{C}$, same 4 loads, 4 higher u 's

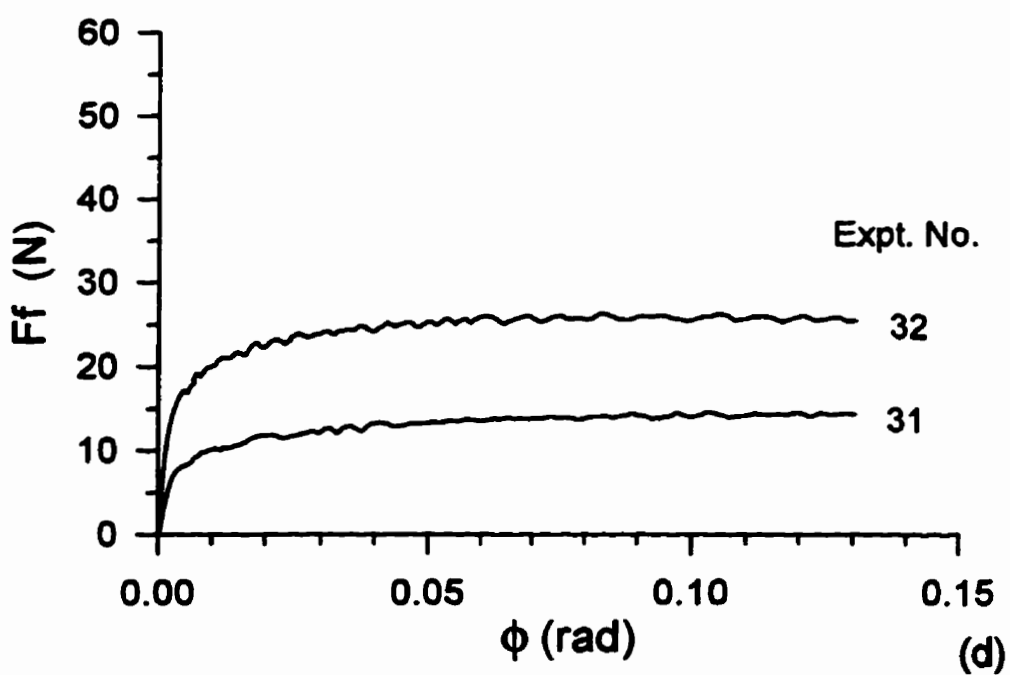
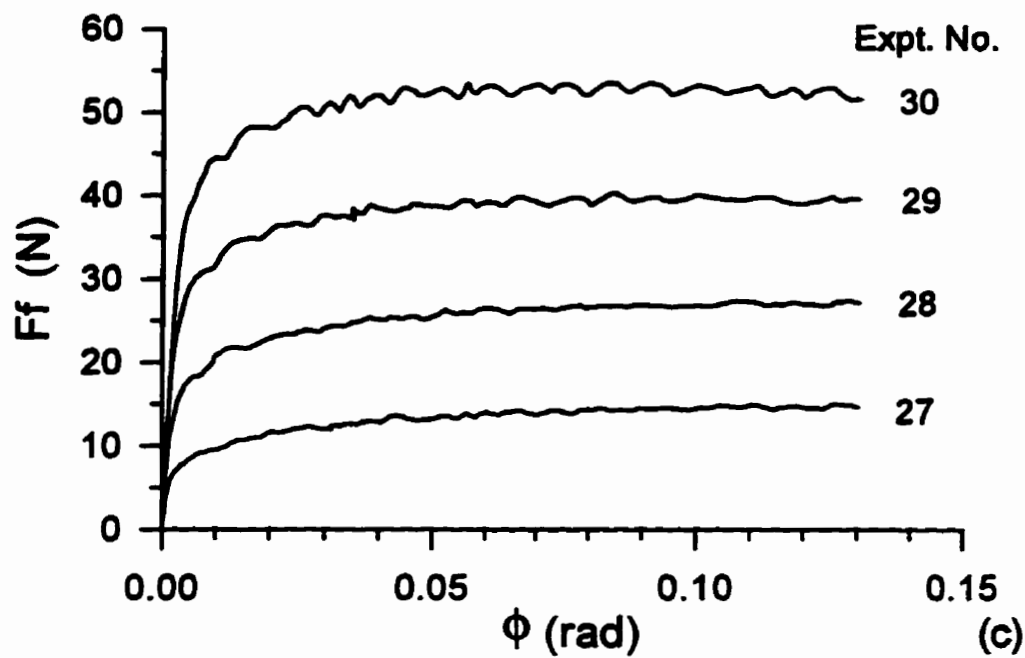


Figure 5.3 Traction curves from smooth disc tests for MCT 5+FM
(c) $T = 40^\circ\text{C}$, 4 load levels, 4 lower u 's
(d) $T = 40^\circ\text{C}$, lower 2 loads, 2 higher u 's

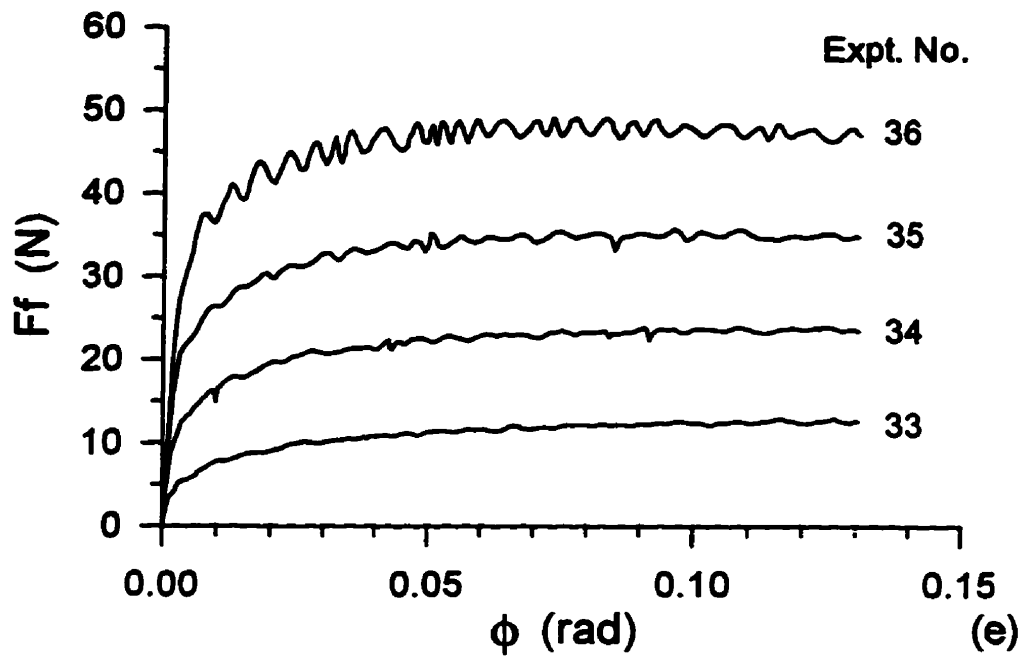


Figure 5.3 Traction curves from smooth disc tests for MCT 5+FM
(e) $T = 55^\circ \text{C}$, 4 load levels, 4 higher u 's

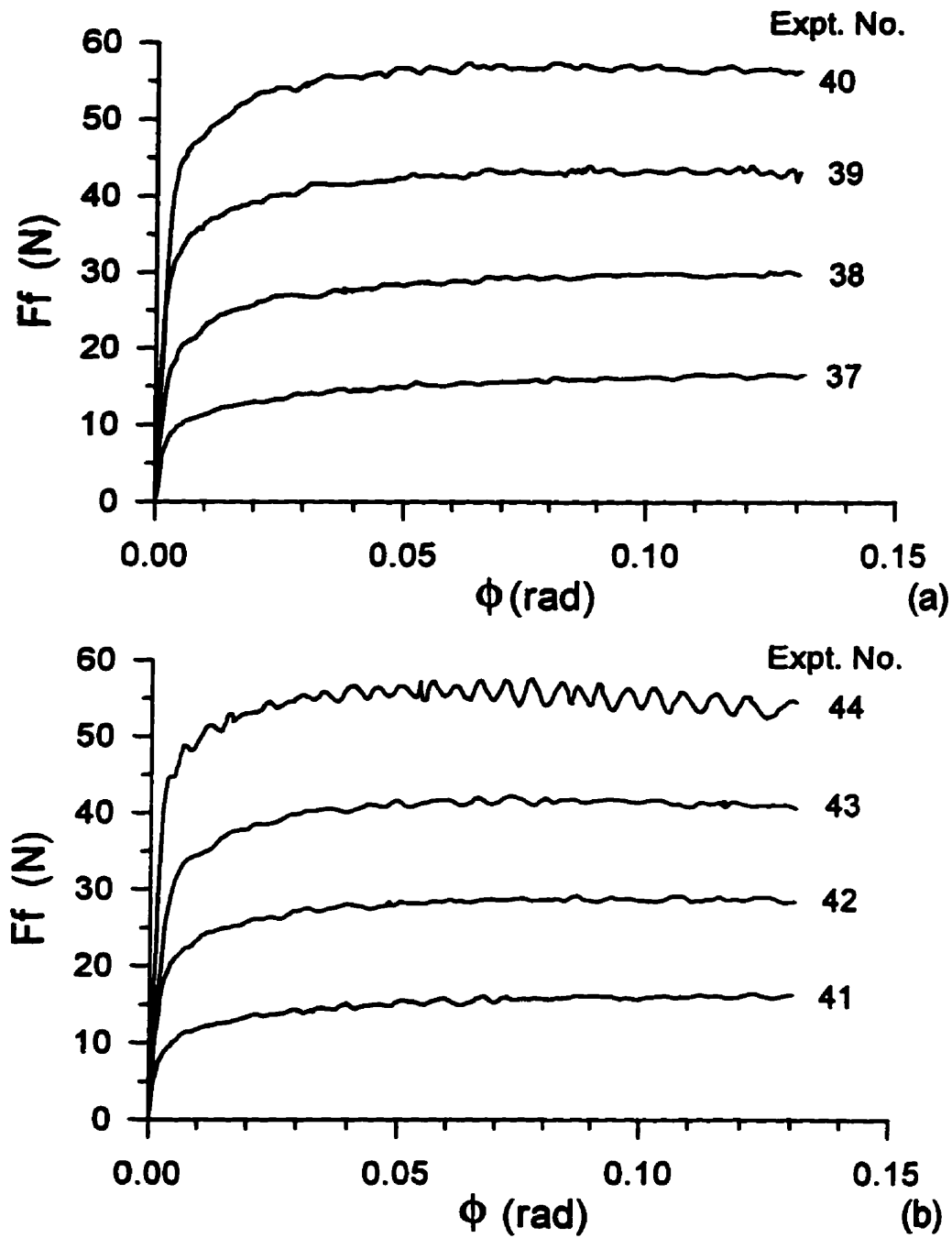


Figure 5.4 Traction curves from smooth disc tests for MCT 5+AW
 (a) $T = 30^\circ \text{C}$, 4 load levels, 4 lower u's
 (b) $T = 30^\circ \text{C}$, same 4 loads, 4 higher u's

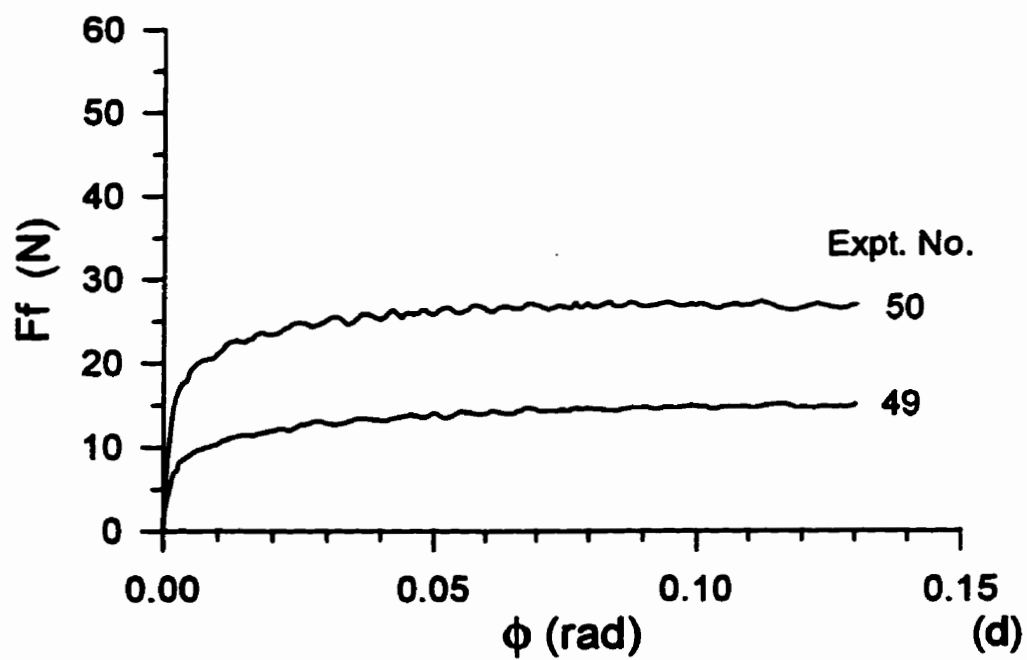
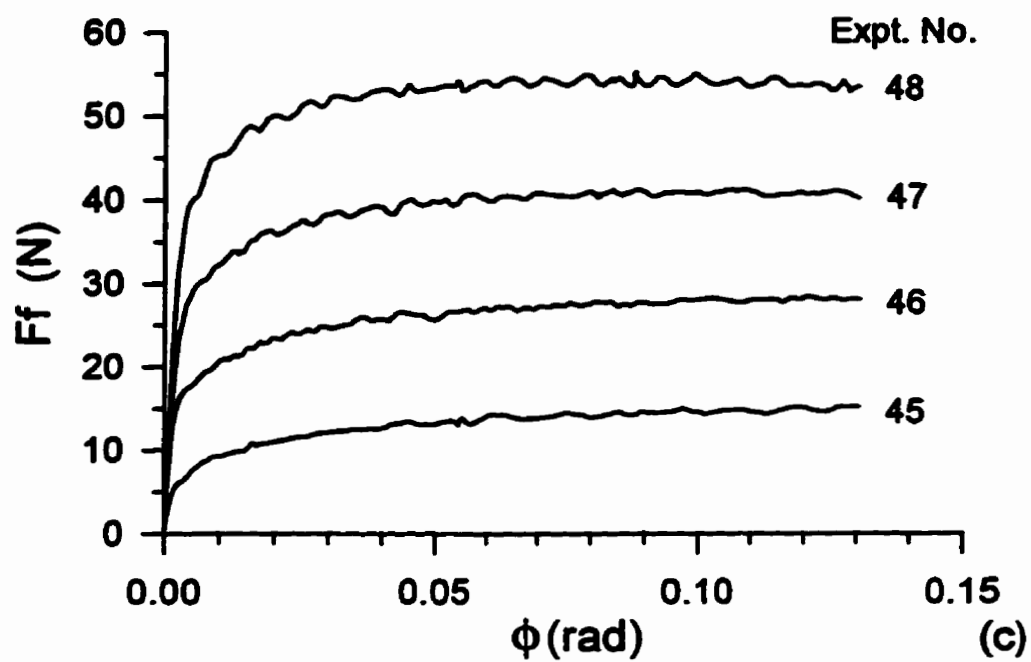


Figure 5.4 Traction curves from smooth disc tests for MCT 5+AW
(c) $T = 40^\circ\text{C}$, 4 load levels, 4 lower u 's
(d) $T = 40^\circ\text{C}$, lower 2 loads, 2 higher u 's

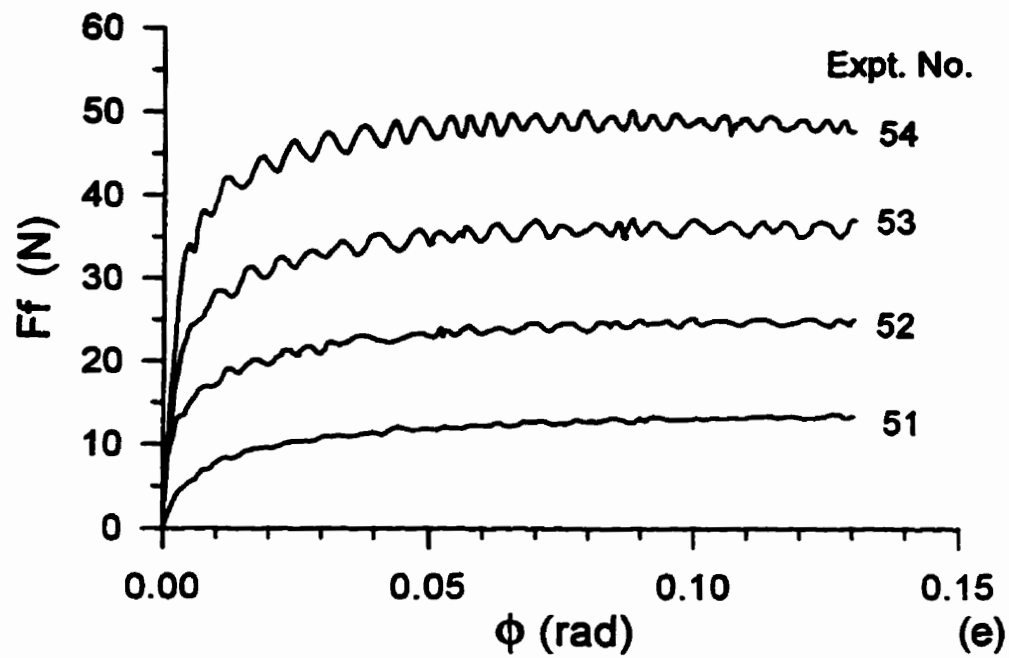


Figure 5.4 Traction curves from smooth disc tests for MCT 5+AW
(e) $T = 55^\circ\text{C}$, 4 load levels, 4 higher u 's

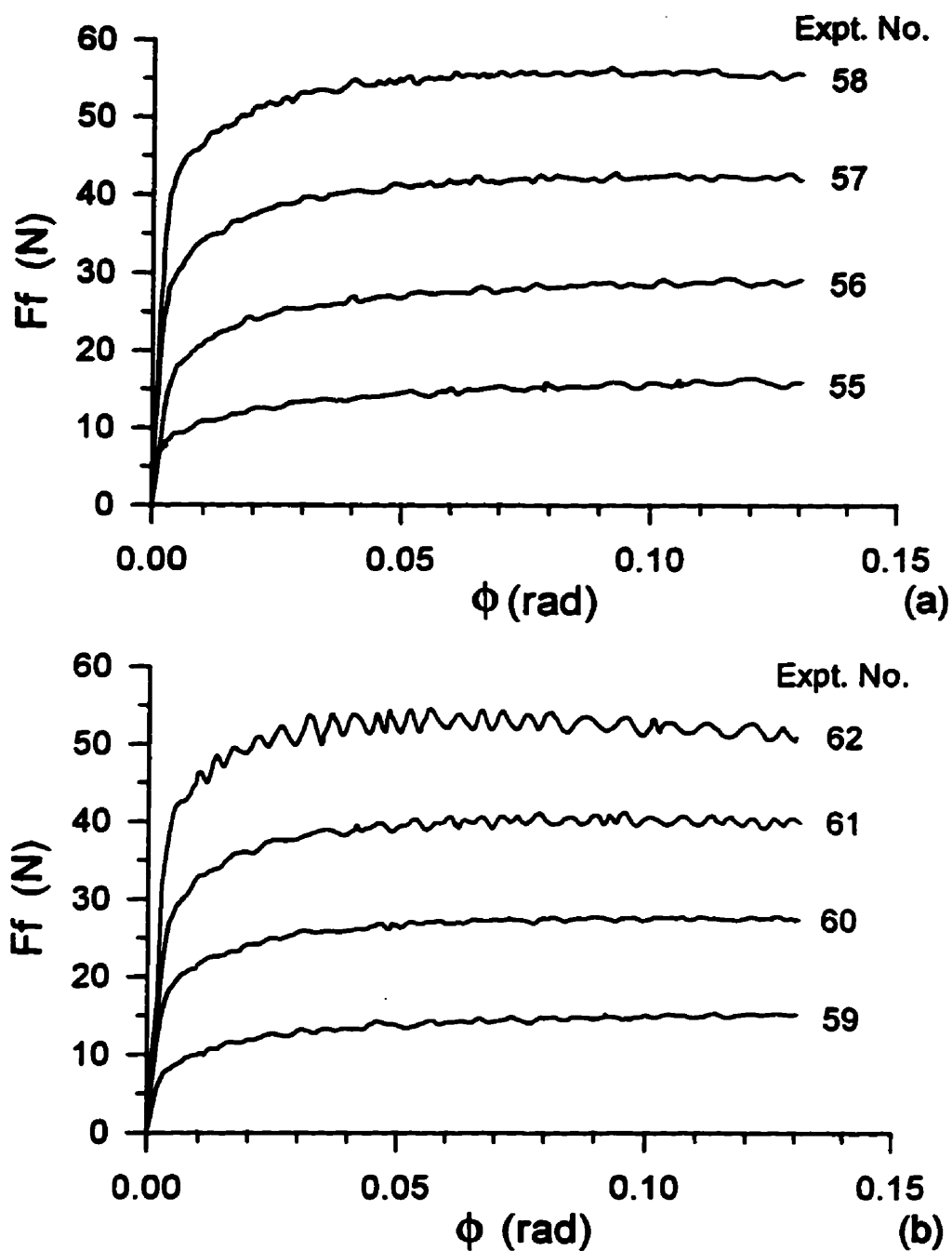


Figure 5.5 Traction curves from smooth disc tests for MCT 5+EP
(a) $T = 30^\circ\text{C}$, 4 load levels, 4 lower u 's
(b) $T = 30^\circ\text{C}$, same 4 loads, 4 higher u 's

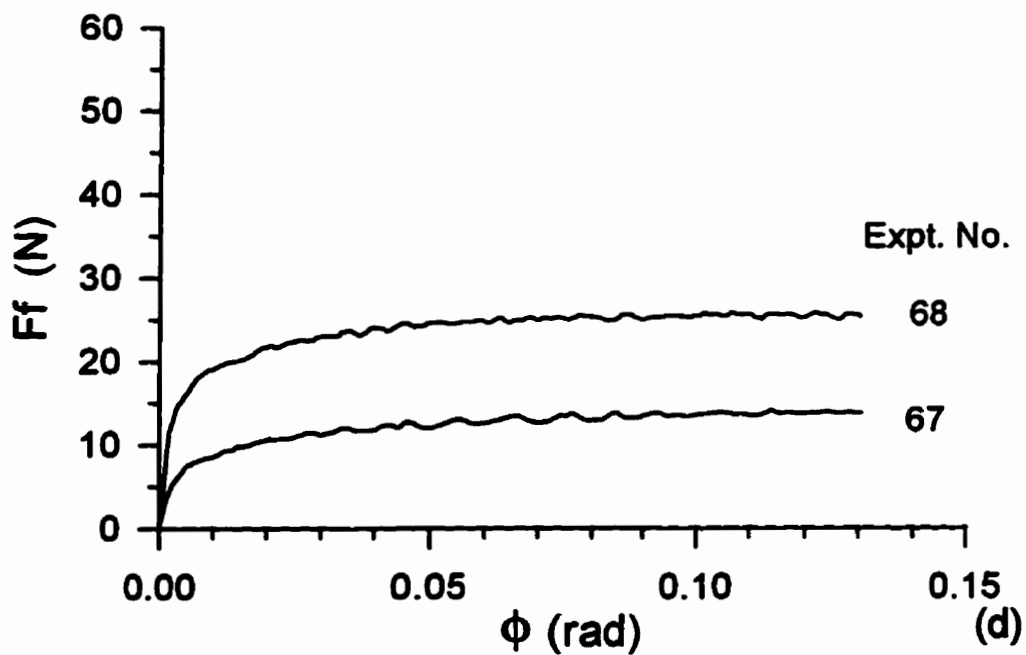
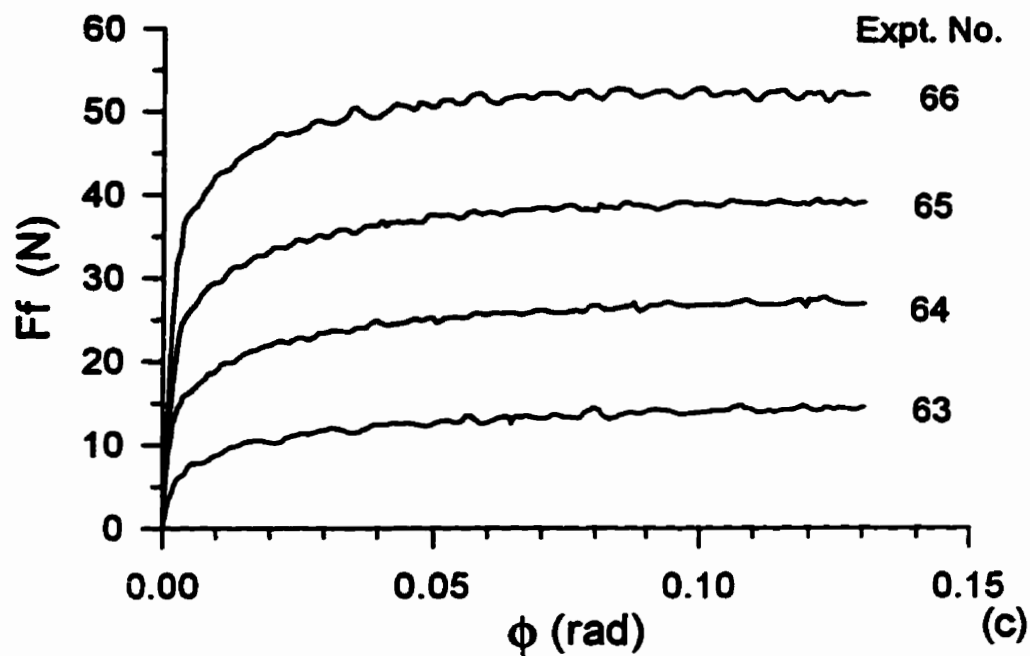


Figure 5.5 Traction curves from smooth disc tests for MCT 5+EP
 (c) $T = 40^\circ\text{C}$, 4 load levels, 4 lower u 's
 (d) $T = 40^\circ\text{C}$, lower 2 loads, 2 higher u 's

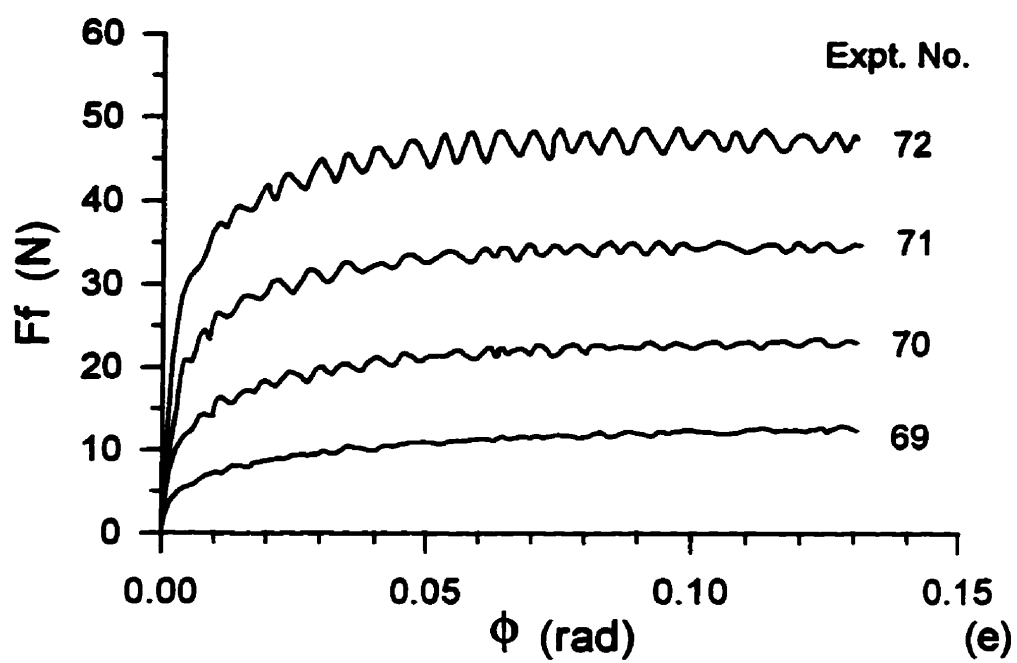


Figure 5.5 Traction curves from smooth disc tests for MCT 5+EP
(e) $T = 55$ C, 4 load levels, 4 higher u 's

● **Maximum friction force**

As described previously, the maximum friction force $F_{f \max}$ was determined for each experiment (Table 5.1). The experiments were organized so that same conditions were imposed on each of the lubricants, and thus Table 5.1 was constructed so that each row present experiments corresponding to the same conditions.

Table 5.1 The $F_{f \max}$ in smooth surface disc measurements

Expt. No.*	$F_{f \max}$ (N) MCT 5	Expt. No	$F_{f \max}$ (N) MCT 5 + FM	Expt. No.	$F_{f \max}$ (N) MCT 5 + AW	Expt. No.	$F_{f \max}$ (N) MCT 5 + EP
1	16.82	19	16.52	37	17.04	55	16.21
2	30.18	20	29.03	38	29.92	56	28.52
3	43.58	21	42.50	39	43.30	57	42.05
4	59.96	22	56.41	40	57.53	58	54.75
5	15.19	23	15.03	41	15.50	59	14.98
6	28.55	24	27.81	42	28.51	60	27.55
7	42.24	25	40.51	43	42.42	61	38.79
8	56.59	26	53.88	44	56.06	62	52.34
9	16.03	27	15.28	45	15.30	63	14.86
10	28.60	28	27.65	46	28.32	64	26.70
11	42.10	29	38.68	47	41.05	65	37.50
12	55.57	30	52.40	48	53.52	66	50.20
13	15.08	31	14.58	49	14.95	67	13.88
14	26.57	32	26.04	50	27.06	68	25.68
15	14.53	33	13.95	51	14.08	69	13.85
16	25.51	34	23.54	52	24.35	70	23.05
17	37.22	35	35.09	53	36.20	71	34.57
18	50.57	36	47.52	54	48.30	72	46.09

* Refer to Table 4.10 for the test conditions of each experiment

5.1.2 Results for mixed film lubrication

- **Traction curves**

The friction force measurements in mixed film lubrication were performed for three formulations: MCT 5, MCT 5 + FM and MCT 5 + EP. All the traction plots were measured under two loads (147.0 N and 244.5 N) and at two temperatures (30°C and 40°C). The traction curves which were measured with the rough top discs R1, R2 and smooth bottom disc BR could be compared with the traction curves which were measured in the matched smooth disc experiments with the smooth top discs S1, S2 and the smooth bottom disc BS.

For each set of the conditions, two traction curves for the same lubricant, at the same temperature, similar λ ratios, slightly varied rolling speeds, but under two different loads, were grouped together and plotted in one figure. The matched smooth disc results which were measured exactly under the same conditions as in the rough disc tests were plotted in the same figure. Therefore, each figure included four traction curves: two thick lined curves for the rough disc tests at two load levels and the other two thin lined curves for the matched smooth disc tests. In this manner, all the results were presented as a series of 30 plots (Figures 5.6a ~ 5.11e) with corresponding experiment numbers which were referred to the conditions in Tables 4.11 and 4.12. As for the full ehl experiments, the shape of each individual traction curve was influenced by experimental conditions, such as the surface roughness, load, rolling velocity, thermal effects and mechanical vibration, as discussed in subsequent sections.

**LIST OF TRACTION CURVES FOR ROUGH TOP DISC EXPERIMENTS
AND MATCHED SMOOTH TOP DISC EXPERIMENTS**

(Figures 5.6a to 5.11e on pages 183 to 200)

Figure	Lubricant	Temp. (°C)	Expt. No.
5.6 (a)	MCT 5	30	91, 96, 151, 156
5.6 (b)			92, 97, 152, 157
5.6 (c)			93, 98, 153, 158
5.6 (d)			94, 99, 154, 159
5.6 (e)			95, 100, 155, 160
5.7 (a)		40	101, 106, 161, 166
5.7 (b)			102, 107, 162, 167
5.7 (c)			103, 108, 163, 168
5.7 (d)			104, 109, 164, 169
5.7 (e)			105, 110, 165, 170
5.8 (a)	MCT 5 + FM	30	111, 116, 171, 176
5.8 (b)			112, 117, 172, 177
5.8 (c)			113, 118, 173, 178
5.8 (d)			114, 119, 174, 179
5.8 (e)			115, 120, 175, 180
5.9 (a)		40	121, 126, 181, 186
5.9 (b)			122, 127, 182, 187
5.9 (c)			123, 128, 183, 188
5.9 (d)			124, 129, 184, 189
5.9 (e)			125, 130, 185, 190
5.10 (a)	MCT 5 + EP	30	131, 136, 191, 196
5.10 (b)			132, 137, 192, 197
5.10 (c)			133, 138, 193, 198
5.10 (d)			134, 139, 194, 199
5.10 (e)			135, 140, 195, 200
5.11(a)		40	141, 146, 201, 206
5.11 (b)			142, 147, 202, 207
5.11 (c)			143, 148, 203, 208
5.11 (d)			144, 149, 204, 209
5.11 (e)			145, 150, 205, 210

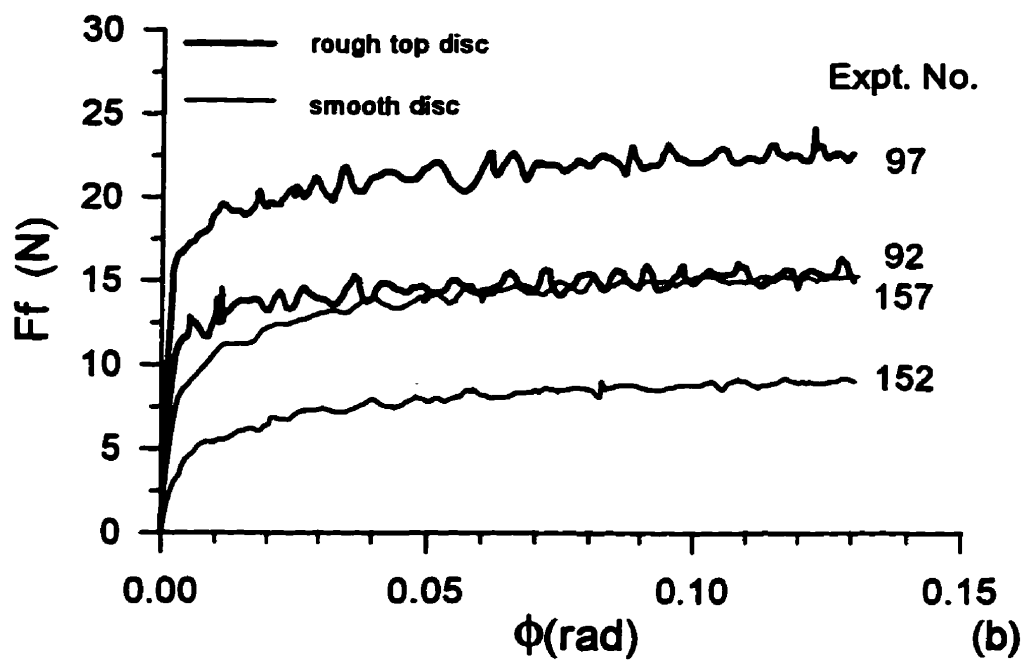
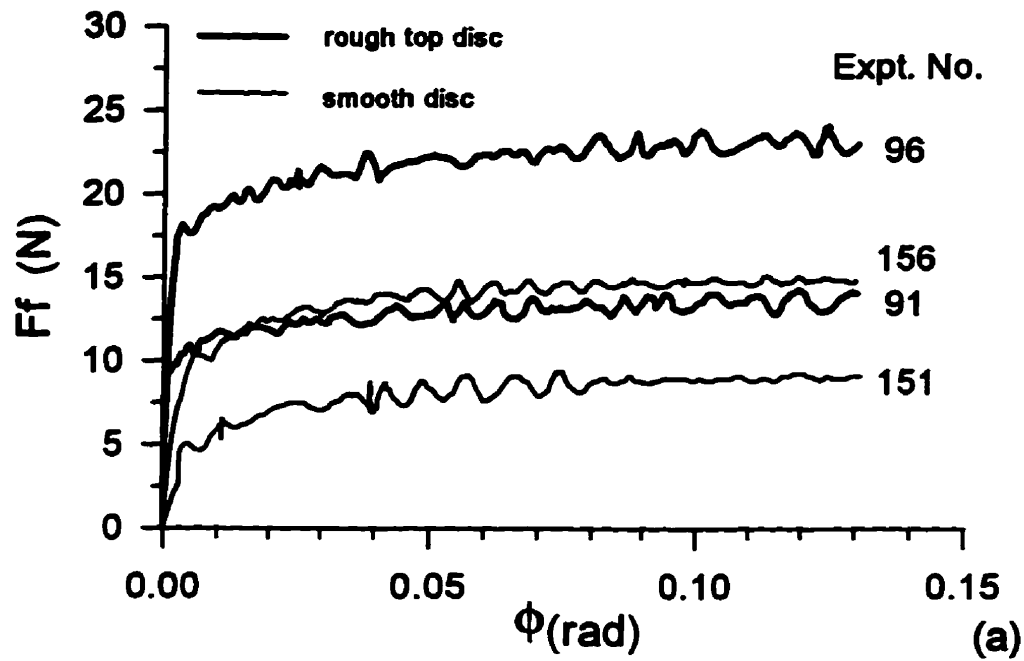


Figure 5.6 Traction curves from rough top disc and matched smooth disc tests for MCT 5 at $T=30^\circ\text{C}$
 (a) 2 load levels, highest u 's
 (b) 2 load levels, high u 's

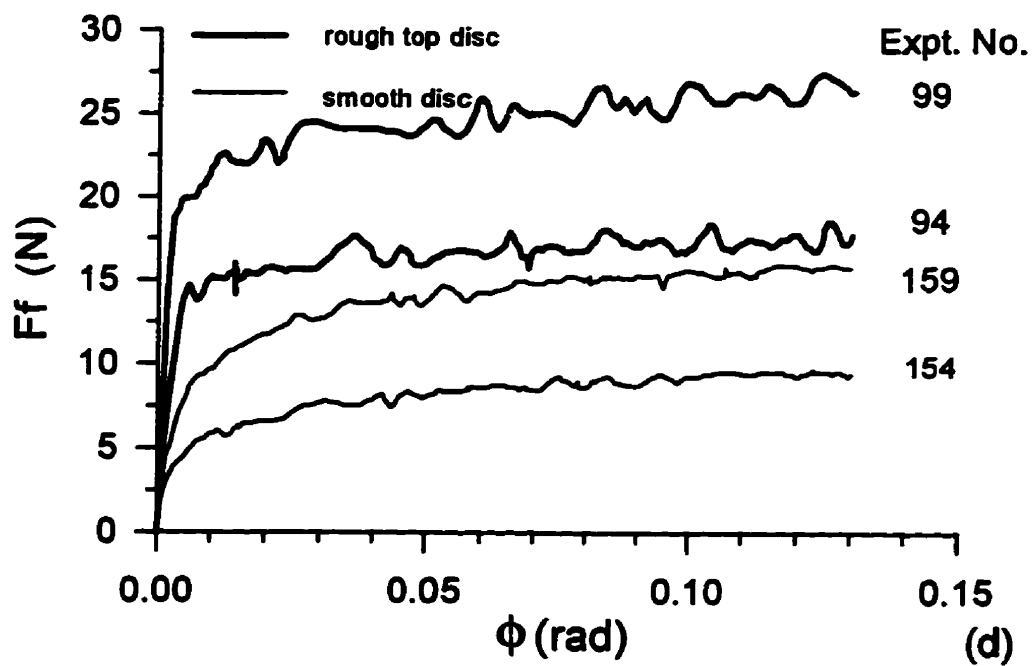
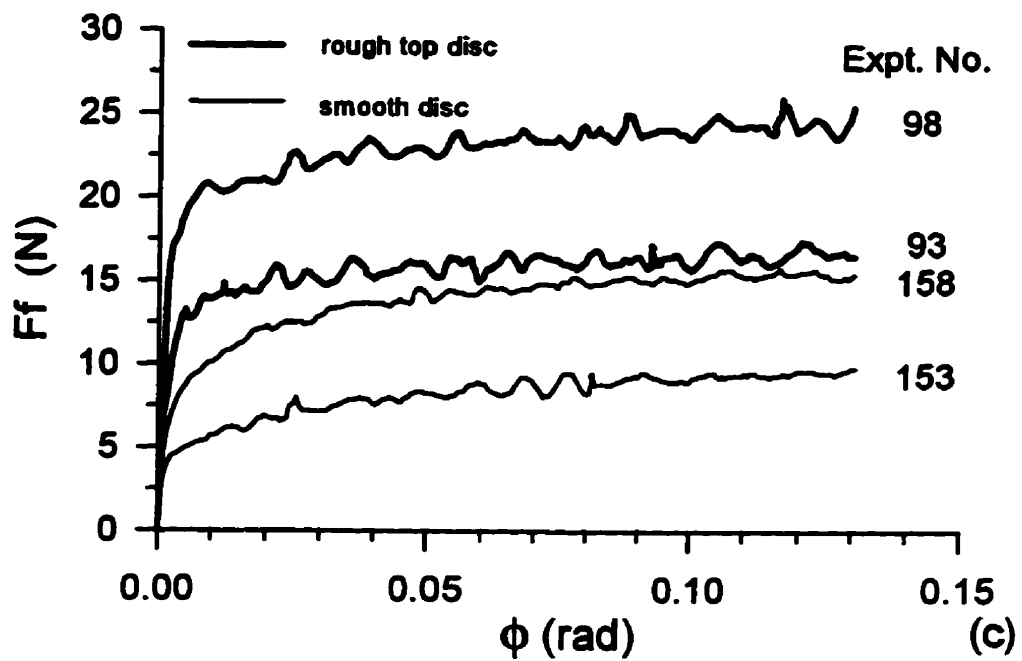


Figure 5.6 Traction curves from rough top disc tests and matched smooth top disc tests for MCT 5 at $T=30^\circ\text{C}$
 (c) 2 load levels, low u 's
 (d) 2 load levels, lower u 's

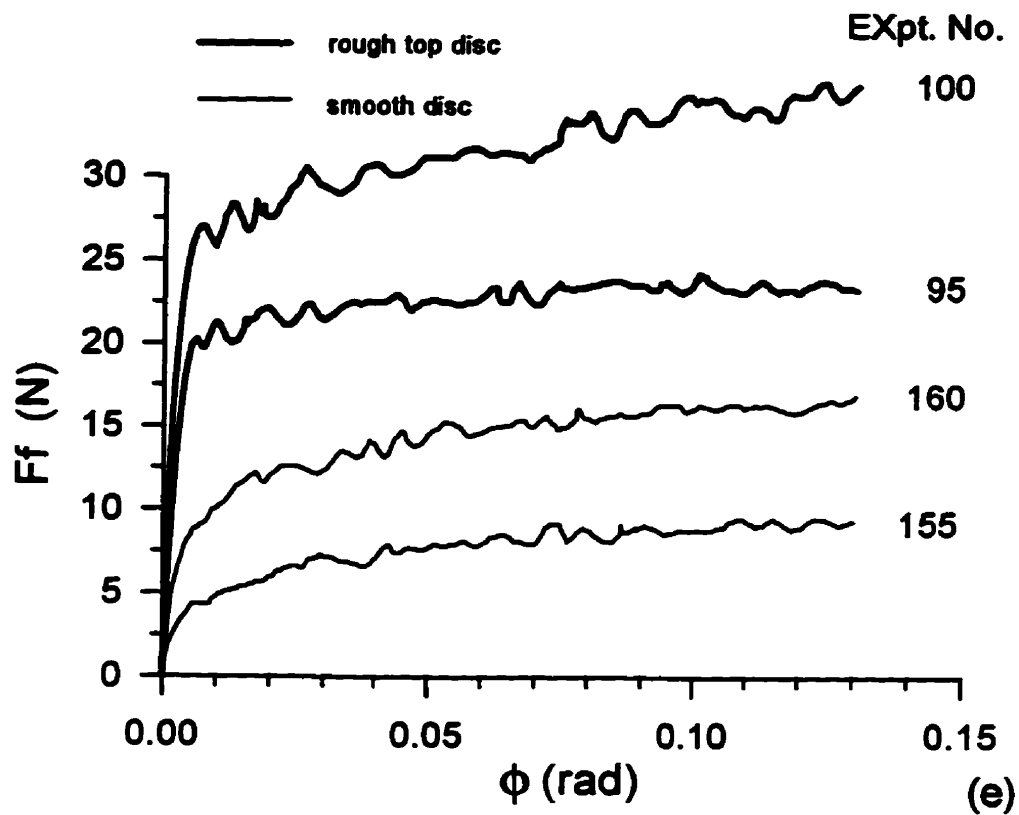


Figure 5.6 Traction curves from rough top disc tests and matched smooth top disc tests for MCT 5 at $T=30^{\circ}\text{C}$
 (e) 2 load levels, lowest u 's

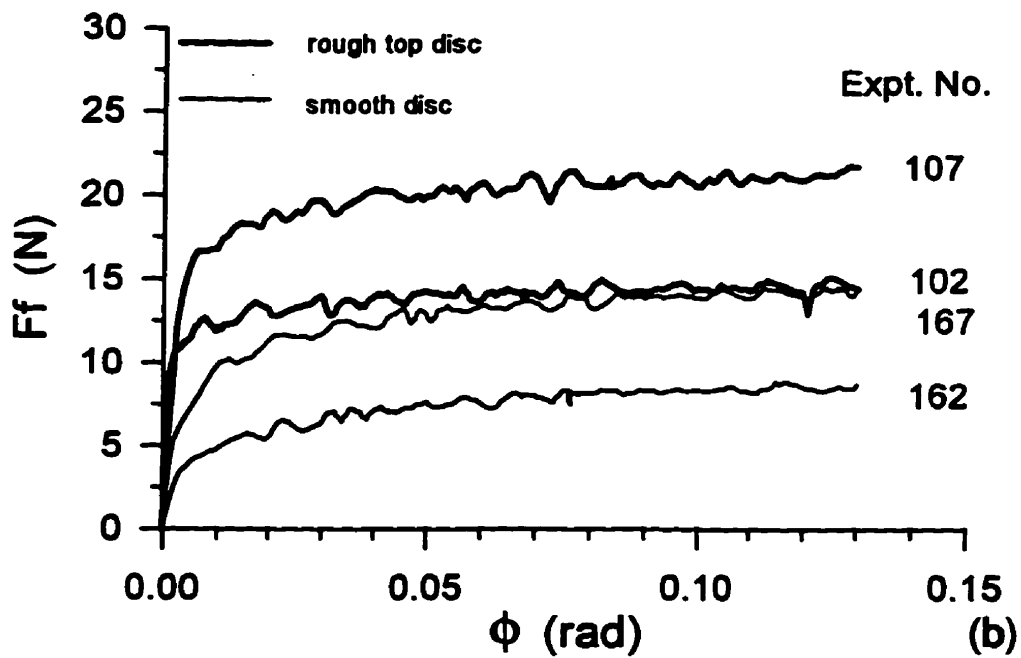
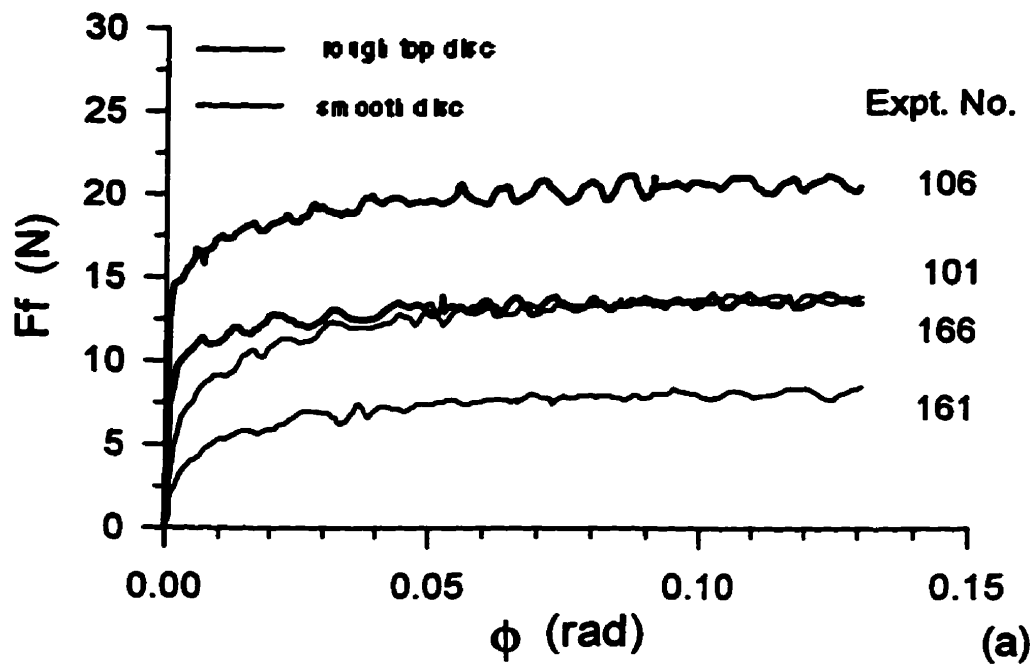


Figure 5.7 Traction curves from rough top disc and matched smooth top disc tests for MCT 5 at $T=40^\circ\text{C}$
 (a) 2 load levels, highest u 's
 (b) 2 load levels, high u 's

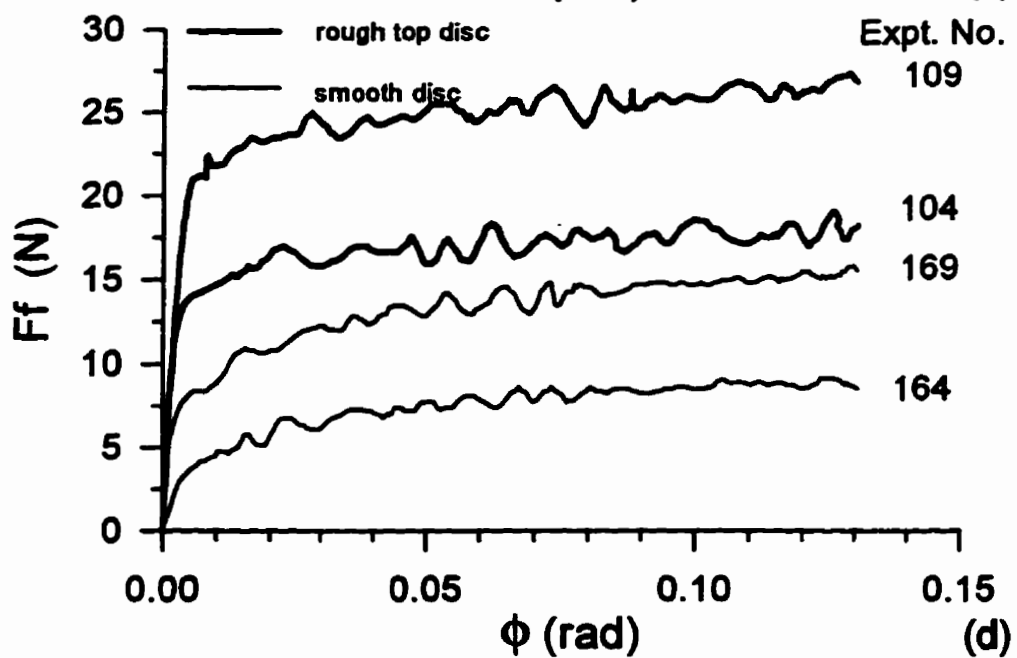
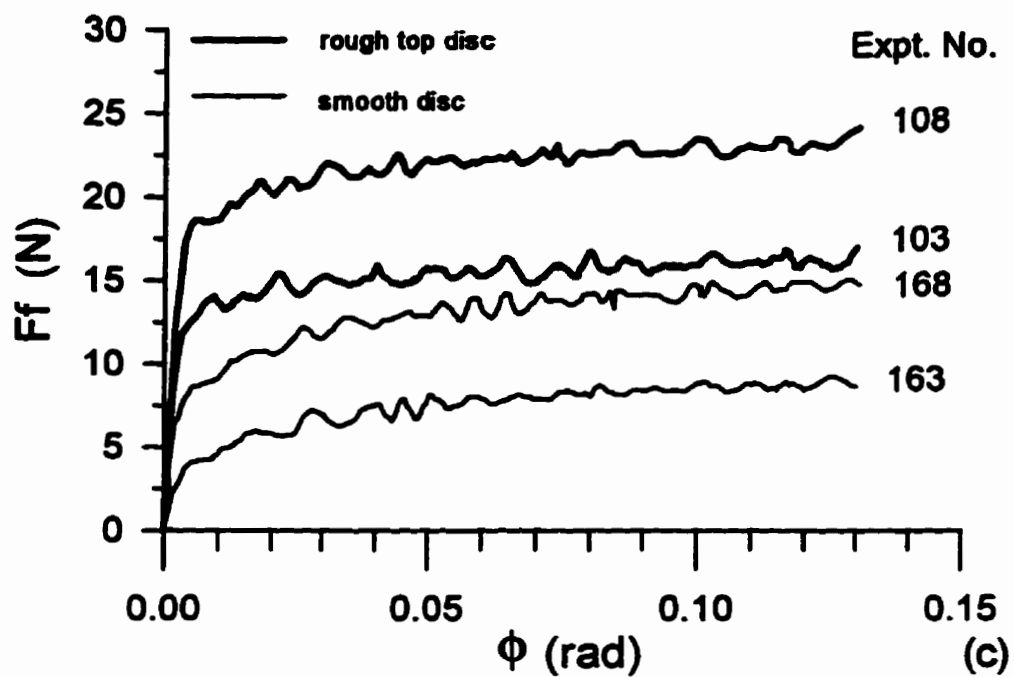


Figure 5.7 Traction curves from rough top disc tests and matched smooth top disc tests for MCT 5 at $T=40^{\circ}\text{C}$
 (c) 2 load levels, low u 's
 (d) 2 load levels, lower u 's

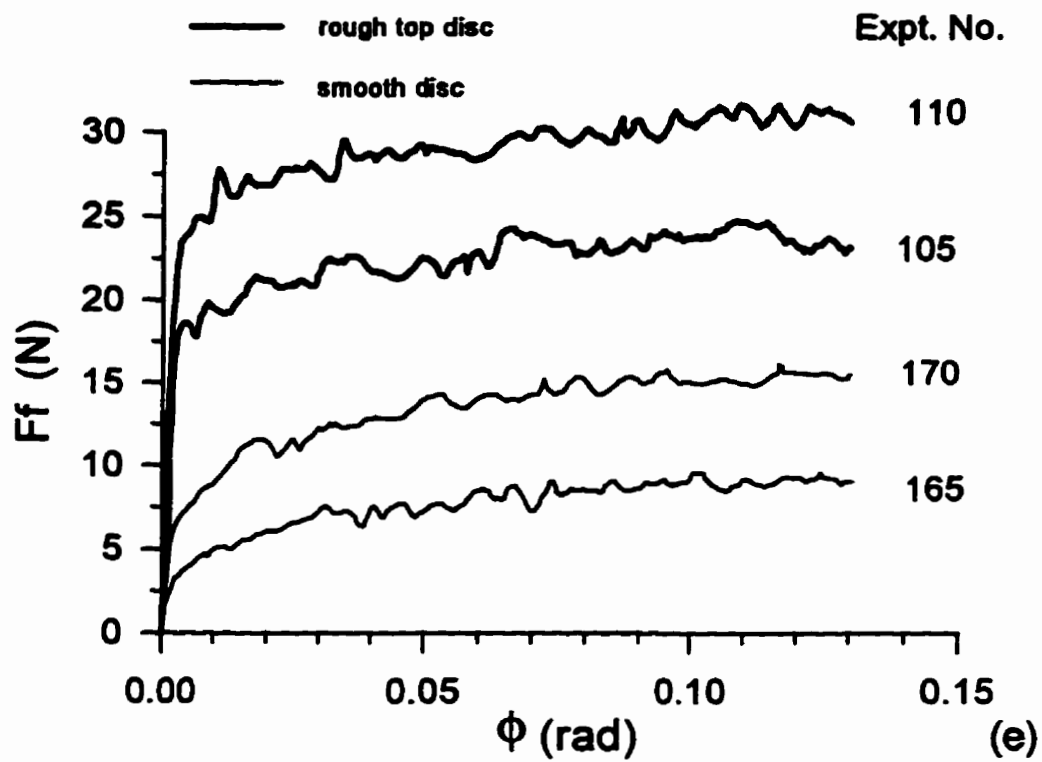


Figure 5.7 Traction curves from rough top disc tests
 matched smooth top disc tests for MCT 5 at $T=40$ °C
 (e) 2 load levels, lowest u 's

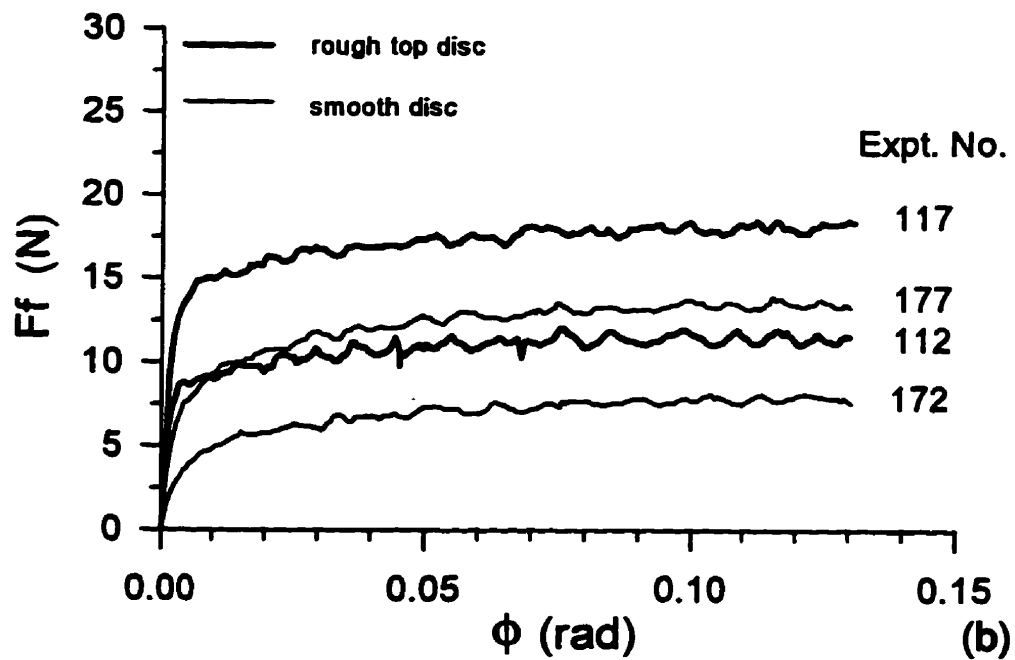
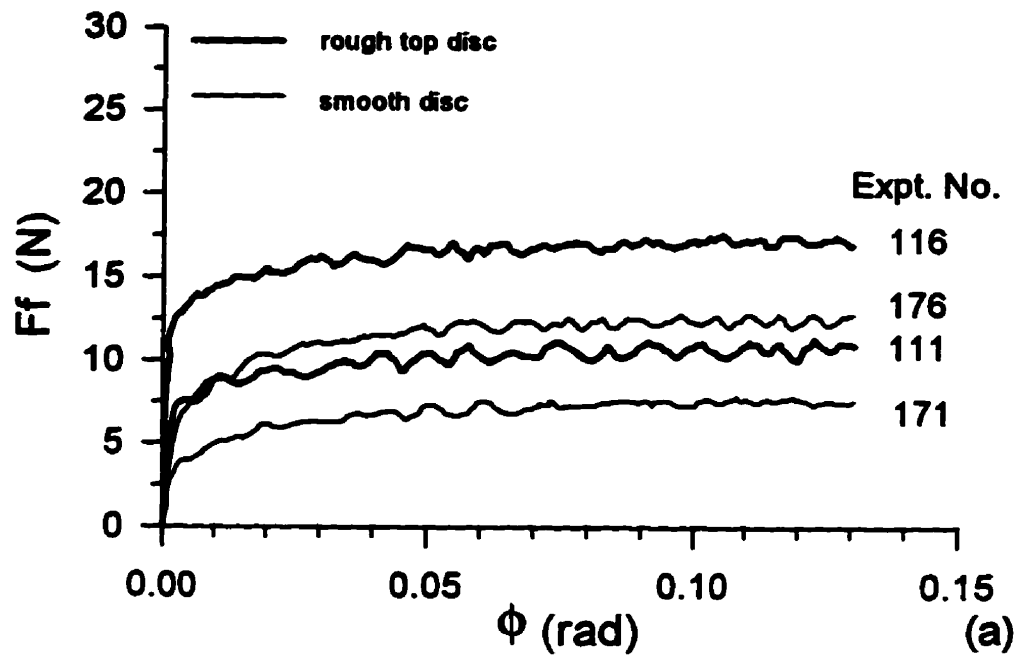


Figure 5.8 Traction curves from rough top disc tests and matched smooth top disc tests for MCT 5+FM at $T=30^\circ\text{C}$
 (a) 2 load levels, highest u 's
 (b) 2 load levels, high u 's

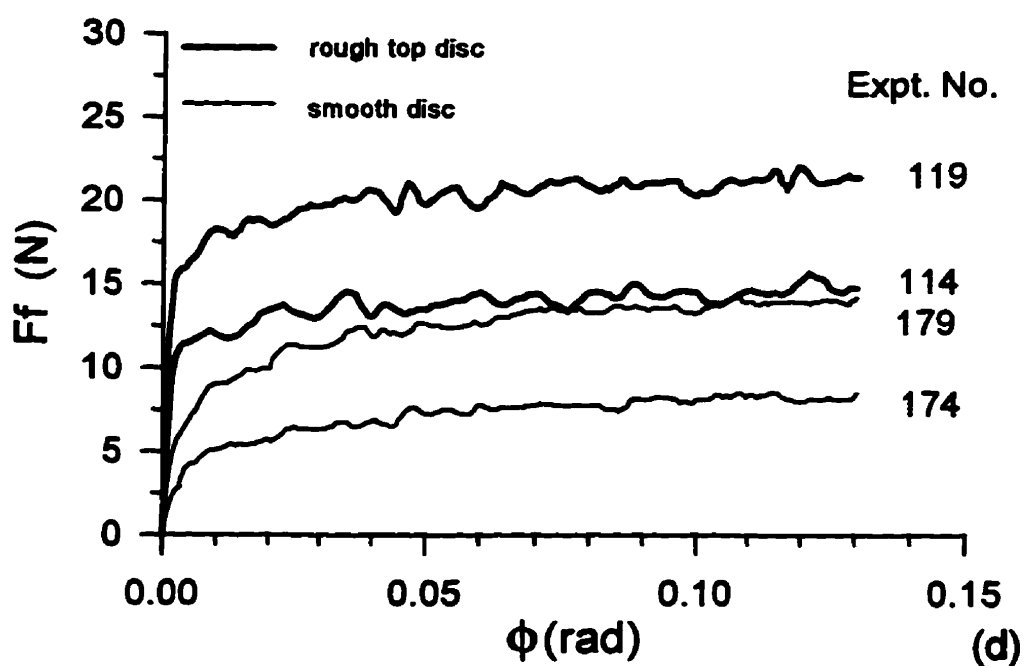
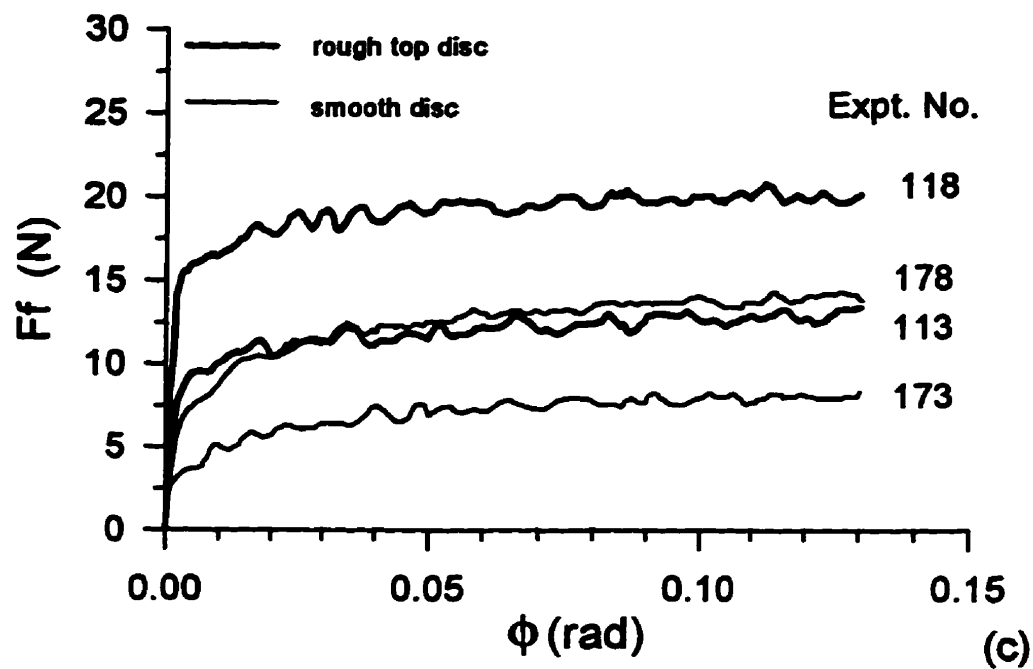


Figure 5.8 Traction curves from rough top disc tests and matched smooth top disc tests for MCT 5+FM at $T=30^\circ\text{C}$
 (c) 2 load levels, low u 's
 (d) 2 load levels, lower u 's

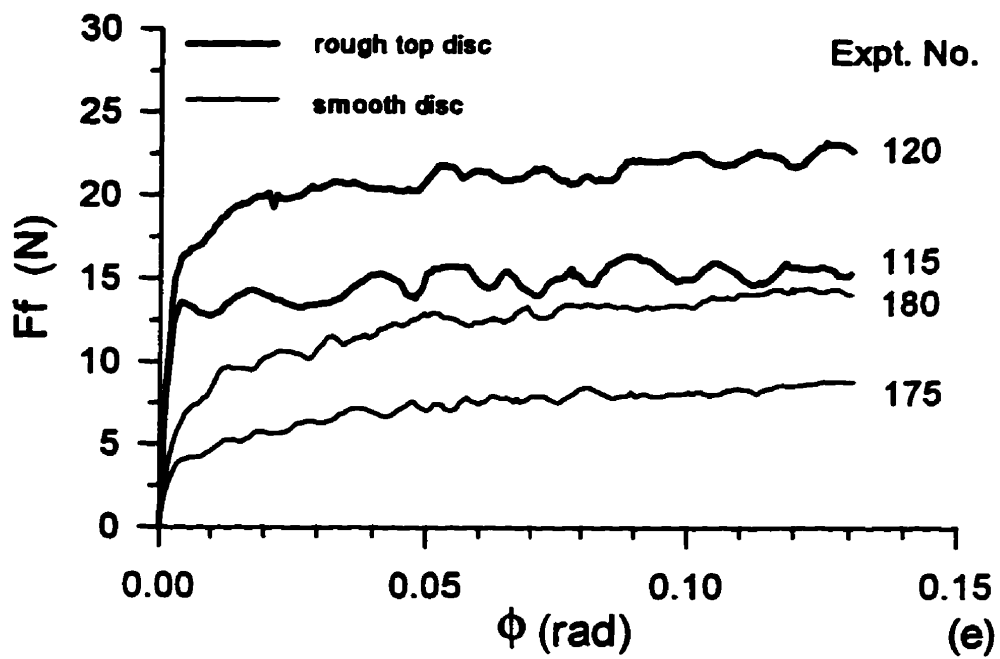


Figure 5.8 Traction curves from rough top disc tests and matched smooth top disc tests for MCT 5+FM at $T=30^{\circ}\text{C}$
(e) 2 load levels, lowest u's

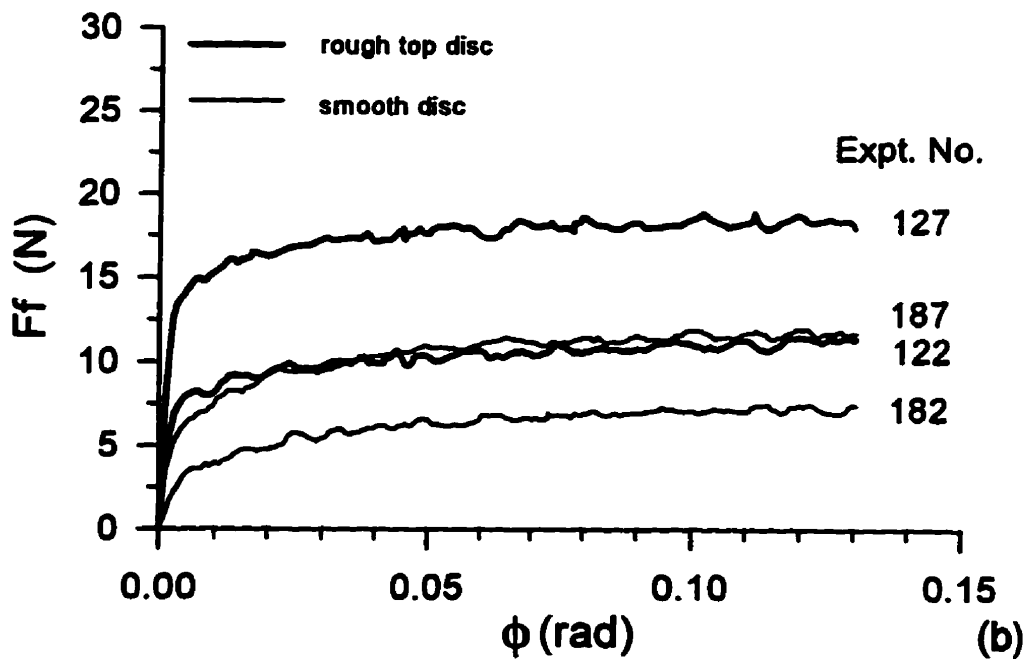
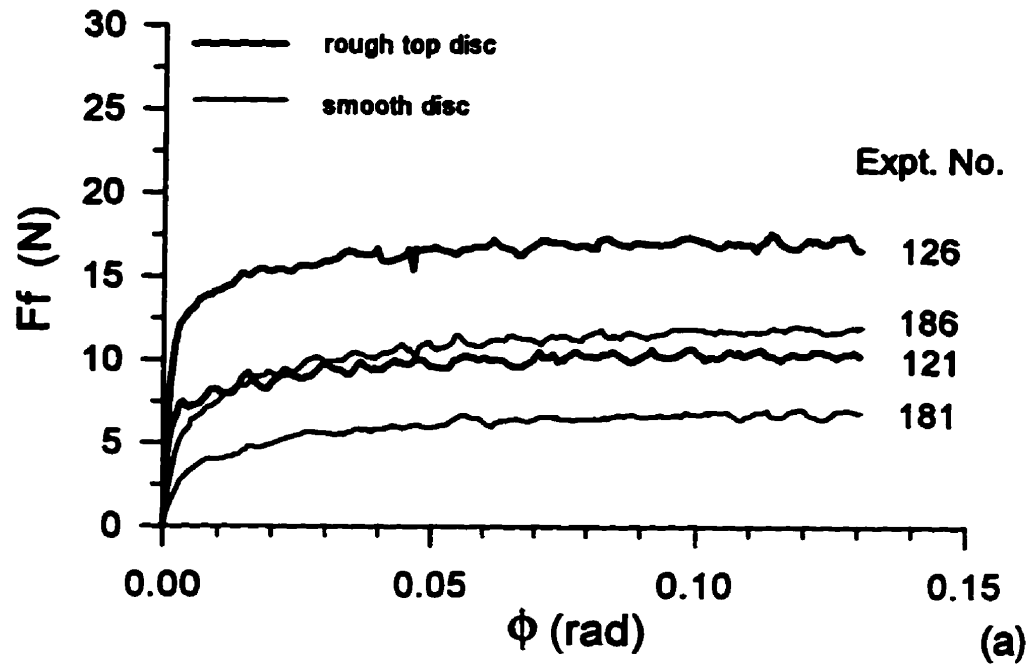


Figure 5.9 Traction curves from rough top disc tests and matched smooth top disc tests for MCT 5+FM at $T=40^\circ\text{C}$
 (a) 2 load levels, highest u 's
 (b) 2 load levels, high u 's

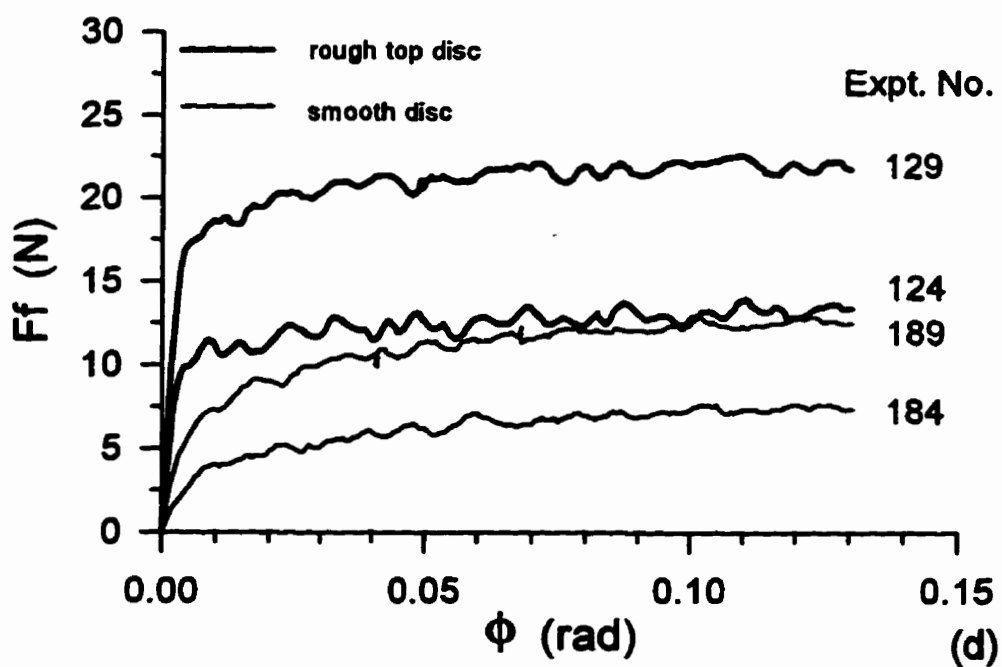
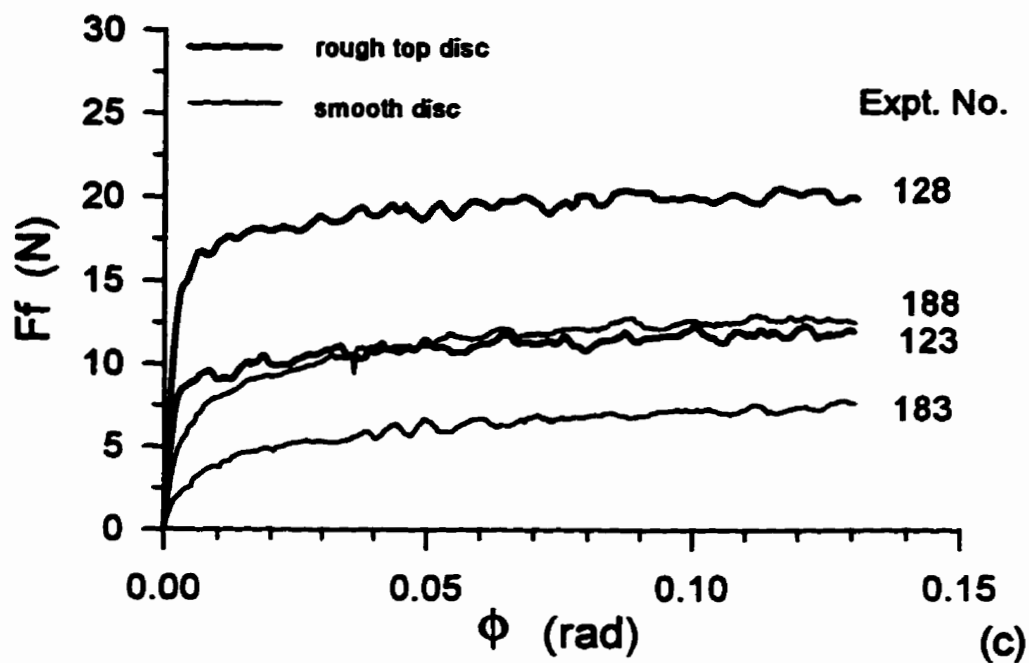


Figure 5.9 Traction curves from rough top disc tests and matched smooth top disc tests for MCT 5+FM at $T=40^\circ\text{C}$
 (c) 2 load levels, low u 's
 (d) 2 load levels, lower u 's

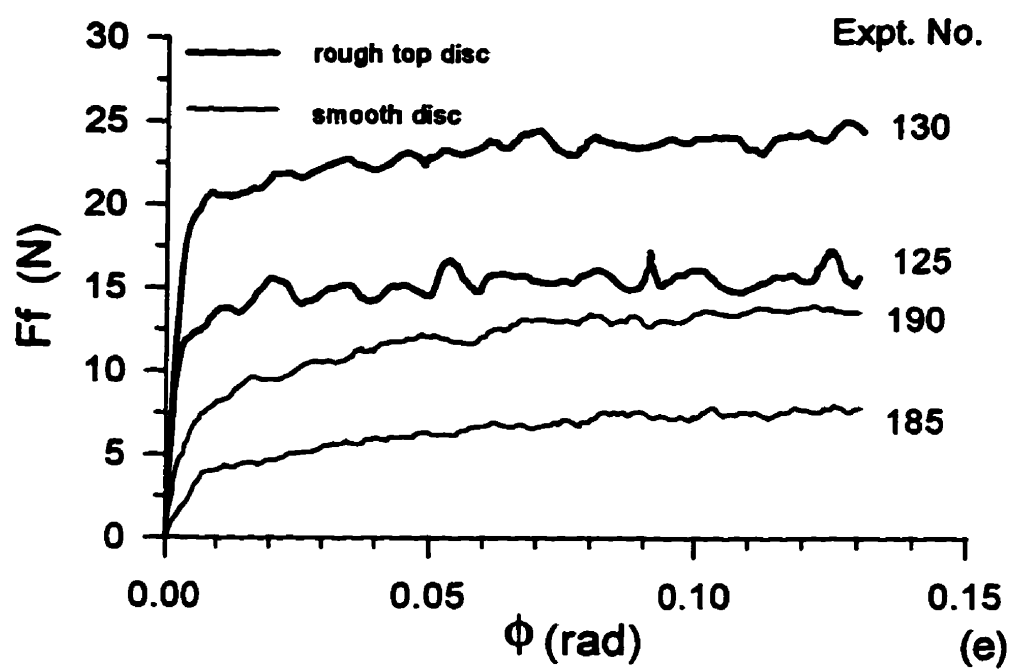


Figure 5.9 Traction curves from rough top disc tests and matched smooth top disc tests for MCT 5+FM at $T=40^{\circ}\text{C}$
(e) 2 load levels, lowest u 's

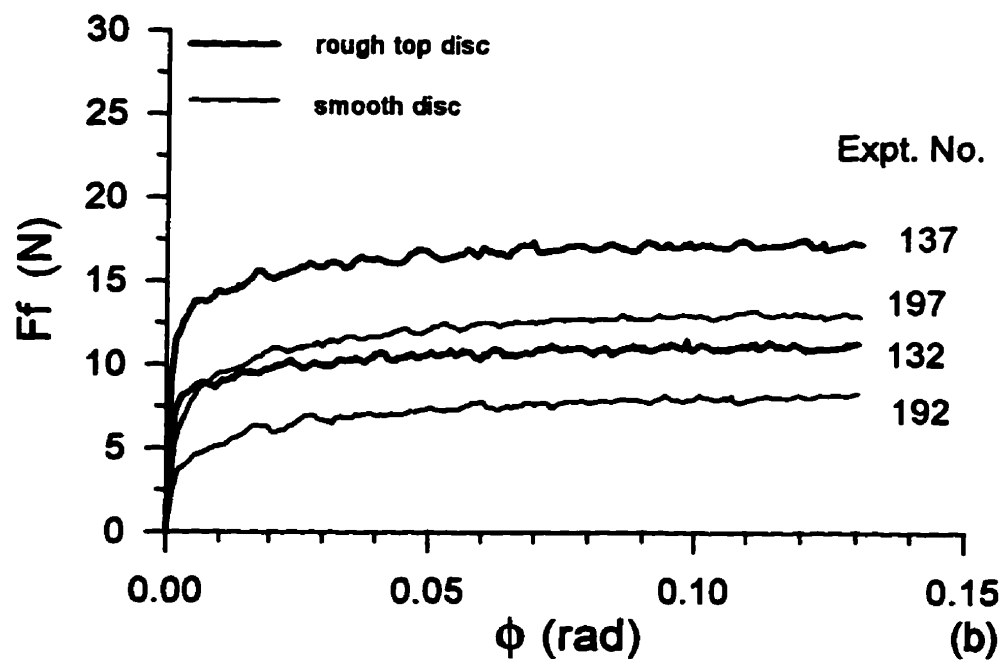
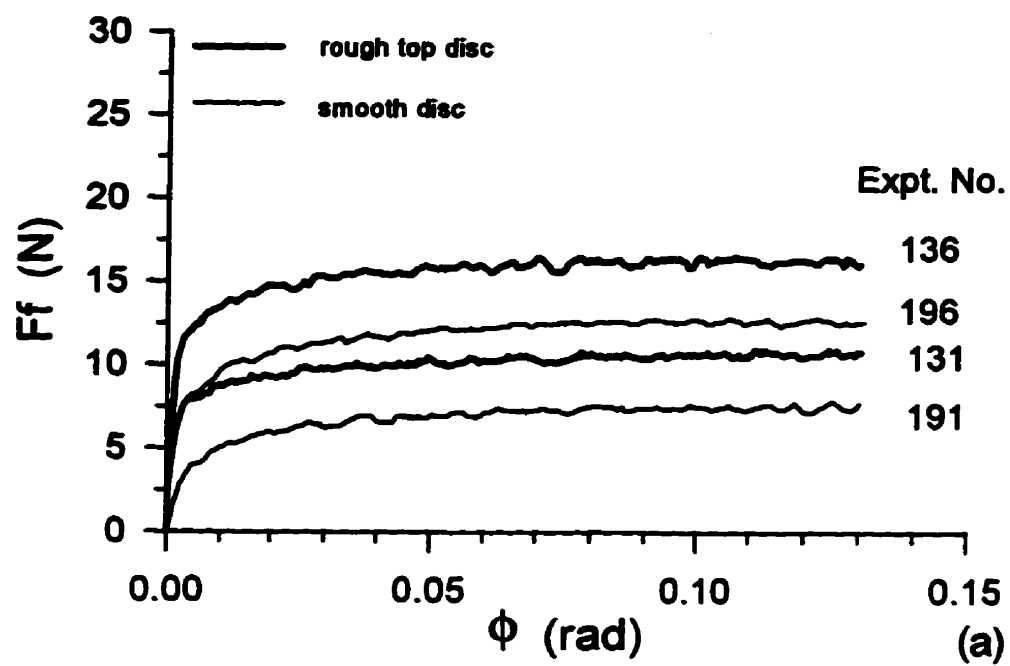


Figure 5.10 Traction curves from rough top disc tests and matched smooth top disc tests for MCT 5+EP at $T=30^\circ\text{C}$
 (a) 2 load levels, highest u 's
 (b) 2 load levels, high u 's

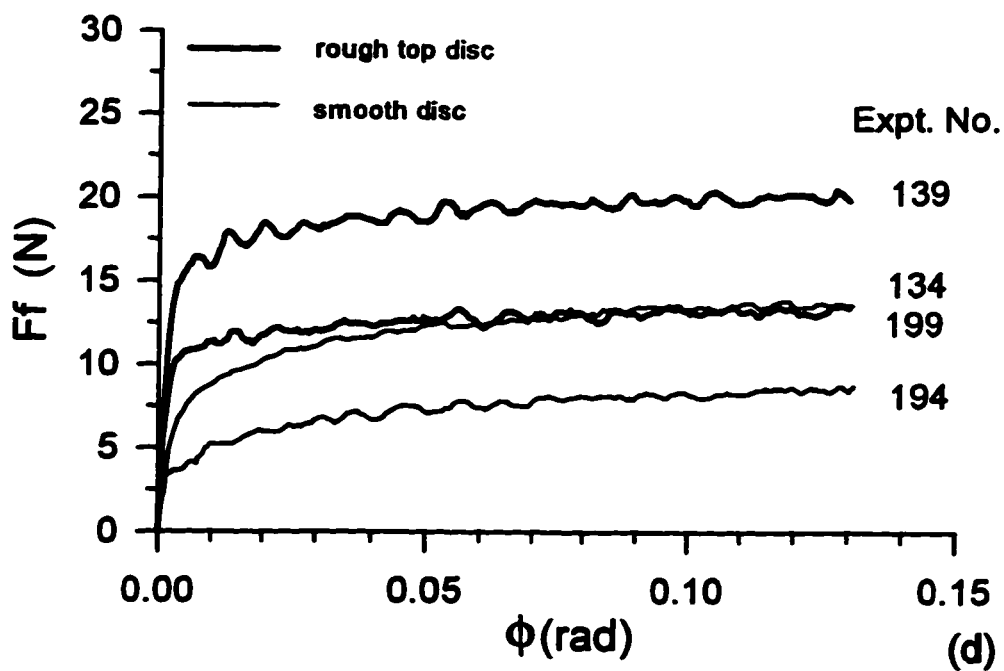
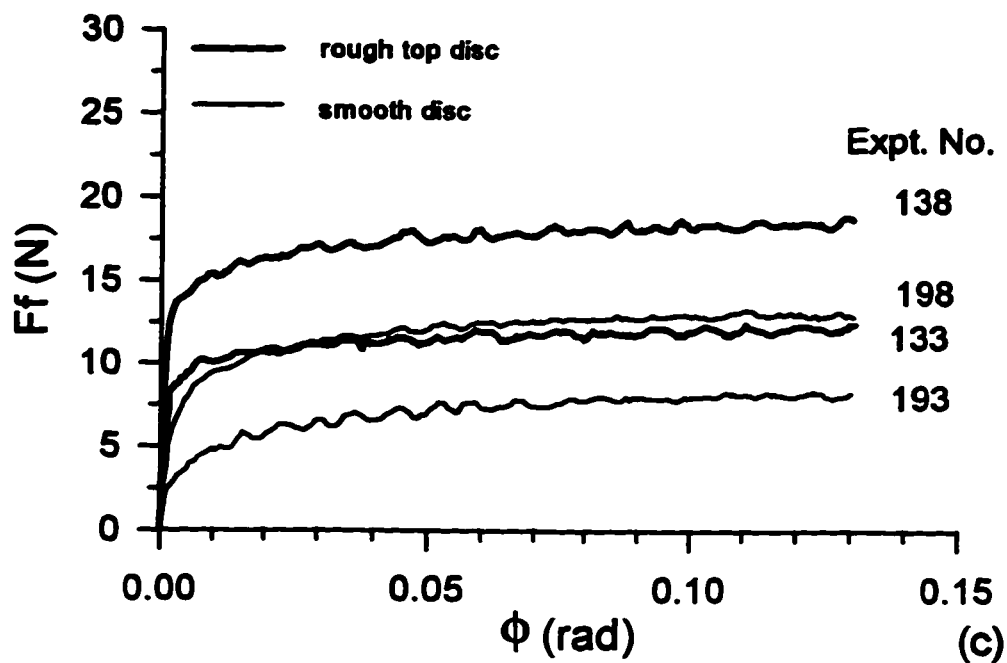


Figure 5.10 Traction curve from rough top disc tests and matched smooth top disc tests for MCT 5+EP at $T=30^{\circ}\text{C}$
 (c) 2 load levels, low u 's
 (d) 2 load levels, lower u 's

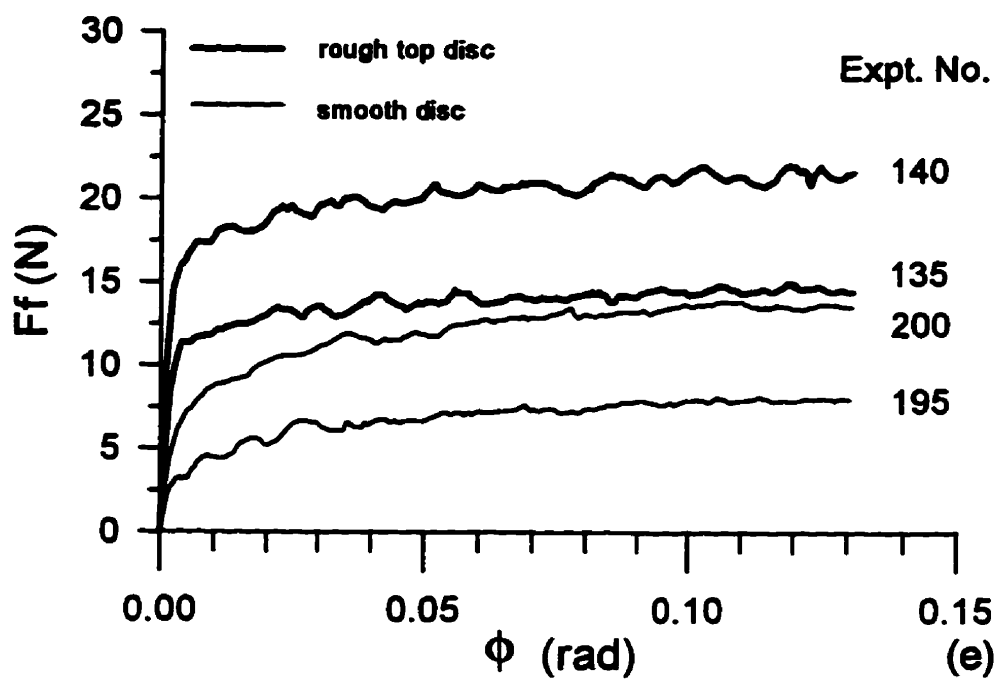


Figure 5.10 Traction curves from rough top disc tests and matched smooth top disc tests for MCT 5+EP at $T=30^{\circ}\text{C}$
(e) 2 load levels, lowest u 's

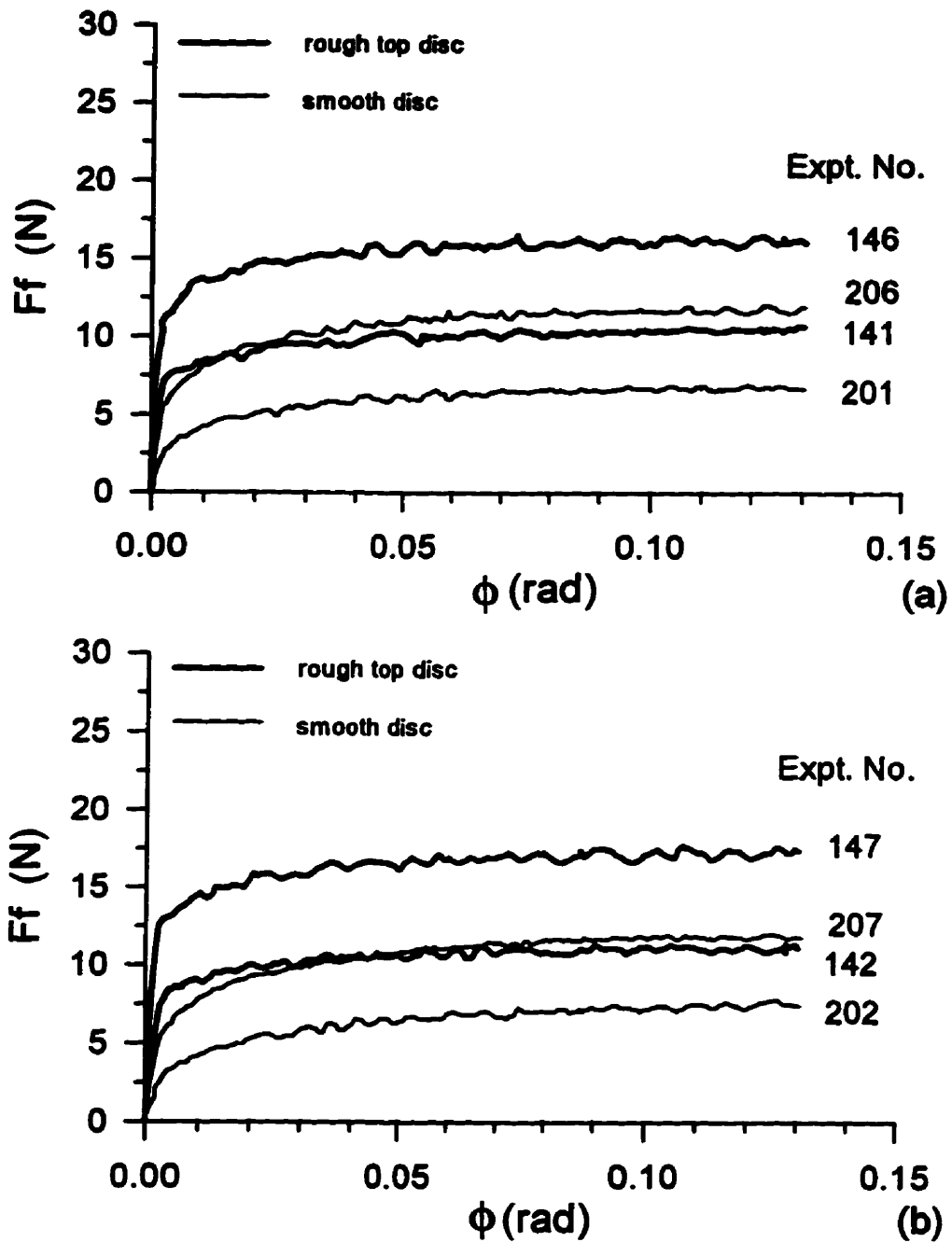


Figure 5.11 Traction curves from rough top disc tests and matched smooth top disc tests for MCT 5+EP at $T=40^\circ\text{C}$
 (a) 2 load levels, highest u 's
 (b) 2 load levels, high u 's

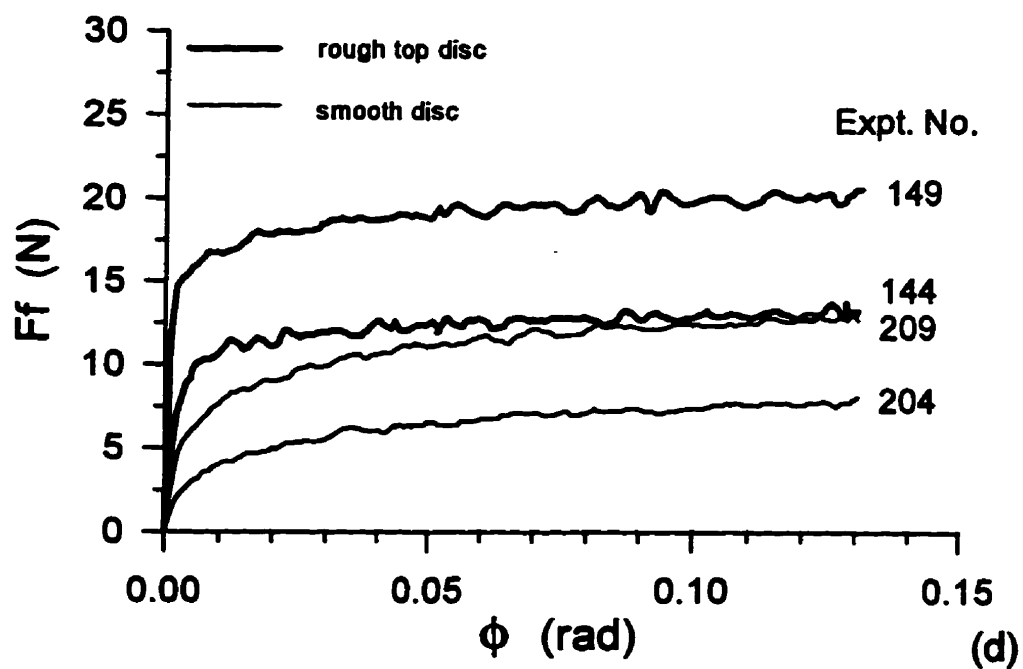
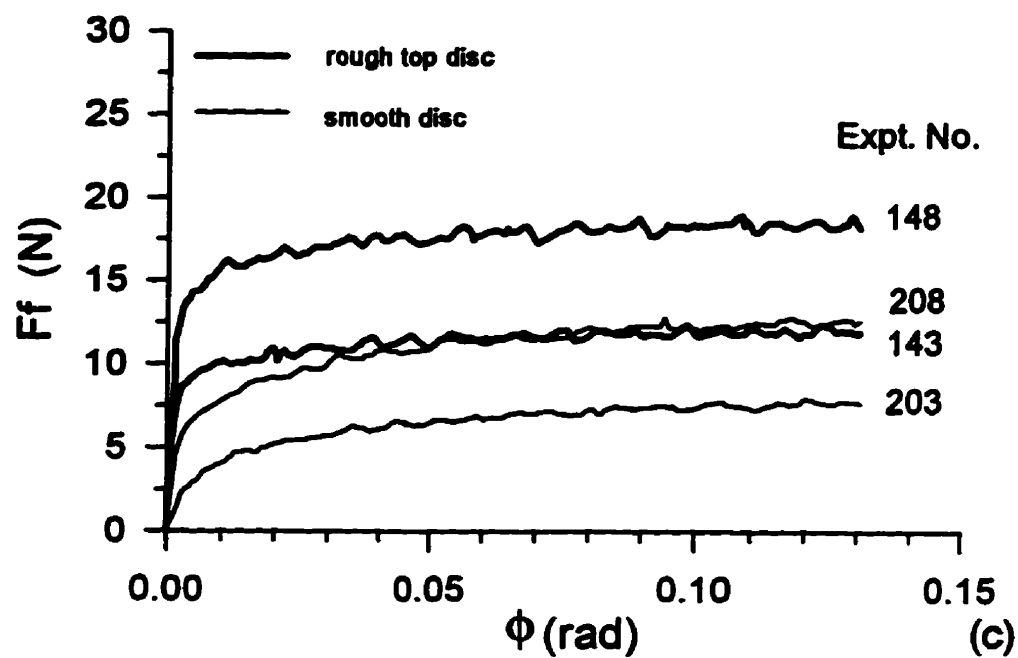


Figure 5.11 Traction curves from rough top disc tests and matched smooth top disc tests for MCT 5+EP at $T=40^\circ\text{C}$
 (c) 2 load levels, low u 's
 (d) 2 load levels, lower u 's

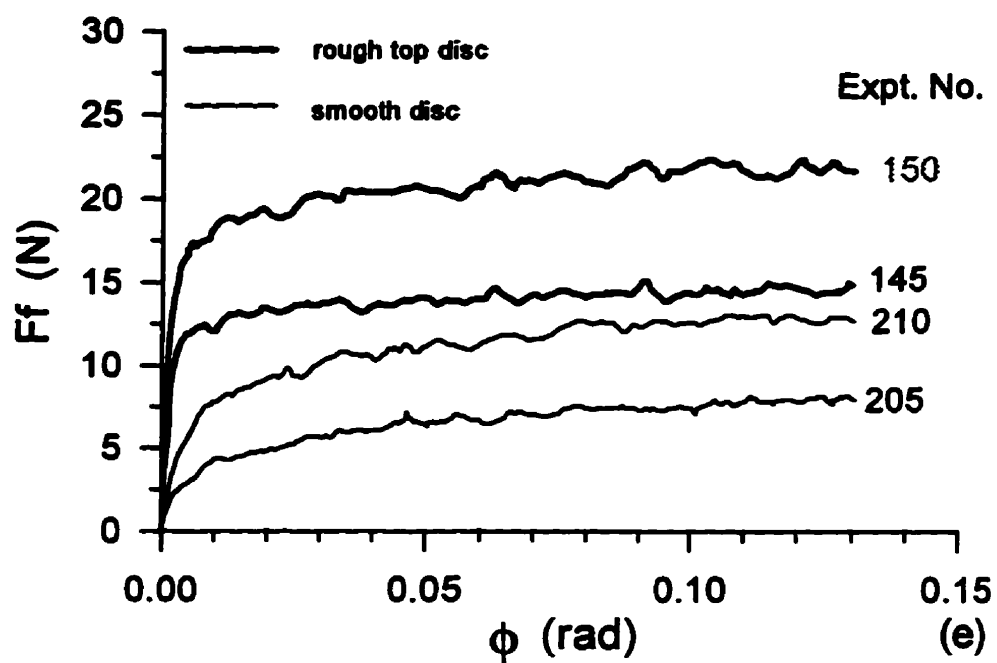


Figure 5.11 Traction curves from rough top disc tests and matched smooth top disc tests for MCT 5+EP at $T=40^\circ\text{C}$
(e) 2 load levels, lowest u 's

- **Maximum friction force**

The $F_{f \max}$ in rough disc experiments (Table 5.2) and the matched smooth disc experiments (Table 5.3) were obtained in the manner described previously at the beginning of this section. Once again, experiments in each row of Tables 5.2 and 5.3 had the same operating conditions but different lubricants.

Table 5.2 The $F_{f \max}$ in rough top disc measurements

Experiment Number*	$F_{f \max}$ (N) MCT 5	Experiment Number	$F_{f \max}$ (N) MCT 5 + FM	Experiment Number	$F_{f \max}$ (N) MCT 5 + EP
91	12.955	111	11.0	131	10.095
92	13.36	112	11.21	132	10.61
93	15.49	113	12.54	133	11.62
94	17.11	114	13.515	134	12.605
95	22.63	115	15.54	135	13.795
96	21.33	116	17.445	136	16.3
97	22.84	117	18.57	137	16.655
98	23.56	118	18.915	138	17.315
99	25.275	119	20.03	139	18.55
100	31.225	120	22.95	140	20.78
101	12.615	121	9.755	141	9.685
102	12.81	122	10.77	142	9.97
103	15.65	123	11.215	143	11.29
104	16.865	124	13.2	144	12.335
105	21.165	125	14.34	145	14.015
106	19.99	126	16.485	146	15.665
107	20.895	127	17.52	147	16.105
108	21.945	128	19.145	148	17.345
109	25.19	129	20.425	149	19.215
110	28.65	130	22.615	150	20.315

* Refer to Table 4.11 for the operating conditions of each experiment

Table 5.3 The F_{rmax} in matched reference smooth top disc measurements

Experiment Number*	F_{rmax} (N) MCT 5	Experiment Number	F_{rmax} (N) MCT 5 + FM	Experiment Number	F_{rmax} (N) MCT 5 + EP
151	8.48	171	7.135	191	7.31
152	7.655	172	7.225	192	7.175
153	7.87	173	7.145	193	7.31
154	7.70	174	7.005	194	7.02
155	7.56	175	7.135	195	7.17
156	14.115	176	12.535	196	12.495
157	13.57	177	12.37	197	12.68
158	13.82	178	12.445	198	12.53
159	14.735	179	12.34	199	12.57
160	13.97	180	12.78	200	12.7
161	7.225	181	6.235	201	6.535
162	7.41	182	6.4	202	6.295
163	7.735	183	6.54	203	6.505
164	7.745	184	6.45	204	6.565
165	7.31	185	6.48	205	6.54
166	13.46	186	10.81	206	11.15
167	12.785	187	10.865	207	10.96
168	12.99	188	11.19	208	11.235
169	13.025	189	11.17	209	11.14
170	13.81	190	11.675	210	11.7

* Refer to Table 4.12 for the operating conditions of each experiment

5.2 Some Observations from the Traction Curves

5.2.1 Characteristics of ehl

- Influences of operating conditions on friction force

The influences of the F , u and T on friction force were drawn from the results of the smooth disc experiments. First, the maximum friction force $F_{f \max}$ increased with increasing load F (Figure 5.12). Slightly lower $F_{f \max}$ tended to occur for the lubricants with additives at the higher F .

Secondly, $F_{f \max}$ decreased with increasing rolling velocity u (Figure 5.13). As u increased, a greater amount of oil was drawn in the contact zone and caused an increase in the central film thickness (h_c), which could be calculated based on the relationship described in Eq. 2.24. On the other hand, the increase of u also caused an increase in the side-slip velocity (v), which could be explained using the relationship shown in Figure 3.6. As mentioned previously, the shear strain rate ($\dot{\gamma}$) expressed by v/h_c affected the friction force as described by rheology models (Eqs. 2.42, 2.43, 2.45 and 2.46). There was no simple and direct relationship to describe the comprehensive results of the above influence of rolling velocity on the friction force. However, at a small and constant skew angle $\phi = 0.05$, by which the $F_{f \max}$ was determined, and with the limited velocity variation ($u < 4$ m/s) on the side-slip disc machine, the maximum friction force decreased with an increase in rolling velocity.

Thirdly, the maximum friction force $F_{f \max}$ decreased with increasing inlet lubricant temperature (Figure 5.14). However, the influence of T was significant only at the higher loads.

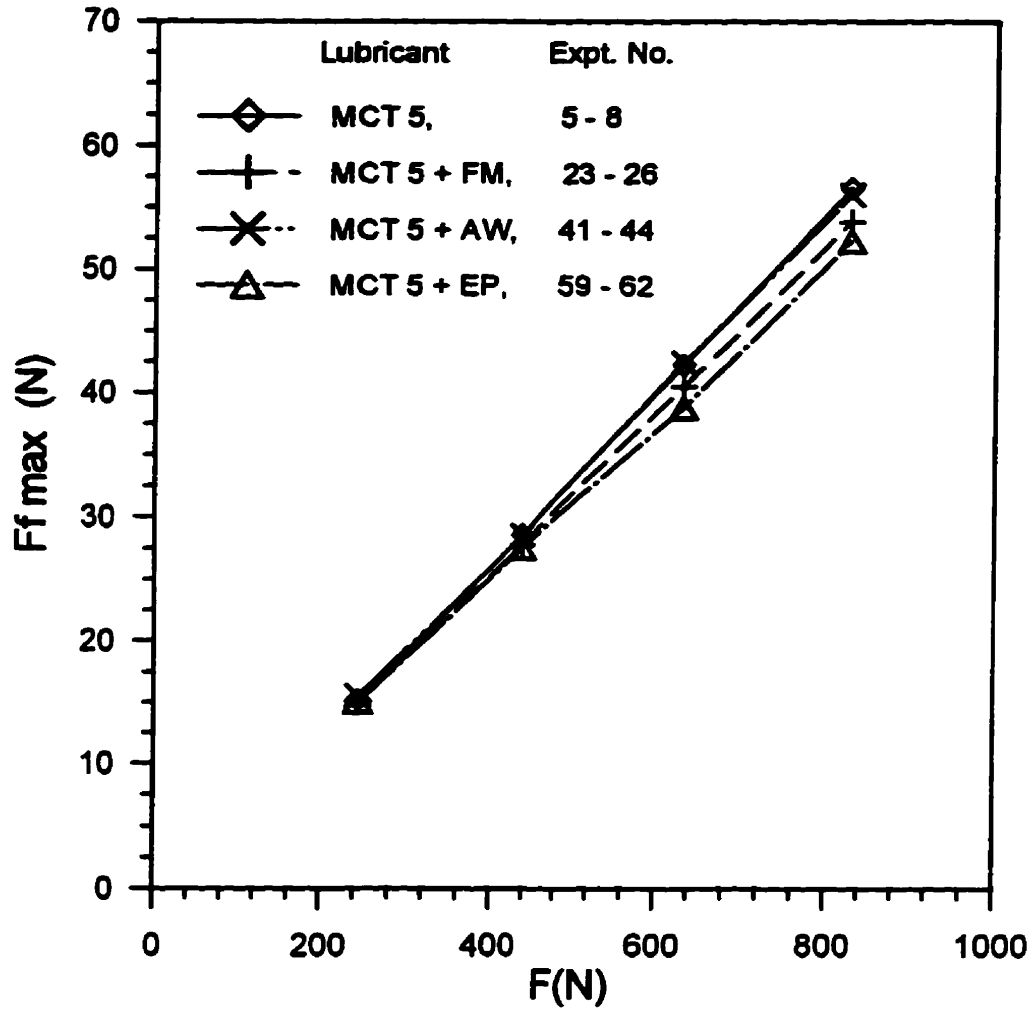


Figure 5.12 Influence of applied loads on friction force in smooth disc tests
(for $T = 30\text{ C}$ and various rolling speed about 2 m/s)

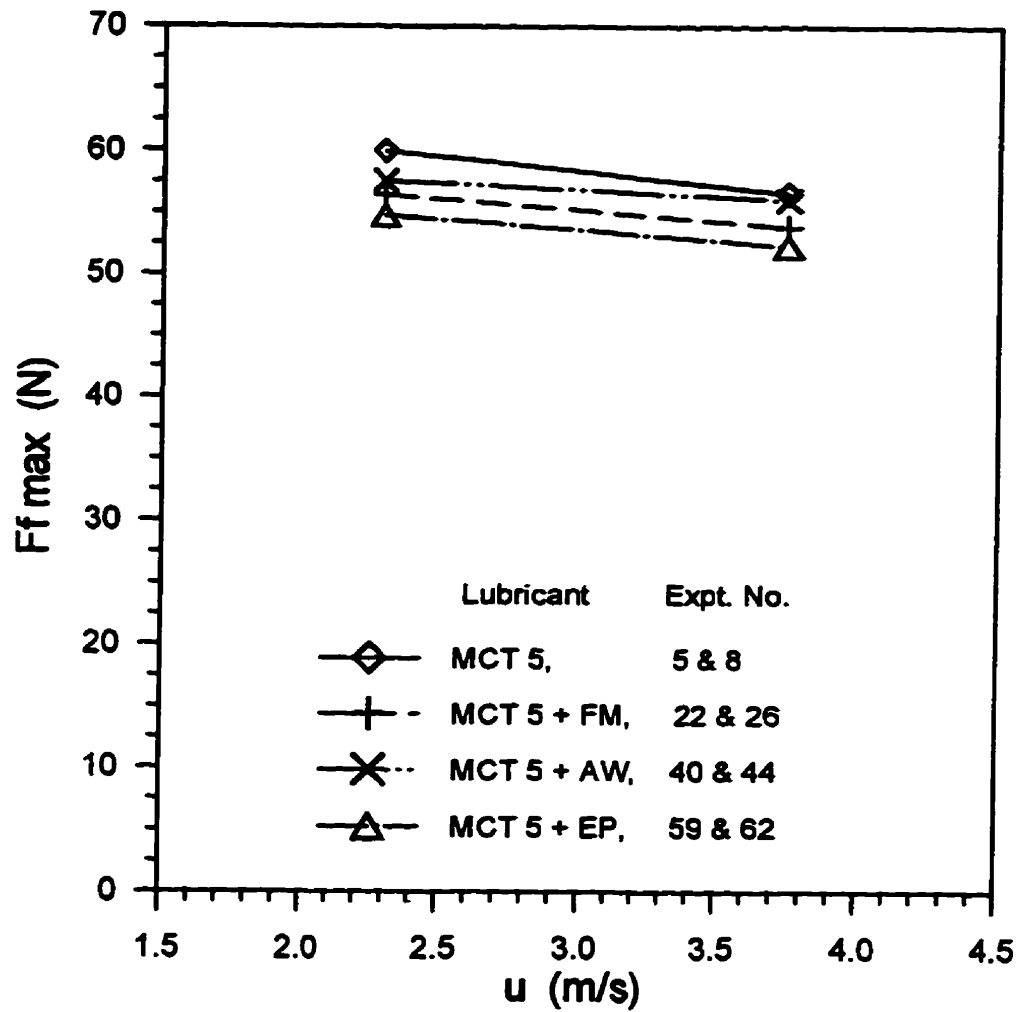


Figure 5.13 Influence of rolling speed on friction force in smooth disc tests
(for $T = 30\text{ C}$ and $F = 829.5\text{ N}$)

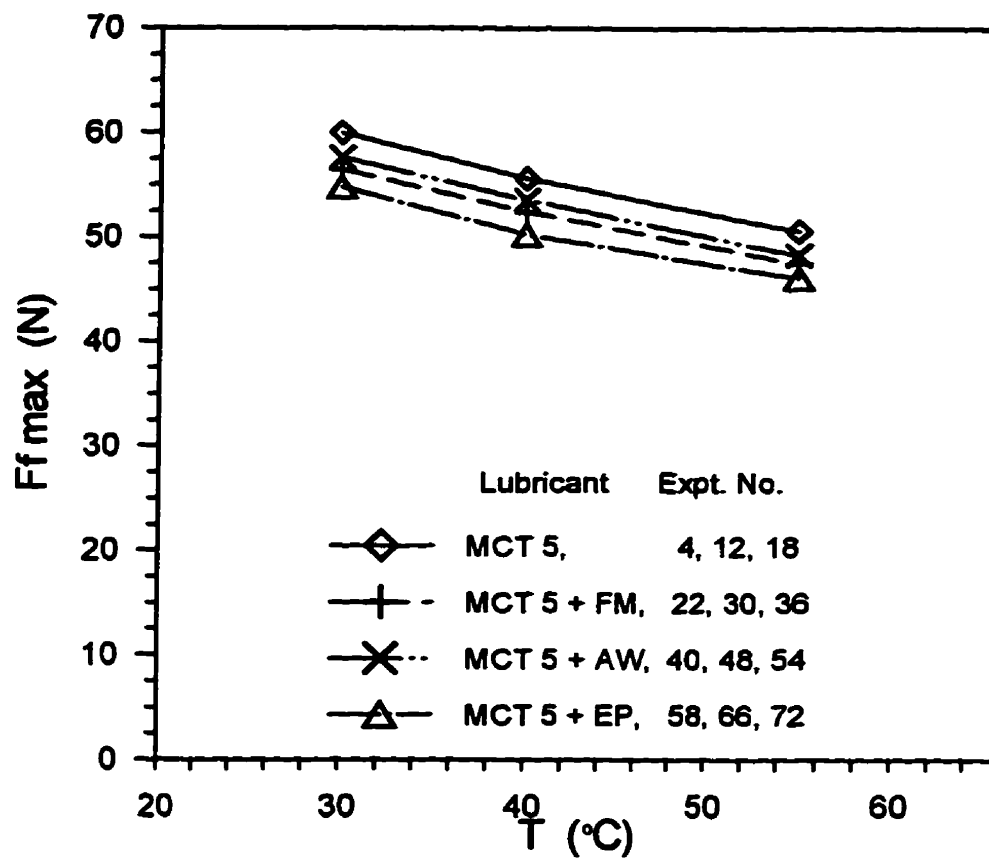


Figure 5.14 Effects of inlet zone temperature on friction force in smooth disc tests
(a) for $F = 829.5 \text{ N}$ and $u = 2.3 \text{ m/s} \sim 4 \text{ m/s}$

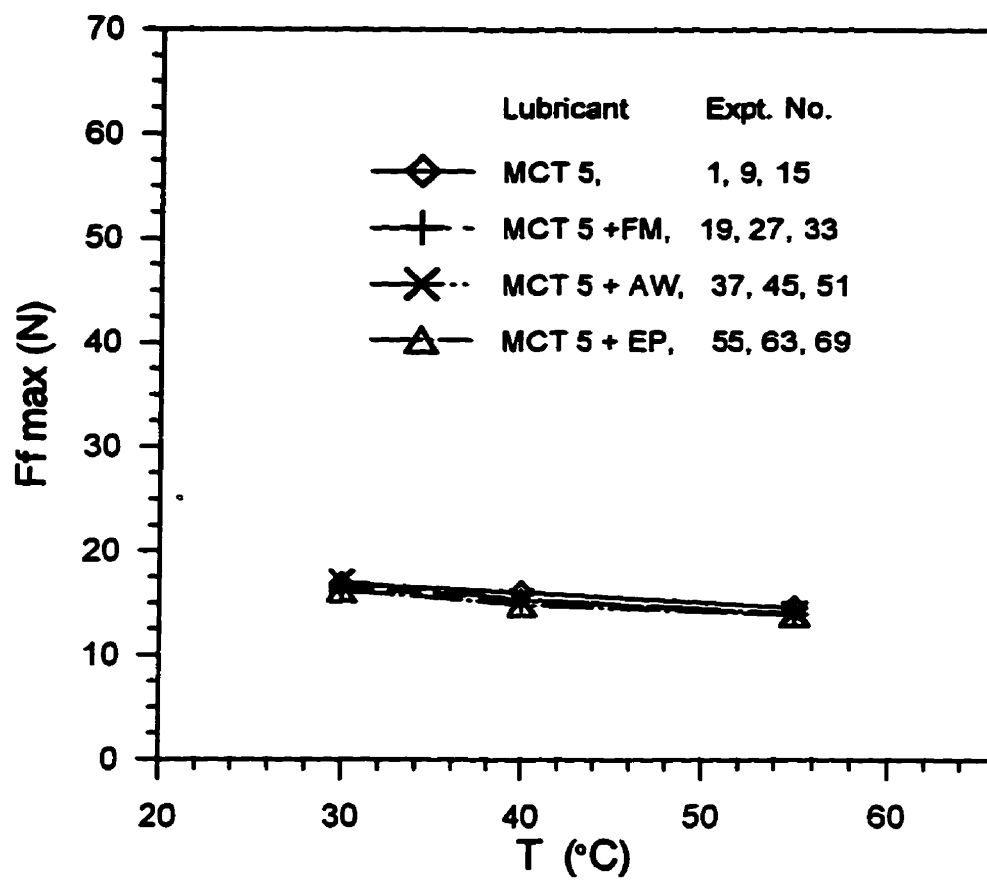


Figure 5.14 Effects of inlet zone temperature on friction force in smooth disc tests (b) for $F = 244.5 \text{ N}$ and $u = 1.6 \text{ m/s} \sim 3.5 \text{ m/s}$

- **Lubricant additives in smooth disc experiments**

There was a small but distinct and repeatable decrease in $F_{r\max}$ as a result of the additives in the lubricant. This decrease was shown clearly by comparing the values in each row of Table 5.1. The effects of additives was enhanced by high loads.

Both the FM and EP additives decreased the $F_{r\max}$ compared with the MCT 5 base stock alone under the same testing conditions. The differences increased with an increase in load and varied from less than 1 N under a load of 244.5 N to about 3 ~ 4 N under a load of 829.5 N. However, the AW additive had the least effect on $F_{r\max}$ with almost the same values for loads of 244.5 N, 439.5 N and 634.5 N, and dropped only 1 ~ 2 N for a load of 829.5 N. Subsequent analysis was expected to show little difference between MCT 5 and MCT 5 + AW oils. Thus, not all additives influence the rheology to the same extent. When the influence was less, there was less need for further examination in the present study. For this reason, and the reputed difficulty in removing the ZDDP in the AW additive from disc surfaces (Snyder, et al., 1984), no further work was performed with the AW additive.

The effect of inlet lubricant temperature was interesting. It was expected that a more significant influence of additives would occur at higher temperatures. However, at the highest load, all of the additives were as effective at low inlet temperature of 30 °C as at higher inlet temperatures of 40 °C and 55°C (Figure 5.14a). Since most additives, particularly the EP additive, were designed to be chemically activated on a surface by high temperatures, this insensitivity to inlet temperature suggested a different and unknown chemistry in full ehl films.

5.2.2 Characteristics of mixed film lubrication

- **Effects of surface roughness on friction force**

A comparison of the results of the experiments with rough top discs R1 and R2, and the matched experiments with smooth top discs S1 and S2, gave a clear view of the effect of surface roughness on friction. The F_f increased with increase in the composite surface roughness σ_c . All the traction curves from rough disc tests showed higher maximum friction force than that of smooth disc tests when they were measured under the same F , u and T (Figures 5.6a ~ 5.11e and Tables 5.2 ~ 5.3). Also, the traction curves showed much steeper initial slopes in the rough disc experiments compared with those from the smooth disc experiments under the same operating conditions.

The dependence of $F_{f \max}$ on u was more pronounced for the rough disc experiments than for the smooth disc experiments, particularly when $u < 2$ m/s (Figure 5.15). In Figure 5.15, the variation of $F_{f \max}$ with F could be found by measuring the length of vertical bars, where the upper end was the $F_{f \max}$ measured under the $F = 244.5$ N and the lower end was that measured under the $F = 147.0$ N. The $F_{f \max}$ increased when the load increased, both in the rough and smooth disc experiments. In general, the solid bars, which represented the results of the rough disc experiments, were longer than the dashed bars, which represented the results of the matched smooth disc experiments. Thus, $F_{f \max}$ had larger increases with F in the rough disc experiments than the smooth disc ones at the same test conditions.

Inlet lubricant temperature had a slight effect on $F_{f \max}$ in rough disc experiments, similarly to the behaviour described in the last section for the smooth disc experiments with top disc S0 and at the lowest F . However, under higher loads, the inlet temperatures might have a more pronounced effect on $F_{f \max}$.

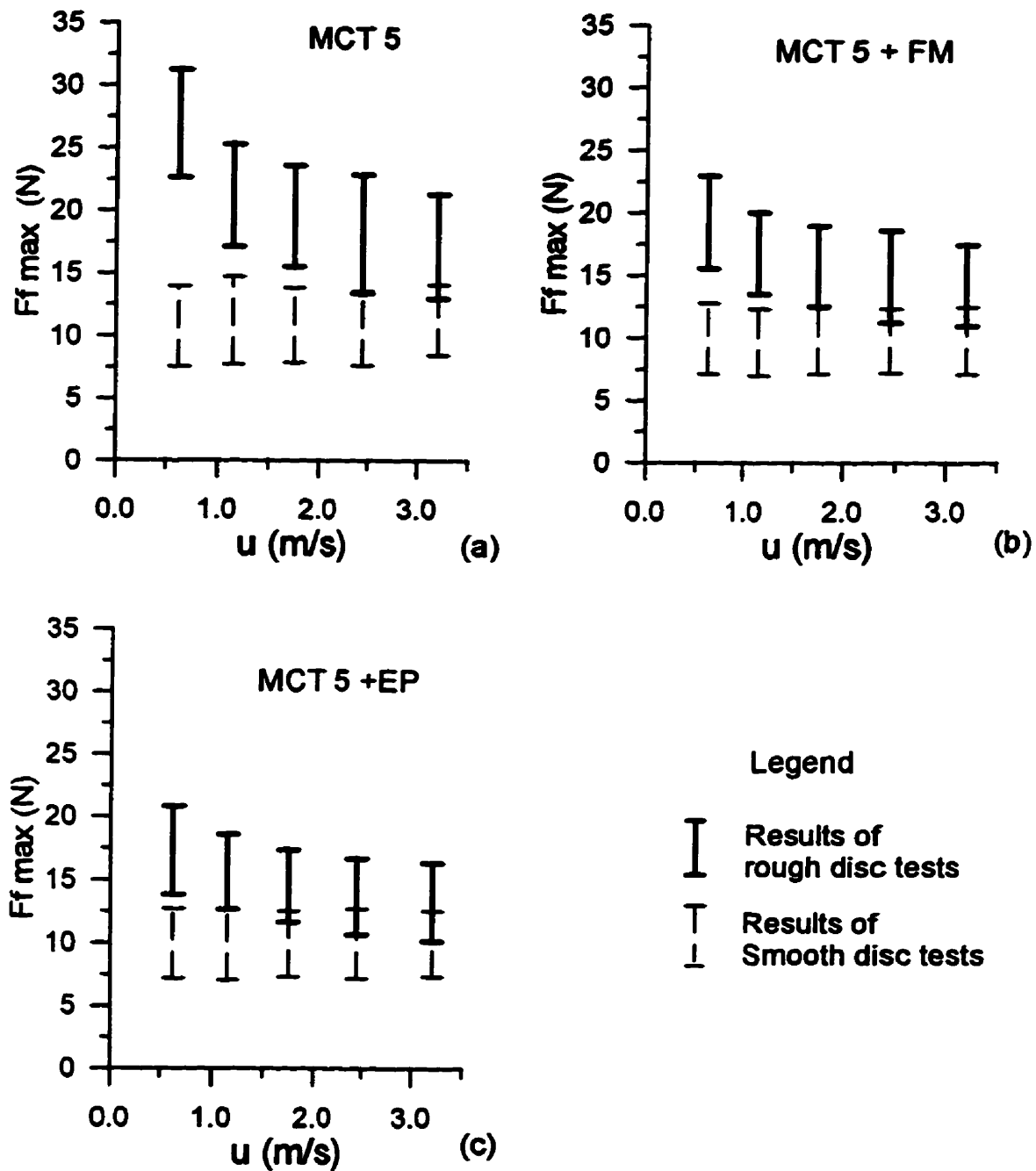


Figure 5.15 Effects of surface roughness on maximum friction force ($F_f \text{ max}$ vs. u plots, at $T=30^\circ\text{C}$)
 (a) for MCT 5, (b) for MCT 5 + FM, (c) for MCT 5 + EP

- **Effects of lubricant additives in rough disc experiments**

Both the FM and EP additive formulated oils reduced the friction force significantly under all the rough disc testing conditions, especially at lower rolling speeds. By comparing Figure 5.15a with Figures 5.15b and 5.15c over the whole range of u , the $F_{f\max}$ decreased about 5.5 N for MCT 5 + FM and 4.5 N for MCT 5 + EP. This behaviour was significantly different from the very small influence of lubricant additives in smooth disc experiments in general, and showed specifically in Figure 5.15 when comparing with the matched smooth disc experiments.

Comparing the traction curves for MCT 5 (Figures 5.6 and 5.7) with that for MCT 5 + EP (Figures 5.10 and 5.11), the EP additive not only reduced the friction force, but also effectively reduced the oscillations in the traction curves. As mentioned in Chapter 3, the application of the oil damper reduced the major mechanical vibrations. However, oscillations still existed in traction curves for both smooth and rough disc experiments, especially under high loads, high temperature and high rolling velocities. In the smooth disc experiments, the oscillations had a regular harmonic pattern which might be related to the mechanical vibration directly (Figures 5.3e and 5.4e). However, in the rough disc experiments, the oscillations occurred more randomly. Supposedly, they might include both the mechanical vibration and the variation of the number of interacting asperities in the contact. But nevertheless, there were much less of these oscillations in the experiments with MCT 5 + EP than that in the experiments with MCT 5.

5.3 Accuracy and Precision

Generally, the evaluation of any experimental results must consider ultimately accuracy and precision. Accuracy can be studied by considering the underlying physics, checking calibrations, modifying procedures to remove unwanted signals and using alternative

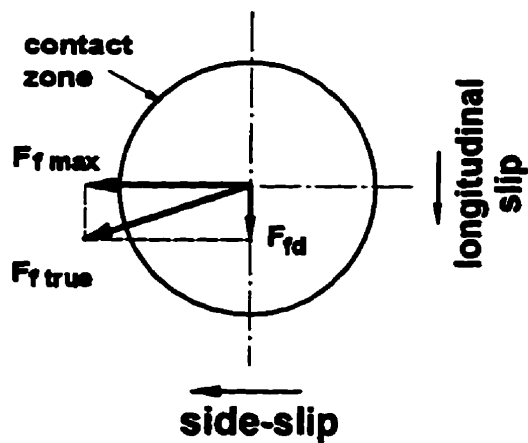
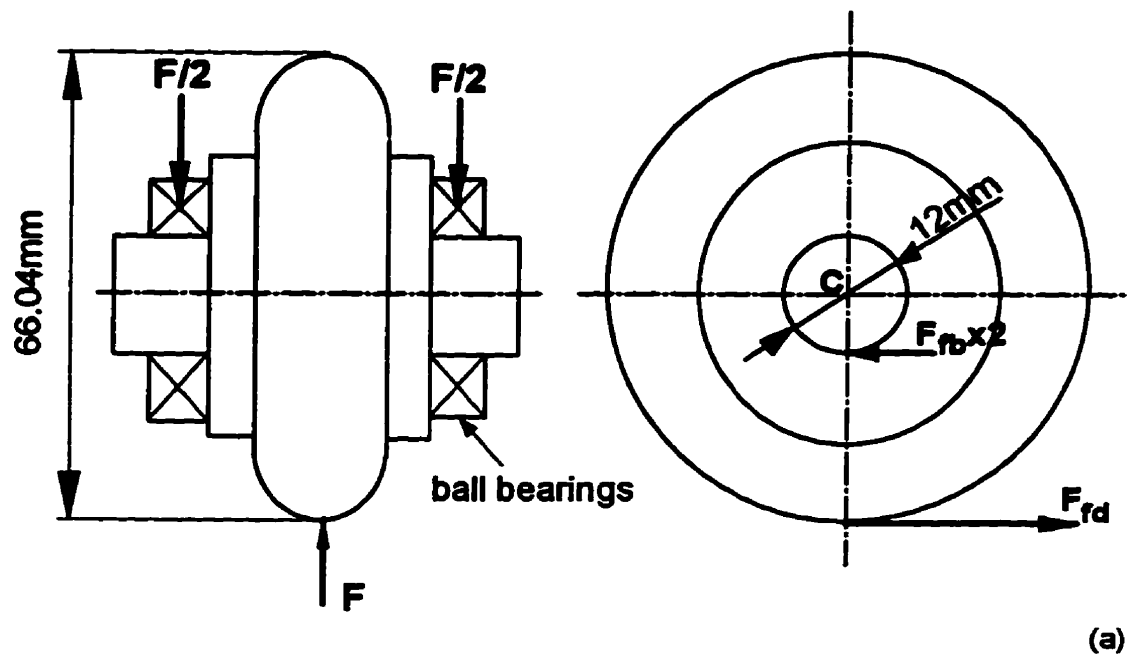
approaches to obtain similar results. Precision is often studied by repeating the experiment under identical conditions to observe how close the results are to each other. This approach to studying precision is known as repeatability. In Chapter 3, the working principle, calibrations and some modifications of the side-slip disc machine were discussed in detail. In the present section, certain issues regarding the accuracy and repeatability of the results from the friction force measurements on the disc machine are discussed.

- **Determining the origin of friction force at zero skew angle**

Side-slip was introduced by skewing the top disc from $\phi = + 0.125$ rad to $\phi = - 0.125$ rad. However, the majority of results reported in the present thesis were from $\phi = 0$ rad to $\phi = 0.125$ rad and gave $F_{f \max}$. The determination of the zero friction point, where $\phi = 0$, was important in determining the $F_{f \max}$. It was almost impossible to set an absolute zero position because of the high sensitivity of the F_f to small shifts in ϕ in the rising region of a traction curve. However, the reversal in rolling direction allowed the origin of the F_f versus ϕ to be determined with high accuracy. The FWD and REV directions of rolling changed the direction of the friction force but not its value. Therefore, a symmetrical “traction plot” (Figure 5.1) was constructed with the two traction curves and the zero friction point was given at the intersection point.

- **Error in F_f caused by friction of top disc supporting bearing**

The top disc in the disc machine is driven by a small friction force through the lubricant film between the top and bottom discs. This driving friction force applied to the top disc must overcome the frictional resistance of the ball bearings which support the top disc shaft. This ball bearing friction causes some slip in the rolling direction and thus subject the lubricant to some shear stress even when the skew angle is zero (and zero slip has been assumed).



$$F_{ftrue} = \sqrt{F_{fmax}^2 + F_{fd}^2}$$

$$= \sqrt{F_{fmax}^2 + (0.18182 \times \mu_b \cdot F)^2}$$

(b)

Figure 5.16 Error caused by friction of top disc supporting bearings
 (a) Free body diagram of top disc and shaft assembly
 (b) True friction force

The frictional resistance of a rolling bearing arises from the rolling and sliding of the balls over the inner races. Considering the top disc shown in Figure 5.16a, $\sum M_c = 0$ implies that

$$F_{fd} \times 0.033 - 2 \times (F/2) \cdot \mu_b \times 0.006 = 0$$

$$F_{fd} = 0.18182 \times \mu_b \cdot F$$

$$\text{where } \mu_b = \frac{F_b}{(1/2) \cdot F}$$

For example, in a smooth disc test of MCT 5 with $F = 634.5$ N and the friction coefficient of self-aligning ball bearing considered as $\mu_b = 0.0010$ (Hamrock, 1994; SKF General Catalogue, 1980), a driving friction force in the rolling direction is of $F_{fd} = 0.115$ N.

Compared with the maximum friction force measured in side slip direction of $F_{f \max} = 42.24$ N, the friction force in the rolling direction is about 0.272 % of the shear in the side slip direction.

If there is longitudinal friction in the contact zone caused by the bearing frictional resistance, then the true friction force acting on the lubricant is as shown in Figure 5.16b. So the percent error in using $F_{f \max}$ rather than $F_{f \text{ true}}$ is

$$\%err = \frac{F_{f \text{ true}} - F_{f \max}}{F_{f \text{ true}}} \times 100 = \left[1 - \frac{1}{\sqrt{1 + \left(0.18182 \frac{\mu_b}{\mu_{\max}} \right)^2}} \right] \times 100 \quad (5.1)$$

$$\text{where } \mu_{\max} = \frac{F_{f \max}}{F}$$

The calculation for various test conditions are summarized in Table 5.4. Only if the friction coefficient of ball bearing $\mu_b > 0.1$ would the error exceeds 5%. A value of $\mu_b > 0.1$ is not likely to have occurred.

Table 5.4 Error in friction force caused by friction of top disc supporting bearings

F (N)	F_{rmax} (N)	μ_{max}	μ_b	%err
147.0	8.48	0.0577	0.0010	0.0005
147.0	8.48	0.0577	0.010	0.05
147.0	8.48	0.0577	0.10	4.6
244.5	15.19	0.0621	0.0010	0.00043
439.5	28.55	0.0650	0.0010	0.00039
634.5	42.24	0.0666	0.0010	0.00037
829.5	56.59	0.0682	0.0010	0.00036

- **Top disc alignment**

The symmetry of the measured friction force variations in the four quadrants of the traction plot provided a check on the accuracy of the disc machine alignment. Before friction force measurements were started, some preliminary tests were performed to check whether the top disc was aligned with the bottom disc. If the whole top disc assembly was not aligned properly, the zero skew angle on the protractor would not corresponded the zero value from the direct current displacement transducer (DCDT), and the plot of the FWD and REV traction curves would lose their symmetry. To overcome this misalignment problem, the top assembly was continuously repositioned until the ϕ value from the protractor matched the DCDT output. If the top disc was tilted in y-z plane, it introduced an extra spin force perpendicular to the rolling direction, which would have sheared the film in the contact. This extra force, either positive or negative, showed clearly in the recorded data, in that, the zero of ϕ from the crossing of FWD and REV traction curves did not occur at zero of F_t . To overcome this tilting problem, the top disc yoke was balanced by resetting the leaf springs. Then, the top disc axis was adjusted by a worm and gear drive, as well as an adjustable protractor and traction plots were generated until the required zero tilt was achieved.

• Disc surface cleaning

The tests always started from using pure base stock oil MCT 5 first and, subsequently, the additive formulations. The three additive formulations for the major smooth disc experiments with top disc $S0_1$ proceeded from the FM to AW and then EP additive oils. The two additive formulations for the rough disc experiments with top discs R1 and R2, and the matched smooth disc experiments with top discs S1 and S2 were performed first with the FM additive oil and then the EP additive oil. Before introducing a new lubricant, all the components in the whole lubricant circulation system, such as the oil tank, valves, heating pipes, oil reservoir and two discs, were cleaned thoroughly by varsol and then acetone. Also, the oil filter was replaced. The new lubricant was always run through the system before the real test and dumped out. Then the tests were performed with a second quantity of the new lubricant. One top disc was used for only one group of tests. For example, after the EP additive oil was tested on the disc machine, the top disc was replaced by a new (or repolished) one. The used disc was sent back to the machine shop to be lightly cut (to a depth of 1 ~ 2 μm) on a lathe and repolished with a fine diamond paste to the same RMS roughness level. The bottom disc was also repolished from time to time, especially when the top disc was changed from smooth to rough, or vice versa.

• Repeatability

For each combination of test conditions (F , u , T and σ_c), the experiments were repeated to produce at least two and sometimes four traction plots. The friction force measurements showed very good repeatability as shown by the four traction plots in Figure 5.1. To check repeatability more rigorously, a set of experiments was performed with new discs ($S0_2$ and $B0_2$), which had almost the same RMS roughness as discs ($S0_1$ and $B0_1$), using only MCT 5 base stock lubricant but varying F , u and T . Thus, the experiments numbered 73 ~ 90 were under exactly the same testing conditions as the experiments between numbers 1 ~ 18. The $F_{t\text{max}}$ values for the corresponding experiments were very close (Table 5.5).

Table 5.5 The $F_{f\max}$ in two repeated sets of smooth disc tests for MCT 5

Experiment No.*	$F_{f\max}$ (N)	Experiment No.	$F_{f\max}$ (N)	Difference (%)
1	16.82	73	16.23	3.5
2	30.18	74	29.52	2.2
3	43.58	75	43.02	1.3
4	59.96	76	59.05	1.5
5	15.19	77	15.49	2.0
6	28.55	78	28.27	1.0
7	42.24	79	42.66	1.0
8	56.59	80	56.97	0.67
9	16.03	81	14.98	6.55
10	28.60	82	28.32	0.98
11	42.10	83	41.56	1.28
12	55.57	84	54.53	1.87
13	15.08	85	13.90	7.82
14	26.57	86	26.85	1.05
15	14.53	87	13.23	8.95
16	25.51	88	24.35	4.55
17	37.22	89	36.94	1.03
18	50.57	90	48.57	3.95

* Refer to Table 4.10 for the test conditions of each experiment

However, much later in the research program when a final set of experiments with a smooth top disc was performed under conditions which matched those of the rough disc experiments, $F_{f\max}$ seemed to decrease compared with the previous smooth disc test results (Figure 5.17). The new top discs (S1 and S2) with the repolished bottom disc (BS) gave approximately the same composite RMS surface roughness as the one for the top discs S0₁ or S0₂ and bottom discs B0₁ or B0₂. When the testing conditions were exactly the same as in the previous tests, the difference in $F_{f\max}$ was about 2 ~ 3 N. Fortunately, the $F_{f\max}$ for the lubricants with additives fell below that of the base stock as before, and thus, the overall average $F_{f\max}$ for the base stock remained above that of the lubricants with additives.

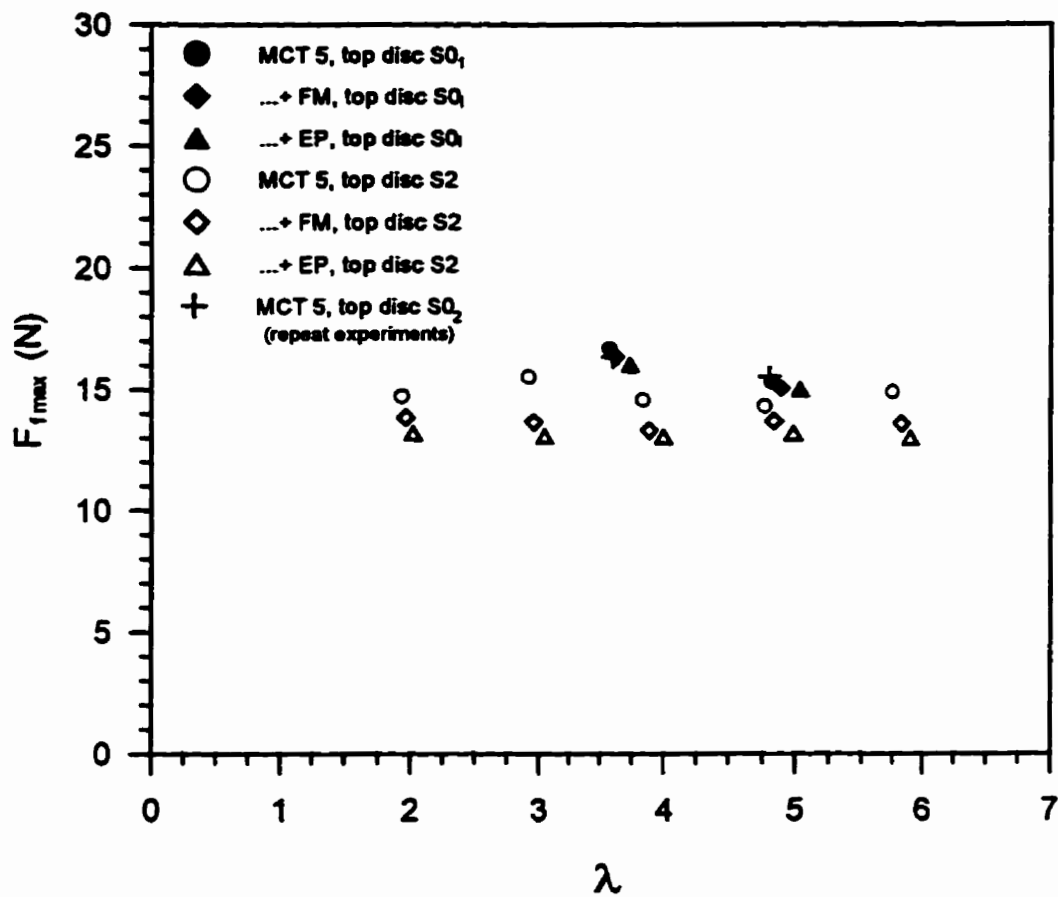


Figure 5.17 Comparison of $F_{f \max}$ of smooth top disc experiments before and after rough disc experiments ($T=30C$, $F=244.5N$)

To further explore this difference, original records of these experiments were checked for all of the measured $F_{r\max}$ possibilities from the traction plots and the data files for a particular set of testing conditions with base stock oil (Table 5.6 and Figure 5.18). Clearly, the differences in the results did not seem to be statistically significant and thus the physics of the experiments had not changed in a major way. However, it was necessary to make multiple friction measurements in individual full ehl experiments and to test the different lubricants in a sequential manner. When this was done, small but consistent differences were always found in the $F_{r\max}$ for the various lubricants.

Table 5.6 Multiple $F_{r\max}$ measurements
(Performed in experiments at the beginning, middle and end of the present study for MCT 5, $F = 244.5$ N, $T = 30$ °C, $u = 2.5$ m/s)

$F_{r\max}$ (N)	$F_{r\max}$ (N)	$F_{r\max}$ (N)
Early Expt. No. 5	Repeat Expt. No. 77	Later Expt. No.157
14.26	14.36	13.20
13.28	14.38	14.57
16.07	14.91	13.22
17.09	14.10	13.49
15.68	16.77	13.64
14.61	16.47	14.42
12.60	16.24	13.92
14.80	16.54	13.05
15.91		
14.96		
15.83		
14.91		

The reason for the scatter shown in Figure 5.18 was not determined, although reduced friction in the top disc skewing assembly by introducing a brass shim between sliding surfaces of steel ring and brass block did seem to be responsible for reduced scatter and improved symmetry in the traction plots in the later experiments. It was suspected that a combination of minor influences might have conspired to shift the average values in Figure 5.17. In any case, changing the lubricant formulation for a particular set of discs did change the average

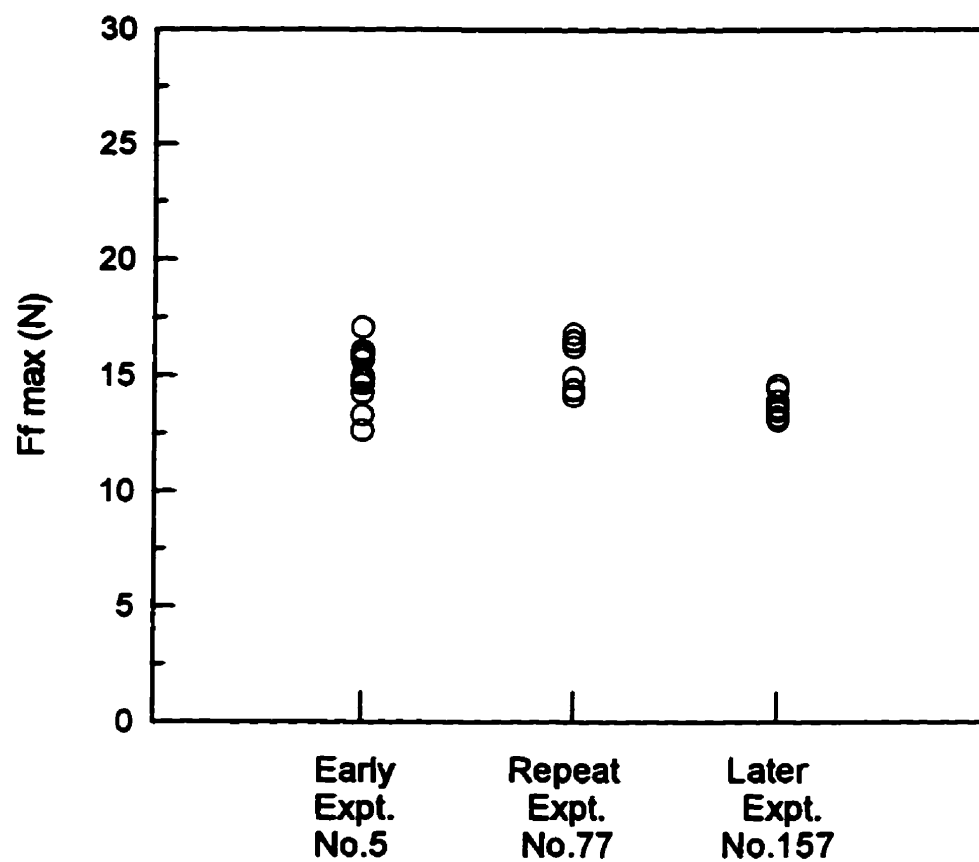


Figure 5.18 Comparison of multiple $F_{f\max}$ measurements
(Performed in experiments at the beginning, middle and end of
the present study for MCT 5, $F=244.5\text{N}$, $T=30\text{C}$ and $u=2.5\text{m/s}$)

F_{max} in a repeatable manner, while it would be preferable to have a more “global” repeatability, subsequent analysis did show that the differences in averages of F_{max} for various lubricants could still give useful rheological information. Future improvements in experimental protocols might lead to a better global repeatability.

Chapter 6 Analysis and Discussion

This chapter analyzes and discusses the results collected from all the groups of friction force measurements on the disc machine. First, the maximum coefficient of friction for each experiment was plotted versus λ ratio. Secondly, the maximum friction force ($F_{f \max}$) from each experiment with full ehl (the smooth top disc, $\lambda > 3$) was used in an empirical procedure to determine the limiting shear stress as a function of film pressure for each of the formulated lubricants. The third analysis examined $F_{f \max}$ from the experiments with micro-ehl (the rough top disc, $\lambda \ll 1$), estimated the real area of contact, and calculated both the average limiting shear stress and average film pressure. For each of the formulated lubricants, the limiting shear stress obtained by extrapolating the functional relationship with pressure, which was derived from the experiments under full ehl conditions, was compared with the value based on the measurements under micro-ehl conditions. The efficacy of using disc machine friction measurements under full ehl conditions to examine the influence of lubricant additives on the fundamental rheological parameter of limiting shear stress was discussed based on the analysis.

6.1 Influence of λ Ratio on Friction Coefficient

As mentioned in the previous chapters, the λ ratio was used to characterize the extent of asperity interaction and to distinguish the lubrication regimes. The λ ratio was the central film thickness (h_c), predicted by an ehl formula, divided by the composite RMS roughness (σ_c) of the contact surfaces (Eq. 2.35). In the present study, the friction force measurements on the side-slip disc machine were arranged in groups, which were assigned to various lubrication regimes by their λ ratio (Tables 4.10 – 4.12). However, Jefferis and Johnson (1968) found little change in friction with increasing asperity interaction. If the side-slip machine was to provide rheological information, it was expected that differences in λ ratio should correspond

to detectable change in friction. Therefore, a simple analysis was performed which consisted of plotting the λ ratio versus the maximum friction coefficient (μ_{\max}).

In the experimental work with the side-slip disc machine, the friction force increased rapidly as the skew angle (ϕ) increased from zero, until an almost constant value was reached when $\phi \geq 0.05$ rad (corresponding to a slide-roll ratio of about 5%). Therefore, $\phi = 0.05$ rad was specified to correspond to the maximum friction force ($F_{f \max}$) in the analysis and the μ_{\max} was

$$\mu_{\max} = \frac{F_{f \max}}{F} \quad (6.1)$$

The $F_{f \max}$ results were taken from Table 5.2 for the rough surface disc tests and from Table 5.3 for the matched smooth surface disc tests. As mentioned in Chapter 5, the $F_{f \max}$ listed in these two tables are the average of at least four traction measurements for each operating conditions, which could be found in Tables 4.11 and 4.12 following the specified experiment number. Therefore, the calculated results of μ_{\max} are the average values, which are given in Table 6.1 for the rough surface disc experiments and in Table 6.2 for the matched smooth surface disc experiments.

Table 6.1 The μ_{max} in rough surface disc experiments

Experiment Number	μ_{max} MCT 5	Experiment Number	μ_{max} MCT 5 + FM	Experiment Number	μ_{max} MCT 5 + EP
91	0.0881	111	0.0748	131	0.0687
92	0.0909	112	0.0763	132	0.0722
93	0.1054	113	0.0853	133	0.0790
94	0.1164	114	0.0919	134	0.0857
95	0.1539	115	0.1057	135	0.0938
96	0.0872	116	0.0713	136	0.0667
97	0.0934	117	0.0760	137	0.0681
98	0.0964	118	0.0774	138	0.0708
99	0.1034	119	0.0819	139	0.0759
100	0.1277	120	0.0939	140	0.0850
101	0.0858	121	0.0664	141	0.0659
102	0.0871	122	0.0733	142	0.0678
103	0.1065	123	0.0763	143	0.0768
104	0.1147	124	0.0898	144	0.0839
105	0.1440	125	0.0976	145	0.0953
106	0.0818	126	0.0674	146	0.0641
107	0.0855	127	0.0717	147	0.0659
108	0.0898	128	0.0783	148	0.0709
109	0.1030	129	0.0835	149	0.0786
110	0.1172	130	0.0925	150	0.0831

Table 6.2 The μ_{\max} in matched smooth surface disc experiments

Experiment Number	μ_{\max} MCT 5	Experiment Number	μ_{\max} MCT 5 + FM	Experiment Number	μ_{\max} MCT 5 + EP
151	0.0577	171	0.0485	191	0.0497
152	0.0521	172	0.0491	192	0.0488
153	0.0535	173	0.0486	193	0.0497
154	0.0524	174	0.0477	194	0.0478
155	0.0514	175	0.0485	195	0.0488
156	0.0577	176	0.0513	196	0.0511
157	0.0555	177	0.0506	197	0.0519
158	0.0565	178	0.0509	198	0.0512
159	0.0603	179	0.0505	199	0.0514
160	0.0571	180	0.0523	200	0.0519
161	0.0491	181	0.0424	201	0.0445
162	0.0504	182	0.0435	202	0.0428
163	0.0526	183	0.0445	203	0.0443
164	0.0527	184	0.0439	204	0.0447
165	0.0497	185	0.0441	205	0.0445
166	0.0551	186	0.0442	206	0.0456
167	0.0523	187	0.0444	207	0.0448
168	0.0531	188	0.0458	208	0.0460
169	0.0533	189	0.0457	209	0.0456
170	0.0565	190	0.0478	210	0.0479

The overview of the influence of the λ ratio on the μ_{\max} of the matched experiments is shown in the following figures. Figure 6.1a is the results for the F of 147 N with top smooth disc S1 and rough disc R1 at T of 30 °C, and Figure 6.1b is for the F of 244.5 N with discs S2 and R2 respectively at same temperature. Quite similar behaviour of μ_{\max} versus λ is found at T of 40 °C, the results are shown in Figures 6.2a and 6.2b with other conditions as the same as those in Figure 6.1.

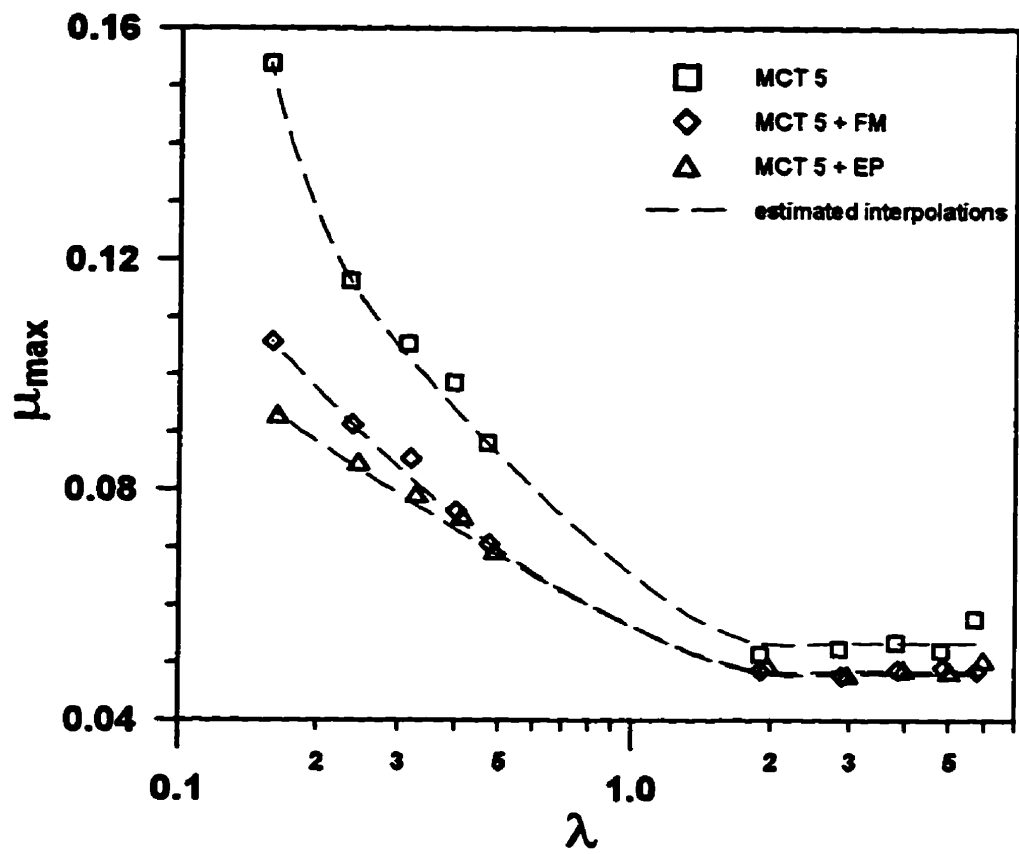


Figure 6.1 Plots of the maximum friction coefficient versus λ ratio at $T=30^{\circ}\text{C}$

(a) top discs S1 and R1, $F=147.0\text{ N}$

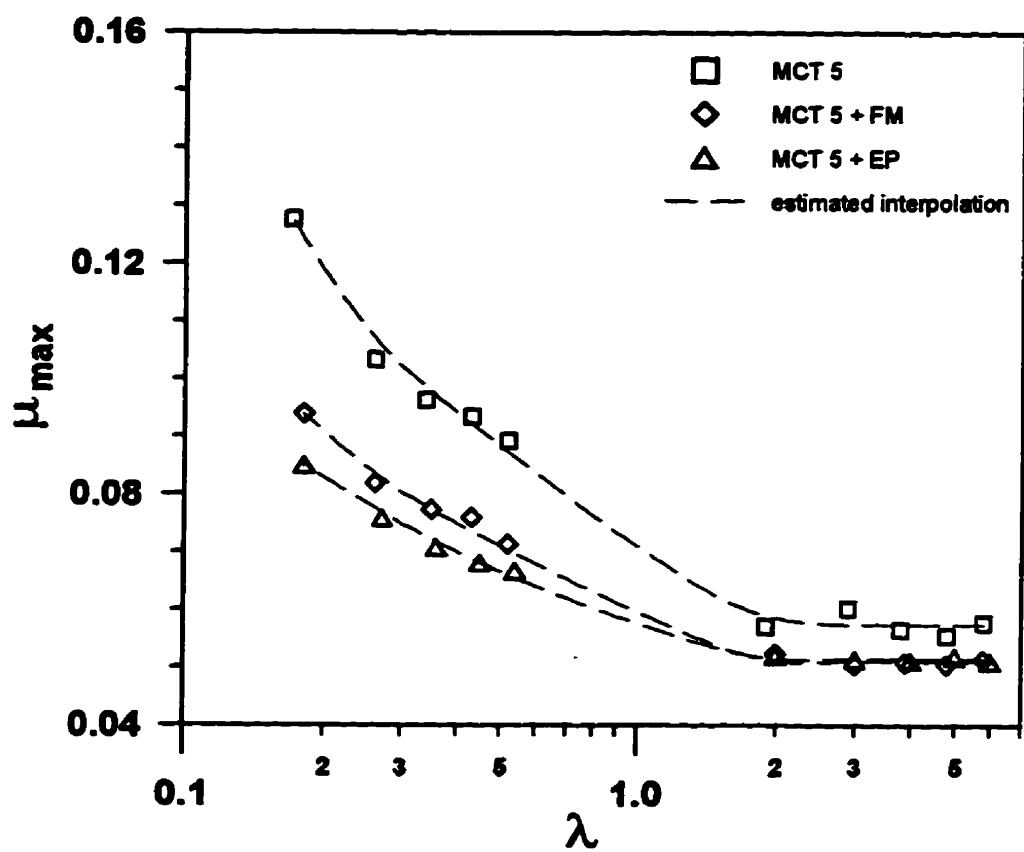


Figure 6.1 Plots of the maximum friction coefficient versus λ ratio at $T=30^{\circ}\text{C}$

(b) top discs S2 and R2, $F = 244.5 \text{ N}$

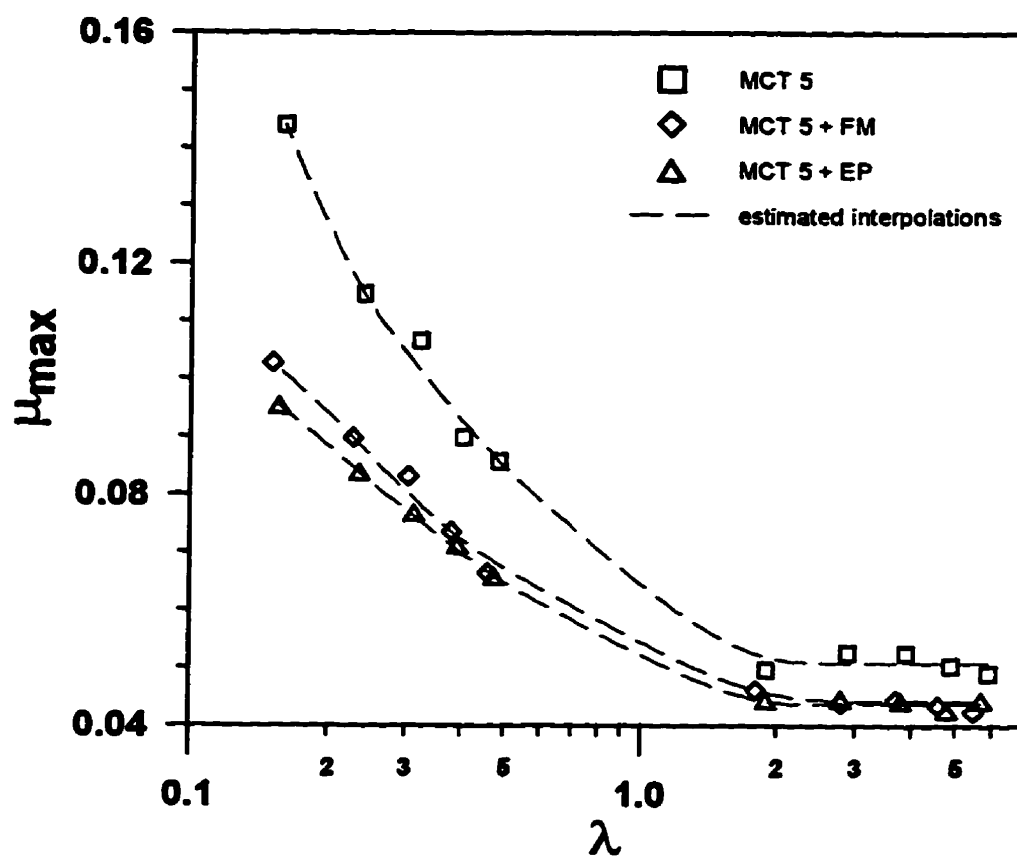


Figure 6.2 Plots of the maximum friction coefficient versus λ ratio at $T=40^{\circ}\text{C}$

(a) top discs S1 and R1, $F = 147.0 \text{ N}$

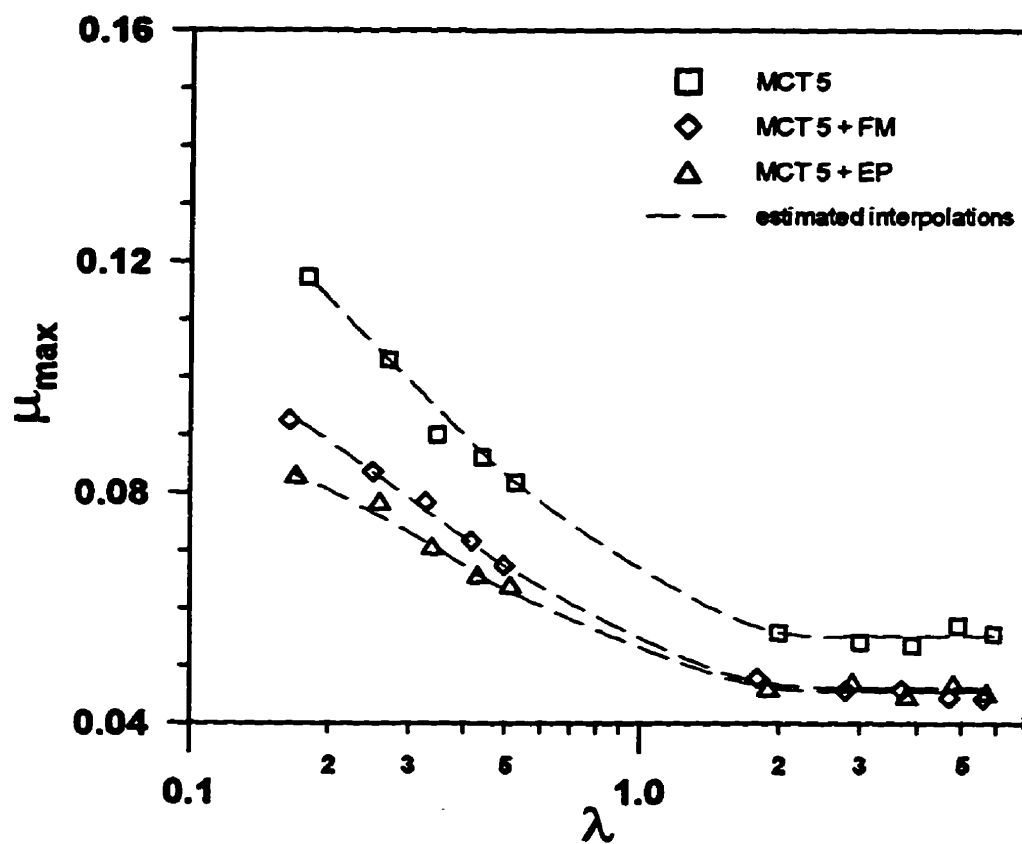


Figure 6.2 Plots of the maximum friction coefficient versus λ ratio at $T=40^{\circ}\text{C}$

(b) top discs S2 and R2, $F = 244.5 \text{ N}$

In these figures, the μ_{\max} was approximately constant for each lubricant as $\lambda > 1.8$ corresponding to the smooth top disc experiments. From the data shown in the Table 6.2, the additives had only some small but repeatable effect on μ_{\max} in these experiments. Both the FM and EP additive lubricants showed slightly lower μ_{\max} than base stock alone. This small effect persisted until $\lambda \ll 1$, whereupon both the FM and EP additives reduced the μ_{\max} significantly compared with base stock alone. This could be a result of the effects of asperity interactions in the rough top disc experiments. When the λ was between 0.24 to 0.55, the μ_{\max} increased gradually between 0.06 and 0.10. In most cases, the EP additive reduced the μ_{\max} more than the FM additives. For λ just below 0.2, an abrupt increase in μ_{\max} occurred for each lubricant, and especially the μ_{\max} value for the MCT 5 was two or three times the value for $\lambda > 1.8$.

As suggested by Hamrock and Dowson (1981), the increase in coefficient of friction (μ) distinguished the transition of lubrication regimes (Figure 2.15). The region of their film parameter ($3 < \lambda^* < 10$) corresponded to the full ehl and gave the lowest μ . In the present experiments, this region extended to λ of 1.8 ($\lambda^* \approx 1.2$) and the μ_{\max} was not over 0.06 for each of the lubricants. But in the lowest λ region, the μ_{\max} was above 0.10, which is conventionally recognized as the value for boundary lubrication (Williams, 1994) and the chemical properties of lubricant additives were considered to dominate the friction, together with the extent of the contact zones at the asperity tips.

6.2 Empirical Approach to Determine Limiting Shear Stress

The intent of the present study was to examine the influence of additives on lubricant rheological parameters in ehl and micro-ehl films using a disc machine. In these ehl and micro-ehl films, the various rheological models discussed in Chapter 2 presented different interpretations of lubricant behaviour at very low shear strain rates and relative low pressures.

However, there was a general agreement that lubricant reached a limiting shear stress (τ_L) at shear strain rates just slightly higher than zero with high film pressure. Since lubricants in many practical contacts are considered to operate under these conditions, τ_L is an important rheological parameter and determining the effect of lubricant additives on it was considered to be consistent with the objectives of the present study.

An empirical approach developed by Wu and Cheng (1994) was used to determine the τ_L from the friction measurements obtained with the side-slip disc machine. Some features of the contact were described in previous chapters and could be summarized as follows:

- (1) isothermal lubricant film
- (2) film pressure close to that given by Hertzian theory
- (3) uniform oil film thickness h_c over a contact zone approximately equal to that given by Hertzian theory
- (4) both surfaces moving with the same velocity (u) in the rolling direction, but with a side-slip velocity (v) superimposed on the lubricant film
- (5) uniaxial shear in the side-slip direction

6.2.1 Determining the limiting shear stress index number

The empirical approach of determining the limiting shear stress index number (m) was described previously in Chapter 2, Section 2.4.3. This approach assumed that the lubricant had reached the limiting shear stress throughout the contact. Since the temperature was considered at a constant, the τ_L was related to pressure only and could be related to the maximum friction force ($F_{f\max}$) by integrating over the circular contact area (πa^2) and taking into account the pressure variation over the contact. For a specified load and temperature, the contact area, maximum pressure (p_{\max}) and $F_{f\max}$ were either calculated or measured and, therefore, Eq. 2.50 could be used to relate τ_L to a function of pressure (p) and index number (m).

To determine the value of m for a particular lubricant at a specific temperature, F_{\max} was measured at each of four applied loads and $\tau_L = f(p)$ was obtained from Eq. 2.50. The experiments involving the smooth top discs ($S0_1, S0_2$) with $\lambda > 3$ were used for these calculations. At the same film pressure (p), the τ_L expression indicated that some value of m must exist such that the same τ_L could be calculated for each applied load.

Wu and Cheng (1994) did not indicate clearly how this m value was determined. In the present study, a value of p was set equal to the maximum Hertzian pressure for the lowest of the four levels of applied load. An m value was specified and Eq. 2.50 was used to calculate for values of τ_L . An average of the four τ_L values ($\bar{\tau}_L$) was calculated and the sum of the squared residuals was determined as follows:

$$\epsilon = \sum_{i=1}^n (\tau_{L_i} - \bar{\tau}_L)^2 \quad (6.2)$$

For example, the traction force measurements for MCT5 at a inlet temperature of $T = 30$ °C, (experiment numbers 5 ~ 8, 23 ~ 26, 59 ~ 62) and Eq. 2.50 gave the following four expressions (corresponding to loads of 244.5 N, 439.5 N, 634.5 N and 829.5 N) for the limiting shear stress

$$\tau_{L1} = 4.303 \times 10^7 (m+1) \left(\frac{p}{1.038 \times 10^9} \right)^{2m}$$

$$\tau_{L2} = 5.469 \times 10^7 (m+1) \left(\frac{p}{1.263 \times 10^9} \right)^{2m}$$

$$\tau_{L3} = 6.336 \times 10^7 (m+1) \left(\frac{p}{1.428 \times 10^9} \right)^{2m}$$

$$\tau_{L4} = 7.111 \times 10^7 (m+1) \left(\frac{p}{1.560 \times 10^9} \right)^{2m}$$

For $p=1.038 \times 10^9$ Pa and $m=0.6$,

$$\tau_{L1} = 68.85 \text{ MPa,}$$

$$\tau_{L2} = 69.15 \text{ MPa,}$$

$$\tau_{L3} = 69.14 \text{ MPa,}$$

$$\tau_{L4} = 69.78 \text{ MPa,}$$

and

$$\bar{\tau}_L = 69.23 \text{ MPa,}$$

$$\epsilon = 0.4614$$

The above calculations were performed automatically by a FORTRAN computer program "TL.FOR". This program was run for ranges of m values, starting from 0 to 1 and refining within that range until the m value was determined to three significant digits, which gave a minimum ϵ . A single minimum ϵ always occurred at about $m = 0.6$. In the above example $m = 0.615$ corresponded to the minimum ϵ .

The same procedures were applied to MCT 5 + FM and $m = 0.565$ was obtained. Similarly, for MCT 5 + EP, $m = 0.523$ was obtained.

In applying this minimum square residual method to determine m , two factors influenced the results. The first was the number of load levels involved in the determination. A slight change in m occurred when three load levels were used instead of four and more substantial change occurred when two load levels were used. Thus, it was apparent that m was influenced by the inevitable scatter in the friction measurements. The recommended course of action was to use at least four load levels and repeat the measurements at each load level more than once. The second factor was the selection of p . The selected p changed from 1.038 GPa (p_{\max} at $F = 244.5$ N) to 0.8 GPa, the m value increased only slightly, thus indicating that the calculated m value was not very sensitive to variation in p .

6.2.2 Empirical expression of τ_L as function of film pressure (p)

Once the index number m was determined, an empirical expression for the relationship between τ_L and p was generated (Eq. 6.3) by substituting the values of F_{\max} , πa^2 and p_{\max} for a particular load level into Eq. 2.50.

$$\tau_L = C \cdot p^{2m} \quad (6.3)$$

where C — an average value calculated from four load levels

For both τ_L and p in Pa, the index number m and the proportionality constant C for the example given in last section were evaluated (Table 6.3). Similar predictions for temperature of 40°C were based on the tests of experiment numbers 9 ~ 12, 27 ~ 30 and 63 ~ 66. The F_{\max} data could be found in Table 5.1 and the corresponding test conditions were listed in Table 4.10. Through the same procedure, the m and C were found and listed in the same table (Table 6.3).

Table 6.3 Constants for the expression of τ_L versus p (Eq. 6.3)

Temp. (°C)	Constant	MCT 5	MCT 5 + FM	MCT 5 + EP
30	C	0.569e-3	0.436e-2	0.243e-1
	m	0.615	0.565	0.523
40	C	0.134e-2	0.3095e-2	0.1305e-1
	m	0.594	0.571	0.536

6.3 Real Area of Contact for Rough Surface Discs

Surface roughness has a significant effect on friction force in mixed film lubrication. This effect is a consequence of the decrease in the real area of contact with increased surface roughness, which then results in high contact pressure. To continue the rheological analysis

in the present study, it is necessary to estimate the real area of contact (A_r) for the rough disc experiments.

A procedure of the determination A_r for a rough surface against a rigid smooth surface was introduced previously in Chapter 2, Section 2.3.3. From the roughness measurements of HSC and BA for rough discs, the contact spot density (n) at various separations between two contact surfaces, the average surface height (d_{avg}), average asperity height (d^*_{avg}) and their deviations (σ and σ^*) were found through a simple stochastic analysis of BA and n/n_{max} . Then, a Greenwood and Williamson type of contact model was applied to determine the real to apparent contact area ratio (A_r/A_a) under a particular load following the methods described by De Vall (1983).

6.3.1 Bearing area and high spot count

A Talysurf 5 profilometer was used to quantify the surface roughness of all discs used in the present study, and gave the BA and HSC at various heights z in the asperity tip region of the rough surface discs (Tables 4.6 and 4.7). Then, the derived formula (Eq. 2.30) can be used to determine the contact spot density n from the BA and HSC, which were measured from rough discs R1 and R2.

However, as mentioned in Chapter 2, the statistical analysis method, which was developed to prepare the parameters for a Greenwood and Williamson type model to determine the A_r , requires plots of BA vs. z and n/n_{max} vs. z on probability papers to check the surface and asperity height distributions. Since the processor of Talysurf 5 selected the z 's internally, it was not always possible to get enough data in the asperity tip region. To generate more data, three traverses were taken on the same rough surface disc (for example R1). Then, additional values were obtained by interpolation with piecewise third order polynomial curves which fit $BA \times 100$ versus z on a linear co-ordinate system (Figure 6.3). The coefficient of

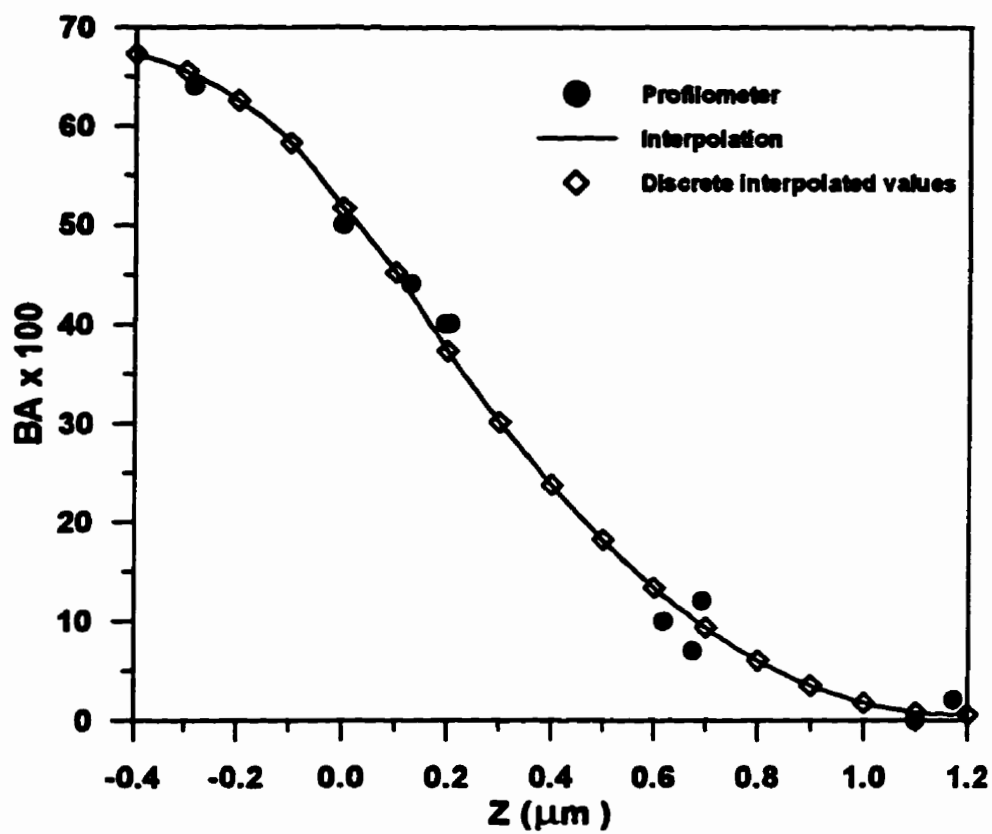


Figure 6.3 Polynomial curve fitting of BA versus z for rough disc R1

determination¹, R-Squared value reached 0.982585. Discrete data obtained from this curve fits and similar ones for HSC (Figure 6.4) allow many discrete n values to be calculated and n_{\max} to be determined (Table 6.4).

Table 6.4 Results of curve fitting for rough surface disc R1

z (μm)	BA	HSC (1/mm)	n (1/mm ²)	$(n/n_{\max}) \times 100$
-0.4	0.673537	44.2141	2279.42	-
-0.3	0.653722	45.0881	2442.42	100
-0.2	0.624427	43.2059	2347.98	96.13
-0.1	0.585690	38.9272	2032.02	83.20
0.0	0.538656	32.7303	1561.99	63.95
0.1	0.451894	27.3070	1295.99	53.06
0.2	0.372834	22.3892	1055.97	43.23
0.3	0.301475	17.9770	841.92	34.47
0.4	0.237818	14.0703	653.81	26.77
0.5	0.181862	10.6691	491.59	20.13
0.6	0.133608	7.7734	355.21	14.54
0.7	0.093055	5.3833	244.59	10.01
0.8	0.060204	3.4987	159.69	6.54
0.9	0.035054	2.1197	100.67	4.12
1.0	0.017606	1.2462	69.28	2.84
1.1	0.007859	0.8782	(77.07)	-
1.2	0.005814	1.0157	(139.37)	-

The above data were plotted as $BA \times 100$ vs. z on a probability paper (Figure 6.5). For the rough disc R1, the BA data were fit with a straight line in the asperity tip region of the surfaces. The roughness profiles were measured after run-in and did not have an overall Gaussian distribution as shown in Figure 4.5b. However, the surface height distribution was Gaussian in the asperity tip region, which made intimate contact with the smooth disc surface. The features of the distribution included the average surface height (d_{avg}) and standard deviation (σ), both of which were determined from this plot. Following Eqs. 2.31 and 2.32, $d_{\text{avg}} = 0$ and $\sigma = 0.48 \mu\text{m}$ for rough disc R1.

¹ The coefficient of determination, R-squared value equals $1 - \text{SSE}/(\text{SSE} + \text{SSr})$, where SSE is the Residual sum of squares, and SSr is the Regression sum of squares (Grapher for Windows Reference Manual, 1994).

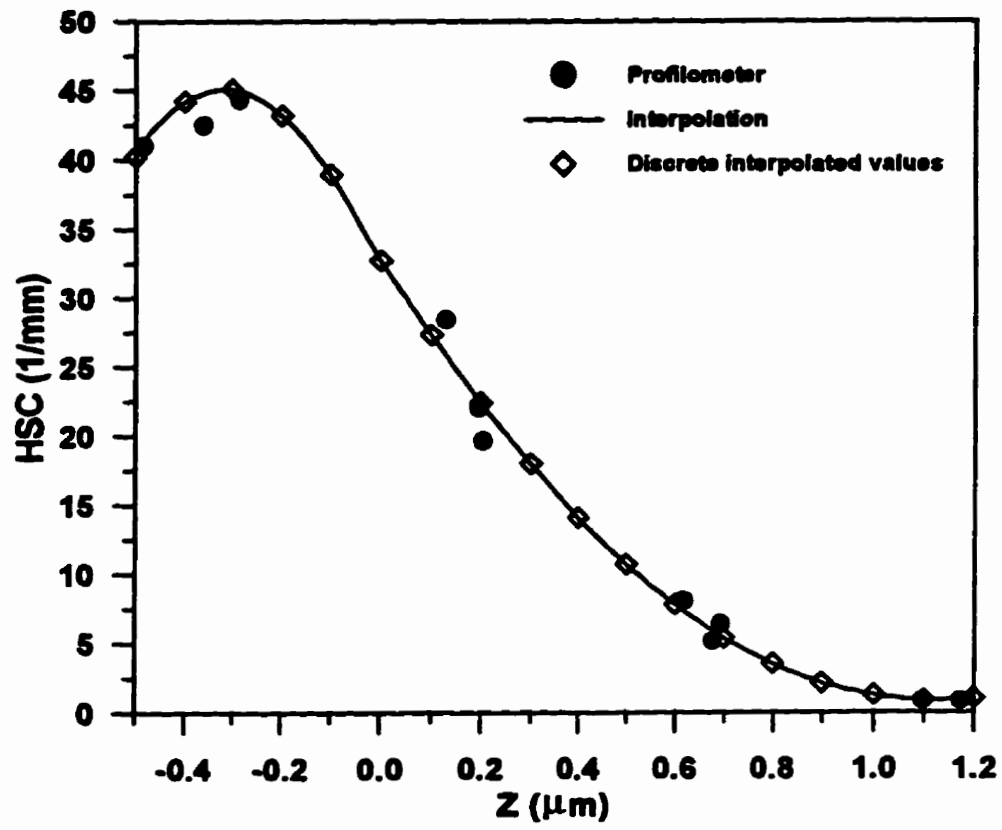


Figure 6.4 Polynomial curve fitting of HSC versus z for rough disc R1

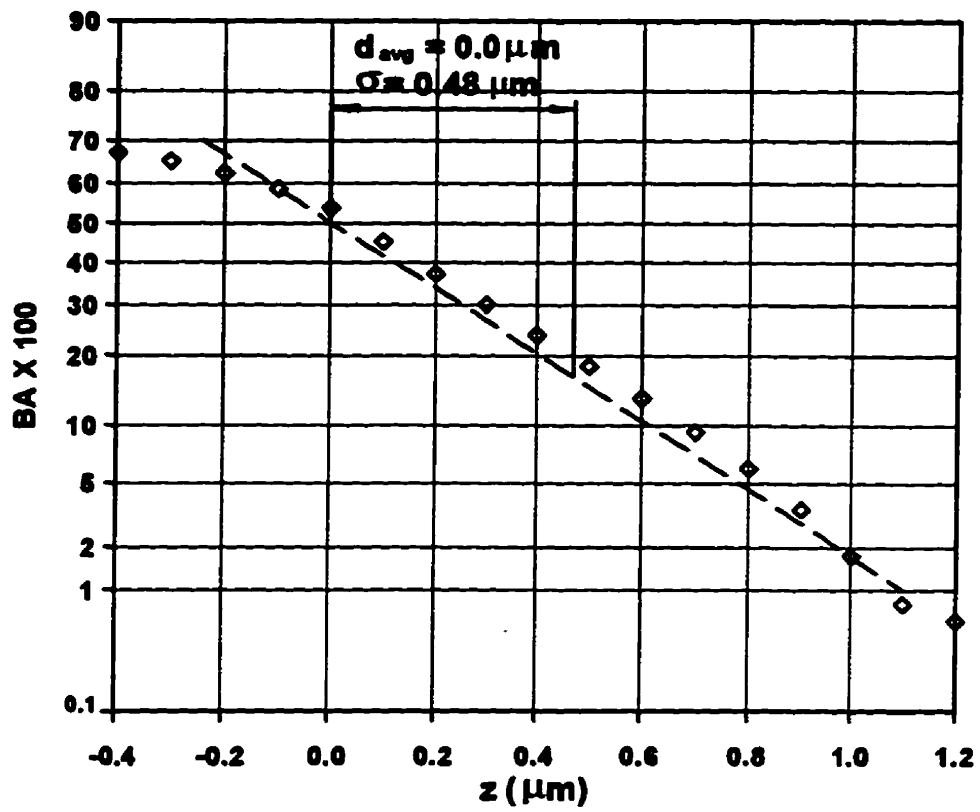


Figure 6.5 Plot of BA on probability paper to determine d_{avg} and σ for disc R1

In the similar manner, piecewise third order polynomial curve was fit to the HSC data (Figure 6.4). The coefficient determination, R-squared value was 0.980137. Data interpolated using the curve fit were substituted together with BA data into Eq. 2.30 to calculate the n and n/n_{\max} for each z (Table 6.4). Finally, the $n/n_{\max} \times 100$ versus z was plotted on a probability paper (Figure 6.6). Following the Eqs. 2.33 and 2.34, the average asperity height was found as, $d^*_{\text{avg}} = 0.11 \mu\text{m}$ and $\sigma^* = 0.47 \mu\text{m}$ for rough disc R1.

Both the BA and HSC plots on probability paper had lines fitted manually. Software might be developed eventually to perform this task automatically and would have to include an “exclusion criterion” for points in the low and very high z regions which were not distributed in a Gaussian fashion. However, such software would have to be carefully crafted to outperform such a manual fit in which both slope and exclusion criterion can be considered simultaneously.

6.3.2 Surface separation and real area of contact

To estimate the A_r , it was decided to temporarily ignore the presence of lubricant. Also, it was assumed the A_r was represented accurately by a flat rough surface with a Hertzian apparent area (A_a) against a smooth flat surface. Although, the A_a was influenced by the surface roughness (Greenwood et. al., 1984), for an elastic contact of surfaces with Gaussian distributions of surface and asperity heights, the A_r depended mostly on the load and was relatively independent of the A_a .

A Greenwood and Williamson type model (Section 2.3.3) was used to determine the A_r for the present study. In this model, the separation (z) between a rough and a smooth contact surfaces was found and used to determine the A_r for a specific load. A FORTRAN computer program was written to find the separation z by using a secant algorithm for the non-linear Eq. 2.40 (repeated below).

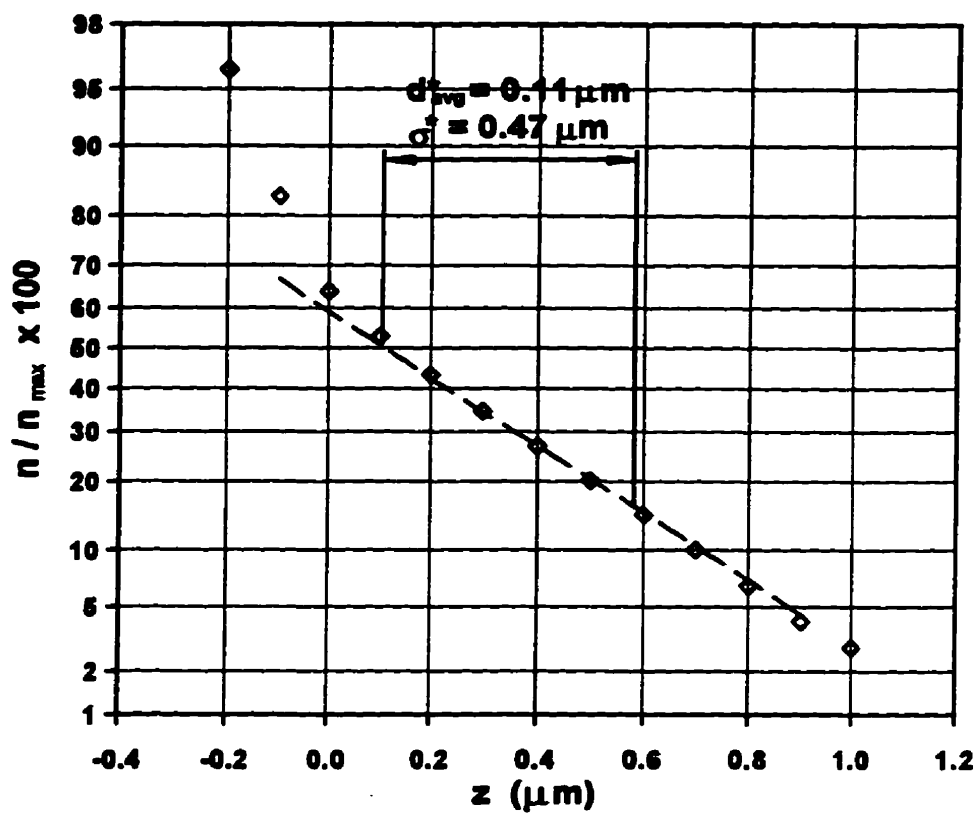


Figure 6.6 Plot of HSC on probability paper to determine d_{avg}^* and σ^* for disc R1

$$F_0(z_m) - \frac{45 \cdot \pi}{n_{\max}} \cdot \left(\frac{F}{\sigma^* \cdot E' \cdot A_a} \right)^2 \cdot \frac{F_1(z_m^*)}{[F_{1.5}(z_m^*)]^2} = 0$$

In this equation, z_m and z_m^* were implicit in the probability density functions $F_0(z_m)$, $F_1(z_m^*)$ and $F_{1.5}(z_m^*)$. For any given z_m or z_m^* , the corresponding functions were evaluated by interpolation from the discrete values in Table 2.3 (McCool, 1986) using a natural cubic spline routine (Davidson, 1988).

The aforementioned example (Section 6.3.1) was used to demonstrate the calculation of the β , A_r and A_r/A_a . For the applied load F of 147.0 N, reduced elastic modulus E' of 219.8×10^9 Pa and reduced radius R of 22.58×10^{-3} m, the apparent contact area from Hertzian formula (Eqs. 2.10 and 2.11) was

$$A_a = \pi \cdot \left(\frac{3F \cdot R}{2E'} \right)^{\frac{2}{3}} = 2.515 \times 10^{-7} (m^2)$$

The surface roughness parameters from Section 6.3.1 were: $d_{\text{avg}} = 0 \mu\text{m}$, $\sigma = 0.48 \mu\text{m}$, $d_{\text{avg}}^* = 0.11 \mu\text{m}$, $\sigma^* = 0.47 \mu\text{m}$ and $n_{\max} = 2442.42 \text{ mm}^{-2}$. Inserting these values and the test condition parameters, F , E' and A_a into Eq. 2.40 and using the secant algorithm with cubic spline interpolation gave

$$z_m = 0.2373, \text{ and } z_m^* = 0.00835.$$

The corresponding values of $F_j(\zeta)$'s were:

$$F_0(z_m) = 0.4070, \quad F_1(z_m^*) = 0.3958, \quad F_{1.5}(z_m^*) = 0.4249$$

It was now possible to calculate the β , A_r and A_r/A_a :

(1) the asperity tip radius (Eq. 2.39)

$$\beta = \frac{F_0(z_m)}{2\pi \cdot \sigma^* \cdot F_1(z_m^*) \cdot n_{\max}} = 1.423 \times 10^{-4} (m)$$

(2) the real area of contact (Eq. 2.36)

$$A_r = \pi \cdot \beta \cdot A_a \cdot n_{\max} \cdot \sigma^* \cdot F_1(z_m^*) = 5.108 \times 10^{-8} (m^2)$$

(3) the ratio of the real to apparent contact areas

$$\frac{A_r}{A_a} = \frac{5.108 \times 10^{-8}}{2.515 \times 10^{-7}} = 0.2031$$

All of the above calculations were performed by a computer program SECANT.FOR. Despite distinct differences in input data, results for discs R1 and R2 exhibited remarkable similarity in their output data (Table 6.5).

Table 6.5 Calculation of β , A_r and A_d/A_r

Parameter		Disc R1	Disc R2
Input	F (N)	147.0	244.5
	d_{avg} (μm)	0.0	0.0
	σ (μm)	0.48	0.55
	d^*_{avg} (μm)	0.11	0.03
	σ^* (μm)	0.47	0.45
	n_{max} (mm^{-3})	2442.42	3116.27
	A_o (mm^2)	0.25151	0.35307
Output	z_m	0.2373	0.1574
	z_m^*	0.00735	0.1257
	$F_0(z_m)$	0.4062	0.4375
	$F_1(z_m^*)$	0.3958	0.3319
	$F_{1.5}(z_m^*)$	0.4249	0.3574
	β (mm)	0.1423	0.1132
	A_r (mm^2)	0.05108	0.07723
	A_d/A_r	0.2031	0.2187

6.4 Comparison of τ_L from Experiments with Smooth and Rough Top Discs

A number of experiments was performed under full ehl with various applied loads and the measured maximum friction forces were used to find a functional relationship between limiting shear stress and pressure for each lubricant (Eq. 6.3 and Table 6.3) as described previously in Section 6.1. Could this rheological equation be applied to predict the average limiting shear stress for each lubricant ($\tau_{Lavg} = F_{fmax} / A_r$) as measured in the experiments with the rough top discs? If so, strong circumstantial evidence would be found for the existence of micro-ehl. The reduction in the maximum friction force as observed for the lubricants with additives in the rough top disc experiments could be attributed to a change in the limiting shear stress which had been evaluated under full ehl conditions. To develop the application of Eq. 6.3, it was used first to predict τ_{Lavg} in full ehl.

• $\tau_{L,avg}$ from friction measurements with a smooth top disc

One approach to using Eq. 6.3 to predict $\tau_{L,avg}$ was to simply substitute in $p = p_{avg}$ and expect that $\tau_L = \tau_{L,avg}$. Since Eq. 6.3 was derived from Eq. 2.50 which contained the exact $\tau_{L,avg}$, the error in the substitution of $p = p_{avg}$ could be derived as follows:

$$\%err = \left| 1 - \frac{m+1}{15^{2m}} \right| \times 100 \quad (6.4)$$

Evaluating this expression for the m values obtained for the present study gave a maximum error of less than 2 %.

To check the approximation of $\tau_{L,avg}$ by substituting p_{avg} into Eq. 6.3, a comparison with the measured $\tau_{L,avg}$ was performed (Table 6.6). The agreement was excellent, well within the expected 2 % maximum. However, it was noted that the C and m values in Eq. 6.3 had been derived directly from these experiments, and thus, excellent agreement had to occur if the precision of the experiments was good. Nevertheless, it was established that an accurate prediction of $\tau_{L,avg}$ was possible by substituting $p = p_{avg}$ into Eq. 6.3.

Table 6.6 Measured and predicted τ_{LAVG} for ehl conditions

Experiment Number	τ_{LAVG} (MPa)	
	Measured	Predicted
5	43.03	42.51
6	54.69	54.11
7	63.36	62.93
8	71.11	70.24
9	43.35	42.57
10	54.68	53.75
11	63.24	62.19
12	70.29	69.16
23	42.55	42.54
24	53.27	53.10
25	60.76	61.00
26	67.59	67.48
27	39.27	38.55
28	49.08	48.23
29	56.46	55.50
30	62.50	61.46
59	42.41	42.89
60	52.78	52.66
61	58.18	59.88
62	65.65	65.74
63	39.49	39.10
64	48.70	48.26
65	55.53	55.04
66	61.09	60.58

- **τ_{LAVG} from friction measurements with a rough top disc**

The friction forces measured in the experiments with the rough top disc were assumed to arise from isolated micro-ehl. In isolated micro-ehl of a surface with spherically tipped asperities, the film pressure could be approximated as a number of localized Hertzian distributions. In the present study, it seemed reasonable to use Eq. 6.3 with $p = p_{avg}$ for all of the micro-contacts to predict τ_{LAVG} . The predicted τ_{LAVG} could be compared to the directly measured τ_{LAVG}

that was obtained from dividing the measured maximum friction force $F_{f \max}$ by the estimated real area of contact A_r .

As λ decreased, either a transition from cooperative to isolated micro-ehl or film breakdown occurred in some of the micro-contacts, both of which could cause increasing $F_{f \max}$. To obtain an appropriate range of $F_{f \max}$ values for the directly measured τ_{LAVG} , it was assumed that isolated micro-ehl dominated approximately when $0.23 < \lambda < 0.54$. The friction of the base stock oil did seem to have a big increase below $\lambda = 0.23$, which suggested a breakdown of micro-ehl and gave a basis for selecting the above lower limit for the range of λ . The upper limit was chosen because no friction measurements were available for $0.54 < \lambda < 1.8$ and at $\lambda = 1.8$ the $F_{f \max}$ values were as low as for full ehl thus indicating little micro-ehl took place. For subsequent comparisons, two values of τ_{LAVG} were calculated from the $F_{f \max}$ obtained for the highest and the lowest λ values in this specified range. In this manner, a range of τ_{LAVG} values were estimated with a corresponding p_{avg} for the lubricants in each of the experiments with top discs R1 and R2 (Table 6.7).

Table 6.7 Measured and predicted τ_{LAVG} for micro-ehl conditions

Lubricating Oil	Expt. Number	τ_{LAVG} (MPa)		
		Measured ($\lambda=0.5$)	Measured ($\lambda=0.4$)	Predicted
MCT 5	91, 92	253.62	261.52	245.33
	96, 97	276.19	295.74	275.88
	101, 102	246.97	250.75	231.46
	106, 107	258.84	270.56	259.24
MCT 5+FM	111, 112	215.37	219.46	212.92
	116, 117	225.88	240.48	237.16
	121, 122	190.97	210.85	196.29
	126, 127	213.45	226.85	218.89
MCT 5+EP	131, 132	197.63	212.80	190.45
	136, 137	207.68	211.00	210.44
	141, 142	189.60	195.27	180.19
	146, 147	202.84	208.53	199.59

• Comparison of τ_{Lavg} values

The predicted τ_{Lavg} could be compared with the directly measured one in the isolated micro-ehl (Table 6.7). A more obvious comparison was made by plotting the data of Table 6.7 in Figure 6.7a for $T = 30^\circ\text{C}$ and Figure 6.7b for $T = 40^\circ\text{C}$. The predicted τ_{Lavg} included values from Table 6.7 and further discrete values listed in Table 6.8, which were generated by substituting p_{avg} values into Eq. 6.3. All of these values were linked by a solid line generated using a cubic spline interpolation.

Table 6.8 Predicted τ_{Lavg} from empirical expression with p_{avg}

p_{avg} (GPa)	τ_{Lavg} (MPa) ($T = 30^\circ\text{C}$)			τ_{Lavg} (MPa) ($T = 40^\circ\text{C}$)		
	MCT 5	MCT 5+FM	MCT 5+EP	MCT 5	MCT 5+FM	MCT 5+EP
0.5	28.500	29.466	30.530	28.984	26.758	27.697
1.0	66.852	64.489	63.039	66.036	59.063	58.235
1.5	110.079	101.969	96.338	106.899	93.857	89.947
2.0	156.812	141.140	130.162	150.452	130.371	122.445
2.5	206.338	181.618	164.381	196.122	168.222	155.541
3.0	258.209	223.169	198.918	243.552	207.171	189.122
3.5	312.116	265.634	233.723	292.499	247.060	223.110

The agreement between the directly measured and predicted τ_{Lavg} was quite good, particularly for the tests at $F = 244.5$ N (with top disc R2). Since two test temperature had only a 10°C difference, an influence of temperature on additive performance was not found. All of the lubricants showed a slight decrease in τ_{Lavg} with increasing temperature.

The comparison indicated that in the rough disc experiments with λ ratio greater than about 0.24, micro-ehl occurred and the shear stresses throughout the contact reached the limiting shear stress. Therefore, the limiting shear stress model can describe the lubrication in the present isolated micro-ehl regime.

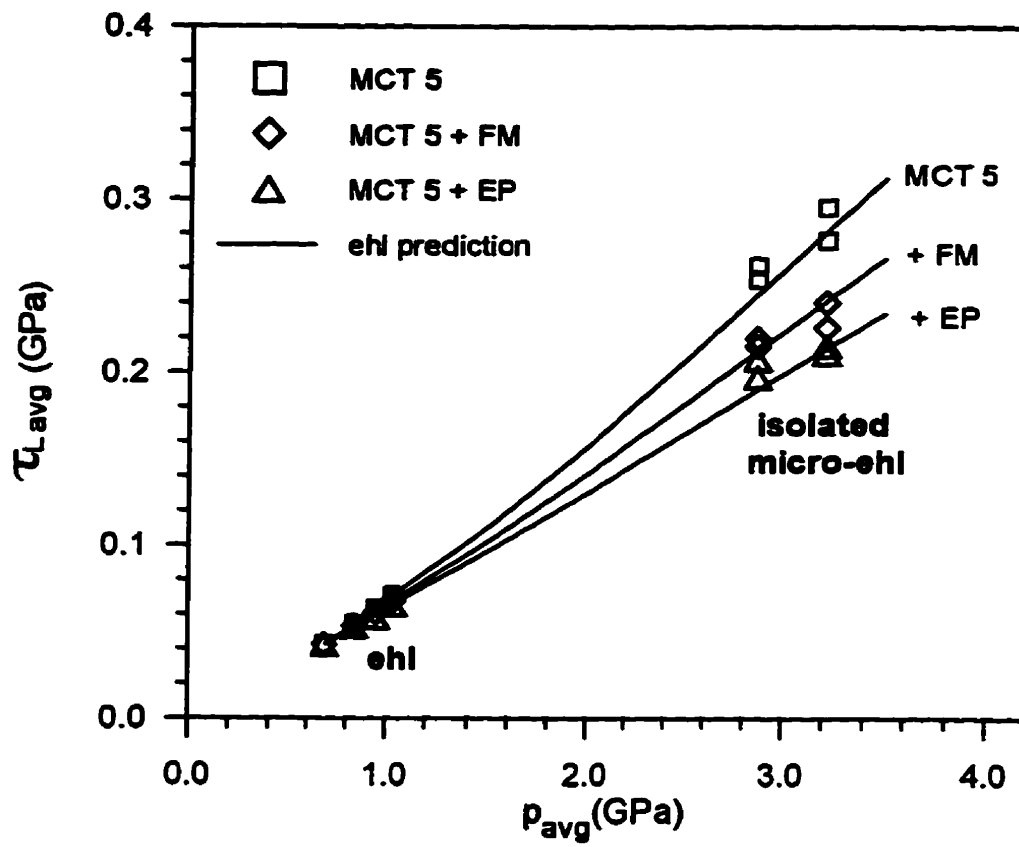


Figure 6.7 Comparison of predicted and measured $\tau_{L,avg}$ in ehl and micro-ehl

(a) $T=30^\circ\text{C}$

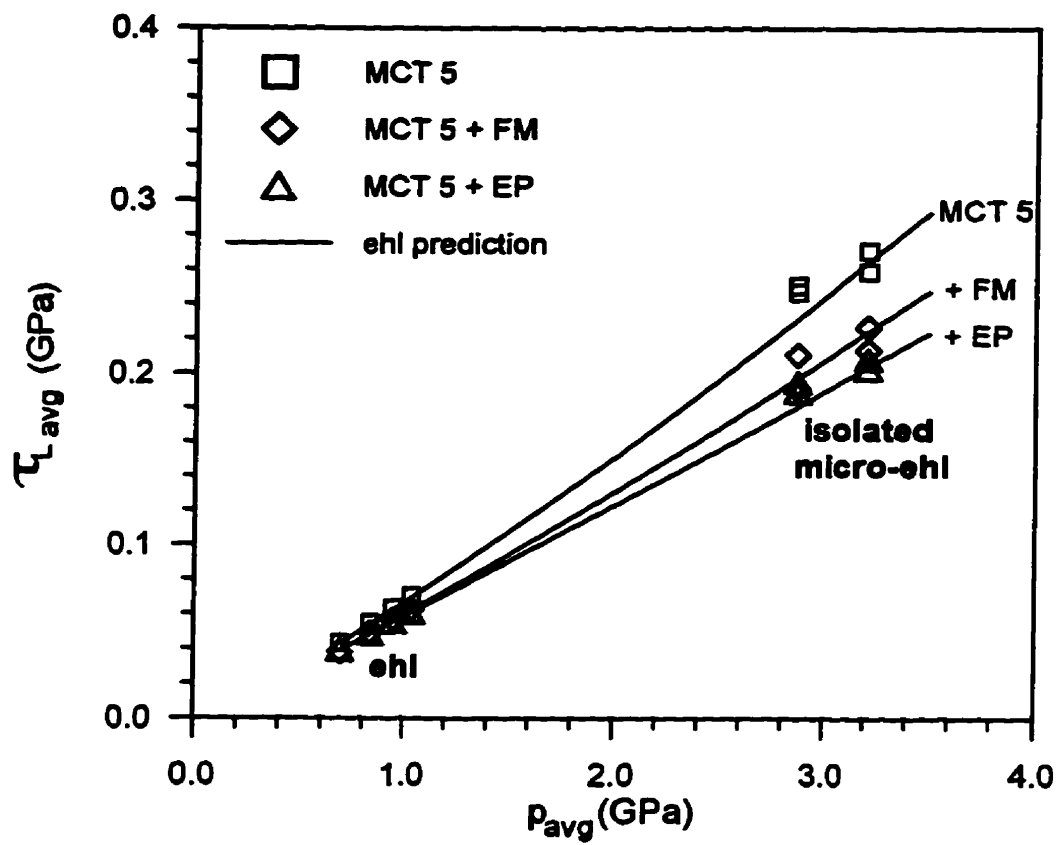


Figure 6.7 Comparison of predicted and measured $\tau_{L,avg}$ in ehl and micro-ehl

(b) at $T = 40^\circ\text{C}$

From the engineering point of view, determining the τ_L from friction measurement in a side-slip disc machine under full ehl is a useful technique. Although smooth discs are required, long run-in is not required and experiments can be performed with minimal surface damage. It is a simple and low cost procedure as compared with the expensive full engine tests and field tests. It is also more precise than some simple pure sliding tests in which extensive surface damage occurred from sliding action. The present method gives a direct evaluation of the τ_L , a controlling rheological parameter in micro-ehl, and is sensitive enough to give different values for different additives.

Although no other research groups have tested MCT 5, the limiting shear stress versus pressure results of the present study can be compared with those obtained by others using various oils to ascertain whether the present results are in the same range. They are indeed in the same range (Figure 6.8).

In summary, the disc machine can be used as a test apparatus to screen a large number of lubricant additives. Disc machine results can provide useful information on rheology for the designers and users of lubricant additives. However, the present method should be applied to more other additives and high temperatures to explore the generality of this approach.

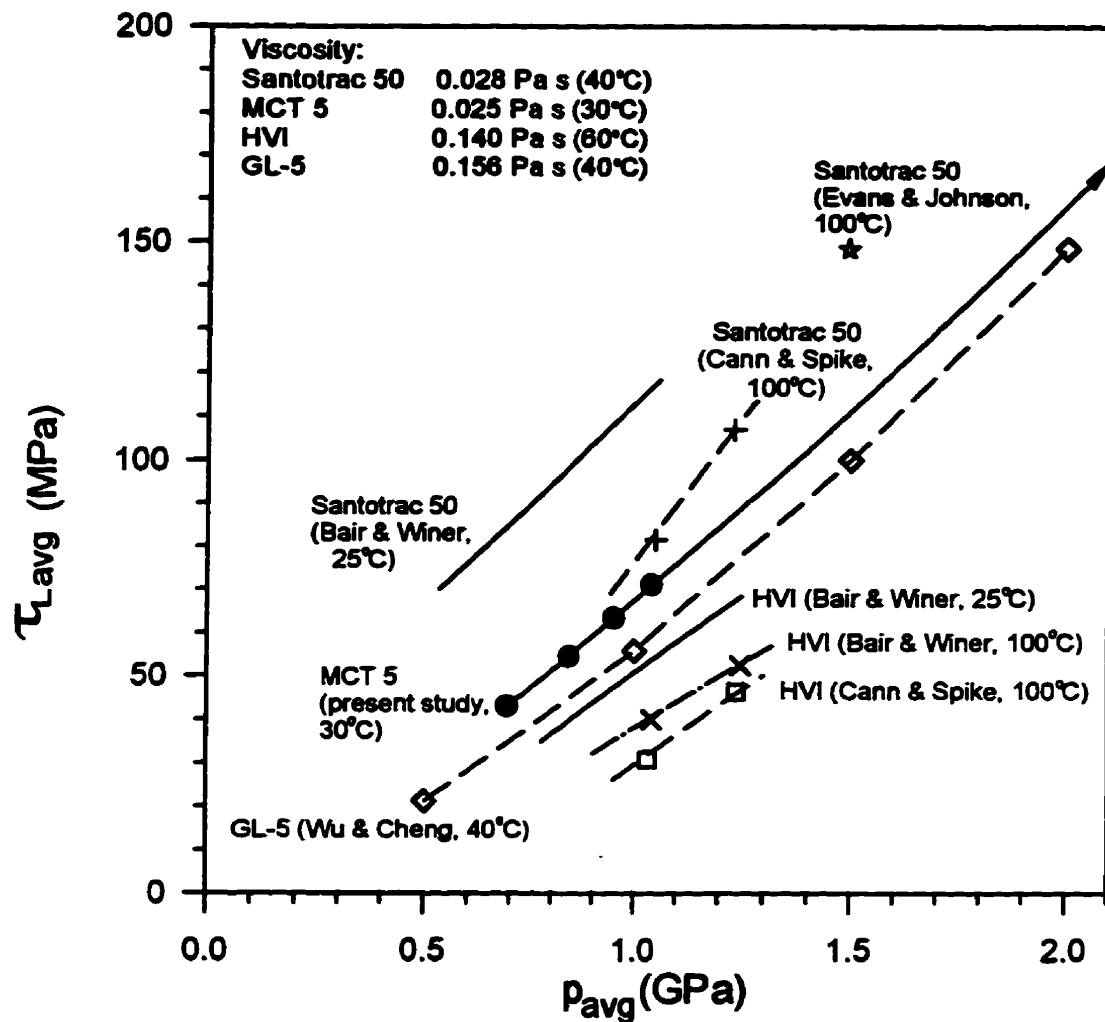


Figure 6.8 Comparison of present τ_{Lavg} vs. p_{avg} with other researchers' values

(Presented data from Bair and Winer, 1979; Cann and Spike, 1989; Evans and Johnson, 1986; Wu and Cheng, 1994)

Chapter 7 Summary, Conclusions and Recommendations

7.1 Summary

The work reported in this thesis dealt mainly with the investigation of the friction behaviour of formulated lubricating oils in both ehl and micro-ehl regimes. A side-slip disc machine was used to provide a simple method of measuring the friction force due to shearing of the lubricant film in the contact between the rolling discs. The disc machine subjected a lubricating oil to high pressures, while maintaining an almost constant ehl film thickness.

The friction force measurements were performed using both smooth and rough discs. The composite RMS surface roughnesses were about $0.1\mu\text{m}$ for the smooth disc experiments and 1.0 to $1.5\mu\text{m}$ for the rough disc experiments. The first group of experiments were performed using base stock oil (MCT 5) alone combined with three type of additives (FM, AW and EP) with smooth top and bottom discs and under four load levels of 244.5 N , 439.5 N , 634.5 N and 829.5 N . The entrainment velocities were varied between 1.6 m/s and 4.0 m/s . Three inlet lubricant temperatures of 30°C , 40°C and 55°C were used. The second group of experiments involved both rough and smooth top discs with smooth bottom discs, which were performed under identical loads, rolling velocities and temperatures in “matched” experiments. In other words, the operating conditions for each matched experiments were the same except the composite RMS roughness of disc surface. Two load levels of 147.0 N and 244.5 N , five entrainment velocities between 0.6 m/s and 3.3 m/s , and two inlet lubricant temperatures of 30°C and 40°C were applied. The results in all experiments consisted of the traction curves of friction force (F_f) versus the skew angle (ϕ) of the top disc (which equaled the ratio of side-slip to rolling velocities).

To analyze the results, an effective film thickness parameter (λ) was defined in this thesis as the ratio of the theoretical central film thickness (h_c) to the composite RMS surface roughness

(σ_c) of the discs (Eq. 2.28). This parameter was used to determine the lubrication regimes in an approximate manner. For all of the smooth disc experiments, λ was greater than 3 and there was, in theory, a continuous fluid film between discs without asperity interactions. For the rough disc experiments, the λ ratio was within the range of 0.15 to 0.5, and the asperity interactions had to be considered. The experimental results were summarized by plots of friction coefficient (μ) versus λ ratio (Figures 6.1 and 6.2). The influence of lubricant additives on friction was shown and discussed by referring directly to these plots.

Subsequent analyses focused on the mechanical behaviour, especially on the rheological behaviour, of the lubricants with additives in ehl and micro-ehl. It was assumed that the lubricant films were sheared at a limiting shear stress (τ_L). This assumption was examined by using the smooth disc friction measurements for full ehl ($\lambda > 3$) to determine the limiting shear stress for each lubricant. Following the approach developed by Wu and Cheng (1994), an empirical expression of the relationship between τ_L and p was found (Eq. 6.3). In the rough disc experiments, assuming isolated micro-ehl occurred, the friction force was predicted as the product of the average limiting shear stress (at the average pressure) and the real area of contact. The real area of contact had been determined from the roughness measurements of discs and other experimental parameters by using a Greenwood and Williamson type model, with an assumption of the entire load was only carried by the asperity contacts. The comparison of the predicted friction force with the measured results from the rough disc experiments showed quite good agreement.

The results and analysis of part of the data for $T = 30$ °C was presented at the 23rd Leeds-Lyon Symposium on Tribology in September, 1996. The associated paper was accepted for publication in the "Fundamentals and Applications in Lubrication and Traction", Tribology Series, 32, Elsevier, edited by C. Taylor et al., and included some reviewers' questions and authors replies (Appendix A).

7.2 Conclusions

1. Friction force was measured on a side-slip disc machine with various disc surface roughnesses for base stock and three formulated lubricating oils. The friction force measurements of the smooth disc experiments showed only slight but repeatable differences between the base stock and formulated oils. The friction force measurements of the rough disc experiments showed significant effects of additives on the friction force. Both the friction modifier (FM) and extreme pressure (EP) additives reduced the friction force. In most cases, the EP additive reduced friction more than the FM additive. The antiwear (AW) additive had somewhat more erratic behaviour, sometimes marginally reducing friction force, while at other time, giving the same friction force as the base stock oil in the smooth disc experiments.

2. The output voltage in the electrical resistance circuit dropped at $\lambda = 3$ (Figure 4.7), as expected (Section 4.2.2, Chapter 4), thus, providing experimental support for the Hamrock and Dowson (1977) formula (Eq. 2.24) for central film thickness, which was developed from their theoretical numerical analysis.

3. The plots of the maximum friction coefficient (μ_{max}) versus λ ratio suggested that additives had a very small effect on friction coefficient until λ ratio dropped below 0.55 whereupon both the FM and EP additives reduced the friction force compared with base stock alone. It was suggested that the additives worked more efficiently in the mixed film regime than in full ehl.

4. Following an empirical approach (Wu and Cheng, 1994), in which it was assumed that all of the lubricant films were being sheared at the limiting shear stress (τ_L), results of the disc machine friction force measurements under conditions of full ehl ($\lambda > 3$) yielded an expression (Eq. 6.3) for τ_L in terms of the film pressure (p) for each lubricant formulation.

5. The τ_L expression was used to estimate $\tau_{L,avg}$ in the rough disc experiments assuming isolated micro-ehl. The $\tau_{L,avg}$ value agree well with the measured values of the maximum friction force ($F_{r,max}$) divided by the real area of contact (A_r) for the base stock oil alone and when it had the FM and EP additives. This agreement supported the validity of the empirical approach used to find τ_L and showed how limiting shear stress can be used to predict friction forces in isolated micro-ehl.

6. A procedure was developed to quantify the influence of lubricant additives on limiting shear stress by friction force measurements in a disc machine under full ehl. This finding suggested that lubricants could be designed to have an optimal limiting shear stress using disc machine measurements as a guidance. The measurement of the friction force in a disc machine provided a simple, low cost method to assess the influence of additives compared with high cost engine tests and extensive field testing. Also, this procedure may be particularly suitable for selecting additives to exhibit a desired behaviour from a large number of candidate formulations.

7.3 Recommendations of Further Research

Further research should focus on two directions: continuation of the work on the friction measurement using the disc machine and studies of the fundamental lubrication mechanisms in micro-ehl. The continuing work should include improvements to the accuracy, precision and range of operating conditions of the testing facility, experiments on more lubricant formulations under various conditions, and a development of the analytical procedures. The studies of fundamental mechanisms should use various experimental and analytical methods to clarify the relationship between the rheological properties, such as the limiting shear stress, to the chemical properties of the lubricant additives. Thus, the mechanism of additive influence on friction in micro-ehl would be explained thoroughly.

1. There were some limitations of the disc machine which should be removed in the future research. For example, the oil temperature cannot be higher than 60°C in the present disc machine. However, many lubricant additives are designed for use in an elevated temperature environment to protect the contact surfaces, such as piston ring, and cylinder by forming a film as a result of some special thermally activated chemical reactions. The current inlet lubricant temperature upper limit does not allow the effects of such additives be seen clearly. A new design for a high temperature lubricant circulation system would give better evaluation of the influence of additives on friction at higher temperatures.

2. The manual system of skewing the top disc introduces some difficulties and errors during the friction force measurements. In the present experiments, it is very difficult to make a uniform operation of skew angle to match the sampling time for the data acquisition system and to obtain a symmetrical traction plot. Therefore, an automatically controlled system of skewing the top disc is needed to satisfy these requirements, simplify the operation and get more precise results.

3. A hydraulic loading system can be used in the side-slip disc machine, instead of the suspended weight assembly. This would allow the applied loads be adjusted continuously and avoid some mechanical vibrations.

4. In the present research only a few lubricant additives have been studied using limited range of disc surface roughnesses. However, many new lubricant additives were designed for various applications. The additive designers put more of their efforts on the chemical compositions and properties, but pay less attention to the high pressure rheological properties. Useful results would come from further tests on new lubricant additives using the procedures described in the present thesis, and would be available to the machine designers and users.

5. The experiments in the present study have concentrated on very smooth and very rough disc surfaces, which are expected to simulate the ehl and isolated micro-ehl regimes respectively. In practice, the intermediate surface roughness exists and makes the lubricant work in the cooperative micro-ehl regime. The mechanical behaviour of lubricant additives in this regime has attracted considerable attention. Thus, further experimental studies of the influence of lubricant additives within this regime could be performed, perhaps using the disc machine.

6. It should not be expected that the influence of lubricant additives on friction in micro-ehl could be completely determined by using only the disc machine. All the related fundamental studies, such as determination of the chemical and physical properties of lubricant additives, and the experimental techniques, such as visualization of the shear deformation of lubricant film under high pressure and high temperature, could provide rheological evaluation of lubricants in ehl and micro-ehl. It would be beneficial to compare the results of the present study to those of alternative experimental techniques (Cann and Spike, 1989; Bair et al., 1993) for the same oils and additives.

REFERENCES

Aramaki, H., Cheng, H.S. and Chung, Y.W. (1993) The contact between rough surfaces with longitudinal texture - Part I: Average contact pressure and real contact area. *ASME J. of Trib.*, **115**, 419-424.

Baglin, K.P. (1986) Elastohydrodynamic pressure rippling in cylinder finished with a circumferential lay. *Proc. Ins. Mech. Eng.*, Part C, **200** (6), 335-347.

Bair, S., Qureshi, F. and Winer, W.O. (1993) Observations of shear localization in liquid lubricants under pressure. *ASME J. of Trib.*, **115**, 507-514.

Bair, S. and Winer, W.O. (1979a) Shear strength measurements at high pressure. *ASME J. of Lubr. Technol.*, **101**(3), 251-257.

Bair, S. and Winer, W.O. (1979b) A rheological model for elastohydrodynamic contacts based on primary laboratory data. *ASME J. of Lubr. Technol.*, **101**(3), 258-265.

Bair, S. and Winer, W.O. (1980) Friction/traction measurements with continuously variable slide-roll ratio and slid slip at various lambda ratio. *Proceedings of the 7th Leeds-Lyon Symposium on Tribology*, 296-301.

Bair, S. and Winer, W.O. (1982) Regimes of traction in concentrated contact lubrication. *ASME J. of Lubr. Technol.*, **104**, 382-391.

Bair, S. and Winer, W.O. (1990) The high shear stress rheology of liquid lubricants at pressures of 2 to 200 MPa. *ASME J. of Trib.*, **112**, 246-253.

Bair, S. and Winer, W.O. (1992) The high pressure high shear stress rheology of liquid lubricants. *ASME J. of Trib.*, 114, 1-13.

Bendat, J.S. and Piersol, A.G. (1980) *Random Data: Analysis and Measurement Procedures*, Wiley-Interscience, a division of John Wiley & Sons, Inc.

Booser, E.R. (Editor) (1984) *CRC Handbook of Lubrication (Theory and Practice of Tribology) Volume II, Theory and Design*, CRC Press, Inc. Boca Raton, Florida, USA.

Briant, J., Denis, J. and Parc, G., (1989) *Rheological Properties of Lubricants*, Editions Technip, Paris, French.

Bush, A.W., Gibson, R.D. and Thomas, T.R. (1975) The elastic contact of a rough surface. *Wear*, 35, 87-111.

Cameron, A. (1981) *Basic Lubrication Theory*, (3rd Edition). Ellis Horwood Ltd., Chichester, England.

Cann, P.M. and Spike, H.A. (1989) Determination of the shear stresses of lubricants in elastohydrodynamic contacts. *STLE Tribology Trans.*, 32, 414-422.

Chang, L. and Webster, M.N. (1991) A study of elastohydrodynamic lubrication of rough surfaces. *ASME J. of Trib.*, 113, 110-115.

Cheng, H.S. (1970) A numerical solution of the EHD film thickness in an elliptical contact. *ASME Trans.J. Lub. Tech.*, 92F(1) 155-162.

Cheng, H.S. (1978) On some aspects of microelastohydrodynamic lubrication. *Proceeding of the 4th Leeds-Lyon Symposium on Tribology*, 71-79.

Cheng, H.S. (1993) Mixed lubrication and lubricated wear. *Proceeding of the 19th Leeds-Lyon Symposium on Tribology*, 181-191.

Christensen, H. (1969) Stochastic models for hydrodynamic lubrication of rough surfaces. *Proc. Ins. Mech. Eng.*, **184** (55), 1013-1026.

Cooper, M.G., Mikic, B.B. and Yovanovich, M.M. (1969) Thermal contact conductance. *Int. J. Heat Mass Transfer.*, **12**, 279-300.

Crook, A.W. (1961) The lubrication of rollers, III. A theoretical discussion of friction and the temperatures in the oil film. *Philosophical Transactions, A*, **254**, 237-258.

De Silva, G.M.S., Leather, J.A. and Sayles, R.S., (1985) The influence of surface topography on the lubricant film thickness in an elastohydrodynamic (EHD) point contact. *Proceedings of the 12th Leeds-Lyon Symposium on Tribology*. 258-272.

De Vaal, J.W., (1983) Thermal contact conductance of rough surfaces. *MASc thesis, Mechanical Engineering, University of Waterloo*.

Dowson, D., (1992) Developments in lubrication - the thinning film. *J. Phys. D: Appl. Phys.* **25**, 334-339.

Dowson, D., (1995) Elastohydrodynamic and micro-elastohydrodynamic lubrication. *Wear*, **190**, 125-138.

Dowson, D. and Higginson, G.R. (1966) *Elastohydrodynamic Lubrication: The Fundamentals of Roller and Gear Lubrication*. Pergamon. Oxford.

Esfahanian, M. and Hamrock, B.J., (1991) Fluid-film lubrication regimes revisited. *STLE Tribology Trans.*, 34, 628-632.

Evans, C.R. and Johnson, K.L. (1986a) The rheological properties of elastohydrodynamic lubricants. *Proc. Inst. Mech. Engrs. Pt C*, 200, 303-312.

Evans, C.R. and Johnson, K.L. (1986b) Regimes of traction in elastohydrodynamic lubrication. *Proc. Inst. Mech. Engrs. Pt C*, 200, 313-324.

Evans, C.R. and Johnson, K.L. (1987) The influence of surface roughness on elastohydrodynamic traction. *Proc. Inst. Mech. Engrs. Pt C*, 201, 145-150.

Fein, R.S. (1983) Characteristics of boundary lubrication. *Handbook of Lubrication*, Volume II, 49-68.

Fein, R.S. (1986) A perspective on boundary lubrication. *Industrial Engineering Chemistry Fundamentals*, 25, 518-524.

Fowles, P.E. (1971) A thermal elastohydrodynamic theory for individual asperity-asperity collisions. *J. of Lubrication Technology, Trans. ASME, (F)*, 93, (3), 383-397.

Furey, F.W. (1961) Metallic contact and friction between sliding surfaces. *ASLE Transactions*. 4, 1-11.

Gecim, B. and Winer, W.O. (1980) Lubricant limiting shear stress effect on EHD film thickness. *ASME J. of Lubr. Technol.*, 102, 213-221.

Gohar, R. (1988) *Elastohydrodynamics*. Ellis Horwood Limited, Chichester, England.

Grapher for Windows Reference Manual (Technical Graphics for Scientists and Engineers) (1994) Golden Software, Inc. Golden, CO, USA.

Greenwood, J.A. Johnson, K.L. and Matsubara, E., (1984) A surface roughness parameter in hertz contact. *Wear*, 100, 47-57.

Greenwood, J.A. and Tripp, J.H., (1967) The elastic contact of rough spheres. *ASME J. of Appl. Mech.*, 89, 153-159.

Greenwood, J.A. and Williamson, J.B.P., (1966) Contact of nominally flat surfaces. *Proc. R. Soc. A*, 295, 300~319.

Grubin, A.N. (1949) Fundamentals of hydrodynamic theory of lubrication of heavily loaded cylindrical surfaces. *Investigation of the contact machine components*. Kh. F. ketova, (Ed.). Translation of Russian Book No. 30, Central Scientific Institute for Technology and Mechanical Engineering, Moscow, chap.2. (Available from Dept. of Sci. and Ind. Research, Great Britain, Trans. CTS-235 and Special Libraries Association, Trans. R-3554).

Hamrock, B.J. (1994) *Fundamentals of Fluid Film Lubrication*. McGraw-Hill, Inc.

Hamrock, B.J. and Dowson, D. (1981) *Ball Bearing Lubrication - The Elastohydrodynamics of Elliptical Contacts*. John Wiley & Sons, Inc.

Hamrock, B.J., Jacobson, B.O. and Bergström, S.I. (1987) Measurement of the density of base fluid at pressure to 2.2 GPa. *ASLE Trans.*, 30 (2), 196-202.

Halling, J. (1976) *Introduction to Tribology*. Wykeham Publications, London.

Hilburn, J.L. and Johnson, D.E. (1983) *Manual of Active Filter Design*. Second Edition. McGraw-Hill Book Company.

Hist, W. and Moore, A.J. (1974) Non-Newtonian behavior in ehd lubrication. *Proc. Roy. Soc. Lond.*, **A337, 217-242.**

Houpert, L.G. and Hamrock, B.J. (1985) Elastohydrodynamic lubrication calculations used as a tool to study scuffing. *Proceeding of the 12th Leeds-Lyon symposium*. 146-155.

Höglund, E. and Jacobson, B.O. (1986) Experimental Investigations of the shear strength of lubricants subjected to high pressure and temperature. *J. of Tribology*, **108 (4), 571-578.**

Huang, P. and Wen, S.Z. (1993) Sectional micro-elastohydrodynamic lubrication. *ASME J. of Trib.*, **115, 148-151.**

Imai, Y. and Brown, N. (1976) Environmental crazing and intrinsic tensile deformation in PMMA. *J. Mater. Sci.*, **11, 417-424.**

Jefferis, J.A. and Johnson, K.L. (1968) Sliding friction between lubricated rollers. *Proc. Instn mech. Engrs*, Part C, **182 (1), 281-292.**

Johnson, G.W. (1994) *LabVIEW Graphic Programming*. McGraw-Hill, Inc.

Johnson, K.L. (1970) Regimes of elastohydrodynamic lubrication. *J. Mech. Eng. Sci.*, **12 (1), 9-16.**

Johnson, K.L. (1992) Non-Newtonian effects in elastohydrodynamic lubrication. *Proceeding of the 19th Leeds-Lyon symposium*. 15-26.

Johnson, K.L. and Cameron, A. (1967) Shear behavior of elastohydrodynamic oil films at high rolling contact pressures. *Proc. Inst. Mech. Eng., Part C*, **182**(1), 292-299.

Johnson, K.L., Greenwood, J.A. and Poon, S.Y. (1972) A simple theory of asperity contact in elastohydrodynamic lubrication. *Wear*, **19**, 91-108.

Johnson, K.L. and Higginson, J.G. (1988) A non-Newtonian effect of sliding in micro-ehl. *Wear*, **128**, 249-264.

Johnson, K.L. and Roberts, A.D. (1974) Observations of viscoelastic behaviour of an elastohydrodynamic lubricant film. *Proc. Roy. Soc. Lond., Ser. A*, **337**, 217-242.

Johnson, K.L. and Tevaarwerk, J.L. (1977) Shear behavior of elastohydrodynamic oil film. *Proc. Roy. Soc. Lond., Ser. A*, **356**, 215-236.

Karami, G., Evans, H.P. and Snidle, R.W. (1987) Elastohydrodynamic lubrication of circumferentially-finished rollers having sinusoidal roughness. *Proc. Int. Mech. Eng., Part C*, **201** (1), 29-36.

Kato, K., Iwasaki, T., Kato, M. and Inoue, K. (1993) Evaluation of limiting shear stress of lubricants by roller test. *JSME International Journal, Series C*, **36** (4), 515-522.

Kingsbury, E. (1985) Parched elastohydrodynamic lubrication. *ASME J. of Tribol.*, **107**(2), 229-232.

Kunz, R.K. and Winer, W.O. (1977) Discussion on page 275-276 of Hamrock. B.J. and Dowson, D., Isothermal elastohydrodynamic lubrication of point contacts, Part III - Fully flooded results. *ASME J. of Tribology*, **99** (2), 264-275.

Kweh, C.C, Evans, H.P. and Snidle, R.W. (1989) Micro-elastohydrodynamic lubrication of an elliptical contact with transverse and three-dimensional sinusoidal roughness. *ASME J. of Trib.*,111, 577-584.

***LabVIEW for Windows Analysis VI Reference Manual* (1993) National Instruments Corporation, Austin, TX, USA.**

***LabVIEW for Windows Data Acquisition VI Reference Manual* (1993) National Instruments Corporation, Austin, TX, USA.**

***LabVIEW for Windows User Manual* (1993) National Instruments Corporation, Austin, TX, USA.**

Lai, and Cheng, H.S. (1985) Computer simulation of elastic rough contacts. *ASLE Trans.*, 28 (2), 172-180.

Lee, S.C. and Cheng, H.S. (1992) On the relation of load to average cap in the contact between surfaces with longitudinal roughness. *ASLE Trans.*, 35 (3), 523-529.

Lee, R.T. and Hamrock, B. J. (1991a) A circular non-Newtonian fluid model: Part I - Used in elastohydrodynamic lubrication. *ASME J. of Tribology*, 112 (3), 486-496.

Lee, R.T. and Hamrock, B. J. (1991b) A circular non-Newtonian fluid model: Part II - Used in elastohydrodynamic lubrication. *ASME J. of Tribology*, 112 (3), 497-505.

Liston, T.V. (1992) Engine lubricant additives, what they are and how they function. *STLE Lubrication Engineering*, 389-397.

Lubrecht, A.A., Napel, W.E.T. and Bosma, R. (1988) The influence of longitudinal and transverse roughness on the elastohydrodynamic lubrication of circular contacts. *ASME J. of Trib.*, **110**, 421-426.

McCool, J.I. (1986) Comparison of models for the contact of rough surface. *Wear*, **107**, 37-60.

McCool, J.I. and Gassel, S.S. (1981) The contact of two surfaces having anisotropic roughness geometry, *ASLE Spec. Publ. SP-7*, 29-38.

Mobil EHL Guidebook (4th Edition) (1992) Mobil Oil Corporation, Fairfax, VI, USA.

Onions, R.A. and Archard, J.F. (1973) The contact of surfaces having a random surface structure. *J. of Phys. D., Applied Physics*, **6**, 289-304.

O'Brien, J.A. (1983) Lubricating oil additives, *CRC Handbook of Lubrication (Theory and Practice of Tribology)*, Vol. II, *Theory and Design*. CRC press, Inc., 301-315.

Patir, N. and Cheng, H.S. (1978a) An average flow model for determining effects of three dimensional roughness on partial hydrodynamic lubrication. *ASME J. of Lubr. Technol.*, **100**, 12-17.

Patir, N. and Cheng, H.S. (1978b) Effect of surface roughness orientation on the central film thickness in E.H.D. contacts. *Proceedings of the 5th Leeds-Lyon Symposium on Tribology*, 15-21.

PC-LPM-16 Data Acquisition Board User Manual (1993) National Instruments Corporation, Austin, TX, USA.

Plint, M.A. (1967) Traction in elastohydrodynamic contacts. *Prec. Inst. Mech. Eng., Part C*, **182**(1), 300-306.

Ramesh, K.T. and Clifton, R.J. (1987) A pressure shear plate experiment for studying the rheology of lubricants at high pressures and high shearing rates. *ASME J. of Tribology*, **109** (2), 215-222.

Roelands, C.J.A., Vlugter, J.C. and Waterman, H.I. (1963) The viscosity-temperature-pressure relationship of lubricating oils and its correlation with chemical constitution. *ASME J. of Basic Engineering*, 601-610.

Sheasby, J.S. and Caughlin, T.A. (1993) The direct observation of the anti-wear action of ZDDP. *Proceedings of the 21st Leeds-Lyon Symposium on Tribology*, 399-408.

Shieh, J.A. and Hamrock, B.J. (1991) Film collapse in ehl and micro-ehl. *ASME J. of Tribology*, **113**(2), 372-377.

Siripongse, C. and Cameron, A. (1958) Thin film lubrication: 2 - lubrication of the four ball machine. *Engineering*. **186** (August), 147-149.

Siripongse, C., Rogers, P.R. and Cameron, A. (1958) Thin film lubrication: 1 - discharge through thin oil film. *Engineering*. **186** (August), 146-147.

Smith, F. W. (1959) Lubricant behavior in concentrated contact — the castor oil-steel system. *Wear*, **2**, 250-263.

Smith, F. W. (1960) Lubricant behavior in concentrated contact — some rheological problems. *ASLE Transactions*, **3**, (1) 18-25.

Smith, F. W. (1962) The effect of temperature in concentrated contact lubrication. *ASLE Trans.* **5**, (1), 142-148.

Snyder, F.L. (1982) The effects of oil additives and contacting materials on lubricant film thickness. *MASc. Thesis, Mechanical Engineering, University of Waterloo.*

Snyder, F.L., Tevaarwerk, J.L. and Schey, J.A. (1984) Effects of oil additives on lubricant film thickness and traction. *SAE Tech. Paper Series, 840263*, SAE, Warrendale, Pennsylvania.

Spikes, H.A. (1994) The behaviour of lubricants in contacts: current understanding and future possibilities. *Proc Instn Mech Engrs, Part J: J. of engineering Tribology*, **208**, 3-15.

Sutcliffe, M.P.F. (1991) Traction measurements in mixed elastohydrodynamic lubrication with a controlled circumferential roughness. *Proc Instn Mech Engrs, Part C: J. of Mech. Eng.* **205**, 265-273.

Talysurf 5 System, Operator's Handbook Rank Taylor Hobson, Leicester, England.

Tallian, T.E. (1972) The theory of partial elastohydrodynamic contacts. *Wear*, **21**, 49-101.

Tripaldi, G., Vettor, A. and Spikes, H.A. (1996) Friction behavior of ZDDP films in the mixed, boundary/ehd regime. *SAE Tech. Paper Series, 962036*, SAE, Warrendale, Pennsylvania.

Webster, M.N., Ioannides, E. and Sayles, R.S. (1985) The effect of topographical defects on the contact stress and fatigue life in rolling element bearings. *Proceedings of the 12th Leeds-Lyon Symposium on Tribology*, 207-221.

Williams, J.A. (1994) *Engineering Tribology*. Oxford University Press. Oxford, England.

Wu, S. and Cheng, H.S. (1994) Empirical determination of effective lubricant rheological parameters. *ASLE Tribology Trans.*, 37(1), 138-146.

Wu, S. and Cheng, H.S. (1991) A sliding wear model for partial ehl contacts. *ASME J. of Tribol.*, 113(1), 134-141.

Yang, Z., Chung, Y.W. and Cheng, H.S. (1996) Lubricant effects in the transition from boundary to microelastohydrodynamic lubrication. *STLE Tribology Trans.*, 39(4), 974-978.

Zhu, D., Cheng, H.S. and Hamrock, B.J. (1990) Effect of surface roughness on pressure spike and film constriction in elastohydrodynamically lubricated line contacts. *STLE Tribology Trans.*, 33(2), 267-273.

Appendix A

Influence of Lubricant Additives on Friction in a Disc Machine

**(Paper accepted for publication in the
“Fundamentals and Applications in Lubrication and Traction”
Tribology Series, 32, Elsevier)**

Influence of Lubricant Additives on Friction in a Disc Machine

H. Yu and J.B. Medley

Department of Mechanical Engineering
University of Waterloo, Waterloo, ON N2L 3G1, Canada

The friction behaviour of base stock and formulated lubricating oils under conditions of continuous elastohydrodynamic lubrication (ehl) and micro-ehl were investigated in a side-slip disc machine by varying the surface roughness of the discs. Under micro-ehl conditions, the friction was 2 - 3 times larger than under ehl conditions and the additives produced significant differences in the friction. For ehl, small but distinct and repeatable differences in friction were produced by the additives. These differences permitted the derivation of a limiting shear stress expression as a function of pressure, using an empirical approach suggested in the literature, for each of the lubricants. The friction measured under micro-ehl conditions along with an estimation of the real area of contact allowed an alternative evaluation of the limiting shear stress which agreed quite well with the predictions based on the friction measured under ehl conditions. Thus, it was suggested that friction measurements under ehl conditions could be used to evaluate and explore the influence of additives on the limiting shear stress. Furthermore, a simple model for friction in micro-ehl was developed which was consistent with the results of the present investigation.

NOMENCLATURE

a	radius of Hertzian contact circle
A_s, A_r	apparent, real area of contact
d_{avg}, d_{avg}^*	average surface, asperity height
E^*	reduced elastic modulus
F	load
F_f	friction force
h_c	central film thickness
m	limiting shear stress index number
n	asperity density
p	pressure
R	reduced radius
T	lubricant supply temperature
u	entrainment velocity
z_m, z_m^*	dimensionless surface, asperity separation
α	pressure-viscosity coefficient
β	average asperity tip radius at separation z
η_0	viscosity at atmospheric pressure
λ	lambda ratio
μ	coefficient of friction
ν	kinematic viscosity
ρ	lubricant density
σ, σ^*	std deviation of surface, asperity heights
σ_c	composite RMS surface roughness
σ_T, σ_B	RMS roughness of top, bottom discs
τ_L	limiting shear stress
ϕ	skew angle

1. INTRODUCTION

Crankcase oils are "graded" according to their viscosity variation with temperature but their "service category" depends on performance in full engine tests which is influenced significantly by the efficacy of their additive packages. One aspect of additive performance is how they accommodate shear. This rheological behaviour influences friction and, in engines, friction is an important part of the overall energy efficiency and is related ultimately to engine wear.

New additives are proposed frequently by lubricant chemists but it is much too expensive to evaluate them in full engine tests. The simplified standard lubricant tests, such as those involving 4-ball (ASTM D2266) and Timken (ASTM D2509) devices, may be helpful indicators of the combined rheological-chemical additive behaviour but cannot be related, with precision, to performance in full engine tests. Therefore, it is useful to develop new simple and inexpensive tests for evaluating rheological behaviour of lubricant additives which, on their own or in conjunction with existing standard tests, can give a better indication of lubricant performance in full engine tests.

In many engine bearings, elastohydrodynamic lubrication (ehl) films are thin enough to allow individual asperities to play a role in the tribology. These asperity interactions may be "cooperative" in that

they interact with each other to maintain a relatively continuous lubricant film. However, as the surfaces approach more closely, there may be a transition to "isolated" micro-ehl in which each asperity contact acts as an individual bearing. Eventually, surface films of molecular dimensions may begin to interact and the friction is governed by the chemical behaviour of these surface films rather than lubricant rheology. This is known as boundary lubrication. Additive packages are often considered to be developed for boundary lubrication but micro-ehl may be a much more common state and thus performance of additives under these conditions may be important.

The purpose of the present study is to explore the influence of additives on friction in ehl and micro-ehl using a side-slip disc machine of a particular nominal point contact geometry. In the long term, a simple, low cost test procedure for quantifying additive rheological behaviour is sought.

Disc machines have been used to study ehl for many years. The lubricant film can be subjected to various combinations of rolling and sliding velocity and friction forces can be measured accurately.

Jefferis and Johnson (1968) used a disc machine to study the influence of surface roughness on friction in lubricated contacts. They found that when lubricant film thickness decreased, friction increased only slightly with asperity interaction and suggested that, even with very rough surfaces, the lubricant rheology dominated the traction between the discs. More recently, disc machine experiments by Evans and Johnson (1987), Johnson and Higginson (1988) and Sutcliffe (1991) supported this view with more data, directly linking friction at asperity contacts to bulk lubricant rheology. Unfortunately, the role of lubricant additives on the friction at asperity contacts was not examined.

Lubricant additives were examined by Snyder et al (1984) using the disc machine of the present study but their investigation emphasized the influence of additives on ehl film thickness rather than rheology. Much of their work was performed under conditions of continuous fluid film lubrication and they reported that no significant changes in their peak traction coefficients were seen with any of the additives.

Recently, sophisticated instrumentation has been developed for measuring two dimensional maps of shear stress within ehl contacts (Cann and Spikes, 1989; Spikes, 1994) and profiles of shear through ehl film thicknesses (Bair et al. 1993). Such devices provide a much more direct measurement of lubricant rheology

than an overall friction force measurement from a disc machine and can be used to investigate additive behaviour, but they may not be so suitable as simple, low cost test procedures.

2. MATERIALS AND METHODS

2.1. Lubricants

Three formulations of a low viscosity mineral oil (from Imperial Oil Ltd) were used in the present study (Table 1). The first oil was base stock alone (MCT 5) while the second was base stock with 0.5 % by weight of a friction modifier (MCT 5 + FM). The friction modifier was a long chain polar molecule that attached ionically to the metal surfaces. In automobile engine tests, the fuel consumption would decrease because of this additive. The third oil was the base stock with 2 % by weight of an extreme pressure additive (MCT 5 + EP). The extreme pressure additive was *anglamol 33*, a sulphur-phosphorus compound, and the efficacy of this additive could be demonstrated in a 4-ball test (ASTM D2566).

The supplier (Imperial Oil Ltd) provided the kinematic viscosity (ν) and the density (ρ) at the appropriate standard temperatures for each lubricant (Table 1). Following the established ASTM procedures, an absolute viscosity (η_0) was predicted at the lubricant supply temperature in the present experiments for each of the lubricants. These values of η_0 were checked by measurements with a Brookfield viscometer and showed acceptable agreement.

Table 1
Lubricant Specifications

	T (°C)	MCT 5	MCT 5 + FM	MCT 5 + EP
ν (cSt)	40	18.47	19.12	18.46
ν (cSt)	100	3.796	3.803	3.800
ρ (g/ml)	15	0.851	0.854	0.858

2.2. Disc machine

A side-slip disc machine (Fig 1 and 2) was used to provide a simple method of subjecting a lubricating oil to high pressures and a range of low shear rates, while maintaining an almost constant ehl film thickness. The load was applied by hanging weights on the top disc.

An oil damper was placed below the weights and a pivot was provided in the hanger rod so that the weights did not move when the top disc was skewed (rotated in the plane of the contact zone). Both of these features acted to reduce the mechanical vibrations at the higher rolling speeds and loads. A DC motor drove the bottom disc which in turn drove the top disc, at about the same surface velocity, by virtue of friction acting through the contact. By skewing the top disc manually, a side-slip velocity was imposed and continuously increased, thus causing a friction (traction) force which acted sideways (perpendicular to the rolling direction). The friction force was measured by a load cell which used strain gauges and the skew angle (ϕ) was measured with a displacement transducer. A digital data acquisition board (PC-LPT-16 from National Instruments, Austin, Texas) was used with a purpose-built signal conditioning unit (Wheatstone bridge, amplifier and an analog anti-aliasing filter). To help record and process the data, a software package (LabView for Windows from National Instruments) was employed.



Figure 1. Side-slip disc machine which is mounted on a high stand with the weights hanging below.

Thermocouples were placed in light contact with the disc surfaces and in the inlet oil stream in order to determine an appropriate inlet oil temperature. In addition, a simple circuit was fabricated to determine the electrical resistance of the oil film. The resistance measurements provided some insight into the beginning and extent of asperity interaction.

It is important to realize that if the application of this disc machine is established for evaluating additive performance, much of the instrumentation described above can be simplified or eliminated.

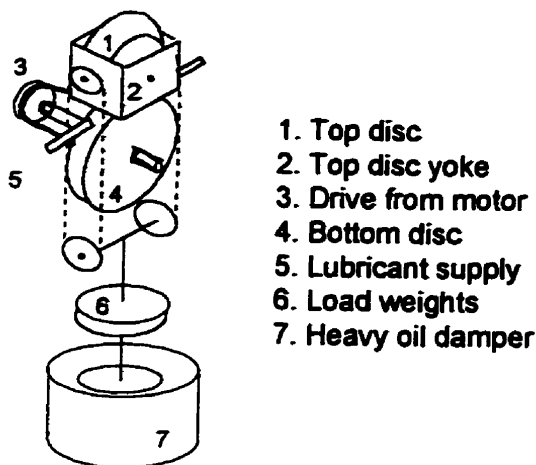


Figure 2. Schematic representation of the side-slip disc machine.

2.3. Disc fabrication

The discs were machined from wrought tool steel (SAE O1 for the bottom disc and Atlas Steel's Keewatin for the top disc). Then, they were hardened by heat treatment to a Rockwell C value of 63, precision cut on a lathe with a diamond tip cutting tool and lapped with fine diamond paste until an RMS roughnesses (σ_T and σ_B) in the range of 0.08 - 0.11 μm were measured with a profilometer device (Talysurf 5, made by Rank Taylor Hobson, Leicester, UK). Two rough top discs were fabricated by adding the additional step of sand blasting with a graded silica sand (No. 60 AFA with a mean diameter of about 1.5 mm) to achieve a σ_T in the range of 1.0 - 1.5 μm .

2.4. Operating conditions

A number of procedural guidelines were developed to select the operating conditions. The thermocouples in the inlet zone were monitored and rolling speeds kept low enough that inlet shear heating was not detected.

When using the smooth discs at a particular load, the electrical resistance measurements allowed a range of rolling speeds to be set that proceeded gradually through the initial breakdown of the ehl film. Likewise, with the rough top discs, the rolling speeds were set to approach the point at which the resistance dropped close to zero, thus suggesting a breakdown of micro-ehl films had occurred. It was recognized that the electrical resistance could give an inaccurate indication of the extent of film breakdown because of oil deposit and oxide layers on

the surface. However, by choosing a range of rolling speeds and various load, it was ensured that measurements were made in regions of experimental interest.

Loads up to about 829.5 N were applied to the smooth disc contacts but the testing with the rough upper discs used only loads of 147.0 N and 244.5 N because of the risk of progressive plastic deformation changing the surface roughness continually. In all testing, run-in was allowed to occur until the surface roughness had stabilized in the contact zone.

The tests always proceeded from using pure base stock oil to using base stock oil with FM and then EP additives. Before introducing a new lubricant, the top disc was cleaned with solvents (varsol and acetone) and lightly polished with abrasives while the bottom disc was just cleaned with the solvents.

A total of 84 individual tests were included in the present study, with the lubricant supply temperature (T) always at 30 °C. Each test consisted of manually skewing the top disc from one side to the other, repeating this act for the opposite direction of rolling (Fig 3) and, finally, repeating the entire procedure a second time. The reversal in rolling direction, allowed the origin of the friction force versus skew angle to be determined exactly and the symmetry of the friction in the four quadrants provided a check on the precision of the disc machine. In most cases, a single quadrant was selected to represent the friction in each individual test and the other seven values only provided an indication of reliability. While an "averaging" procedure might be appropriate, it was not implemented at this stage.

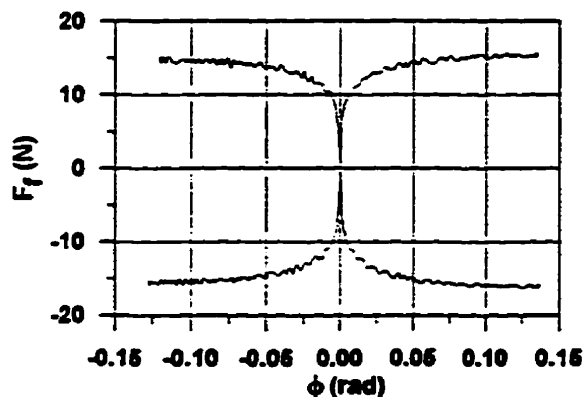


Figure 3. Typical traction curve from the side-slip disc machine for smooth disc surfaces.

An outline of the experimental input parameters is provided in Table 2. Detailed data lists will be available

¹ The composite roughness of top disc S0 is $\sigma_c = 0.092 \mu\text{m}$ in Table 2 of this paper.

in the first author's PhD thesis. In Table 2, a composite root mean square (RMS) roughness is calculated as follows:

$$\sigma_c = \sqrt{\sigma_T^2 + \sigma_B^2} \quad (1)$$

Also, the rough top discs R1 and R2 have the same combinations of loads and velocities as the smooth top discs S1 and S2, respectively.

Table 2
Input parameters for the experiments

Top Disc	σ_c (μm) ¹	F (N)	u (m/s)
S0	0.094	244.5 -829.5	1.6 - 3.8
S1	0.095	147.0	0.6 - 3.1
S2	0.095	244.5	0.7 - 3.3
R1	1.146	147.0	0.6 - 3.1
R2	1.061	244.5	0.7 - 3.3

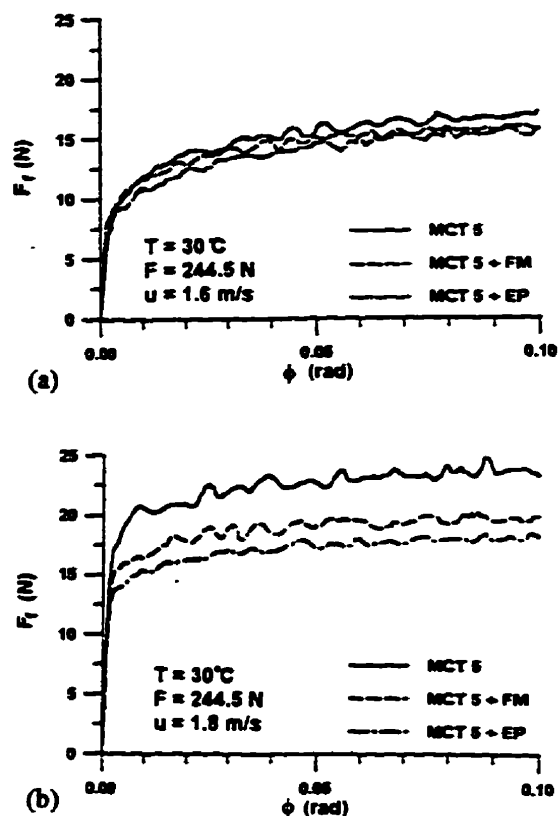


Figure 4. Typical effect of additives on friction for (a) smooth top disc (S2) and (b) rough top disc (R2).

3. RESULTS

As expected with a side-slip disc machine (Johnson and Tevaarwerk, 1977), the friction force (F_f) increased rapidly to a maximum value as the skew angle (ϕ) increased from zero (Fig 3 and 4). Although, F_f was not much influenced by the additives for the smooth top disc, a distinct and repeatable decrease in friction did occur. This effect was much more pronounced when the rough top disc was used. In general, the EP additive reduced F_f more than the FM additive. At $\phi > 0.05$ rad (corresponding to a slide-roll ratio of about 5%), the friction force remained relatively constant and thus this value was considered to correspond to $F_{f, \max}$ in the subsequent analysis of the present study.

4. ANALYSIS

4.1. Friction and lambda ratio

One rather obvious analysis to perform in tribology is to examine the influence of the lambda ratio (λ) on the maximum friction coefficient (μ_{\max}) where

$$\lambda = \frac{h_c}{\sigma_c} \quad (2)$$

The central film thickness (h_c) is calculated, assuming isothermal ehl, for η_0 at 30 °C of 24.5 mPa s, E' of 219.8 GPa, R of 22.58 mm and α of 22.1 GPa⁻¹ along with various values of u and F using

$$\frac{h_c}{R} = 1.90 \left(\alpha E' \right)^{0.53} \left(\frac{\eta_0 u}{E' R} \right)^{0.67} \left(\frac{F}{E' R^2} \right)^{-0.067} \quad (3)$$

from Hamrock and Dowson (1981).

The σ_c values are taken from Table 2. Electrical resistance measurements through the contact indicated that a continuous fluid film occurred for about $\lambda > 3$. As mentioned previously, the $F_{f, \max}$ was specified as occurring at $\phi = 0.05$ rad (corresponding to a slide-roll ratio of 5%) and dividing by the load gives the maximum friction coefficient (μ_{\max}). By eliminating ϕ from further consideration, a concise overview of the present experiments can be shown in Figure 5 (except the testing with top disc S0).

Broadly similar behaviour of μ_{\max} versus λ was found using top discs S1 and R1 with $F = 147.0$ N (Fig 5a) and top discs S2 and R2 with $F = 244.5$ N (Fig 5b). However, the friction for the rough disc tests,

corresponding to the low λ regions, differed enough to suggest that the variations in their surface texture such as asperity tip radius (β) and maximum contact density (n_{\max}) influenced friction.

In general, μ_{\max} remained constant for $\lambda > 1$ but increased significantly as λ dropped further. For λ just below 0.2, μ_{\max} was two or three times its value for $\lambda > 1$. The additives had a small but repeatable effect of reducing μ_{\max} in the region of $\lambda > 3$ which persisted until $\lambda < 1$, whereupon both types of additives reduced the μ_{\max} significantly compared with base stock alone.

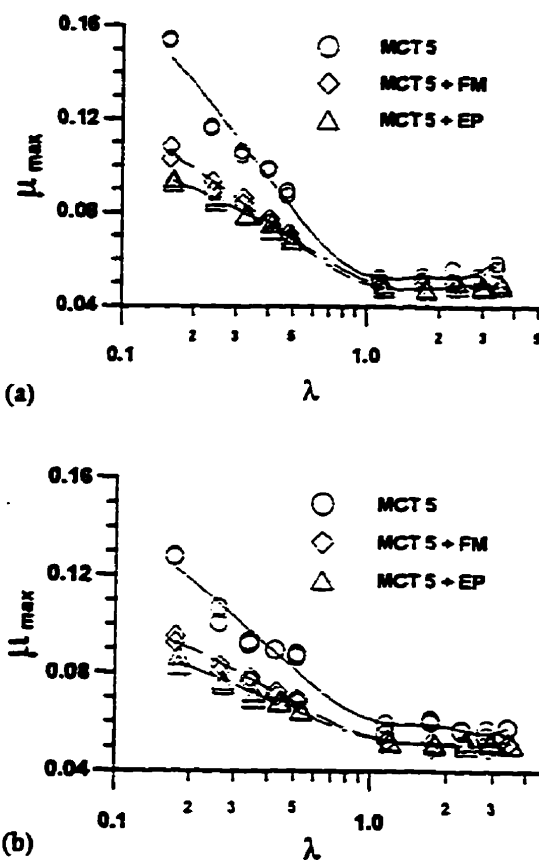


Figure 5.¹ Plots of μ_{\max} versus λ for (a) $F = 147.0$ N (top discs S1 and R1) and (b) $F = 244.5$ N (top discs S2 and R2).

4.2. Limiting shear stress from ehl friction

The effect of the additives when $\lambda > 3$ was puzzling because a continuous fluid film sufficient to separate the asperities occurred and was verified by electrical resistance measurements. To quantify this behaviour, it was decided to estimate the limiting shear stress from

¹ The final version of plots of μ_{\max} versus λ in Figures 5 (a) and (b) in this paper can be found in Figures 6.1 (a) and (b) on pages 226 - 227.

the $F_{t,max}$ obtained for the tests with top disc S0. These tests involved four loads (244.5 N, 439.5 N, 634.5 N and 829.5 N). Following the procedure of Wu and Cheng (1994), the values of the limiting shear stress index number (m) were determined for the lubricants as described in detail in Appendix A.

Once m was determined, eqn (A4) was used to generate an expression of the form (with τ_L and p in Pa)

$$\tau_L = C p^{2m} \quad (4)$$

where C = average of the four load levels,

which was evaluated (Table 3) for the lubricants of the present study.

Table 3
Constants for eqn (4)

	MCT 5	MCT 5 + FM	MCT 5 + EP
m	0.615	0.565	0.523
C	0.000569	0.00436	0.0243

4.3. Real area of contact for the rough discs

To analyze the friction behaviour for the rough discs (discs R1 and R2) which had $\lambda < 1$, it was decided to ignore the lubricant, for the moment, and estimate the real area of contact. The "alpha" roughness parameter of Greenwood et al (1984) was 0.135 for disc R1 and 0.111 for disc R2. According to Greenwood et al, the apparent area of contact (A_a) was influenced by the rough surface such that if Hertzian theory (which assumed smooth surfaces) was used to calculate A_a , it would be about 20% smaller than the actual value. However, it was considered relevant to note that for elastic contact of a surface with Gaussian distributions of surface and asperity heights, the real area of contact (A_r) might depend mostly on the load and be relatively independent of the A_a .

In any case, it was assumed that the A_r was represented accurately by a flat rough surface, with an A_a equal to the smooth surfaced Hertzian value, loaded against a smooth flat surface. A portion of a typical Talysurf profilometer trace of one of the rough top discs is shown in Figure 6. The data from the profilometer

processing unit was analyzed to give the characteristic features of the surface and asperity height distributions (Appendix B and C). The Hertzian value for A_a was calculated with the following standard expression.

$$A_a = \pi \left(\frac{1.5FR}{E'} \right)^{2/3} \quad (5)$$

Then, the procedure outlined in Appendix D was used to estimate A_r (Table 4). The standard deviation of the surface heights (σ) was not equal to the RMS roughness of the disc (σ_r) because the actual surface height distribution was only Gaussian in the region of the asperity tips (Appendix C, Fig C1) because of the deep valleys and rounded peaks found in the run-in surface profile (Fig 6).

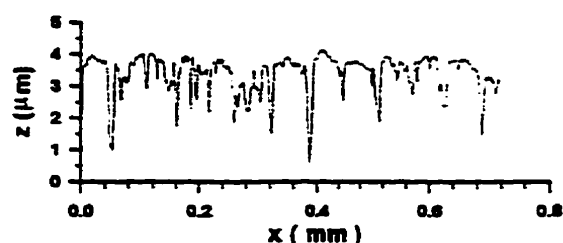


Figure 6. Typical surface of one of the rough top discs after run-in.

Table 4
Calculation of the real area of contact

Parameter	Disc	
	R1	R2
F (N)	147.0	244.5
d_{avg} (μm)	0.	0.
σ (μm)	0.48	0.55
d_{avg}^* (μm)	0.11	0.03
σ^* (μm)	0.47	0.45
n_{max} (mm^{-2})	2442.	3116.
z_m	0.2373	0.1574
z_m^*	0.00735	0.1257
β (mm)	0.1423	0.1132
A_r (mm^2)	0.05108	0.07723

4.4. Limiting shear stress from micro-ehl friction

Assuming that isolated micro-ehl occurred for the rough disc tests somewhere in the range $0.25 < \lambda < 0.5$, the measured $F_{i,max}$ divided by the calculated A_r gave an estimate for $\tau_{L,avg}$. These values of $\tau_{L,avg}$ were calculated for $\lambda = 0.25$ and 0.5 and the corresponding pressure was taken to be the average value obtained by dividing F by A_r . In this manner, a small range of $\tau_{L,avg}$ values were estimated with a corresponding p_{avg} for the lubricants in each of the tests with top discs R1 and R2.

4.5. Comparison of the limiting shear stress from ehl and micro-ehl friction measurements

In the experiments involving top disc S0, $\tau_{L,avg}$ was determined by dividing the measured $F_{i,max}$ by the Hertzian contact area which was calculated using eqn (5). Substituting p_{avg} into eqn (4) gave a prediction of $\tau_{L,avg}$ and when the measured values were compared to the predicted ones for the example of the base stock oil (MCT 5) close agreement was obtained (Table 5). Assuming an absolutely precise value of m had been obtained from Appendix A, eqn (A4) was manipulated to show that the percent error (% err) in estimating a value of $\tau_{L,avg}$ using p_{avg} in an expression such as eqn (4) would be

$$\% \text{ err} = \left| \frac{m + 1}{1.5^{2m}} - 1 \right| \times 100 \quad (6)$$

and evaluating this equation for the m values obtained in the present study gave a maximum percent error of less than 2%. Thus, for the present ehl experiments, eqn (4) with $p = p_{avg}$ could give an accurate estimate of $\tau_{L,avg}$

Table 5
The use of eqn (4) in predicting $\tau_{L,avg}$ for the base stock lubricant (MCT 5)

F (N)	p_{avg} (GPa)	$\tau_{L,avg}$ (MPa)	
		measured	predicted
244.5	0.692	43.0	42.5
439.5	0.842	54.7	54.1
634.5	0.952	63.4	62.9
829.5	1.041	71.1	70.2

Remembering that the film pressure in isolated micro-ehl of a surface with spherical tipped asperities could be approximated as number of localized Hertzian

distributions, it seemed reasonable to use eqn (4) to predict the average limiting shear stress in micro-ehl with the understanding that the pressure in eqn (4) would be the average pressure of all the micro-contacts.

Finally, a direct comparison could be made between the $\tau_{L,avg}$ predicted from ehl friction and that predicted from micro-ehl (Fig 8). Surprisingly, considering the assumptions and simplifications made in the analysis, the agreement was quite good, particularly for the testing at $F = 244.5$ N with top disc R2. This agreement suggested that the τ_L expression given by eqn (4) which was determined from ehl friction measurements was reasonably accurate and thus a useful technique for finding τ_L had been found which was sensitive enough to give different values for the different additives.

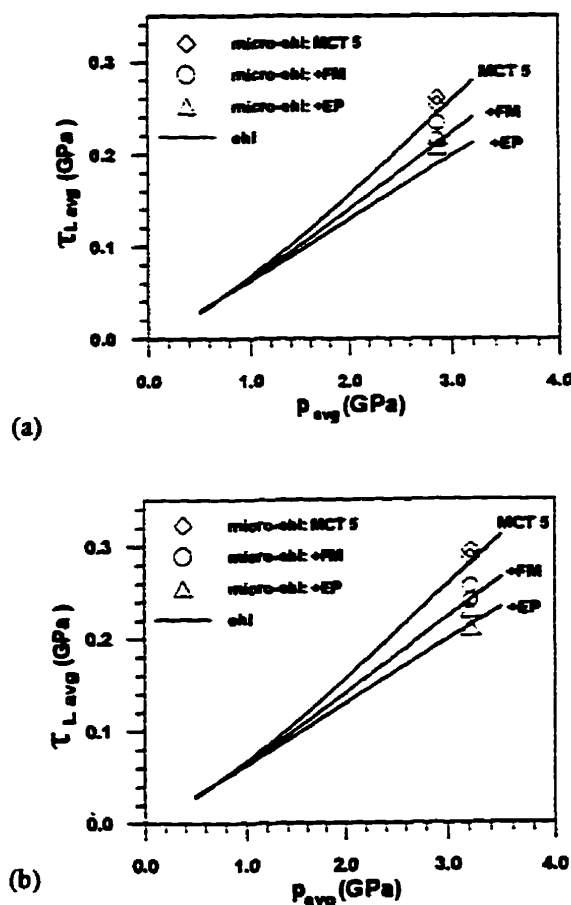


Figure 8. Comparison of the average limiting shear stress predictions based on ehl and micro-ehl friction measurements for (a) $F = 147.0$ N and (b) $F = 244.5$ N.

5. DISCUSSION

A disc machine of relatively simple construction has been used to investigate the influence of additives on lubricant rheology. For the present experiments, a plausible analysis has been made which explains the friction as arising from the lubricant reaching a limiting shear stress. This analysis remains consistent for lambda ratio greater than 0.25, thus suggesting that micro-ehl can persist down to these low values. The limiting shear stress was influenced by the additives used in the present experiments.

The limiting shear stress could be evaluated at a lambda ratio greater than 3, where full fluid film lubrication occurs and where neither extensive characterization of the disc surfaces nor frequent monitoring of progressive damage to the disc surfaces is required. *It is here that we believe the main contribution of the present study lies.* Side-slip disc machine friction measurements can be used under conditions of continuous ehl to evaluate limiting shear stress that is a useful parameter for predicting friction in the mixed film regime under conditions of micro-ehl. The limiting shear stress is influenced by the additives, thus suggesting that lubricant chemistry could be designed to give an optimal limiting shear stress using the disc machine measurements for guidance.

However, our enthusiasm for this approach must be tempered with some uncertainty regarding the generality of the procedure. Although additional data has been generated for the first author's PhD thesis and it seems to support the findings of the present paper, more testing is required with other additives and higher lubricant temperatures. The developed procedures for finding the limiting shear stress index value and the real area of contact are both very sensitive to small changes in the input parameters. Continued work is required to improve the precision of all of the procedures described in the present study. Maintaining the experimental studies under micro-ehl conditions is advocated to check the estimated values of limiting shear stress obtained under continuous ehl conditions and another type of viscometer (as opposed to a disc machine) is recommended to provide additional, perhaps more precise, confirmation of these estimated values. Devices such as those used by Cann and Spikes (1989) and Bair et al (1993) may be good choices for this future work.

5. CONCLUSIONS

- The limiting shear stress was estimated from friction measurements under continuous ehl conditions and agrees quite closely with that obtained under isolated micro-ehl conditions.
- The limiting shear stress was influenced by lubricant additives.
- The limiting shear stress combined with an evaluation of the real area of contact provided a simple friction model for isolated micro-ehl.
- A simple, low cost test procedure using a side-slip disc machine under conditions of continuous ehl was suggested for screening lubricant additives.

ACKNOWLEDGEMENTS

Financial support was provided by Imperial Oil Ltd and NSERC and skillful technical assistance was provided by E. Huber, P. Renkma and D. Raude.

REFERENCES

- Bair, S., Qureshi, F. and Winer, W.O. (1993) Observations of shear localization in liquid lubricants under pressure. *ASME J. of Trib.*, 115, 507-514.
- Bair, S. and Winer, W.O. (1992) The high pressure high shear stress rheology of liquid lubricants. *ASME J. of Trib.*, 114, 1-13.
- Bair, S. and Winer, W.O. (1979) A rheological model for elastohydrodynamic contacts based on primary laboratory data. *ASME J. of Lubr. Technol.*, 101, 258-265.
- Cann, P.M. and Spikes, H.A. (1989) Determination of the shear stresses of lubricants in elastohydrodynamic contacts. *STLE Tribology Trans.*, 32, 414-422.
- Cooper, M.G., Milkic, B.B. and Yovanovich M.M. (1969) Thermal contact conductance. *Int. J. Heat Mass Transfer*, 12, 279-300.
- Evans, C.R. and Johnson, K.L. (1987) The influence of surface roughness on EHD traction. *Proc. Inst. Mech. Engrs.* Pt C, 201, 145-150.
- Greenwood, J.A., Johnson, K.L. and Matsubara, E. (1984) A surface roughness parameter in hertz contact. *Wear*, 100, 47-57.
- Greenwood, J.A. and Tripp, J.H. (1967) The elastic contact of rough spheres. *ASME J. of Appl. Mech.*, 89, 153-159.
- Greenwood, J.A. and Williamson, J.B.P. (1966) Contact of nominally flat surfaces. *Proc. Royal Soc. A*, 295, 300-319.

Hamrock, B.J. and Dowson, D. (1981) *Ball Bearing Lubrication - The Elastohydrodynamics of Elliptical Contacts*. McGraw-Hill

Jefferis, J.A. and Johnson, K.L. (1968) Sliding friction between lubricated rollers. *Proc Instn Mech Engrs*, 182 (1), 281-92.

Johnson, K.L. and Higginson, J.G. (1988) A non-Newtonian effect of sliding in micro-chl. *Wear*, 128, 249-264.

Johnson, K.L. and Tevaarwerk, J.L. (1977) Shear behavior of elastohydrodynamic oil film. *Proc. Roy. Soc. Lond., Ser. A*. 356. 215-236.

McCool, J.L. (1986) Comparison of models for the contact of rough surface. *Wear*, 107, 37-60.

Snyder, F.L., Tevaarwerk, J.L. and Schey, J.A. (1984) Effects of oil additives on lubricant film thickness and traction. *SAE Tech. Paper Series*, 840263. SAE, Warrendale, Pennsylvania.

Spikes, H.A. (1994) The behaviour of lubricants in contacts: current understanding and future possibilities. *Proc Instn Mech Engrs, Part J: J of Eng Tribology*, 208, 3-15.

Sutcliffe, M.P. (1991) Traction measurements in mixed elastohydrodynamic lubrication with a controlled circumferential roughness. *Proc Instn Mech Engrs, Part C: J.Mech Engineering Science*, 205, 265-273.

Wu, S. and Cheng, H.S. (1994) Empirical determination of effective lubricant rheological parameters. *STLE Tribology Trans.*, 37(1), 138-46.

APPENDIX A

Determining the limiting shear stress index number from friction measurements with a disc machine

In elastohydrodynamic contacts, the lubricant may be subjected to high pressures and shear rates. The resisting shear stress in the lubricant often reaches a limiting value (τ_L) which depends on pressure and temperature but is independent of the shear rate (Johnson and Tevaarwerk, 1977; Bair and Winer, 1979). This model for lubricant behaviour is very simple and there is some debate regarding the extent to which it applies in elastohydrodynamic contacts (Bair and Winer, 1992; Bair et al. 1993).

In the present study, an empirical approach following Wu and Cheng (1994) was adopted to determine a limiting shear stress index number (m). This approach used friction measurements from a disc machine and was based on the assumption that the lubricant had reached limiting shear stress throughout

the contact zone, the values of which depended on local film pressure. It was further assumed that the limiting shear stress was reached before shear heating was significant and thus the inlet temperature of the lubricant prevailed throughout the contact.

Wu and Cheng (1994) applied their technique to a nominal point contact with circular contact area and approximated the local film pressure as Hertzian using the standard formula

$$p = p_{\max} \sqrt{1 - \left(\frac{r}{a}\right)^2} \quad (\text{A1})$$

$$\text{where } p_{\max} = \frac{1.5 F}{\pi a^2} \quad . \quad a = \left(\frac{1.5 F R}{E'}\right)^{\frac{1}{3}}$$

and then assumed that the limiting shear stress has the following distribution

$$\tau_L = \tau_{L \max} \left(1 - \left(\frac{r}{a}\right)^2\right)^m \quad (\text{A2})$$

where m = limiting shear stress index number.

It followed that the maximum friction force as measured with a disc machine was

$$F_{f \max} = \int_0^{2\pi} \int_0^a \tau_L r \, dr \, d\theta$$

and substituting in from eqn (A2) along with elementary integrations gave

$$F_{f \max} = \tau_{L \max} \frac{\pi a^2}{m + 1} \quad (\text{A3})$$

Eqns (A1), (A2) and (A3) were combined to give

$$\tau_L = (m + 1) \frac{F_{f \max}}{\pi a^2} \left(\frac{p}{p_{\max}}\right)^{2m} \quad (\text{A4})$$

To determine the value of m for a particular lubricant, the maximum friction force was measured at each of four applied loads (244.5 N, 439.5 N, 634.5 N, 829.5 N). At the same pressure (p), eqn (A4) indicated that some value of m must exist such that the same limiting shear stress could be calculated for each applied load.

Wu and Cheng (1994) did not indicate clearly how this m value was determined. In the present study, a value of p was chosen equal to the maximum Hertzian pressure for the lowest of four levels of applied load. An m value was specified and eqn (A4) used to calculate four values for τ_L . An average of the four τ_L values was

calculated and then the sum of the squared residuals were determined as follows:

$$\epsilon = \sum_{i=1}^4 [\tau_{z,i} - \tau_{z,avg}]^2 \quad (A5)$$

This calculation was repeated for ranges of m values, starting from 0 - 1 and refining within that range until the m value to three significant digits was determined which gave a minimum ϵ . In the present study, a single minimum occurred at around $m = 0.6$ in all cases. Slight changes in m occurred when a different value of p was chosen. More substantial changes in m occurred when 2 or 3 rather than 4 load levels were used but the changes between 3 and 4 load levels were much less than those between 2 and 3 load levels. Thus, it was apparent that m was influenced by the inevitable scatter in the friction measurements and the best course of action was to use at least 4 load levels and perhaps repeat the measurements at each load level more than once. In this respect, the present study was deemed adequate but in future work more load levels and friction measurements would be used and continuing efforts would be made to improve the precision of the measurements.

APPENDIX B

Contact spot density between flat rough and smooth surfaces

If the topography of a nominally flat surface region can be measured giving an accurate three dimensional map, it is relatively simple to ascertain the number of asperity contacts when a smooth flat plane is located at a particular separation. With a specified apparent area of contact (A_c), a direct measurement of contact spot density (n) could be made at that separation.

However, if a profilometer trace is used to measure surface topography giving a two dimensional graph, it is somewhat more difficult to establish an expression for contact spot density which is related to the features of the profilometer trace. To address this problem, a rigid smooth plane (represented in two dimensions as a horizontal line) located at some separation (z), is considered to be in contact with an isotropically rough surface which is measured by a profilometer (Fig B1). A line representing the average of the rough surface heights is also horizontal and the rough surface undergoes perfectly plastic deformation. The n at z is the same if the two surfaces deform elastically but it is

convenient for visualization in the present development to consider the above rigid-plastic pair.

An expression relating n to the high spot count (HSC) and bearing area (BA) at z can be developed. Following standard definitions, the HSC is one half the number of times the rough surface profile crosses the horizontal line representing the smooth surface divided by the profile length while the BA is the sum of the length of the horizontal line segments contained within the rough surface profile divided by the profile length (Fig B1). The HSC and BA are provided as functions of height (or separation) z by the 5M processor of the Talysurf profilometer which was used in the present study. However, this processor selects the heights internally and often does not supply the required parameters at enough heights. When this occurred, additional values were obtained by interpolation with a third order polynomial.

Following Greenwood and Tripp (1967), the asperities are assumed to have spherical tips of about the same radius of curvature but various heights. When a smooth flat plane is pressed into such a spherical tip the contact circle increases rapidly after initial contact, then more slowly as the separation z decreases. As a result, the contact spots all have about the same radius of curvature (\bar{a}) when the smooth flat surface is at some height z despite the variation in asperity heights.

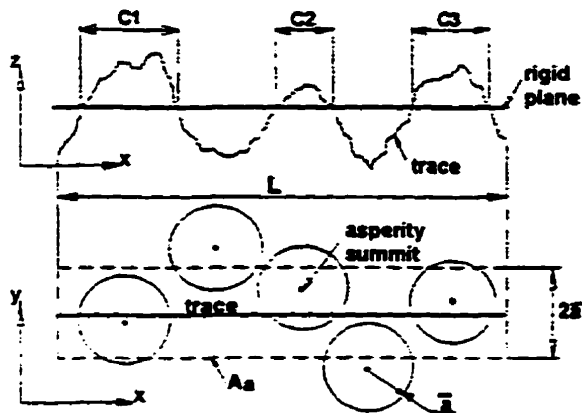
It is convenient to consider the A_c shown in Fig B1 and to note that if asperity contact areas are larger and smaller than those shown, some extra contact spots would be include and some would be missed but on a long trace n should stay about the same. It follows that

$$n = \frac{HSC}{2\bar{a}} \quad (B1)$$

To determine an expression for \bar{a} , consider a long trace that, for the given z , intersects many contact spots. The average length of trace within the contact spots (Fig B2) is

$$\frac{BA}{HSC} = 2\bar{x} \quad (B2)$$

$$\text{where from calculus } \bar{x} = \frac{\frac{1}{2} \pi \bar{a}^2}{2\bar{a}} = \frac{\pi \bar{a}}{4}$$



in this case

$$BA = \frac{C_1 + C_2 + C_3}{L} \quad HSC = \frac{3}{L} \quad n = \frac{3}{A_a}$$

Figure B1. Representation of a rigid plane in contact with a perfectly plastic rough surface, obtained from a two dimensional profilometer trace.

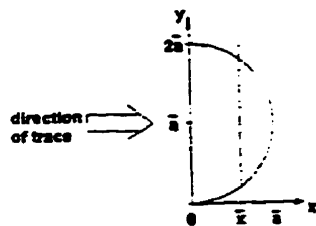


Figure B2. Half of a contact spot.

Eqns (B1) and (B2) imply that

$$n = \frac{\pi}{4} \frac{HSC^2}{BA} \tag{B3}$$

The above expression is valid for elastic surfaces because only size and not the number or the location of the contact spots changes. This same expression was derived in a somewhat different way by Cooper et al (1969).

APPENDIX C

Determining the surface and asperity height distributions

The HSC and BA were measured for decreasing z using a profilometer with interpolation as mentioned in Appendix B. It was then possible to determine n for

each z value using eqn (B3). As expected, n increased with decreasing z until a maximum value (n_{max}) was reached at a particular separation (z_c) as a result of the merging of asperities.

Since the BA represented a cumulative frequency plot of the surface heights, the type and features of the surface height distribution was obtained by plotting BA on probability paper (Fig C1). For both disc 1 and 2, the BA data fit a straight line on the probability paper for the asperity tip region of the surfaces. In other words, the surface height distribution was Gaussian in the part of the surface which would make intimate contact with the smooth disc surface. The features of the distribution included the average surface height (d_{avg}) and the standard deviation (σ) both of which could be determined from the plot on probability paper. The location of the z-axis was adjusted so that z = 0 corresponded to the average surface height for convenience in later calculations.

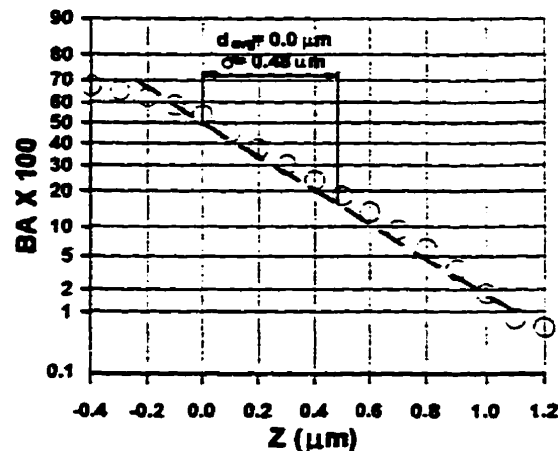


Figure C1. Plot of BA on probability paper (disc R1).

If an asperity was considered to be any summit on the surface which has a height greater than z_c , then the cumulative frequency of the asperity (as opposed to surface) height distribution was given by n/n_{max} which could then be plotted on probability paper (Fig C2). Once again, the data fit a straight line for the outermost region of the surfaces for both disc 1 and 2, thus indicating a Gaussian distribution. The features of the distribution included the average asperity height (d_{avg}^*) and the standard deviation (σ^*) which could be determined from the plot on probability paper.

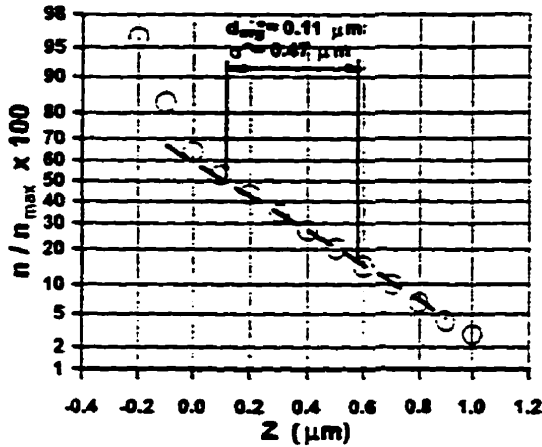


Figure B2. Plot of n/n_{\max} on probability paper (disc R1).

In both the BA and the n/n_{\max} plots on probability paper, the fitted lines were estimated "by eye". Clearly, software must be developed to perform the curve fits and a criterion must be developed for excluding the points in the low z regions which are not distributed in a Gaussian fashion. However, this shortcoming in the present analysis was not expected to influence the overall findings significantly.

APPENDIX D

Determining the real area of contact for a specified load

If the separation z were known for a specified load and the deformation was perfectly plastic, the ratio of real to apparent area of contact would equal the BA at that z (considering an apparent area that was the length of the trace and of infinitesimally width). Unfortunately, z was not known and the deformation was elastic in the present study. However, assuming that all contacting asperities at a particular z have spherical tips with about the same radii of curvature, which could be represented adequately by an average value, and that they deform independently, a procedure was developed to find z . Following Greenwood and Williamson (1966), Hertzian equations were applied to individual asperity contacts and Gaussian distributions of surface and asperity height distributions were employed to yield the following equations:

(i) for the surface heights

$$A_r = \frac{1}{2} A_a F_0(z_m) \quad (D1)$$

(because Hertzian contact areas were half those of purely plastic deformation)

(ii) for the asperity heights

$$A_r = \pi \beta A_a n_{\max} \sigma^* F_1(z_m^*) \quad (D2)$$

$$F = \frac{2}{3} \beta^{0.5} E' A_a n_{\max} (\sigma^*)^{1.5} F_{1.5}(z_m^*) \quad (D3)$$

$$\text{where } z_m = \frac{z - d_{\text{avg}}}{\sigma}, \quad z_m^* = \frac{z - d_{\text{avg}}}{\sigma^*}$$

$$F_j(\zeta) = \frac{1}{\sqrt{2\pi}} \int_{\zeta}^{\infty} (s - \zeta)^j e^{-\frac{s^2}{2}} ds$$

for $j = 0, 1, 1.5$

E' = effective elastic modulus

β = average tip radius for all contacting asperities at separation z

Eqs (D1) and (D2) gave an expression for the asperity tip radius at a particular z

$$\beta = \frac{F_0(z_m)}{2 \pi n_{\max} \sigma^* F_1(z_m^*)} \quad (D4)$$

and substituting into eqn (D3) yielded

$$F_0(z_m) - \frac{9\pi}{4} \left(\frac{1}{n_{\max}} \right) \left(\frac{F}{\sigma^* E' A_a} \right)^2 \frac{F_1(z_m^*)}{[F_{1.5}(z_m^*)]^2} = 0 \quad (D5)$$

which was solved for the separation z which corresponded to the specified load F . A computer program was written in Fortran to perform the solution of eqn (D5) which contained a secant root finding algorithm that used the discrete values of the F_j 's given by McCool (1986) and a natural cubic spline routine to provide interpolated values when required.

Once the z value had been determined, the corresponding z_m value was calculated and eqn (D1) gave the real area of contact. Also, it was possible to calculate the average tip radius for all contacting asperities using eqn (D4).

Discussion of the Paper by Yu and Medley in the 23rd Leeds-Lyon Symposium on Tribology

Question 1: J.A.Williams, Cambridge University, Dept. Engineering

You demonstrate the importance of the λ ratio on the overall friction coefficient of your rough surface experiments for which you assumed, I think, a Greenwood and Williamson type of topography. This requires that the surface can be ascribed a single characteristic value of asperity curvature - how did you assess its value from your topographical measurements and could you indicate the sorts of values you have used.

Question 2: Marnix Visscher, The University of Leeds

The authors derived average pressure and average shear stress values for the "real contacts". To this end they used the Greenwood and Williamson contact model to calculate the real area of contact. This, and other, contact models make use, however, of parameters which are not intrinsic properties of the surface but depend on the measurement parameters [D1, D2]. The mean peak radius, e.g., varies significantly with the sampling interval. Hence, by manipulating the roughness measurement, one can get any value one likes. My question, therefore, is: have the authors considered this fact, and how have they overcome the problem?

References

- [D1] Greenwood, J.A., (1992), "Fundamentals of Friction" Macroscopic and Microscopic Processes (Proc. NATO Adv. study Inst. on Fundamental of Friction)", NATO ASI Series E, Vol. 220, pp. 57 - 76.
- [D2] Visscher, M., Dowson, D. and Taylor, C.M. (1996), "The Third Body Concept: Interpretation of Tribological Phenomena (Proc. 22nd Leeds-Lyon Symposium on Tribology).

Question 3: J.C. Bell, Shell Research Ltd. UK

The authors have estimated the contribution of friction of lubricant additives by the use of the limiting shear stress (τ_L) model of Wu and Cheng. The mechanism by which additives affect τ_L is far from clear. Would the authors please clarify this mechanism and how it is reflected in the Wu and Cheng model.

Authors' Reply

Drs. Williams and Visscher seem to be asking essentially the same question. In our presentation, we did not elaborate on our "Greenwood and Williamson" type model but, in our paper, details are provided in Section 4.3 and Appendices B, C and D. The influence of Greenwood and Williamson led us to assume that asperities had spherical tips, deformed independently and that Gaussian distributions could be applied to surface and asperity height distributions. However, using the relationship for contact spot density, derived by Cooper et al. (1969) and also in Appendix B of our paper in a somewhat different manner, we assumed that all contacting asperities at a particular separation z (Figure B1) had spherical tips of about the same radius of curvature (but various heights) which could be represented adequately by an average value (β). The method of obtaining the separation z and corresponding β for a given load can be found in De Vaal (1983) and also in Appendix D of our paper, and the numerical values for our two rough surface (discs R1 and R2) are listed in Table 4. By determining a separation z and an average β , both related to the applied load, we allowed small surface ripples and/or noise which might be part of the trace of the surface heights (Figure 6), details of which would be sensitive to sampling interval, to merge when the surfaces are at separation z and thus not influence the calculated real area of contact significantly. In this manner, our calculated β was not a single constant value for the surface but a function of the applied load which, in turn, set the separation z . For our surface topography and loads, the β value was not likely to change much unless the load was reduced significantly.

This approach differs from that of Visscher et al [D2] but it seems to achieve a somewhat similar result in that it eliminates smaller scale “asperities” from consideration. Since our surfaces were run-in before testing so that virtually all asperities would be deforming elastically under load, plasticity index could not have been used to determine a sampling interval. However, our approach might provide a versatile alternative which would be useful in the modeling of Visscher et al.

If a Greenwood and Williamson model requires a “mean peak radius” as stated by Dr. Visscher or a “single characteristic value of asperity curvature” as stated by Dr. Williams, then perhaps we should not have associated Greenwood and Williamson so directly with our model. Since the calculation of real areas of contact was only a means to an end in our paper, we make no claims to have a universal model based on “intrinsic” surface properties. However, we do feel that the adopted approach gives a unique prediction of real area of contact which is reasonably accurate for the run-in surfaces in our study.

In response to the question of Dr. Bell, we have found that under our conditions of high pressure and low temperature, the friction can be controlled by the limiting shear stress and the additives cause a decrease in the limiting shear stress as predicted by Equation 4 of our paper by reducing the value of m which is the index number from the model of Wu and Cheng (1994). The determination of m is described in detail in Appendix A of our paper. One can speculate that the additives influence the formation of the shear bands, described by Bair et. al. (1993) by allowing the lubricant to “slide over itself” more readily. However, Dr. Bell may be seeking a specific and verified mechanism related to the lubricant chemistry and including the influence of temperature. It was beyond the scope of the present study to determine these important aspects of the mechanism, but nevertheless we do feel that some experimental evidence of its existence has been obtained.

Additional Reference

De Vaal, J.W. (1983) Thermal contact conductance of rough surface. *MASc Thesis*, University of Waterloo, 76-80.